

# Journal of Advances in Information Fusion

A semi-annual archival publication of the International Society of Information Fusion

Regular Papers	Page
<b>Bias Estimation for Moving Optical Sensor Measurements with Targets of Opportunity</b> ..... 101 <i>Djedjiga Belfadel, University of Connecticut, USA</i> <i>Richard W. Osborne, III, University of Connecticut, USA</i> <i>Yaakov Bar-Shalom, University of Connecticut, USA</i>	101
<b>Fusion of Multipath Data with ML-PMHT for Very Low SNR Track Detection in an OTHR</b> ..... 113 <i>Kevin Romeo, University of Connecticut, USA</i> <i>Yaakov Bar-Shalom, University of Connecticut, USA</i> <i>Peter Willett, University of Connecticut, USA</i>	113
<b>Tracking Targets with Multiple Measurements per Scan Using the Generalized PHD Filter</b> ..... 125 <i>Christoph Degen, Fraunhofer FKIE, Germany</i> <i>Felix Govaers, Fraunhofer FKIE, Germany</i> <i>Wolfgang Koch, Fraunhofer FKIE, Germany</i>	125
<b>An improved measurement model for target tracking under measurement origin uncertainty</b> ..... 143 <i>Viji Paul Panakkal, BEL, India</i> <i>Rajbabu Velmurugan, Indian Institute of Technology Bombay, India</i>	143
<b>Bistatic Measurement Fusion from Multistatic Configurations for Air Collision Warning</b> ..... 163 <i>Wenbo Dou, University of Connecticut, USA</i> <i>Yaakov Bar-Shalom, University of Connecticut, USA</i> <i>Peter Willett, University of Connecticut, USA</i>	163
<b>Early Fusion and Query Modification in Their Dual Late Fusion Forms</b> ..... 183 <i>Leszek Kalciak, AmbieSense Ltd., UK</i> <i>Hans Myrhaug, AmbieSense Ltd., UK</i> <i>Ayse Goker, AmbieSense Ltd., UK</i> <i>Dawei Song, Open University in Milton Keynes, UK</i>	183
<b>Fusion of Asynchronous Passive Measurements</b> ..... 199 <i>Richard W. Osborne, III, University of Connecticut, USA</i> <i>Yaakov Bar-Shalom, University of Connecticut, USA</i> <i>Peter Willett, University of Connecticut, USA</i>	199

# INTERNATIONAL SOCIETY OF INFORMATION FUSION

The International Society of Information Fusion (ISIF) is the premier professional society and global information resource for multidisciplinary approaches for theoretical and applied INFORMATION FUSION technologies. Technical areas of interest include target tracking, detection theory, applications for information fusion methods, image fusion, fusion systems architectures and management issues, classification, learning, data mining, Bayesian and reasoning methods.

## JOURNAL OF ADVANCES IN INFORMATION FUSION: DECEMBER 2015

---

<b>Editor-In-Chief</b>	Uwe D. Hanebeck	Karlsruhe Institute of Technology (KIT), Germany; +49-721-608-43909; uwe.hanebeck@ieee.org
Associate	Stefano Coraluppi	Systems & Technology Research, USA; +1 781-305-4055; stefano.coraluppi@ieee.org
<b>Administrative Editor</b>	Robert Lynch	University of Connecticut, USA; +1 860-705-3321; lynch@enr.uconn.edu
Associate	Ruixin Niu	Virginia Commonwealth University, Richmond, Virginia, USA; +1 804-828-0030; rniu@vcu.edu
Associate	Marcus Baum	Karlsruhe Institute of Technology (KIT), Germany; +49-721-608-46797; marcus.baum@kit.edu

## EDITORS FOR TECHNICAL AREAS

---

<b>Tracking</b>	Stefano Coraluppi	Systems & Technology Research, USA; +1 781-305-4055; stefano.coraluppi@ieee.org
Associate	Huimin Chen	University of New Orleans, New Orleans, Louisiana, USA; +1 504-280-1280; hchen2@uno.edu
Associate	Paulo Braca	NATO Science & Technology Organization Centre for Maritime Research and Experimentation, Italy; +39 0187 527 461; paolo.braca@cmre.nato.int
<b>Detection</b>	Pramod Varshney	Syracuse University, Syracuse, New York, USA; +1 315-443-1060; varshney@syr.edu
<b>Fusion Applications</b>	Ben Slocumb	Numerica Corporation; Loveland, Colorado, USA; +1 970-461-2000; bjslocumb@numerica.us
Associate	Ramona Georgescu	United Technologies Research Center, East Hartford, Connecticut, USA; 860-610-7890; georgera@utrc.utc.com
<b>Image Fusion</b>	Lex Toet	TNO, Soesterberg, 3769de, Netherlands; +31 346356237; lex.toet@tno.nl
Associate	Ting Yuan	Mercedes Benz R&D North America, USA; +1 669-224-0443; dr.ting.yuan@ieee.org
<b>Fusion Architectures and Management Issues</b>	Chee Chong	BAE Systems, Los Altos, California, USA; +1 650-210-8822; chee.chong@baesystems.com
<b>Classification, Learning, Data Mining</b>	Nageswara S. V. Rao	Oak Ridge National Laboratory, USA; +1 865-574-7517; raons@ornl.gov
Associate	Robert Lynch	University of Connecticut, USA; +1 860-705-3321; lynch@enr.uconn.edu
<b>Bayesian and Other Reasoning Methods</b>	Claude Jauffret	Université de Toulon, La Garde, France; +33 (0) 4 94 14 24 14; jauffret@univ-tln.fr
Associate	Jean Dezert	ONERA, Chatillon, 92320, France; +33 146734990; jean.dezert@onera.fr

Manuscripts are submitted at <http://jaif.msubmit.net>. If in doubt about the proper editorial area of a contribution, submit it under the unknown area.

## INTERNATIONAL SOCIETY OF INFORMATION FUSION

---

Darin Dunham, *President*  
Jean Dezert, *President-elect*  
Stefano Coraluppi, *Secretary*  
Chee Chong, *Treasurer*  
Dale Blair, *Vice President Publications*

Robert Lynch, *Vice President Communications*  
Lance Kaplan, *Vice President Conferences*  
Anne-Laure Jousselme, *Vice President Membership*  
Garfield Mellema, *Vice President Working Groups*  
Roy Streit, *Perspectives EIC*

Journal of Advances in Information Fusion (ISSN 1557-6418) is published semi-annually by the International Society of Information Fusion. The responsibility for the contents rests upon the authors and not upon ISIF, the Society, or its members. ISIF is a California Nonprofit Public Benefit Corporation at P.O. Box 4631, Mountain View, California 94040. **Copyright and Reprint Permissions:** Abstracting is permitted with credit to the source. For all other copying, reprint, or republication permissions, contact the Administrative Editor. Copyright© 2015 ISIF, Inc.

# Bias Estimation for Moving Optical Sensor Measurements with Targets of Opportunity

DJEDJIGA BELFADEL  
RICHARD W. OSBORNE, III  
YAAKOV BAR-SHALOM

Integration of space based sensors into a Ballistic Missile Defense System (BMDS) allows for detection and tracking of threats over a larger area than ground based sensors. This paper examines the effect of sensor bias error on the tracking quality of a Space Tracking and Surveillance System (STSS) for the highly non-linear problem of tracking a ballistic missile. The STSS constellation consists of two or more satellites (on known trajectories) for tracking ballistic targets. Each satellite is equipped with an IR sensor that provides azimuth and elevation to the target. The tracking problem is made more difficult due to a constant or slowly varying bias error present in each sensor's line of sight measurements. The measurements provided by these sensors are assumed time-coincident (synchronous) and perfectly associated. The Line Of Sight (LOS) measurements from the sensors are used to estimate simultaneously the Cartesian target of opportunity positions, and the sensor biases. The evaluation of the Cramér-Rao Lower Bound (CRLB) on the covariance of the bias estimates, which serves as a quantification of the available information about the biases, and the statistical tests on the results of simulations show that this method is statistically efficient, even for small sample sizes (as few as two sensors and six points on the (unknown) trajectory of a single target of opportunity). We also show that the Root Mean Square (RMS) position error is significantly improved with bias estimation compared with the target position estimation using the original biased measurements.

Manuscript received April 14, 2014; revised December 24, 2014; released for publication March 3, 2015.

Refereeing of this contribution was handled by Ramona Georgescu.

Approved for Public Release 14-MDA-7763 (27 March 14).

Partially funded by ARO W911NF-10-1-0369.

Authors' address: Electrical and Computer Engineering, University of Connecticut, Storrs, CT, U.S.A. (e-mail: djedjiga.belfadel@uconn.edu, rosborne@enr.uconn.edu, ybs@enr.uconn.edu).

1557-6418/15/\$17.00 © 2015 JAIF

## I. INTRODUCTION

Space-based sensors can expand the range and effectiveness of the capabilities of a Ballistic Missile Defense System (BMDS) to counter future projected threats. A space based tracking system utilizing an IR sensor will allow detection and tracking of targets outside of terrestrial radar coverage. This is possible because a sensitive IR sensor in relatively close proximity can detect and track a target against the cold background of space. Multisensor systems use fusion of data from multiple sensors to form accurate estimates of a target track. To fuse multiple sensor data the individual sensor data must be expressed in a common reference frame. A problem encountered in multisensor systems is the presence of errors due to sensor bias. Some sources of bias errors include: measurement biases due to the deterioration of initial sensor calibration over time; attitude errors caused by biases in the gyros of the inertial measurement units of (airborne, seaborne, or spaceborne) sensors; and timing errors due to the biases in the onboard clock of each sensor platform [6].

In [6] time varying bias estimation based on a non-linear least squares formulation and the singular value decomposition using truth data was presented. However, this work did not discuss the CRLB for bias estimation. An approach using maximum a posteriori (MAP) data association for concurrent bias estimation and data association based on sensor-level track state estimates was proposed in [7] and extended in [8].

Sensor calibration using in-situ celestial observations to estimate bias in space-based missile tracking was discussed in [5]. In [4] simultaneous sensor bias and targets position estimation using fixed passive sensors was presented. In the present paper, bias estimation is investigated when only targets of opportunity are available. The tracking system consists of two or three satellites tracking a ballistic target. We assume the sensors are synchronized, their locations are known, and the data association is correct; and we estimate their orientation biases. We investigate the use of the minimum possible number of moving sensors and measurements. Two cases are considered. In the first case, we use three moving optical sensors to estimate 3 points on the (unknown) trajectory of a single target of opportunity simultaneously with the biases of the three optical sensors [3]. In the second case, we estimate the position of 6 points on the trajectory of a single target of opportunity simultaneously with the biases of two space-based optical sensors[2]. First, we discuss the observability requirement related to the bias estimation. We evaluate the Cramér-Rao lower bound (CRLB) on the covariance of the bias estimates, which is the quantification of the available information on the sensor biases, and show via statistical tests that the estimation is statistically efficient—it meets the CRLB. Section II

presents the problem formulation and solution in detail. Section III describes the simulations performed and gives the results. Finally, Section IV gives the conclusions.

## II. PROBLEM FORMULATION

The fundamental frame of reference used in this paper is the Earth Centered Inertial (ECI) Coordinate System. The ECI is defined by the orthogonal set of unit vectors  $\{e_x, e_y, e_z\}$ . The  $X$ -axis is directed toward the vernal Equinox, the  $Y$ -axis is in the equatorial plane and normal to the  $X$ -axis, and the  $Z$ -axis is directed along the rotation axis of the Earth (i.e., normal to the equatorial plane). In a multisensor scenario, sensor platform  $s$  will typically have a sensor reference frame associated with it (measurement frame of the sensor) defined by the orthogonal set of unit vectors  $\{e_{\xi_s}, e_{\eta_s}, e_{\zeta_s}\}$ . The origin of the measurement frame of the sensor is a translation of the ECI origin, and its axes are rotated with respect to the ECI axes. The rotation between these frames can be described by a set of Euler angles. We will refer to these angles  $\phi_s + \phi_s^n, \rho_s + \rho_s^n, \psi_s + \psi_s^n$  of sensor  $s$  as roll, pitch, and yaw respectively [6], where  $\phi_s^n$  is the nominal roll angle,  $\phi_s$  is the roll bias, etc.

Each angle defines a rotation about a prescribed axis, in order to align the sensor frame axes with the ECI axes. The  $xyz$  rotation sequence is chosen, which is accomplished by first rotating about the  $x$  axis by  $\phi_s^n$ , then rotating about the  $y$  axis by  $\rho_s^n$ , and finally rotating about the  $z$  axis by  $\psi_s^n$ . The rotations sequence can be expressed by the matrices

$$\begin{aligned} T_s(\psi_s^n, \rho_s^n, \phi_s^n) &= T_z(\psi_s^n) \cdot T_y(\rho_s^n) \cdot T_x(\phi_s^n) \\ &= \begin{bmatrix} \cos \psi_s^n & \sin \psi_s^n & 0 \\ -\sin \psi_s^n & \cos \psi_s^n & 0 \\ 0 & 0 & 1 \end{bmatrix} \\ &\quad \cdot \begin{bmatrix} \cos \rho_s^n & 0 & -\sin \rho_s^n \\ 0 & 1 & 0 \\ \sin \rho_s^n & 0 & \cos \rho_s^n \end{bmatrix} \\ &\quad \cdot \begin{bmatrix} 1 & 0 & 0 \\ 0 & \cos \phi_s^n & \sin \phi_s^n \\ 0 & -\sin \phi_s^n & \cos \phi_s^n \end{bmatrix} \end{aligned} \quad (1)$$

Assume there are  $N_s$  synchronized passive sensors, with known positions in ECI coordinates at times  $t_i$ ,  $\xi_s(t_i) = [\xi_s(t_i), \eta_s(t_i), \zeta_s(t_i)]'$ ,  $s = 1, 2, \dots, N_s$ , and  $N_t$  target locations at  $\mathbf{x}(t_i) = [x(t_i), y(t_i), z(t_i)]'$ ,  $i = 1, 2, \dots, N_t$ , also in ECI coordinates. We assume that each sensor sees all the target locations (same physical target at different times).<sup>1</sup> With the previous convention, the operations

<sup>1</sup>This can also be different targets at a common time or at different times, as long as the sensors are synchronized.

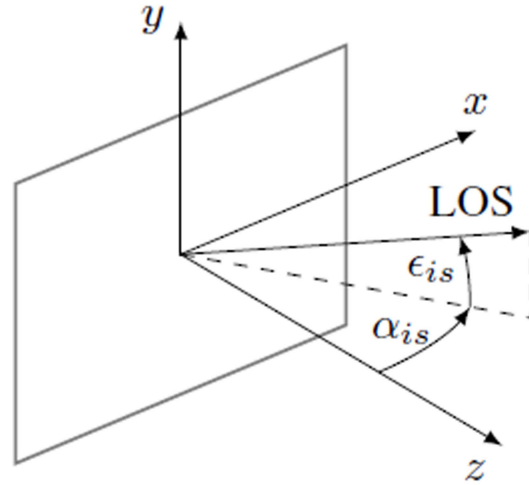


Fig. 1. Optical sensor coordinate system with the origin in the center of the focal plane.

needed to transform the position of a given target location at  $t_i$  expressed in ECI coordinates into the sensor  $s$  coordinate system (based on its nominal orientation) is

$$\begin{aligned} \mathbf{x}_s^n(t_i) &= T(\omega_s(t_i))(\mathbf{x}(t_i) - \xi_s(t_i)) \\ i &= 1, 2, \dots, N_t, \quad s = 1, 2, \dots, N_s \end{aligned} \quad (2)$$

where  $\omega_s(t_i) = [\phi_s^n(t_i), \rho_s^n(t_i), \psi_s^n(t_i)]'$  is the nominal orientation of sensor  $s$  at times  $t_i$ ,  $T(\omega_s(t_i))$  is the appropriate rotation matrix, and the translation  $(\mathbf{x}(t_i) - \xi_s(t_i))$  is the difference between the vector position of the target  $i$  and the vector position of the sensor  $s$ , both expressed in ECI coordinates. The superscript “n” in (2) indicates that the rotation matrix is based on the nominal sensor orientation.

As shown in Figure 1, the azimuth angle  $\alpha_s(t_i)$  is the angle in the sensor  $xz$  plane between the sensor  $z$  axis and the line of sight to the target, while the elevation angle  $\epsilon_s(t_i)$  is the angle between the line of sight to the target and its projection onto the  $xz$  plane, i.e.,

$$\begin{bmatrix} \alpha_s(t_i) \\ \epsilon_s(t_i) \end{bmatrix} = \begin{bmatrix} \tan^{-1} \left( \frac{x_s(t_i)}{z_s(t_i)} \right) \\ \tan^{-1} \left( \frac{y_s(t_i)}{\sqrt{x_s^2(t_i) + z_s^2(t_i)}} \right) \end{bmatrix} \quad (3)$$

The model for the biased noise-free LOS measurements is then

$$\begin{aligned} \begin{bmatrix} \alpha_s^b(t_i) \\ \epsilon_s^b(t_i) \end{bmatrix} &= \begin{bmatrix} g_1(\mathbf{x}(t_i), \xi_s(t_i), \omega_s(t_i), \mathbf{b}_s) \\ g_2(\mathbf{x}(t_i), \xi_s(t_i), \omega_s(t_i), \mathbf{b}_s) \end{bmatrix} \\ &\triangleq \mathbf{g}(\mathbf{x}(t_i), \xi_s(t_i), \omega_s(t_i), \mathbf{b}_s) \end{aligned} \quad (4)$$

where  $g_1$  and  $g_2$  denote the sensor Cartesian coordinates-to-azimuth/elevation angle mapping that can be found by inserting (2) and (3) into (4), and the bias vector of

sensor  $s$  is

$$\mathbf{b}_s = [\phi_s, \rho_s, \psi_s]' \quad (5)$$

For a given target, each sensor provides the noisy LOS measurements

$$\mathbf{z}_s(t_i) = \mathbf{g}(\mathbf{x}(t_i), \boldsymbol{\xi}_s(t_i), \boldsymbol{\omega}_s(t_i), \mathbf{b}_s) + \mathbf{w}_s(t_i) \quad (6)$$

where

$$\mathbf{w}_s(t_i) = [w_s^\alpha(t_i), w_s^\epsilon(t_i)]' \quad (7)$$

The measurement noises  $\mathbf{w}_s(t_i)$  are zero-mean, white Gaussian with

$$R_s = \begin{bmatrix} (\sigma_s^\alpha)^2 & 0 \\ 0 & (\sigma_s^\epsilon)^2 \end{bmatrix} \quad (8)$$

and are assumed mutually independent. The problem is to estimate the bias vectors for all sensors and the locations of the targets of opportunity. We shall obtain the maximum likelihood (ML) estimate of the augmented parameter vector

$$\boldsymbol{\theta} = [\mathbf{x}(t_1)', \dots, \mathbf{x}(t_{N_t})', \mathbf{b}_1', \dots, \mathbf{b}_{N_s}]' \quad (9)$$

consisting of the (unknown) target locations and sensor biases, by maximizing the likelihood function (LF) of  $\boldsymbol{\theta}$

$$\Lambda(\boldsymbol{\theta}) = \prod_{i=1}^{N_t} \prod_{s=1}^{N_s} p(\mathbf{z}_s(t_i) | \boldsymbol{\theta}) \quad (10)$$

where

$$p(\mathbf{z}_s(t_i) | \boldsymbol{\theta}) = |2\pi R_s|^{-1/2} \cdot \exp(-\frac{1}{2}[\mathbf{z}_s(t_i) - \mathbf{h}_{is}(\boldsymbol{\theta})]' R_s^{-1} [\mathbf{z}_s(t_i) - \mathbf{h}_{is}(\boldsymbol{\theta})]) \quad (11)$$

and we use the compact notation

$$\mathbf{h}_{is}(\boldsymbol{\theta}) \triangleq \mathbf{g}(\mathbf{x}(t_i), \boldsymbol{\xi}_s(t_i), \boldsymbol{\omega}_s(t_i), \mathbf{b}_s) \quad (12)$$

The ML estimate (MLE) is then

$$\hat{\boldsymbol{\theta}}^{ML} = \arg \max_{\boldsymbol{\theta}} \Lambda(\boldsymbol{\theta}) \quad (13)$$

In order to find the MLE, one has to solve a nonlinear least squares problem for the exponent in (11). This will be done using a numerical search via the Iterated Least Squares (ILS) technique [1].

#### A. Requirements for Bias Estimability

*Minimum number of measurements.* The number of equations (size of the measurement vector) has to be at least equal to the number of parameters to be estimated (target location and bias components). Each passive sensor provides two-dimensional measurement (the two LOS angles to the target), and it is assumed that each sensor sees all the target locations at a common time. Stacking together each measurement of  $N_t$  target locations seen by  $N_s$  sensors results in an overall measurement vector of dimension  $2N_tN_s$ . Therefore we must have

$$2N_tN_s \geq 3(N_t + N_s) \quad (14)$$

This is a necessary condition but not sufficient because (13) has to have a unique solution, i.e., the parameter vector has to be estimable [1].

#### *Invertibility of the Fisher Information matrix (FIM).*

In order to have parameter observability, the FIM must be invertible. If the FIM is not invertible (i.e., it is singular), then the CRLB (the inverse of the FIM) will not exist—the FIM will have one or more infinite eigenvalues, which means total uncertainty in a subspace of the parameter space, i.e., ambiguity [2].

For the examples of bias estimability discussed in the sequel, to estimate the biases of 3 sensors (9 bias components) we need 3 target locations (9 position components), i.e., the search is in an 18-dimensional space, while for 2 sensors (6 bias components) we need at least 6 target locations (18 position components) in order to meet the necessary requirement (14). As stated previously, the FIM must be invertible, so the rank of the FIM has to be equal to the number of parameters to be estimated (9 + 9 = 18, or 6 + 18 = 24, in the previous examples). The full rank of the FIM is a necessary and sufficient condition for estimability.

#### B. Iterated Least Squares for Maximization of the LF of $\boldsymbol{\theta}$

Given the estimate  $\hat{\boldsymbol{\theta}}^j$  after  $j$  iterations, the ILS estimate after the  $(j + 1)$ th iteration will be

$$\hat{\boldsymbol{\theta}}^{j+1} = \hat{\boldsymbol{\theta}}^j + [(H^j)' R^{-1} H^j]^{-1} (H^j)' R^{-1} [\mathbf{z} - \mathbf{h}(\hat{\boldsymbol{\theta}}^j)] \quad (15)$$

where

$$\mathbf{z} = [z_1(t_1)', \dots, z_s(t_1)', \dots, z_s(t_i)', \dots, z_{N_s}(t_{N_t})']' \quad (16)$$

$$\mathbf{h}(\hat{\boldsymbol{\theta}}^j) = [h_{11}(\hat{\boldsymbol{\theta}}^j)', \dots, h_{is}(\hat{\boldsymbol{\theta}}^j)', \dots, h_{N_tN_s}(\hat{\boldsymbol{\theta}}^j)]' \quad (17)$$

$$R = \begin{bmatrix} R_1 & 0 & \dots & 0 \\ 0 & R_2 & \dots & 0 \\ \vdots & \vdots & \ddots & \vdots \\ 0 & \dots & 0 & R_{N_s} \end{bmatrix} \quad (18)$$

where  $R_s$  is the measurement noise covariance matrix of sensor  $s$ , and

$$H^j = \left. \frac{\partial \mathbf{h}(\boldsymbol{\theta}^j)}{\partial \boldsymbol{\theta}} \right|_{\boldsymbol{\theta}=\hat{\boldsymbol{\theta}}^j} \quad (19)$$

is the Jacobian matrix of the vector consisting of the stacked measurement functions (17) w.r.t. (9) evaluated at the ILS estimate from the previous iteration  $j$ . In this case, the Jacobian matrix is, with the iteration index omitted for conciseness,

$$H = [H_{11} \quad H_{21} \dots H_{N_t1} \quad H_{12} \dots H_{N_tN_s}]' \quad (20)$$

where

$$H_{is} = \begin{bmatrix} \frac{\partial g_{1s}(t_i)}{\partial x(t_1)} & \frac{\partial g_{2s}(t_i)}{\partial x(t_1)} \\ \frac{\partial g_{1s}(t_i)}{\partial y(t_1)} & \frac{\partial g_{2s}(t_i)}{\partial y(t_1)} \\ \frac{\partial g_{1s}(t_i)}{\partial z(t_1)} & \frac{\partial g_{2s}(t_i)}{\partial z(t_1)} \\ \vdots & \vdots \\ \frac{\partial g_{1s}(t_i)}{\partial x(t_{N_i})} & \frac{\partial g_{2s}(t_i)}{\partial x(t_{N_i})} \\ \frac{\partial g_{1s}(t_i)}{\partial y(t_{N_i})} & \frac{\partial g_{2s}(t_i)}{\partial y(t_{N_i})} \\ \frac{\partial g_{1s}(t_i)}{\partial z(t_{N_i})} & \frac{\partial g_{2s}(t_i)}{\partial z(t_{N_i})} \\ \frac{\partial g_{1s}(t_i)}{\partial \psi_1} & \frac{\partial g_{2s}(t_i)}{\partial \psi_1} \\ \frac{\partial g_{1s}(t_i)}{\partial \rho_1} & \frac{\partial g_{2s}(t_i)}{\partial \rho_1} \\ \frac{\partial g_{1s}(t_i)}{\partial \phi_1} & \frac{\partial g_{2s}(t_i)}{\partial \phi_1} \\ \vdots & \vdots \\ \frac{\partial g_{1s}(t_i)}{\partial \psi_{N_s}} & \frac{\partial g_{2s}(t_i)}{\partial \psi_{N_s}} \\ \frac{\partial g_{1s}(t_i)}{\partial \rho_{N_s}} & \frac{\partial g_{2s}(t_i)}{\partial \rho_{N_s}} \\ \frac{\partial g_{1s}(t_i)}{\partial \phi_{N_s}} & \frac{\partial g_{2s}(t_i)}{\partial \phi_{N_s}} \end{bmatrix} \quad (21)$$

The appropriate partial derivatives are given in the appendix.

### C. Initialization

In order to perform the numerical search via ILS, an initial estimate  $\hat{\theta}^0$  is required. Assuming that the biases are null, the LOS measurements from the first and the second sensor  $\alpha_1(t_i)$ ,  $\alpha_2(t_i)$ , and  $\epsilon_1(t_i)$  can be used to solve for each initial Cartesian target position, in ECI coordinates, using (22)–(24).

$$x(t_i)^0 = \frac{\xi_2(t_i) - \xi_1(t_i) + \zeta_1(t_i) \tan \alpha_1(t_i) - \zeta_2(t_i) \tan \alpha_2(t_i)}{\tan \alpha_1(t_i) - \tan \alpha_2(t_i)} \quad (22)$$

$$y(t_i)^0 = \frac{\tan \alpha_1(t_i)(\xi_2(t_i) + \tan \alpha_2(t_i)(\zeta_1(t_i) - \zeta_2(t_i))) - \xi_1(t_i) \tan \alpha_2(t_i)}{\tan \alpha_1(t_i) - \tan \alpha_2(t_i)} \quad (23)$$

$$z(t_i)^0 = \eta_1(t_i) + \tan \epsilon_1(t_i) \left| \frac{(\xi_1(t_i) - \xi_2(t_i)) \cos \alpha_2(t_i) + (\zeta_2(t_i) - \zeta_1(t_i)) \sin \alpha_2(t_i)}{\sin(\alpha_1(t_i) - \alpha_2(t_i))} \right| \quad (24)$$

### D. Cramér-Rao Lower Bound

In order to evaluate the efficiency of the estimator, the CRLB must be calculated. The CRLB provides a lower bound on the covariance matrix of an unbiased estimator as [1]

$$E\{(\theta - \hat{\theta})(\theta - \hat{\theta})'\} \geq J(\theta)^{-1} \quad (25)$$

where  $J$  is the Fisher Information Matrix (FIM),  $\theta$  is the true parameter vector to be estimated, and  $\hat{\theta}$  is the estimate. The FIM is

$$J(\theta) = E\{[\nabla_{\theta} \ln \Lambda(\theta)][\nabla_{\theta} \ln \Lambda(\theta)]'\}_{\theta=\theta_{\text{true}}} \quad (26)$$

where the gradient of the log-likelihood function is

$$\lambda(\theta) \triangleq \ln \Lambda(\theta) \quad (27)$$

$$\nabla_{\theta} \lambda(\theta) = \sum_{i=1}^{N_i} \sum_{s=1}^{N_s} H'_{is} R_s^{-1} (\mathbf{z}_s(t_i) - \mathbf{h}_{is}(\theta)) \quad (28)$$

which, when plugged into (26), gives

$$\begin{aligned} J(\theta) &= \sum_{i=1}^{N_i} \sum_{s=1}^{N_s} H'_{is} (R_s^{-1}) H_{is} |_{\theta=\theta_{\text{true}}} \\ &= H'(R^{-1})H |_{\theta=\theta_{\text{true}}} \end{aligned} \quad (29)$$

Since  $\theta_{\text{true}}$  is not available in practice,  $J$  will be evaluated at the estimate, and, as it's pointed out later, the two results are practically the same.

### E. Test for Efficiency with Monte Carlo Runs

The Normalized Estimation Error Squared (NEES) for the parameter  $\theta$  (under the hypothesis of efficiency), defined as

$$\epsilon_{\theta} = (\theta - \hat{\theta})' P^{-1} (\theta - \hat{\theta}) = (\theta - \hat{\theta})' J(\theta) (\theta - \hat{\theta}) \quad (30)$$

is chi-square distributed with  $n_x$  (the dimension of  $\theta$ ) degrees of freedom, that is,

$$\epsilon_{\theta} \sim \chi_{n_x}^2 \quad (31)$$

The hypothesis test for efficiency whether (31) can be accepted, i.e., that  $P = J^{-1}$  is discussed in [2] and outlined next. The NEES is used in simulations to check whether the estimator is efficient, that is, the errors are statistically consistent with the covariance given by the CRLB—this is the efficiency check. Thus the efficiency

check of the estimator (in simulation—because this is the only situation where  $\theta$  is available) consists of verifying whether (31) holds. The practical procedure to check the estimator efficiency is using the sample average NEES from  $N$  independent Monte Carlo runs defined as

$$\bar{\epsilon}_x = \frac{1}{N} \sum_{i=1}^N \epsilon_x^i \quad (32)$$

The quantity  $N\bar{\epsilon}$  is chi-square distributed with  $Nn_x$  degrees of freedom.

Let the  $1 - Q$  ( $Q$  is the type I error probability of the test) two-sided probability region for  $N\bar{\epsilon}$  be the interval  $[\epsilon'_1, \epsilon'_2]$ .

$$\epsilon'_1 = \chi_{Nn_x}^2 \left( \frac{Q}{2} \right) \quad (33)$$

$$\epsilon'_2 = \chi_{Nn_x}^2 \left( 1 - \frac{Q}{2} \right) \quad (34)$$

where in view of the division by  $N$  in (32), one has

$$\epsilon_i = \frac{\epsilon'_i}{N} \quad (35)$$

Thus, if the estimator is efficient, one has to have

$$P\{\bar{\epsilon}_x \in [\epsilon'_1, \epsilon'_2]\} = 1 - Q \quad (36)$$

### III. SIMULATIONS

We simulate a space based tracking system tracking a ballistic missile. The missile and satellite trajectories are generated using System Tool Kit (STK).<sup>2</sup> The target modeled represents a ballistic missile with a flight time of about 20 minutes. STK provides the target and sensor positions in three dimensional Cartesian coordinates at 1 s intervals. The target launch time is chosen so that the satellite sensors were able to follow the missile trajectory throughout its flight path.

#### A. Three-Sensor Case

We simulated three space based optical sensors at various known orbits observing a target at three points in time at unknown locations. In this case, an 18-dimensional parameter vector is to be estimated. Figure 2 shows each target position observed by the sensors (Figure 3 gives an image of this). As discussed in the previous section, the three sensor biases are roll, pitch, and yaw angle offsets. The biases for each sensor were set to  $0.5^\circ = 8.72$  mrad. We ran 100 Monte Carlo runs. In order to establish a baseline for evaluating the performance of our algorithm, we also ran the simulations without biases, and with biases but without bias estimation. The horizontal and vertical fields-of-view of each sensor are assumed to be  $60^\circ$ . The measurement noise standard deviation  $\sigma_s$  (identical across sensors for both

<sup>2</sup>STK Systems Tool Kit are registered trademarks of Analytical Graphics, Inc.

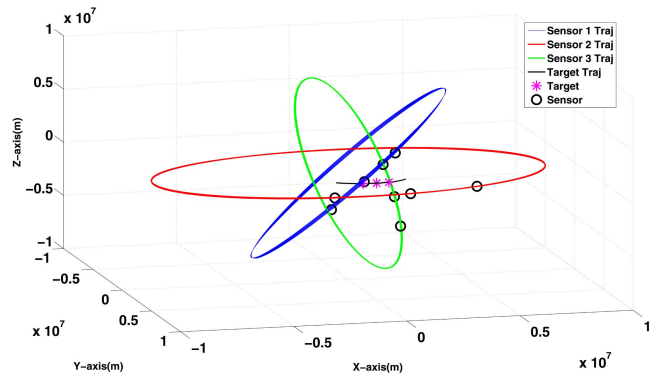


Fig. 2. Target and satellite trajectories for the three-sensor case.

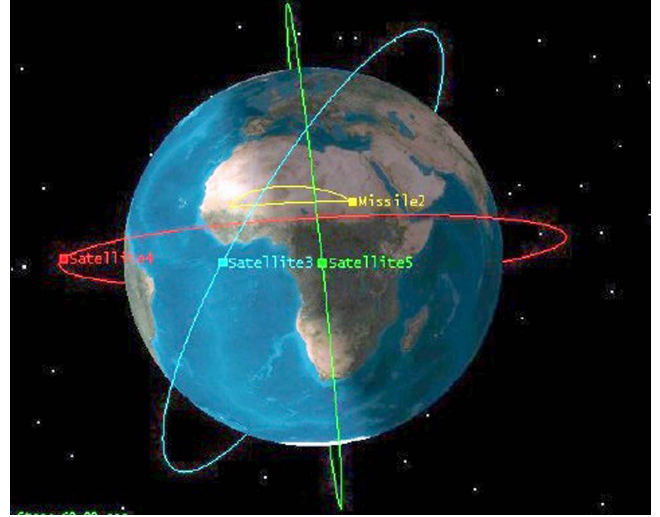


Fig. 3. Target and satellite trajectories for the three-sensor case.

azimuth and elevation measurements,  $\sigma_s^\alpha = \sigma_s^\epsilon = \sigma_s$ ) was assumed to be  $30 \mu\text{rad}$ .

1) *Description of the scenarios.* The sensors are assumed to provide LOS angle measurements. We denote by  $\xi_1, \xi_2, \xi_3$  the 3D Cartesian sensor locations, and  $\mathbf{x}(t_1), \mathbf{x}(t_2), \mathbf{x}(t_3)$  the 3D Cartesian target locations (all in ECI). The three target locations were chosen from a trajectory of a ballistic target as follows (in km)

$$\mathbf{x}(t_1) = [7,518 \quad -1,311 \quad -1,673]' \quad (37)$$

$$\mathbf{x}(t_2) = [7,942 \quad -509 \quad -1,375]' \quad (38)$$

$$\mathbf{x}(t_3) = [7,988 \quad 317 \quad -1,012]' \quad (39)$$

Table I summarizes the sensor positions (in km).

2) *Statistical efficiency of the estimates.* In order to test for the statistical efficiency of the estimate (of the 18 dimensional vector (9)), the NEES [1] is used, with the CRLB as the covariance matrix. The sample average NEES over 100 Monte Carlo runs calculated using the FIM evaluated at the true bias values and target locations is approximately 17.3, and the sample average NEES calculated using the FIM evaluated at the estimated biases and target locations is approximately 17.6 and both fall in the interval given below. According to

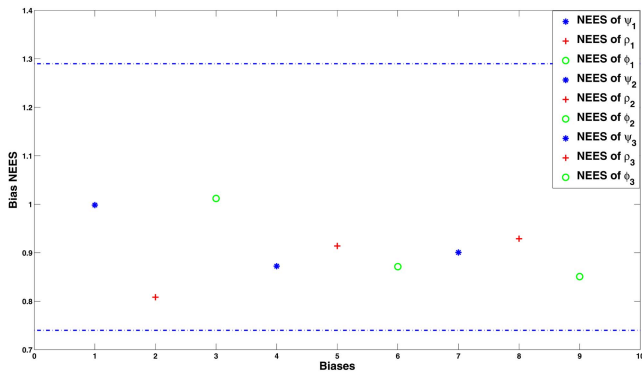


Fig. 4. Sample average bias NEES (CRLB evaluated at the estimate), for each of the 9 biases, over 100 Monte Carlo runs (Three-sensor case).

TABLE I  
Sensor positions (km).

	$t_1$	$t_2$	$t_3$
$\xi_1$	1,235	1,062	887
$\eta_1$	158	-174	-507
$\zeta_1$	6,927	6,955	6,963
$\xi_2$	5,549	3,061	112
$\eta_2$	1,116	2,993	4,418
$\zeta_2$	6,285	7,295	7,212
$\xi_3$	6,499	7,897	8,389
$\eta_3$	-279	-719	-1,074
$\zeta_3$	-5,407	-2,944	-143

the CRLB, the FIM has to be evaluated at the true parameter. Since this is not available in practice, however, it is useful to evaluate the FIM also at the estimated parameter, the only one available in real world implementations [9], [10]. The results are very close regardless of which values are chosen for evaluation of the FIM. The 95% probability region for the 100 sample average NEES of the 18 dimensional parameter vector is [16.84, 19.19]. This NEES is found to be within this interval and the MLE is therefore statistically efficient. Figure 4 shows the individual bias component NEES. The 95% probability region for the 100 sample average single component NEES is [0.74, 1.29]. The NEES values are found to be within this interval.

The RMS position errors for the 3 target locations are summarized in Table II. In this table, the first estimation scheme was established as a baseline using bias-free LOS measurements to estimate the target locations.<sup>3</sup> For the second scheme, we used biased LOS measurements but we only estimated target locations. In the last scheme, we used biased LOS measurements and we simultaneously estimated the target locations and sensor biases. Bias estimation yields significantly

<sup>3</sup>As shown in [9], [10] the unbiased LOS measurements yield composite measurements (full position MLEs) whose errors are zero-mean and their covariance is equal to the corresponding CRLB.

TABLE II  
Sample average position RMSE (m) for the 3 targets, over 100 Monte Carlo runs, for the 3 estimation schemes (Three-sensor case).

Scheme	1	2	3
First Target	127	69,391	673
Second Target	98	41,713	484
Third Target	82	16,271	343

TABLE III  
Sample average bias ( $\mu\text{rad}$ ) RMSE over 100 Monte Carlo runs and the corresponding bias standard deviation from the CRLB (Three-sensor case).

	RMSE	$\sigma_{\text{CRLB}}$
$\psi_1$	138.009	138.211
$\rho_1$	176.073	195.808
$\phi_1$	150.108	149.209
$\psi_2$	178.507	191.110
$\rho_2$	147.752	154.675
$\phi_2$	230.009	246.231
$\psi_3$	229.131	241.389
$\rho_3$	134.680	139.726
$\phi_3$	708.588	768.215

TABLE IV  
Sample average bias ( $\mu\text{rad}$ ) error  $\bar{b}$  over 100 Monte Carlo runs (Three-sensor case).

	$\bar{b}$	$2 \frac{\sigma_{\text{CRLB}}}{\sqrt{N}}$
$\psi_1$	-1.728	27.642
$\rho_1$	16.945	39.161
$\phi_1$	4.545	29.841
$\psi_2$	-17.323	38.222
$\rho_2$	5.262	30.935
$\phi_2$	22.804	49.246
$\psi_3$	20.580	48.277
$\rho_3$	-7.454	27.945
$\phi_3$	79.386	153.643

improved target RMS position errors in the presence of biases.

Each component of  $\theta$  should also be individually consistent with its corresponding  $\sigma_{\text{CRLB}}$  (the square root of the corresponding diagonal element of the inverse of the FIM). In this case, the sample average bias RMSE over 100 Monte Carlo runs should be within 15% of its corresponding bias standard deviation from the CRLB ( $\sigma_{\text{CRLB}}$ ) with 95% probability. Table III demonstrates the consistency of the individual bias estimates. This complements the NEES evaluations from Figure 4.

To confirm that the bias estimates are unbiased, the average bias error  $\bar{b}$ , from Table IV (over 100 Monte Carlo runs) confirms that  $|\bar{b}|$  is less than  $2\sigma_{\text{CRLB}}/\sqrt{N}$  (which it should hold with 95% probability), i.e., these estimates are unbiased.

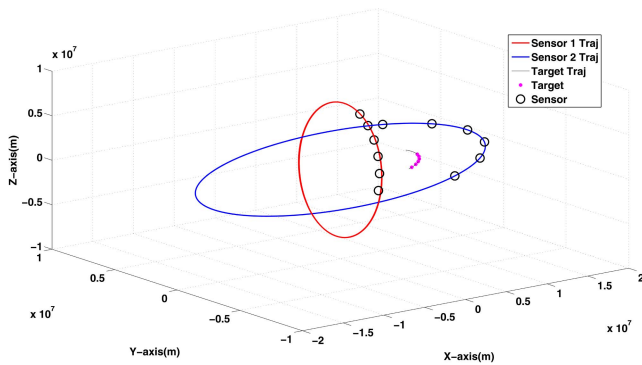


Fig. 5. Target and satellite trajectories for the two-sensor case

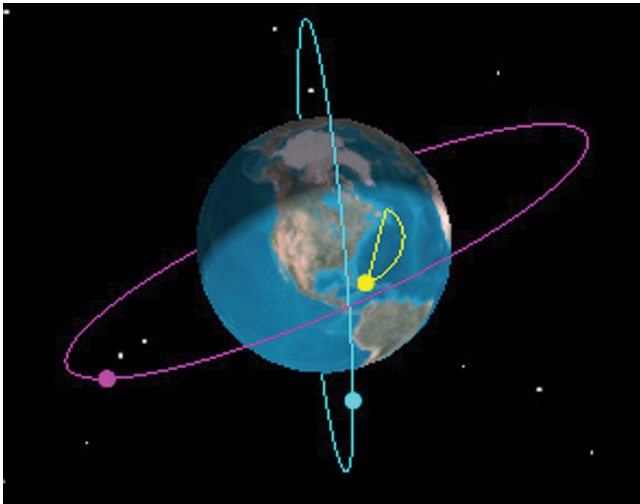


Fig. 6. Target and satellite trajectories for the two-sensor case

## B. Two-Sensor Case

We simulated two space-based optical sensors at various known orbits observing a target at six (unknown) locations (which is equivalent to viewing six different targets at unknown locations). In this case, a 24-dimensional parameter vector is to be estimated. As shown in Figure 5, each target position can be observed by all sensors. As discussed in the previous section, the three sensor biases were roll, pitch and yaw angle offsets. All the biases for each sensor were set to  $50 \mu\text{rad}$ .

We made 100 Monte Carlo runs. In order to establish a baseline for evaluating the performance of our algorithm, we also ran the simulations without bias, and with bias but without bias estimation. The measurement noise standard deviation  $\sigma_s$  (identical across sensors for both azimuth and elevation measurements) was assumed to be  $30 \mu\text{rad}$ .

1) *Description of the scenarios.* The sensors are assumed to provide LOS angle measurements. We denote by  $\xi_1, \xi_2$  the 3D Cartesian sensor positions at six different times, and  $\mathbf{x}(t_1), \mathbf{x}(t_2), \mathbf{x}(t_3), \mathbf{x}(t_4), \mathbf{x}(t_5), \mathbf{x}(t_6)$  the six 3D Cartesian target locations (all in ECI). The six target locations were chosen from a trajectory of a ballistic

TABLE V  
Sensor positions (km).

	$t_1$	$t_2$	$t_3$	$t_4$	$t_5$	$t_6$
$\xi_1$	187	-902	-1,934	-2,840	-3,559	-4,046
$\eta_1$	-1,439	-2,786	-3,951	-4,858	-5,447	-5,680
$\zeta_1$	6,886	6,400	5,494	4,229	2,687	968
$\xi_2$	-3,966	123	4,195	7,646	9,965	10,810
$\eta_2$	-5,969	-7,238	-7,436	-6,533	-4,664	-2,105
$\zeta_2$	8,519	8,458	7,145	4,774	1,698	-1,630

target as follows (in km)

$$\mathbf{x}(t_1) = [-1,167 \quad -5,782 \quad 3,028]' \quad (40)$$

$$\mathbf{x}(t_2) = [-1,054 \quad -6,027 \quad 3,436]' \quad (41)$$

$$\mathbf{x}(t_3) = [-922 \quad -6,148 \quad 3,772]' \quad (42)$$

$$\mathbf{x}(t_4) = [-774 \quad -6,155 \quad 4,036]' \quad (43)$$

$$\mathbf{x}(t_5) = [-611 \quad -6,056 \quad 4,228]' \quad (44)$$

$$\mathbf{x}(t_6) = [-435 \quad -5,852 \quad 4,344]' \quad (45)$$

Table V summarizes the sensor positions.

2) *Statistical Efficiency of the Estimates.* In order to test for the statistical efficiency of the estimate (of the 24 dimensional vector), the NEES is used, with the CRLB as the covariance matrix. The sample average NEES over 100 Monte Carlo runs calculated using the FIM evaluated at the true bias values and target locations is approximately 23.995, and the sample average NEES calculated using the FIM evaluated at the estimated biases and target locations is approximately 23.996 and both fall in the interval given below. The results are practically identical regardless of which values are chosen for evaluation of the FIM. The 95% probability region for the 100 sample average NEES of the 24 dimensional parameter vector is  $[22.66, 25.37]'$ . This NEES is found to be within this interval and the MLE is therefore statistically efficient. Figure 7 shows the individual bias component NEES. The 95% probability region for the 100 sample average single component NEES is  $[0.74, 1.29]'$ . These NEES are found to be within this interval, except for one component, which is slightly outside this region.

The RMS position errors for the 6 target locations are summarized in Table VI. In this table, the first estimation scheme was established as a baseline using bias-free LOS measurements to estimate the target locations. For the second scheme, we used biased LOS measurements but we only estimated target locations. In the last scheme, we used biased LOS measurements and we simultaneously estimated the target locations and sensor biases. Once again, bias estimation yields significantly improved target RMS position errors in the presence of biases.

Each component of  $\theta$  should also be individually consistent with its corresponding  $\sigma_{\text{CRLB}}$  (the square root of the corresponding diagonal element of the inverse

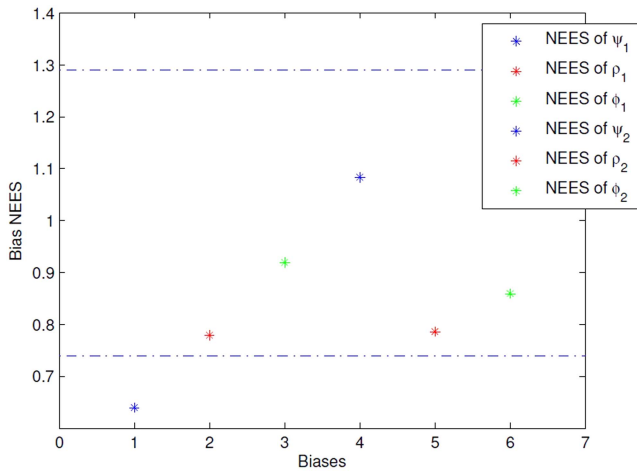


Fig. 7. Sample average bias NEES (CRLB evaluated at the estimate), for each of the 6 biases, over 100 Monte Carlo runs (Two-sensor case).

TABLE VI

Sample average position RMSE (m) for the 6 targets, over 100 Monte Carlo runs, for the 3 estimation schemes (Two-sensor case).

Scheme	1	2	3
First Target	234	93,123	521
Second Target	235	70,902	417
Third Target	212	60,840	403
Fourth Target	501	57,113	677
Fifth Target	637	262,712	754
Sixth Target	580	163,104	703

of FIM). In this case, the sample average bias RMSE over 100 Monte Carlo runs should be within 15% of its corresponding bias standard deviation from the CRLB ( $\sigma_{\text{CRLB}}$ ) with 95% probability. Table VII demonstrates the efficiency of the individual bias estimates.

To confirm that the bias estimates are unbiased, the average bias error  $\tilde{b}$ , from Table VIII, over 100 Monte Carlo runs confirms that  $|\tilde{b}|$  is less than  $2\sigma_{\text{CRLB}}/\sqrt{N}$  (which it should hold with 95% probability), i.e., these estimates are unbiased.

#### IV. CONCLUSIONS AND FUTURE WORK

Previous research into the simultaneous estimation of the 3D Cartesian locations of the targets of opportunity and the angle measurement biases of fixed sensors [4] demonstrated that the maximum likelihood estimator via the ILS algorithm was able to provide statistically efficient estimates. In the three-sensor case it was shown that one has complete observability of the sensor biases. In the two-sensor case a rank deficiency of 1 in the FIM was observed. A suitable geometric explanation was provided for this. In the present paper we presented a new algorithm that uses targets of opportunity for estimation of measurement biases for moving sensors. The first step was formulating a general bias model for synchronized space-based (moving) optical sensors

TABLE VII

Sample average bias ( $\mu\text{rad}$ ) RMSE over 100 Monte Carlo runs and the corresponding bias standard deviation from the CRLB (Two-sensor case).

	RMSE	$\sigma_{\text{CRLB}}$
$\psi_1$	74.945	72.334
$\rho_1$	108.100	99.322
$\phi_1$	88.624	81.117
$\psi_2$	53.548	52.208
$\rho_2$	25.491	30.455
$\phi_2$	140.719	98.743

TABLE VIII

Sample average bias (mrad) error  $\tilde{b}$  over 100 Monte Carlo runs (Two-sensor case).

	$\tilde{b}$	$\frac{\sigma_{\text{CRLB}}}{\sqrt{N}}$
$\psi_1$	-27.248	19.750
$\rho_1$	-13.943	21.213
$\phi_1$	0.289	17.705
$\psi_2$	-9.677	12.289
$\rho_2$	5.167	0.654
$\phi_2$	10.985	19.217

at known locations. The association of measurements is assumed to be perfect. Based on this, we used a ML approach that led to a nonlinear least-squares estimation problem for simultaneous estimation of the 3D Cartesian locations of the targets of opportunity and the angle measurement biases of the sensors. The bias estimates, obtained via ILS, were shown to be unbiased and statistically efficient for all the scenarios considered.

#### APPENDIX

The appropriate partial derivatives of (21) are

$$\frac{\partial g_{1s}(t_i)}{\partial x(t_k)} = \frac{\partial g_{1s}(t_i)}{\partial x_s(t_i)} \frac{\partial x_s(t_i)}{\partial x(t_k)} + \frac{\partial g_{1s}(t_i)}{\partial y_s(t_i)} \frac{\partial y_s(t_i)}{\partial x(t_k)} + \frac{\partial g_{1s}(t_i)}{\partial z_s(t_i)} \frac{\partial z_s(t_i)}{\partial x(t_k)} \quad (46)$$

$$\frac{\partial g_{1s}(t_i)}{\partial y(t_k)} = \frac{\partial g_{1s}(t_i)}{\partial x_s(t_i)} \frac{\partial x_s(t_i)}{\partial y(t_k)} + \frac{\partial g_{1s}(t_i)}{\partial y_s(t_i)} \frac{\partial y_s(t_i)}{\partial y(t_k)} + \frac{\partial g_{1s}(t_i)}{\partial z_s(t_i)} \frac{\partial z_s(t_i)}{\partial y(t_k)} \quad (47)$$

$$\frac{\partial g_{1s}(t_i)}{\partial z(t_k)} = \frac{\partial g_{1s}(t_i)}{\partial x_s(t_i)} \frac{\partial x_s(t_i)}{\partial z(t_k)} + \frac{\partial g_{1s}(t_i)}{\partial y_s(t_i)} \frac{\partial y_s(t_i)}{\partial z(t_k)} + \frac{\partial g_{1s}(t_i)}{\partial z_s(t_i)} \frac{\partial z_s(t_i)}{\partial z(t_k)} \quad (48)$$

$$\frac{\partial g_{1s}(t_i)}{\partial \psi_k} = \frac{\partial g_{1s}(t_i)}{\partial x_s(t_i)} \frac{\partial x_s(t_i)}{\partial \psi_k} + \frac{\partial g_{1s}(t_i)}{\partial y_s(t_i)} \frac{\partial y_s(t_i)}{\partial \psi_k} + \frac{\partial g_{1s}(t_i)}{\partial z_s(t_i)} \frac{\partial z_s(t_i)}{\partial \psi_k} \quad (49)$$

$$\frac{\partial g_{1s}(t_i)}{\partial \rho_k} = \frac{\partial g_{1s}(t_i)}{\partial x_s(t_i)} \frac{\partial x_s(t_i)}{\partial \rho_k} + \frac{\partial g_{1s}(t_i)}{\partial y_s(t_i)} \frac{\partial y_s(t_i)}{\partial \rho_k} + \frac{\partial g_{1s}(t_i)}{\partial z_s(t_i)} \frac{\partial z_s(t_i)}{\partial \rho_k} \quad (50)$$

$$\frac{\partial g_{1s}(t_i)}{\partial \phi_k} = \frac{\partial g_{1s}(t_i)}{\partial x_s(t_i)} \frac{\partial x_s(t_i)}{\partial \phi_k} + \frac{\partial g_{1s}(t_i)}{\partial y_s(t_i)} \frac{\partial y_s(t_i)}{\partial \phi_k} + \frac{\partial g_{1s}(t_i)}{\partial z_s(t_i)} \frac{\partial z_s(t_i)}{\partial \phi_k} \quad (51)$$

$$\frac{\partial g_{2s}(t_i)}{\partial x(t_k)} = \frac{\partial g_{2s}(t_i)}{\partial x_s(t_i)} \frac{\partial x_s(t_i)}{\partial x(t_k)} + \frac{\partial g_{2s}(t_i)}{\partial y_s(t_i)} \frac{\partial y_s(t_i)}{\partial x(t_k)} + \frac{\partial g_{2s}(t_i)}{\partial z_s(t_i)} \frac{\partial z_s(t_i)}{\partial x(t_k)} \quad (52)$$

$$\frac{\partial g_{2s}(t_i)}{\partial y(t_k)} = \frac{\partial g_{2s}(t_i)}{\partial x_s(t_i)} \frac{\partial x_s(t_i)}{\partial y(t_k)} + \frac{\partial g_{2s}(t_i)}{\partial y_s(t_i)} \frac{\partial y_s(t_i)}{\partial y(t_k)} + \frac{\partial g_{2s}(t_i)}{\partial z_s(t_i)} \frac{\partial z_s(t_i)}{\partial y(t_k)} \quad (53)$$

$$\frac{\partial g_{2s}(t_i)}{\partial z(t_k)} = \frac{\partial g_{2s}(t_i)}{\partial x_s(t_i)} \frac{\partial x_s(t_i)}{\partial z(t_k)} + \frac{\partial g_{2s}(t_i)}{\partial y_s(t_i)} \frac{\partial y_s(t_i)}{\partial z(t_k)} + \frac{\partial g_{2s}(t_i)}{\partial z_s(t_i)} \frac{\partial z_s(t_i)}{\partial z(t_k)} \quad (54)$$

$$\frac{\partial g_{2s}(t_i)}{\partial \psi_k} = \frac{\partial g_{2s}(t_i)}{\partial x_s(t_i)} \frac{\partial x_s(t_i)}{\partial \psi_k} + \frac{\partial g_{2s}(t_i)}{\partial y_s(t_i)} \frac{\partial y_s(t_i)}{\partial \psi_k} + \frac{\partial g_{2s}(t_i)}{\partial z_s(t_i)} \frac{\partial z_s(t_i)}{\partial \psi_k} \quad (55)$$

$$\frac{\partial g_{2s}(t_i)}{\partial \rho_k} = \frac{\partial g_{2s}(t_i)}{\partial x_s(t_i)} \frac{\partial x_s(t_i)}{\partial \rho_k} + \frac{\partial g_{2s}(t_i)}{\partial y_s(t_i)} \frac{\partial y_s(t_i)}{\partial \rho_k} + \frac{\partial g_{2s}(t_i)}{\partial z_s(t_i)} \frac{\partial z_s(t_i)}{\partial \rho_k} \quad (56)$$

$$\frac{\partial g_{2s}(t_i)}{\partial \phi_k} = \frac{\partial g_{2s}(t_i)}{\partial x_s(t_i)} \frac{\partial x_s(t_i)}{\partial \phi_k} + \frac{\partial g_{2s}(t_i)}{\partial y_s(t_i)} \frac{\partial y_s(t_i)}{\partial \phi_k} + \frac{\partial g_{2s}(t_i)}{\partial z_s(t_i)} \frac{\partial z_s(t_i)}{\partial \phi_k} \quad (57)$$

Given that (2) can be written as

$$\mathbf{x}_s(t_i) = \begin{bmatrix} x_s(t_i) \\ y_s(t_i) \\ z_s(t_i) \end{bmatrix} = T_s(\mathbf{x}(t_i) - \boldsymbol{\xi}_s) = \begin{bmatrix} T_{s11} & T_{s12} & T_{s13} \\ T_{s21} & T_{s22} & T_{s23} \\ T_{s31} & T_{s32} & T_{s33} \end{bmatrix} \begin{bmatrix} x(t_i) - \xi_s \\ y(t_i) - \eta_s \\ z(t_i) - \zeta_s \end{bmatrix} \quad (58)$$

therefore

$$x_s(t_i) = T_{s11}(x(t_i) - \xi_s) + T_{s12}(y(t_i) - \eta_s) + T_{s13}(z(t_i) - \zeta_s) \quad (59)$$

$$y_s(t_i) = T_{s21}(x(t_i) - \xi_s) + T_{s22}(y(t_i) - \eta_s) + T_{s23}(z(t_i) - \zeta_s) \quad (60)$$

$$z_s(t_i) = T_{s31}(x(t_i) - \xi_s) + T_{s32}(y(t_i) - \eta_s) + T_{s33}(z(t_i) - \zeta_s) \quad (61)$$

and

$$\frac{\partial x_s(t_i)}{\partial x(t_k)} = T_{s11}, \quad \frac{\partial x_s(t_i)}{\partial y(t_k)} = T_{s12}, \quad \frac{\partial x_s(t_i)}{\partial y(t_k)} = T_{s13} \quad (62)$$

$$\frac{\partial y_s(t_i)}{\partial x(t_k)} = T_{s21}, \quad \frac{\partial y_s(t_i)}{\partial y(t_k)} = T_{s22}, \quad \frac{\partial y_s(t_i)}{\partial y(t_k)} = T_{s23}$$

$$\frac{\partial z_s(t_i)}{\partial x(t_k)} = T_{s31}, \quad \frac{\partial z_s(t_i)}{\partial y(t_k)} = T_{s32}, \quad \frac{\partial z_s(t_i)}{\partial y(t_k)} = T_{s33}$$

$$\frac{\partial x_s(t_i)}{\partial \psi_k} = \frac{\partial T_{s11}}{\partial \psi_k}(x(t_i) - \xi_s) + \frac{\partial T_{s12}}{\partial \psi_k}(y(t_i) - \eta_s) + \frac{\partial T_{s13}}{\partial \psi_k}(z(t_i) - \zeta_s) \quad (63)$$

$$\frac{\partial x_s(t_i)}{\partial \rho_k} = \frac{\partial T_{s11}}{\partial \rho_k}(x(t_i) - \xi_s) + \frac{\partial T_{s12}}{\partial \rho_k}(y(t_i) - \eta_s) + \frac{\partial T_{s13}}{\partial \rho_k}(z(t_i) - \zeta_s) \quad (64)$$

$$\frac{\partial x_s(t_i)}{\partial \phi_k} = \frac{\partial T_{s11}}{\partial \phi_k}(x(t_i) - \xi_s) + \frac{\partial T_{s12}}{\partial \phi_k}(y(t_i) - \eta_s) + \frac{\partial T_{s13}}{\partial \phi_k}(z(t_i) - \zeta_s) \quad (65)$$

$$\frac{\partial y_s(t_i)}{\partial \psi_k} = \frac{\partial T_{s21}}{\partial \psi_k}(x(t_i) - \xi_s) + \frac{\partial T_{s22}}{\partial \psi_k}(y(t_i) - \eta_s) + \frac{\partial T_{s23}}{\partial \psi_k}(z(t_i) - \zeta_s) \quad (66)$$

$$\frac{\partial y_s(t_i)}{\partial \rho_k} = \frac{\partial T_{s21}}{\partial \rho_k}(x(t_i) - \xi_s) + \frac{\partial T_{s22}}{\partial \rho_k}(y(t_i) - \eta_s) + \frac{\partial T_{s23}}{\partial \rho_k}(z(t_i) - \zeta_s) \quad (67)$$

$$\frac{\partial y_s(t_i)}{\partial \phi_k} = \frac{\partial T_{s21}}{\partial \phi_k}(x(t_i) - \xi_s) + \frac{\partial T_{s22}}{\partial \phi_k}(y(t_i) - \eta_s) + \frac{\partial T_{s23}}{\partial \phi_k}(z(t_i) - \zeta_s) \quad (68)$$

$$\frac{\partial z_s(t_i)}{\partial \psi_k} = \frac{\partial T_{s31}}{\partial \psi_k}(x(t_i) - \xi_s) + \frac{\partial T_{s32}}{\partial \psi_k}(y(t_i) - \eta_s) + \frac{\partial T_{s33}}{\partial \psi_k}(z(t_i) - \zeta_s) \quad (69)$$

$$\frac{\partial z_s(t_i)}{\partial \rho_k} = \frac{\partial T_{s31}}{\partial \rho_k}(x(t_i) - \xi_s) + \frac{\partial T_{s32}}{\partial \rho_k}(y(t_i) - \eta_s) + \frac{\partial T_{s33}}{\partial \rho_k}(z(t_i) - \zeta_s) \quad (70)$$

$$\frac{\partial z_s(t_i)}{\partial \phi_k} = \frac{\partial T_{s31}}{\partial \phi_k}(x(t_i) - \xi_s) + \frac{\partial T_{s32}}{\partial \phi_k}(y(t_i) - \eta_s) + \frac{\partial T_{s33}}{\partial \phi_k}(z(t_i) - \zeta_s) \quad (71)$$

$$\frac{\partial g_{1s}(t_i)}{\partial x_s(t_i)} = \frac{z_s(t_i)}{z_s(t_i)^2 + x_s(t_i)^2} \quad (72)$$

$$\frac{\partial g_{1s}(t_i)}{\partial y_s(t_i)} = 0 \quad (73)$$

$$\frac{\partial g_{1s}(t_i)}{\partial z_s(t_i)} = -\frac{x_s(t_i)}{x_s(t_i)^2 + z_s(t_i)^2} \quad (74)$$

$$\frac{\partial g_{2s}(t_i)}{\partial x_s(t_i)} = -\frac{x_s(t_i)y_s(t_i)}{\sqrt{(x_s(t_i)^2 + z_s(t_i)^2)(x_s(t_i)^2 + y_s(t_i)^2 + z_s(t_i)^2)}} \quad (75)$$

$$\frac{\partial g_{2s}(t_i)}{\partial y_s(t_i)} = \frac{\sqrt{x_s(t_i)^2 + z_s(t_i)^2}}{x_s(t_i)^2 + y_s(t_i)^2 + z_s(t_i)^2} \quad (76)$$

$$\frac{\partial g_{2s}(t_i)}{\partial z_s(t_i)} = -\frac{z_s(t_i)y_s(t_i)}{(x_s(t_i)^2 + y_s(t_i)^2 + z_s(t_i)^2)(\sqrt{x_s(t_i)^2 + z_s(t_i)^2})} \quad (77)$$

$$\frac{\partial T_{s11}}{\partial \psi_k} = -\sin \psi_k \cos \rho_k \quad (78)$$

$$\frac{\partial T_{s12}}{\partial \psi_k} = -\sin \psi_k \sin \rho_k \sin \phi_k - \cos \psi_k \cos \phi_k \quad (79)$$

$$\frac{\partial T_{s13}}{\partial \psi_k} = -\sin \psi_k \sin \rho_k \cos \phi_k + \cos \psi_k \sin \phi_k \quad (80)$$

$$\frac{\partial T_{s21}}{\partial \psi_k} = \cos \psi_k \cos \rho_k \quad (81)$$

$$\frac{\partial T_{s22}}{\partial \psi_k} = \cos \psi_k \sin \rho_k \sin \phi_k - \sin \psi_k \cos \phi_k \quad (82)$$

$$\frac{\partial T_{s23}}{\partial \psi_k} = \cos \psi_k \sin \rho_k \cos \phi_k + \sin \psi_k \sin \phi_k \quad (83)$$

$$\frac{\partial T_{s31}}{\partial \psi_k} = 0 \quad (84)$$

$$\frac{\partial T_{s32}}{\partial \psi_k} = 0 \quad (85)$$

$$\frac{\partial T_{s33}}{\partial \psi_k} = 0 \quad (86)$$

$$\frac{\partial T_{s11}}{\partial \rho_k} = -\cos \psi_k \sin \rho_k \quad (87)$$

$$\frac{\partial T_{s12}}{\partial \rho_k} = \cos \psi_k \cos \rho_k \sin \phi_k \quad (88)$$

$$\frac{\partial T_{s13}}{\partial \rho_k} = \cos \psi_k \cos \rho_k \cos \phi_k \quad (89)$$

$$\frac{\partial T_{s21}}{\partial \rho_k} = -\sin \psi_k \sin \phi_k \quad (90)$$

$$\frac{\partial T_{s22}}{\partial \rho_k} = \sin \psi_k \cos \rho_k \sin \phi_k \quad (91)$$

$$\frac{\partial T_{s23}}{\partial \rho_k} = \sin \psi_k \cos \rho_k \cos \phi_k \quad (92)$$

$$\frac{\partial T_{s31}}{\partial \rho_k} = -\cos \phi_k \quad (93)$$

$$\frac{\partial T_{s32}}{\partial \rho_k} = -\sin \rho_k \sin \phi_k \quad (94)$$

$$\frac{\partial T_{s33}}{\partial \rho_k} = -\sin \rho_k \cos \phi_k \quad (95)$$

$$\frac{\partial T_{s11}}{\partial \phi_k} = 0 \quad (96)$$

$$\frac{\partial T_{s12}}{\partial \phi_k} = \cos \psi_k \sin \rho_k \cos \phi_k + \sin \psi_k \sin \phi_k \quad (97)$$

$$\frac{\partial T_{s13}}{\partial \phi_k} = -\cos \psi_k \sin \rho_k \sin \phi_k + \sin \psi_k \cos \phi_k \quad (98)$$

$$\frac{\partial T_{s21}}{\partial \phi_k} = 0 \quad (99)$$

$$\frac{\partial T_{s22}}{\partial \phi_k} = \sin \psi_k \sin \rho_k \cos \phi_k - \cos \psi_k \sin \phi_k \quad (100)$$

$$\frac{\partial T_{s23}}{\partial \phi_k} = -\sin \psi_k \sin \rho_k \sin \phi_k - \cos \psi_k \cos \phi_k \quad (101)$$

$$\frac{\partial T_{s31}}{\partial \phi_k} = 0 \quad (102)$$

$$\frac{\partial T_{s32}}{\partial \phi_k} = \cos \psi_k \cos \phi_k \quad (103)$$

$$\frac{\partial T_{s33}}{\partial \phi_k} = -\cos \rho_k \sin \phi_k \quad (104)$$

## REFERENCES

- [1] Y. Bar-Shalom, X.-R. Li, and T. Kirubarajan *Estimation with Applications to Tracking and Navigation: Theory, Algorithms and Software.* Wiley, 2001.
- [2] D. Belfadel, R. W. Osborne, and Y. Bar-Shalom "A Minimalist Approach to Bias Estimation for Passive Sensor Measurements with Targets of Opportunity," in *Proc. SPIE Conf. Signal and Data Processing of Small Targets*, #8857-13, San Diego, California, Aug. 2013.
- [3] D. Belfadel, R. W. Osborne, and Y. Bar-Shalom "Bias Estimation for Optical Sensor Measurements with Targets of Opportunity," in *Proc. FUSION Conf.*, Istanbul, Turkey, July 2013.
- [4] D. Belfadel, R. W. Osborne, and Y. Bar-Shalom "Bias Estimation and Observability for Optical Sensor Measurements with Targets of Opportunity," *Journal of Advances in Information Fusion*, vol. 9, no. 2, pp. 59–74, Dec. 2014.
- [5] T. M. Clemons and K.-C. Chang "Sensor Calibration using In-Situ Celestial Observations to Estimate Bias in Space-Based Missile Tracking," *IEEE Trans. on Aerospace and Electronic Systems*, vol. 48, no. 2, pp. 1403–1427, April 2012.
- [6] B. D. Kragel, S. Danford, S. M. Herman, and A. B. Poore "Bias Estimation Using Targets of Opportunity," *Proc. SPIE Conf. on Signal and Data Processing of Small Targets*, #6699, Aug. 2007.

- [7] B. D. Kragel, S. Danford, S. M. Herman, and A. B. Poore  
“Joint MAP Bias Estimation and Data Association: Algorithms,”  
*Proc. SPIE Conf. on Signal and Data Processing of Small Targets*, #6699-1E, Aug. 2007.
- [8] B. D. Kragel, S. Danford, and A. B. Poore  
“Concurrent MAP Data Association and Absolute Bias Estimation with an Arbitrary Number of Sensors,”  
*Proc. SPIE Conf. on Signal and Data Processing of Small Targets*, #6969-50, May 2008.
- [9] R. W. Osborne, III, and Y. Bar-Shalom  
“Statistical Efficiency of Composite Position Measurements from Passive Sensors,”  
in *Proc. SPIE Conf. on Signal Proc., Sensor Fusion, and Target Recognition*, #8050-07, Orlando, FL, April 2011.
- [10] R. W. Osborne, III, and Y. Bar-Shalom  
“Statistical Efficiency of Composite Position Measurements from Passive Sensors,”  
*IEEE Tans. on Aerospace and Electronic Systems*, vol. 49, no. 4, Oct. 2013.



**Djedjiga Belfadel** is a Ph.D. candidate in the Electrical Engineering department at the University of Connecticut, Storrs, CT. Her research interests include target tracking, data association, sensor fusion, sensor biases, machine vision, and other aspects of estimation. She obtained her B.S., degrees from the University of Mouloud Mammeri in 2003, and her M.S., degrees from the University of New Haven in 2008, both in electrical engineering. Before joining the Estimation and Signal Processing (ESP) Laboratory, she worked, as an Electrical Engineer, from 2009 to 2011, at Evax Systems Inc. in Branford, Connecticut.



**Richard W. Osborne, III** obtained his B.S., M.S., and Ph.D. degrees in electrical engineering from the University of Connecticut in 2004, 2007, and 2012, respectively. From 2012–2014 he was an Assistant Research Professor in the Electrical Engineering department at the University of Connecticut, Storrs, CT. Currently, he is a Senior Research Engineer at BAE Systems, Inc. in Burlington, MA, working in the Performance, Exploitation and Dissemination (PED) Technology and Integration group. His academic interests include target tracking, information fusion, automated systems, and all aspects of estimation.

**Yaakov Bar-Shalom** was born on May 11, 1941. He received the B.S. and M.S. degrees from the Technion, Israel Institute of Technology, in 1963 and 1967 and the Ph.D. degree from Princeton University in 1970, all in electrical engineering. From 1970 to 1976 he was with Systems Control, Inc., Palo Alto, California. Currently he is Board of Trustees Distinguished Professor in the Dept. of Electrical and Computer Engineering and Marianne E. Klewin Professor in Engineering at the University of Connecticut. He is also Director of the ESP (Estimation and Signal Processing) Lab. His current research interests are in estimation theory, target tracking and data fusion. He has published over 500 papers and book chapters in these areas and in stochastic adaptive control. He coauthored the monograph *Tracking and Data Association* (Academic Press, 1988), the graduate texts *Estimation and Tracking: Principles, Techniques and Software* (Artech House, 1993), *Estimation with Applications to Tracking and Navigation: Algorithms and Software for Information Extraction* (Wiley, 2001), the advanced graduate texts *Multitarget-Multisensor Tracking: Principles and Techniques* (YBS Publishing, 1995), *Tracking and Data Fusion* (YBS Publishing, 2011), and edited the books *Multitarget-Multisensor Tracking: Applications and Advances* (Artech House, Vol. I, 1990; Vol. II, 1992; Vol. III, 2000). He has been elected Fellow of IEEE for “contributions to the theory of stochastic systems and of multi-target tracking.” He has been consulting to numerous companies and government agencies, and originated the series of Multitarget-Multisensor Tracking short courses offered via UCLA Extension, at Government Laboratories, private companies and overseas. During 1976 and 1977 he served as Associate Editor of the IEEE Transactions on Automatic Control and from 1978 to 1981 as Associate Editor of *Automatica*. He was Program Chairman of the 1982 American Control Conference, General Chairman of the 1985 ACC, and Co-Chairman of the 1989 IEEE International Conference on Control and Applications. During 1983–87 he served as Chairman of the Conference Activities Board of the IEEE Control Systems Society and during 1987–89 was a member of the Board of Governors of the IEEE CSS. He was a member of the Board of Directors of the International Society of Information Fusion (1999–2004) and served as General Chairman of FUSION 2000, President of ISIF in 2000 and 2002 and Vice President for Publications in 2004–13. In 1987 he received the IEEE CSS Distinguished Member Award. Since 1995 he is a Distinguished Lecturer of the IEEE AESS and has given numerous keynote addresses at major national and international conferences. He is co-recipient of the M. Barry Carlton Award for the best paper in the IEEE Transactions on Aerospace and Electronic Systems in 1995 and 2000 and recipient of the 1998 University of Connecticut AAUP Excellence Award for Research. In 2002 he received the J. Mignona Data Fusion Award from the DoD JDL Data Fusion Group. He is a member of the Connecticut Academy of Science and Engineering. In 2008 he was awarded the IEEE Dennis J. Picard Medal for Radar Technologies and Applications, and in 2012 the Connecticut Medal of Technology. He has been listed by [academic.research.microsoft.com](http://academic.research.microsoft.com) (top authors in engineering) as #1 among the researchers in Aerospace Engineering based on the citations of his work.



# Fusion of Multipath Data with ML-PMHT for Very Low SNR Track Detection in an OTHR

KEVIN ROMEO  
YAAKOV BAR-SHALOM  
PETER WILLETT

The Maximum Likelihood Probabilistic Multi-Hypothesis Tracker (ML-PMHT) is formulated for and applied to an Over-The-Horizon radar (OTHR) scenario. In this scenario there are two ionosphere layers acting as reflectors of the electromagnetic (EM) waves and each scan can contain multiple measurements (up to four) originating from each target; each of these target-originated measurements takes one of four possible round-trip paths. The ML-PMHT likelihood ratio is modified to model this uncertainty in the measurement path which then allows the fusion of multipath data in the presence of false measurements.

This tracker is shown to have a high track detection probability and track accuracy with a low probability of false track in very low signal to noise ratio (SNR) OTHR scenarios. It is also shown to be a statistically efficient estimator. Consequently, the ML-PMHT holds great promise in increasing the sensitivity and robustness of the next generation OTHR.

Results indicate that one can achieve for a very low observable (VLO) target a true track detection probability above 95% and a false track rate under one per 24 hours.

Manuscript received September 24, 2014; revised March 6, 2015; released for publication May 29, 2015.

Refereeing of this contribution was handled by Stefano Coraluppi.

Supported in part by ARO Grant W991NF-10-1-0369.

Authors' address: Dept. of Electrical and Computer Engineering, University of Connecticut, Storrs, CT 06269-4157 (e-mail: {romeo, ybs, willett}@enr.uconn.edu.)

1557-6418/15/\$17.00 © 2015 JAIF

## 1. INTRODUCTION

Over-the-horizon radar (OTHR) relies on signal refraction through the ionosphere to detect targets beyond the horizon. Due to the nature of the ionosphere, the signal from the radar may propagate via multiple paths, resulting in several target-originated detections. There is an ambiguity between detections and paths; the path corresponding to each target detection is not known. There are also measurements from false detections.

There are a wide range of approaches to the OTHR problem, varying in how detection, tracking, and association are handled. The multiple detection multiple hypothesis tracker (MD-MHT) [16] is formulated to solve the data association problem between measurements and measurement paths using an extended multiframe assignment technique. Alternatively, a multihypothesis fusion algorithm, presented in [11, 13–15], is a measurement-level fusion algorithm using only measurements already associated with targets by another filter to calculate the probabilities of association hypotheses. In [1, 2] a method is proposed for joint multiple target ground track estimation and slant track association. Additionally they assume unknown ionospheric conditions. Their method shows an improvement in accuracy and the number of correct track and path assignments. The Signal Inversion for Target Extraction and Registration (SIFTER) signal processing algorithm developed in [9] provides a better detection of low SNR targets in clutter by solving for the scattering surface that reproduces the radar's measurements and has been demonstrated effectively on real OTHR data.

Other approaches include applying the probabilistic data association filter (PDAF) [6–8], the multipath probabilistic data association algorithm (MPDA) [12], and the Probabilistic Multi-Hypothesis Tracker (PMHT) [8] to OTHR data. An extension of the PDAF called the Multiple Model Unified PDAF (MM-UPDAF) is developed in [7]. The MM-UPDAF is designed to handle multiple nonuniform clutter regions. The SNR in [7] is unavailable as the parameters used to determine the performance of the MM-UPDAF are proprietary. The lowest SNR available from [12] and [16] is around 10 dB, with an ionosphere model similar to what we use in our simulations. We show that our algorithm with a VLO target SNR of 4 dB yields a high track detection probability (95%) and a very low false track rate (less than one per day) for the scenario considered.

A multipath Expectation Maximization algorithm is developed and applied to an OTHR scenario in [10]. Similar to the PMHT, it treats data association as missing data. It also treats propagation paths as missing data. The (single path) Maximum Likelihood Probabilistic Multi-Hypothesis Tracker (ML-PMHT) uses the log-likelihood function based on the PMHT model. The ML-PMHT has previously been formulated for single and multitarget [17, 18] scenarios. It has been shown to perform well even with very low target SNR.

In this paper we extend the ML-PMHT formulation from [17, 18]. We present a generalized form of the ML-PMHT that accounts for multiple possible propagation paths. We apply this algorithm to an OTHR scenario. Unlike the MD-MHT [16], no data association is required. The ML-PMHT considers simultaneously all the measurements without knowing their origins or propagation paths and, remarkably, has *linear complexity in the number of measurements*. The ML-PMHT performs fusion of the multipath data in the presence of false measurements.

Section 2 briefly describes the ML-PMHT for a single target case and the extension to allow for multiple paths. Section 3 describes the multiple path extension to the ML-PDA. Section 4 presents the OTHR model used for simulation. Section 5 discusses the performance of the ML-PMHT from Monte Carlo testing. Section 6 develops the Cramér-Rao Lower Bound for the multipath ML-PMHT.

## 2. ML-PMHT

### 2.1. Single Target ML-PMHT

The ML-PMHT log-likelihood ratio (LLR) for the motion parameter of a single target is developed in [17]. This LLR is given by

$$\Lambda(\mathbf{x}; Z) \triangleq \ln \left\{ \frac{p(Z | \mathbf{x})}{p(Z | \text{all false})} \right\} \\ = \sum_{i=1}^{N_w} \sum_{j=1}^{m_i} \ln \{ \pi_0 + \pi_1 V p[\mathbf{z}_j(i) | \mathbf{x}(i)] \rho_j(i) \} \quad (1)$$

with

$$Z \triangleq \{ \{ \mathbf{z}_j(i) \}_{j=1}^{m_i} \}_{i=1}^{N_w} \quad (2)$$

Here  $N_w$  is the number of scans in the batch (the window length), and  $m_i$  is the number of measurements in the  $i$ th scan (frame). The parameter  $\mathbf{x}$  determines the target state  $\mathbf{x}(i)$  in a deterministic way (we use a constant velocity model<sup>1</sup> i.e.,  $\mathbf{x} = [s_t(1), \dot{s}_t]'$ , where  $s_t(1)$  and  $\dot{s}_t$  are the initial position and velocity of the target, respectively). The prior probabilities that a measurement occurred due to clutter or due to a target are given by  $\pi_0$  and  $\pi_1$ , respectively. These values are related to the probability of detection,  $P_D$ , and the probability of false alarm in a resolution cell,  $P_{FA}$ . The volume of the search region is  $V$  and a measurement, which didn't occur due to a target, has a uniform pdf in  $V$ . The  $j$ th measurement in the  $i$ th scan is  $\mathbf{z}_j(i)$  and its associated amplitude likelihood ratio is  $\rho_j(i)$ . Finally,  $p[\mathbf{z}_j(i) | \mathbf{x}(i)]$  is a Gaussian with mean determined by the target state parametrization  $\mathbf{x}(i)$ , and with the measurement noise covariance matrix. The amplitude likelihood ratio serves as a feature discriminant between the target originated measurements and the false ones due to spurious detections.

<sup>1</sup>Any arbitrary deterministic motion model can be used, such as deterministic motion in a known gravitational field [4].

The pdfs  $p[Z(i) | \mathbf{x}(i)]$  (likelihood of the target present hypothesis) and  $p[Z(i) | \text{all false}]$  (likelihood of the target absent hypothesis) are derived using the ML-PMHT assumptions [17]:

- There is a single target with known probability of detection.
- Any number of measurements in a scan can be assigned to the target.
- The motion of the target is deterministic.
- False detections are uniformly distributed.
- The number of false detections is Poisson distributed with known density.
- Amplitudes of target and false detections are Rayleigh distributed with known distribution.
- Target measurements are corrupted with zero-mean Gaussian noise.
- Measurements at different times, conditioned on the parameterized state, are independent.

These likelihoods are then given by

$$p[Z(i) | \mathbf{x}(i)] \\ = \prod_{j=1}^{m_i} \left\{ \frac{\pi_0}{V} p_0^\tau[a_j(i)] + \pi_1 p[\mathbf{z}_j(i) | \mathbf{x}(i)] p_1^\tau[a_j(i)] \right\} \quad (3)$$

$$p[Z(i) | \text{all false}] = \prod_{j=1}^{m_i} \frac{1}{V} p_0^\tau[a_j(i)] \quad (4)$$

where  $p_0^\tau[a_j(i)]$  and  $p_1^\tau[a_j(i)]$  are the pdfs of a false alarm and target measurement amplitude conditioned on exceeding the threshold  $\tau$ , respectively.

### 2.2. The Multipath ML-PMHT Log-Likelihood Ratio for OTHR

The LLR of the generalized ML-PMHT that allows multiple propagation paths is given by

$$\Lambda(\mathbf{x}; Z) \\ = \sum_{i=1}^{N_w} \sum_{j=1}^{m_i} \ln \left\{ \pi_0 + \pi_1 V \rho_j(i) \sum_{\ell=1}^{n_p} p[\mathbf{z}_j(i) | \mathbf{x}(i), \ell] P[\ell] \right\} \quad (5)$$

where  $\ell$  is used to denote which path the signal took,  $P[\ell]$  is the probability of path  $\ell$  being taken, and  $n_p$  is the total number of possible paths. The mean of the Gaussian  $p[\mathbf{z}_j(i) | \mathbf{x}(i), \ell]$  is  $f_\ell(\mathbf{x}(i))$ , where  $f_\ell$  is the function that transforms the target state  $\mathbf{x}(i)$  into the measurement space via path  $\ell$ . The covariance matrix for this Gaussian is the measurement noise covariance for a measurement from path  $\ell$ . Note that, for simplicity, we have assumed that  $\rho_j(i)$  is the same for each path  $\ell$  (a path dependent LLR can be used if available).

## 3. ML-PDA

We can extend the single-path ML-PDA likelihood presented in [17] to allow for multiple paths by applying

the total probability theorem. For a single scan this results in

$$\Lambda(\mathbf{x}; Z) = \sum_{n_d=0}^{n_p} p(\mathbf{z} | \mathbf{x}, n_d) P(n_d) \quad (6)$$

$$P(n_d) = P_D^{n_d} (1 - P_D)^{n_p - n_d} \binom{n_p}{n_d} \quad (7)$$

$$p(\mathbf{z} | \mathbf{x}, n_d) = \frac{1}{\binom{m}{n_d} \binom{n_p}{n_d} n_d!} \sum_{M \in \mathcal{M}_{n_d}} \sum_{A \in \mathcal{A}_{n_d}} \cdot p[\{\mathbf{z}_k\}_{k \notin M} | \text{“clutter”}] \prod_{j=1}^{n_d} p[\mathbf{z}_{M(j)} | \mathbf{x}, A(j)] \quad (8)$$

where  $n_d$  is the number of detections, and  $P_D$  is the probability of detection.  $\mathcal{M}_{n_d}$  is the set of all unordered  $n_d$ -tuples of measurement indices. It contains  $\binom{m}{n_d}$   $n_d$ -tuples.  $\mathcal{A}_{n_d}$  is the set of all ordered  $n_d$ -tuples of path indices. This set contains  $\binom{n_p}{n_d} n_d!$   $n_d$ -tuples. The ML-PDA gives similar results to the ML-PMHT in very low clutter scenarios, but is significantly more complex. For scenarios with a large amount of clutter (like the ones we are exploring in this paper) the ML-PDA becomes intractable due to the number of terms in the double summation in equation (8). Its CRLB is also complicated to determine since it requires extensive Monte Carlo simulations [5]. We choose the ML-PMHT for its simplicity and effectiveness. In a single scan  $i$  the ML-PMHT has  $m_i n_p$  terms—linear complexity—while the ML-PDA has  $\sum_{n_d=0}^{n_p} \binom{m_i}{n_d} \binom{n_p}{n_d} n_d! n_d = m_i n_p \sum_{n_d=0}^{n_p} (n_d - 1)! \binom{m_i - 1}{n_d - 1}$  terms and therefore suffers from a combinatorial explosion with increasing  $m_i$ .

#### 4. OTHR MODEL

We investigate two two-dimensional OTHR scenarios which assume the target to be in a great circle plane on the earth’s surface as shown in Figure 1, and a three-dimensional scenario where the target is on the surface of a sphere. We use a two-layer reflection model (spherical mirror model) for the ionosphere.<sup>2</sup> In this model the signal may reflect from either layer of the ionosphere resulting in multiple (up to four) round-trip propagation paths. In the 2-D and 3-D scenarios the radar measures slant range, slant range rate, and amplitude. In the 3-D scenario it also measures azimuth.

##### 4.1. Measurement Amplitudes

We model the amplitudes of the measurements according to a Swerling I model [4]. The amplitude is

<sup>2</sup>The actual paths are subject to refraction, which requires numerical algorithms for ray tracing. The reflection model used here is a simplified one, which, however, captures the essence of the OTHR.

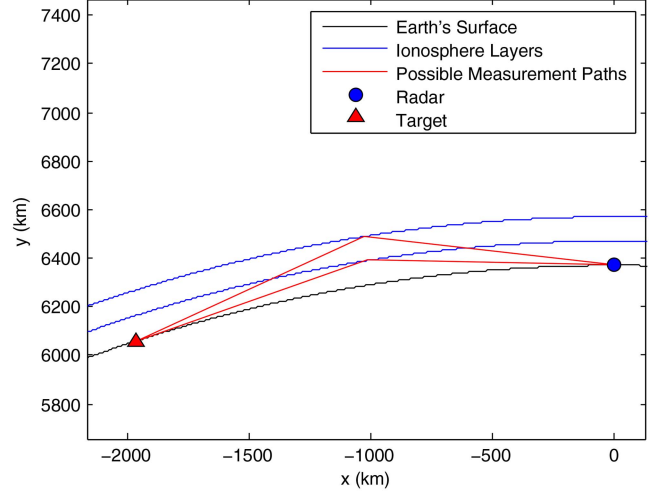


Fig. 1. The 2-D OTHR scenario with a reflection ionosphere model (spherical mirror model).

Rayleigh distributed with pdfs

$$p_0(a) = ae^{-a^2/2} \quad a \geq 0 \quad (9)$$

$$p_1(a) = \frac{a}{1+d} e^{-a^2/2(1+d)} \quad a \geq 0 \quad (10)$$

for the noise only and target, respectively. Here  $d$  is the expected SNR of the target in a resolution cell. For a chosen threshold  $\tau$  we have

$$P_D = \int_{\tau}^{\infty} p_1(a) da \quad (11)$$

$$P_{FA} = \int_{\tau}^{\infty} p_0(a) da \quad (12)$$

The pdfs of the amplitude of a measurement given that it has exceeded the threshold  $\tau$  are

$$p_0^{\tau}(a) = \frac{1}{P_{FA}} p_0(a) \quad a \geq \tau \quad (13)$$

$$p_1^{\tau}(a) = \frac{1}{P_D} p_1(a) \quad a \geq \tau \quad (14)$$

and the amplitude likelihood ratio is then

$$\rho_j(i) = \frac{p_1^{\tau}[a_j(i)]}{p_0^{\tau}[a_j(i)]} \quad (15)$$

##### 4.2. Measurements

The OTHR measures both position and velocity of the target via slant range and slant range rate measurements. The equations of the measurements, given the signal reflected off the lower layer in both directions, are given below.<sup>3</sup> Defining

$$r_1 \triangleq 4 \sqrt{h_1^2 - 2R_{\oplus}(h_1 + R_{\oplus}) \cos\left(\frac{s_r - s_t}{2R_{\oplus}}\right) + 2h_1R_{\oplus} + 2R_{\oplus}^2} \quad (16)$$

<sup>3</sup>The signal propagates forward and is reflected in the plane of the great circle defined by the radar and the target. We assume that the antenna beam illuminating the target is in this plane. This beam corresponds to the measured azimuth of the reflection from the target.

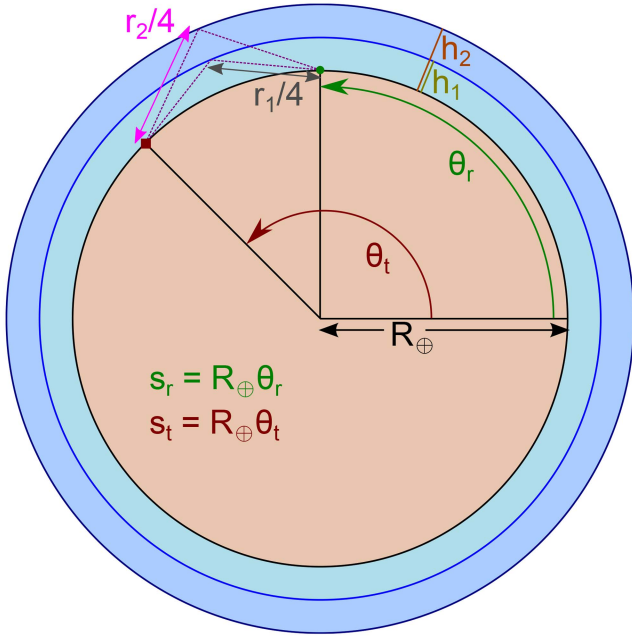


Fig. 2. Illustration of the geometry used to derive the equations for the measurements. Here  $\theta_r$  and  $\theta_t$  are the angles in polar coordinates of the radar and the target, respectively.

$$\dot{r}_1 \stackrel{\Delta}{=} \frac{\partial r_1}{\partial s_t} \frac{\partial s_t}{\partial t}$$

$$= - \frac{2 \sin \left( \frac{s_r - s_t}{2R_{\oplus}} \right) (R_{\oplus} + h_1)}{\sqrt{2R_{\oplus} h_1 + 2R_{\oplus}^2 + h_1^2 - 2R_{\oplus} \cos \left( \frac{s_r - s_t}{2R_{\oplus}} \right) (R_{\oplus} + h_1)}} \dot{s}_t \quad (17)$$

one has

$$z_{r_1} = r_1 + w_{r_1} \quad (18)$$

$$z_{\dot{r}_1} = \dot{r}_1 + w_{\dot{r}_1} \quad (19)$$

Here  $h_1$  is the height of the lower ionosphere layer. The radius of the earth is  $R_{\oplus}$ . The locations of the radar and target on the surface of the earth (on the great circle connecting them) are given by  $s_r$  and  $s_t$ , respectively. An illustration of the geometry of this problem is shown in Fig. 2. The velocity of the target along the great circle is  $\dot{s}_t$ . The noise terms,  $w_{r_1}$  and  $w_{\dot{r}_1}$ , are zero-mean, Gaussian, independent of each other, and with variances  $\sigma_r$  and  $\sigma_{\dot{r}}$ , respectively. We assume, for simplicity, the same noise variances on the other paths.

Given that the signal reflected off the upper layer only (with height  $h_2$ ), we can find similar equations for  $r_2$ ,  $\dot{r}_2$ ,  $z_{r_2}$ , and  $z_{\dot{r}_2}$ , with noises  $w_{r_2}$  and  $w_{\dot{r}_2}$ . The equations for the measurements resulting from the remaining two paths, where the signal reflects off of alternate layers, can then be expressed as

$$z_{r_3} = \frac{1}{2}(r_1 + r_2) + w_{r_3} \quad (20)$$

$$z_{\dot{r}_3} = \frac{1}{2}(\dot{r}_1 + \dot{r}_2) + w_{\dot{r}_3} \quad (21)$$

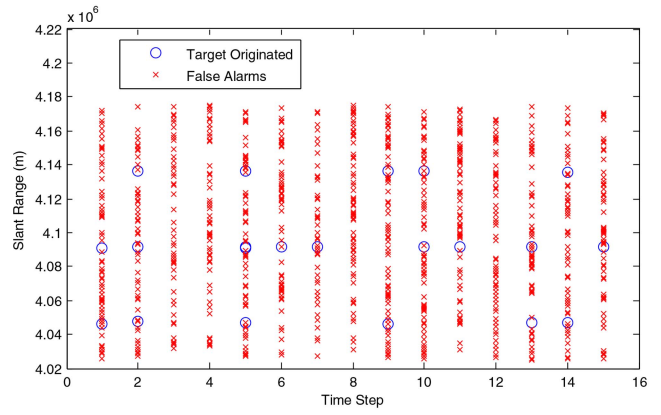


Fig. 3. Slant range measurements in one batch in 2-D scenario 1 (4 dB post-signal processing SNR).

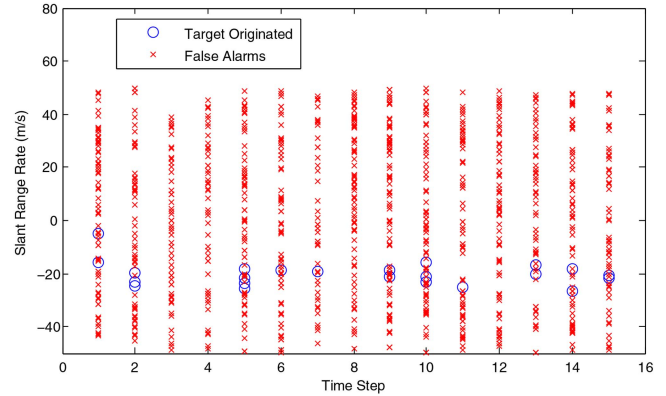


Fig. 4. Slant range rate measurements in one batch in 2-D scenario 1 (4 dB post-signal processing SNR).

$$z_{r_4} = \frac{1}{2}(r_1 + r_2) + w_{r_4} \quad (22)$$

$$z_{\dot{r}_4} = \frac{1}{2}(\dot{r}_1 + \dot{r}_2) + w_{\dot{r}_4} \quad (23)$$

The azimuth measurement (used only in the 3-D scenario) is given by

$$z_{\theta} = \theta + w_{\theta} \quad (24)$$

where  $\theta$  is the true azimuth of the target, and the noise term  $w_{\theta}$  is zero-mean, Gaussian, and has variance  $\sigma_{\theta}$ .

#### 4.3. 2-D Simulation Parameters

We simulated a target with an initial position 2000 km away from the radar, moving with a constant speed of 10 m/s towards it. The other values used in the 2-D simulations are given in Tables I and II. Figures 3 and 4 show the measurements used (after amplitude thresholding) in one run of the tracker from scenario 1. False measurements are generated uniformly in the measurement space. Note that, due to the very low SNR in a cell,  $P_D$  is a meager 0.34 and the high  $P_{FA}$  leads to 60 false measurements per scan. Also note that there are usually zero to three target originated measurements in each scan (rarely all four) and the overwhelming number of false measurements, which, however, can be

TABLE I

Scenario parameters used in the both the 2-D and 3-D simulations.

$N_w$	15
Time between scans	1 s
$\sigma_r$	300 m
$\sigma_v$	5 m/s
SNR in a cell	<b>2.5 = 4 dB</b>
$R_{\oplus}$	6371 km
Ionosphere lower layer height	100 km
Ionosphere upper layer height	200 km
$P[\ell]$ for all $\ell$	0.25

successfully handled by the multipath ML-PMHT track detector.

#### 4.4. 3-D Simulation Parameters

We also simulated a target starting at 2000 km away from the radar and 0 azimuth. It is moving with a constant speed of 10 m/s with an initial course of  $5^\circ$ . The target follows the great circle starting from these initial conditions. The other values used in the 3-D simulation are given in Tables I and II. The very low SNR in a cell now leads to 72 false measurements per scan.

### 5. PERFORMANCE OF THE TRACK DETECTOR

#### 5.1. 2-D Results

The LLR of the ML-PMHT for a single run is shown in Figures 5 and 6 for the first 2-D scenario. The plot is centered at the true target location. There are five peaks resulting from path ambiguity. The central peak (the correct one), however, is easily distinguishable from the side peaks. It is also much higher than any peak occurring due to clutter.

We use a simple grid search with 1 km spacing in range, and 20 m/s spacing in velocity to get into the neighborhood of the global maximum of (5). For simplicity, no target feature was used. We then run a local optimization routine from MATLAB using an interior-point algorithm on the highest valued point from the grid search to produce the final state estimate. In the first 2-D scenario this takes approximately 8 seconds per run in MATLAB (faster than real time), and from 10000 Monte Carlo runs the root mean square

(RMS) errors for position and velocity at the end of the batch were 40.7 m and 0.7 m/s, respectively. There were no false tracks or missed tracks.

We also applied the MD-MHT [16] to the first 2-D scenario. Using perfect initialization and a sliding window of size 2, the RMS errors from 100 Monte Carlo runs for position and velocity at the end of the run were 83 m and 5.8 m/s, respectively, i.e., significantly larger than the ML-PMHT. An extended Kalman filter was used to update the track with the measurement-path combinations chosen by the algorithm. In the MD-MHT, increasing the window size  $N_w$  rapidly increases the computational requirements of the algorithm. The number of hypotheses for a single target scenario depends on the number of paths and measurements and is approximately  $(N_{\text{paths}}N_{\text{meas}})^{N_w}$ , which quickly becomes intractable.

Using the same grid search method for the second scenario 2, the RMS errors from the ML-PMHT for position and velocity at the end of the batch were 27.2 m and 0.4 m/s, respectively, from 100 Monte Carlo runs, also with no false tracks.

We also ran the first 2-D scenario with different values for the SNR and threshold  $\tau$ . We chose  $\tau$  such that  $P_D$  remained fixed at 0.34. These results are shown in Table III. In the lowest SNR case (4 dB) the track was detected in each of the  $10^4$  runs. The algorithm was demonstrated to yield a *track detection probability*,  $P_{DT}$ , higher than 95%. Also no false tracks were detected by the algorithm in these  $10^4$  runs, thus the *probability of false track*,  $P_{FT}$ , is at most  $10^{-4}$  for the 15 s time interval. Based on this, the *false track rate* (over 24 hours) is 0.6/day.

#### 5.2. 3-D Results

Figure 7 shows the LLR surface using the true values for azimuth and course. Similarly, Figure 8 shows the LLR surface using the true values for range and speed. We use MATLAB's GlobalSearch algorithm to perform the optimization. From 100 Monte Carlo runs the RMSE values were 3.3 km in position, 54 m in range, and 21 m/s in velocity (in the range direction 0.86 m/s while in the crossrange direction 21 m/s;

TABLE II  
Scenario parameters used in the 2-D and 3-D simulations.

	2-D Scenario 1	2-D Scenario 2	3-D Scenario
Resolution cell size	600 m $\times$ 10 m/s	15000 m $\times$ 10 m/s	1200 m $\times$ 20 m/s $\times$ 1.2 $^\circ$
Search region size	150 km $\times$ 100 m/s	150 km $\times$ 100 m/s	150 km $\times$ 100 m/s $\times$ 90 $^\circ$
Number of cells	2500	100	46875
V	$1.5 \cdot 10^7$ m <sup>2</sup> /s	$1.5 \cdot 10^7$ m <sup>2</sup> /s	$2.4 \cdot 10^7$ m <sup>2</sup> /s $\times$ rad
$\sigma_\theta$	N/A	N/A	0.3 $^\circ$
Amplitude detection threshold $\tau$	2.7	1.7	3.6
$P_D$ for each path	0.34	0.66	0.16
$P_{FA}$ in a cell	0.024	0.24	0.0015
Expected number of false alarms per scan	60	24	72
$\pi_0$	0.9776	0.8991	0.9913

TABLE III

Results for various SNR values in the first 2-D scenario from 1000 Monte Carlo runs (results for SNR = 4 dB are from 10000 Monte Carlo runs). The measurement detection threshold  $\tau$  is chosen such that the single-measurement  $P_D$  is fixed at 0.34.

	Cell $P_{FA}$	Expected number of false alarms (false measurements) per scan	Position RMSE (m)	Velocity RMSE (m/s)	Position CRLB (m)	Velocity CRLB (m/s)
SNR = 10 dB, $\tau = 4.84$	$7 \cdot 10^{-6}$	0.02	32.90	0.5449	33.11	0.5519
SNR = 7 dB, $\tau = 3.6$	0.0015	4	35.30	0.5647	34.36	0.5727
SNR = 6 dB, $\tau = 3.3$	0.0043	11	37.10	0.6037	35.57	0.5929
SNR = 4 dB, $\tau = 2.73$	0.024	60	40.67	0.6760	39.57	0.6595

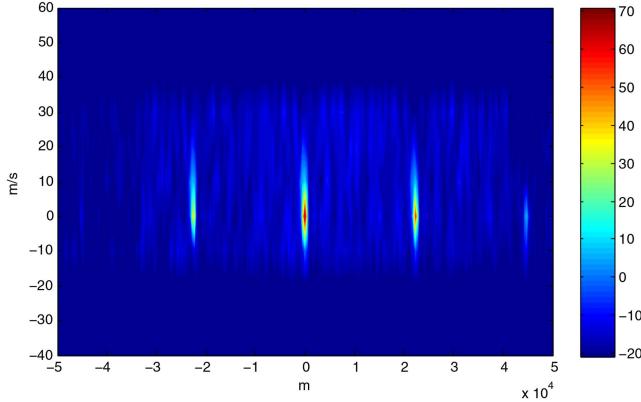


Fig. 5. The log-likelihood ratio centered on the true target state from 2-D scenario 1.

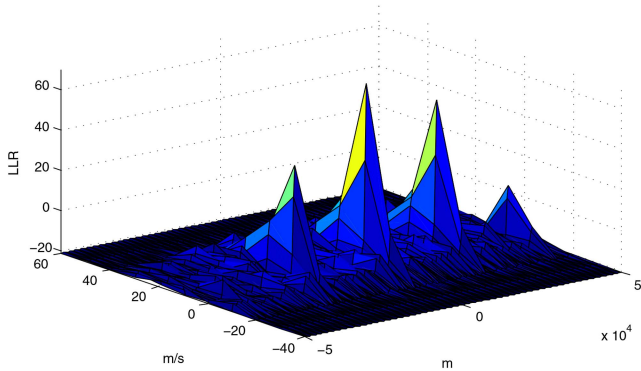


Fig. 6. The log-likelihood ratio centered on the true target state from 2-D scenario 1.

the latter is due to the fact that the crossrange rate is based on the  $0.3^\circ$  azimuth measurement, which maps to  $5 \text{ mrad} \times 2000 \text{ km} = 10 \text{ km}$  crossrange errors, i.e., extremely large).

The algorithm's running time in the 3-D scenario was approximately 2 minutes per run (on 15 s of data) in MATLAB. Therefore, this algorithm can run at least one order of magnitude faster, i.e., it is real time capable if it is implemented in a faster programming language, such as C.

## 6. MULTIPATH FUSION ML-PMHT CRAMÉR-RAO LOWER BOUND

We develop the Cramér-Rao Lower Bound (CRLB) [3] for the multipath fusion ML-PMHT and show that

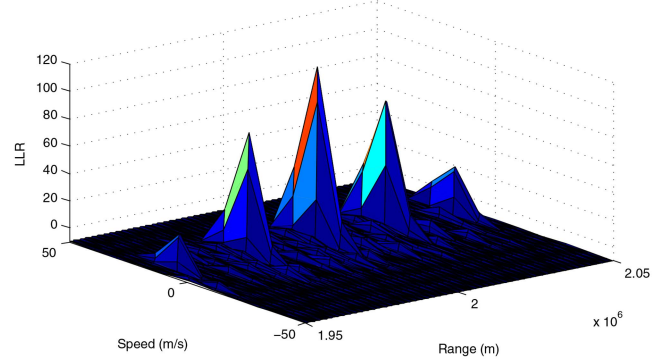


Fig. 7. The log-likelihood ratio at the true values for azimuth and course from the 3-D scenario.

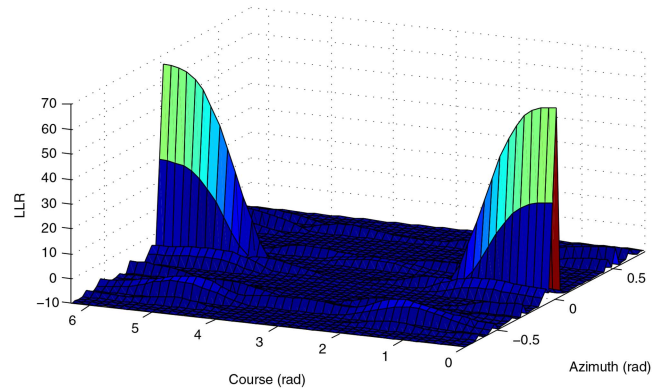


Fig. 8. The log-likelihood ratio at the true values for range and speed from the 3-D scenario.

it is statistically efficient in the first 2-D scenario. We can assume all scans to be independent and also assume the measurements in each scan to be independent. The Fisher Information Matrix (FIM)  $\mathbf{J}$  will then be the sum of the FIMs  $\mathbf{J}_{i,j}$  of each measurement,

$$\mathbf{J} = \mathbb{E}\{(\nabla_{\mathbf{x}} \ln p[\mathbf{Z} | \mathbf{x}])(\nabla_{\mathbf{x}} \ln p[\mathbf{Z} | \mathbf{x}])^T\}_{|\mathbf{x}=\mathbf{x}_0} = \sum_{i=1}^{N_w} \sum_{j=1}^{m_i} \mathbf{J}_{i,j} \quad (25)$$

where

$$\mathbf{J}_{i,j} = \mathbb{E}\{(\nabla_{\mathbf{x}(i)} \ln p[\mathbf{z}_j(i) | \mathbf{x}(i)]) \cdot (\nabla_{\mathbf{x}(i)} \ln p[\mathbf{z}_j(i) | \mathbf{x}(i)])^T\}_{|\mathbf{x}(i)=\mathbf{x}_0(i)} \quad (26)$$

The state vector  $\mathbf{x}(i)$  is given by

$$\mathbf{x}(i) = [s_r(i), \dot{s}_r]' \quad (27)$$

where  $s_t(i)$  is the target's position at time  $i$ , and  $\dot{s}_t$  is the target's velocity. The function that transforms  $\mathbf{x}(i)$  into the measurement space via the path that reflects both ways off the lower layer only is expressed as (28) with derivatives given by (29) and (30). The functions  $f_\ell(\mathbf{x}(i))$  for the other paths (and their derivatives) can be found similarly.

The multipath ML-PMHT likelihood for a single measurement is given by (31). The gradient of the logarithm of this likelihood gives (32), where  $\mathbf{D}_\ell(i)$  is the Jacobian of  $f_\ell(\mathbf{x}(i))$ . Finally, combining equations (26) and (32) gives us the FIM of one measurement, which has to be evaluated numerically, as (33).

$$f_1(\mathbf{x}(i)) = \left[ \begin{array}{c} 4\sqrt{h_1^2 - 2R_\oplus(h_1 + R_\oplus)\cos\left(\frac{s_r - s_t(i)}{2R_\oplus}\right) + 2h_1R_\oplus + 2R_\oplus^2} \\ 2\sin\left(\frac{s_r - s_t(i)}{2R_\oplus}\right)(R_\oplus + h_1) \\ \sqrt{2R_\oplus h_1 + 2R_\oplus^2 + h_1^2 - 2R_\oplus\cos\left(\frac{s_r - s_t(i)}{2R_\oplus}\right)}(R_\oplus + h_1) \end{array} \right] \dot{s}_t(i) \quad (28)$$

$$\frac{\partial}{\partial s_t(i)} f_1(\mathbf{x}(i)) = \left[ \begin{array}{c} 2\sin\left(\frac{s_r - s_t(i)}{2R_\oplus}\right)(R_\oplus + h_1) \\ \sqrt{2R_\oplus h_1 + 2R_\oplus^2 + h_1^2 - 2R_\oplus\cos\left(\frac{s_r - s_t(i)}{2R_\oplus}\right)}(R_\oplus + h_1) \\ \cos\left(\frac{s_r - s_t(i)}{2R_\oplus}\right)(R_\oplus + h_1)\dot{s}_t(i) \\ R_\oplus\sqrt{2R_\oplus h_1 + 2R_\oplus^2 + h_1^2 - 2R_\oplus\cos\left(\frac{s_r - s_t(i)}{2R_\oplus}\right)}(R_\oplus + h_1) \\ \sin\left(\frac{s_r - s_t(i)}{2R_\oplus}\right)^2 (R_\oplus + h_1)^2 \dot{s}_t(i) \\ [2R_\oplus h_1 + 2R_\oplus^2 + h_1^2 - 2R_\oplus\cos\left(\frac{s_r - s_t(i)}{2R_\oplus}\right)(R_\oplus + h_1)]^{3/2} \end{array} \right] \quad (29)$$

$$\frac{\partial}{\partial \dot{s}_t(i)} f_1(\mathbf{x}(i)) = \left[ \begin{array}{c} 0 \\ 2\sin\left(\frac{s_r - s_t(i)}{2R_\oplus}\right)(R_\oplus + h_1) \\ \sqrt{2R_\oplus h_1 + 2R_\oplus^2 + h_1^2 - 2R_\oplus\cos\left(\frac{s_r - s_t(i)}{2R_\oplus}\right)}(R_\oplus + h_1) \end{array} \right] \quad (30)$$

$$p[\mathbf{z}_j(i) | \mathbf{x}(i)] = \frac{\pi_0}{V} p_0^\tau[a_j(i)] + \pi_1 p_1^\tau[a_j(i)] \sum_{\ell=1}^{n_p} p[\mathbf{z}_j(i) | \mathbf{x}(i), \ell] P(\ell) \quad (31)$$

$$\begin{aligned} \nabla_{\mathbf{x}(i)} \ln p(\mathbf{z}_j(i) | \mathbf{x}(i)) &= \frac{\pi_1 p_1^\tau[a_j(i)] \sum_{\ell=1}^{n_p} P(\ell) |2\pi\mathbf{R}|^{-\frac{1}{2}} e^{-\frac{1}{2}[\mathbf{z}_j(i) - f_\ell(\mathbf{x}(i))]'\mathbf{R}^{-1}[\mathbf{z}_j(i) - f_\ell(\mathbf{x}(i))]} \mathbf{D}_\ell^T(i) \mathbf{R}^{-1} [\mathbf{z}_j(i) - f_\ell(\mathbf{x}(i))]}{\frac{\pi_0}{V} p_0^\tau[a_j(i)] + \pi_1 p_1^\tau[a_j(i)] \sum_{\ell=1}^{n_p} P(\ell) |2\pi\mathbf{R}|^{-\frac{1}{2}} e^{-\frac{1}{2}[\mathbf{z}_j(i) - f_\ell(\mathbf{x}(i))]'\mathbf{R}^{-1}[\mathbf{z}_j(i) - f_\ell(\mathbf{x}(i))]} \end{aligned} \quad (32)$$

$$\mathbf{J}_{i,j} = \int_{\tau}^{\infty} \int_V \frac{(\pi_1 p_1^\tau[a_j(i)])^2}{|2\pi\mathbf{R}|} \sum_{\ell=1}^{n_p} \mathbf{A}_\ell(i) \sum_{\ell=1}^{n_p} \mathbf{A}_\ell^T(i) \frac{d\mathbf{z}_j(i) da_j(i)}{\frac{\pi_0}{V} p_0^\tau[a_j(i)] + \pi_1 p_1^\tau[a_j(i)] \sum_{\ell=1}^{n_p} P(\ell) |2\pi\mathbf{R}|^{-\frac{1}{2}} e^{-\frac{1}{2}[\mathbf{z}_j(i) - f_\ell(\mathbf{x}(i))]'\mathbf{R}^{-1}[\mathbf{z}_j(i) - f_\ell(\mathbf{x}(i))]} \quad (33)$$

$$\mathbf{A}_\ell(i) = P(\ell) e^{-\frac{1}{2}[\mathbf{z}_j(i) - f_\ell(\mathbf{x}(i))]'\mathbf{R}^{-1}[\mathbf{z}_j(i) - f_\ell(\mathbf{x}(i))]} \mathbf{D}_\ell^T(i) \mathbf{R}^{-1} [\mathbf{z}_j(i) - f_\ell(\mathbf{x}(i))] \quad (34)$$

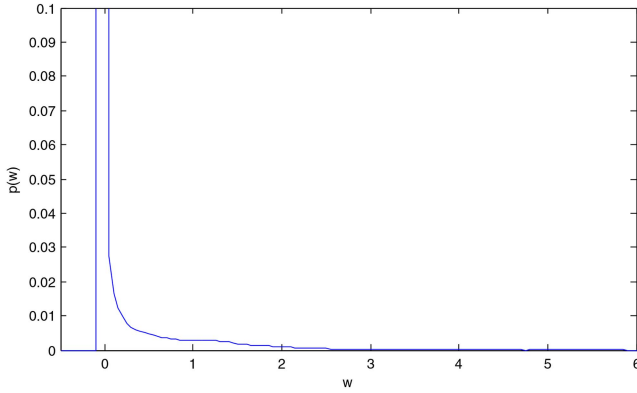


Fig. 9. The pdf of  $w$  (a single *clutter* measurement transformed by the multipath LLR).

Using the parameters given in Table I, the CRLB is 39.57 m and 0.6595 m/s for the position and velocity, respectively. From 10000 Monte Carlo runs for the lowest SNR = 4 dB the standard error of the sample variance is 0.5596 m for position, and 0.009327 m/s for velocity [3]. This gives the 95% (2-sigma) intervals of [38.45 m, 40.69 m] and [0.6408 m/s, 0.6782 m/s] for position and velocity, respectively. Since the RMSE values from the *multipath fusion ML-PMHT* (which were 40.67 m and 0.6760 m/s) are within these intervals, it is a *statistically efficient estimator*. We also include the CRLB for different values of the SNR and  $\tau$  in Table III.

## 7. FALSE TRACK AND TARGET TRACK DETECTION PROBABILITIES

We use the methods in [19, 20] to determine a threshold for the probability of false track,  $P_{FT}$ , and then calculate the probability of track detection,  $P_{DT}$ , for the first 2-D scenario with 4 dB SNR presented in Section 4.3.

### 7.1. Probability of False Track

We begin with the multipath LLR for a single measurement,  $\mathbf{z}_j(i)$ , and its corresponding amplitude LLR,  $\rho_j(i)$ ,

$$\Lambda_{i,j}[\mathbf{z}_j(i)] = \ln \left\{ \pi_0 + \pi_1 V \rho_j(i) \sum_{\ell=1}^{n_p} p[\mathbf{z}_j(i) | \mathbf{x}(i), \ell] P[\ell] \right\} \quad (35)$$

and treat  $\mathbf{z}_j(i) \in \mathbb{R}^2$  and  $\rho_j(i) \in \mathbb{R}^+$  as random variables. Equation (35) is a function that transforms these random variables into a new random variable  $w$ ,

$$w = \Lambda_{i,j}[\mathbf{z}_j(i)], \quad w \in \mathbb{R} \quad (36)$$

While in [19] it was possible to get a closed-form expression for the pdf of  $w$  when using the LLR for a single path ML-PMHT, here we cannot. The sum of exponentials that arises from the multiple paths prevents us from inverting equation (35). We must instead rely on a numerical or empirical approximation of the pdf of  $w$ . This empirical pdf of  $w$  is shown in Figure 9.

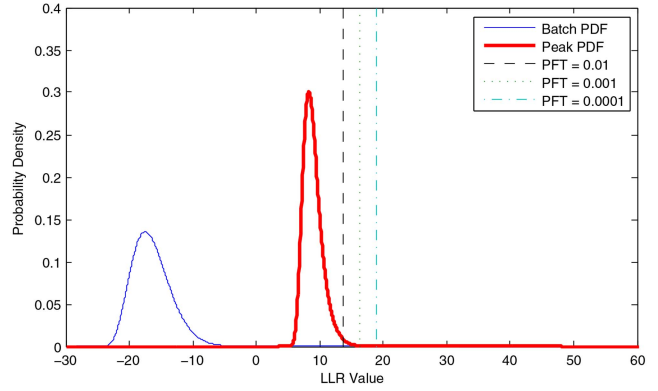


Fig. 10. The batch and peak pdfs (from *clutter*) along with thresholds for several values of  $P_{FT}$ .

We take the pdf of  $w$  and convolve it with itself  $N - 1$  times to find the pdf for a batch of  $N$  measurements from clutter. We refer to this resulting pdf as the “batch” pdf; it is the LLR pdf for a batch of measurements. We use  $N = 900$ , the expected number of measurements from clutter in one batch of measurements in our scenario. Again, following the methodology of [19], we must use the batch pdf to determine the “peak” pdf; this is the pdf of the maximum sample value from  $M$  samples from the batch pdf. This peak pdf is determined from extreme value theory. The determination of  $M$  is discussed in [19]; we use  $M = 10^7$ . The batch and peak pdfs, along with thresholds for several values of  $P_{FT}$  are shown in Figure 10.

### 7.2. Probability of Target Track Detection

Now that we have calculated thresholds using the desired values for  $P_{FT}$ , we can use a similar procedure to evaluate  $P_{DT}$  for these thresholds using the methods in [20]. We again begin with the multipath LLR for a single measurement given by equation (35), but with  $\mathbf{z}_j(i)$  as a Gaussian mixture (for the four paths) random variable (originating from the target) instead of a uniformly distributed random variable (originating from clutter). The approximation of the pdf of a single target measurement transformed by the multipath LLR pdf is shown in Figure 11.

We convolve this pdf with itself  $N - 1$  times to find the pdf for a batch of  $N$  target originated measurements. We use  $N = 20$ , the expected number of target originated measurements in one batch of  $N_w = 15$  scans in our scenario. We do not need to find a peak pdf from this batch pdf; the batch pdf is the peak pdf in this case. The batch pdf and the thresholds calculated in Section 7.1 for several values of  $P_{FT}$  are shown in Figure 12. A  $P_{FT}$  of  $10^{-4}$  yields  $(1 - P_{DT}) = 6 \cdot 10^{-9}$ .

## 8. CONCLUSIONS

We have developed an extension to the single target ML-PMHT to allow for the fusion of data from multiple signal propagation paths. We applied this algorithm to an OTHR scenario. We showed that, with low target

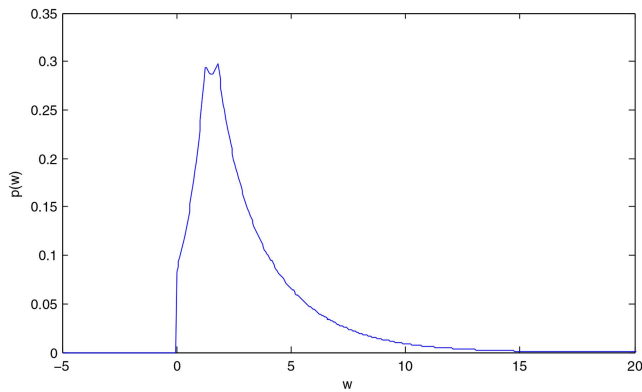


Fig. 11. The pdf of  $w$  (a single *target* measurement transformed by the multipath LLR).

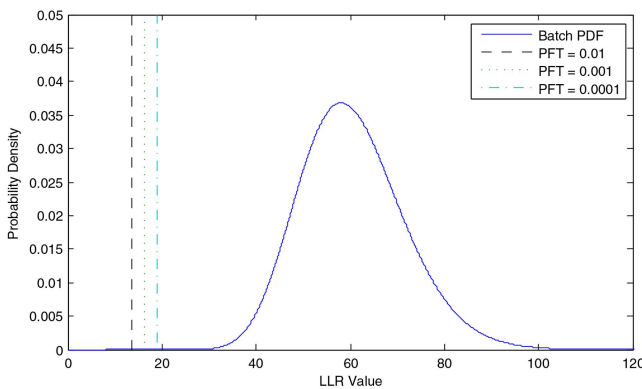


Fig. 12. The batch and peak pdfs (from the *target*) along with thresholds for several values of  $P_{FT}$ .

SNR even down to 4 dB post-signal processing, the fusion ML-PMHT has excellent track detection and accuracy in such a scenario and is statistically efficient. Consequently, the ML-PMHT holds great promise in increasing the sensitivity and robustness of the next generation OTHR.

The results indicate that the ML-PMHT can yield very high  $P_{DT}$  (probability of track detection) and very low  $P_{FT}$  (probability of false track). Future work would include using a more accurate ionosphere model.

## REFERENCES

- [1] R. H. Anderson, and J. L. Krolik  
Multipath track association for over-the-horizon radar using a bootstrapped statistical ionospheric model.  
*In Conference Record of the Thirty-Third Asilomar Conference on Signals, Systems, and Computers*, 1999, 8–14.
- [2] R. H. Anderson, and J. L. Krolik  
Track association for over-the-horizon radar with a statistical ionospheric model.  
*IEEE Transactions on Signal Processing*, 50, 11 (2002), 2632–2643.
- [3] Y. Bar-Shalom, X.-R. Li, and T. Kirubarajan  
*Estimation with Applications to Tracking and Navigation*.  
New York: Wiley, 2001.
- [4] Y. Bar-Shalom, P. K. Willett, and X. Tian  
*Tracking and Data Fusion*.  
Storrs, CT: YBS Publishing, 2011.
- [5] W. R. Blanding, P. K. Willett, and Y. Bar-Shalom  
Offline and real-time methods for ML-PDA track validation.  
*IEEE Transactions on Signal Processing*, 55, 5 (May 2007), 1994–2006.
- [6] S. B. Colegrove, and S. J. Davey  
The probabilistic data association filter with multiple non-uniform clutter regions.  
*In The Record of the IEEE 2000 International Radar Conference*, 2000, 65–70.
- [7] S. B. Colegrove, and S. J. Davey  
PDAF with multiple clutter regions and target models.  
*IEEE Transactions on Aerospace and Electronic Systems*, 39, 1 (Jan. 2003), 110–124.
- [8] S. B. Colegrove, S. J. Davey, and B. Cheung  
PDAF versus PMHT performance on OTHR data.  
*In Proceedings of the International Radar Conference, 2003*, Sep. 2003, 560–565.
- [9] S. V. Fridman, and L. J. Nickisch  
SIFTER: signal inversion for target extraction and registration.  
*Radio Science*, 39, 1 (2004).
- [10] H. Lan, Y. Liang, Q. Pan, F. Yang, and C. Guan  
An EM algorithm for multipath state estimation in OTHR target tracking.  
*IEEE Transactions on Signal Processing*, 62, 11 (2014), 2814–2826.
- [11] D. J. Percival, and K. A. B. White  
Multihypothesis fusion of multipath over-the-horizon radar tracks.  
*In Proceedings of SPIE 3373, Signal and Data Processing of Small Targets*, 1998.
- [12] G. W. Pulford, and R. J. Evans  
A multipath data association tracker for over-the-horizon radar.  
*IEEE Transactions on Aerospace and Electronic Systems*, 34, 4 (Oct. 1998), 1165–1183.
- [13] M. G. Rutten, S. Maskell, M. Briers, and N. J. Gordon  
Multipath track association for over-the-horizon radar using Lagrangian relaxation.  
*In Proceedings of SPIE Signal and Data Processing of Small Targets*, 2004.
- [14] M. G. Rutten, and D. J. Percival  
Comparison of track fusion with measurement fusion for multipath OTHR surveillance.  
*In Proceedings of the 4th International Conference on Information Fusion*, 2001.
- [15] M. G. Rutten, and D. J. Percival  
Joint ionospheric and target state estimation for multipath OTHR track fusion.  
*In Proceedings of SPIE Signal and Data Processing of Small Targets*, 2001.
- [16] T. Sathyan, T.-J. Chin, S. Arulampalam, and D. Suter  
A multiple hypothesis tracker for multitarget tracking with multiple simultaneous measurements.  
*IEEE Journal of Selected Topics in Signal Processing*, 7, 3 (Jun. 2013), 448–460.
- [17] S. Schoenecker, P. Willett, and Y. Bar-Shalom  
Maximum likelihood probabilistic multi-hypothesis tracker applied to multistatic sonar data sets.  
*In Proceedings of SPIE Conference on Signal Processing, Sensor Fusion, and Target Recognition*, Mar. 2011.
- [18] S. Schoenecker, P. Willett, and Y. Bar-Shalom  
ML-PDA and ML-PMHT: Comparing multistatic sonar trackers for VLO targets using a new multitarget implementation.  
*IEEE Journal of Oceanic Engineering*, 39, 2 (Apr. 2014), 303–317.

[19] S. Schoenecker, P. Willett and Y. Bar-Shalom  
Extreme-value analysis for ML-PMHT, part 1: target track-  
ability.  
*IEEE Transactions on Aerospace and Electronic Systems*,  
(2014 in print).

[20] S. Schoenecker, P. Willett and Y. Bar-Shalom  
Extreme-value analysis for ML-PMHT, part 2: false track  
probability.  
*IEEE Transactions on Aerospace and Electronic Systems*,  
(2014 in print).



**Kevin Romeo** received his B.S. degree in 2009 from the Department of Electrical and Computer Engineering, University of Connecticut, Storrs, USA in engineering physics. He is currently working towards the completion of his PhD degree in Electrical Engineering from the University of Connecticut. His main research interests lie in the areas of target tracking and detection.

**Yaakov Bar-Shalom** was born on May 11, 1941. He received the B.S. and M.S. degrees from the Technion, Israel Institute of Technology, in 1963 and 1967 and the Ph.D. degree from Princeton University in 1970, all in electrical engineering. From 1970 to 1976 he was with Systems Control, Inc., Palo Alto, California. Currently he is Board of Trustees Distinguished Professor in the Dept. of Electrical and Computer Engineering and Marianne E. Klewin Professor in Engineering at the University of Connecticut. He is also Director of the ESP (Estimation and Signal Processing) Lab. His current research interests are in estimation theory, target tracking and data fusion. He has published over 500 papers and book chapters in these areas and in stochastic adaptive control. He coauthored the monograph *Tracking and Data Association* (Academic Press, 1988), the graduate texts *Estimation and Tracking: Principles, Techniques and Software* (Artech House, 1993; translated into Russian, MGTU Bauman, Moscow, Russia, 2011), *Estimation with Applications to Tracking and Navigation: Algorithms and Software for Information Extraction* (Wiley, 2001), the advanced graduate texts *Multitarget-Multisensor Tracking: Principles and Techniques* (YBS Publishing, 1995), *Tracking and Data Fusion* (YBS Publishing, 2011), and edited the books *Multitarget-Multisensor Tracking: Applications and Advances* (Artech House, Vol. I, 1990; Vol. II, 1992; Vol. III, 2000). He has been elected Fellow of IEEE for “contributions to the theory of stochastic systems and of multi-target tracking.” He has been consulting to numerous companies and government agencies, and originated the series of Multitarget-Multisensor Tracking short courses offered via UCLA Extension, at Government Laboratories, private companies and overseas. During 1976 and 1977 he served as Associate Editor of the IEEE Transactions on Automatic Control and from 1978 to 1981 as Associate Editor of Automatica. He was Program Chairman of the 1982 American Control Conference, General Chairman of the 1985 ACC, and Co-Chairman of the 1989 IEEE International Conference on Control and Applications. During 1983–87 he served as Chairman of the Conference Activities Board of the IEEE Control Systems Society and during 1987–89 was a member of the Board of Governors of the IEEE CSS. He was a member of the Board of Directors of the International Society of Information Fusion (1999–2004) and served as General Chairman of FUSION 2000, President of ISIF in 2000 and 2002 and Vice President for Publications in 2004–13. In 1987 he received the IEEE CSS Distinguished Member Award. Since 1995 he is a Distinguished Lecturer of the IEEE AESS and has given numerous keynote addresses at major national and international conferences. He is co-recipient of the M. Barry Carlton Award for the best paper in the IEEE Transactions on Aerospace and Electronic Systems in 1995 and 2000 and recipient of the 1998 University of Connecticut AAUP Excellence Award for Research. In 2002 he received the J. Mignona Data Fusion Award from the DoD JDL Data Fusion Group. He is a member of the Connecticut Academy of Science and Engineering. In 2008 he was awarded the IEEE Dennis J. Picard Medal for Radar Technologies and Applications, and in 2012 the Connecticut Medal of Technology. He has been listed by academic.research.microsoft (top authors in engineering) as #1 among the researchers in Aerospace Engineering based on the citations of his work.





**Peter Willett** has been a faculty member in the Electrical and Computer Engineering Department at the University of Connecticut since 1986. Since 1998 he has been a Professor, and since 2003 an IEEE Fellow. He has published 187 journal and 395 conference proceedings articles. His primary areas of research have been statistical signal processing, detection, machine learning, communications, data fusion, and tracking. He is Editor-In-Chief of IEEE Signal Processing Letters and is IEEE Aerospace and Electronic Systems Vice President for Publications. He was editor-in-chief for IEEE Transactions on Aerospace and Electronic Systems from 2006–2011. For 1998–2005 he was associate editor for three active journals { IEEE Transactions on Aerospace and Electronic Systems (for Data Fusion and Target Tracking) and IEEE Transactions on Systems, Man, and Cybernetics, parts A and B. He remains associate editor for the IEEE AES Magazine, and ISIF's Journal of Advances in Information Fusion, and is a member of the editorial board of IEEE's Special Topics in Signal Processing journal and a senior editor for IEEE Signal Processing Letters. He is a member of the IEEE AESS Board of Governors and of the IEEE Signal Processing Society's Sensor-Array and Multichannel (SAM) technical committee (and is now Vice Chair).

# Tracking Targets with Multiple Measurements per Scan Using the Generalized PHD Filter

CHRISTOPH DEGEN  
FELIX GOVAERS  
WOLFGANG KOCH

The task of tracking targets, that generate more than one measurement per scan appears in several applications such as extended object and group tracking. In this case, the target (or group) extent implies that multiple measurements, drawn according to a spatial probability distribution, are measured per sensor-scan. However, applications exist where targets generate several measurements per sensor-scan, which are not geometrically correlated according to a distribution in the measurement space. An example for such an application is Blind Mobile Localization, which is the passive non-cooperative localization and tracking of mobile terminals in urban scenarios. In this paper a Probability Hypothesis Density filter for general models of target-generated measurements is applied to track targets with multiple measurements per scan, where the measurements do not necessarily have to be spatially related in the measurement space. Furthermore, the problem of numerical feasibility is identified and two ways of approximating the update equation of the generalized Probability Hypothesis Density filter are proposed. Finally, two numerical evaluations are carried out to assess sequential Monte Carlo-implementations of the generalized PHD-filter.

Manuscript received June 18, 2014; released for publication June 29, 2015.

Refereeing of this contribution was handled by Paolo Braca.

Authors' address: SDF Dept., Fraunhofer FKIE, Wachtberg, Germany (e-mail: {Christoph.Degen, Felix.Govaers, Wolfgang.Koch}@fkie.fraunhofer.de.)

1557-6418/15/\$17.00 © 2015 JAIF

## I. INTRODUCTION

The purpose of this paper is to investigate the applicability of the generalized PHD-filter [7] to scenarios with arbitrary target-measurement models. To this end, approximation conditions and a generalization of the probability of detection are developed, applied to two different scenarios and compared to existing standard approaches.

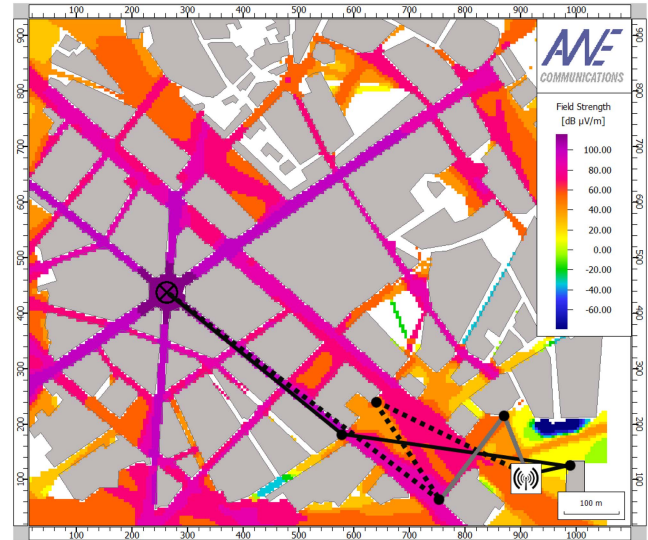


Fig. 1. Visualization of the field-strength prediction given by the ray-tracing simulation: For a given observer (black cross) mobile station (antenna) constellation the color at the emitter location indicates the received field-strength at the observer. Three multipaths are visualized (black solid, block dotted, gray) and the interaction points are plotted as black dots.

Due to the assumption that targets generate conditionally independent observations with at most one observation per target, the standard Probability Hypothesis Density (PHD)-filter [26] is not suited for applications where a target may generate multiple measurements in one sensor-scan. However, for the problem of extended object tracking several modifications of the standard PHD-filter are available (an excellent overview about existing methods is given in [28]). In [26] the target extent is modeled by a set of point scatterers, where each scatterer generates an individual measurement. In [27] an approximation is presented, based on the approximate Poisson model of Gilholm, Godsill, Maskell and Salmon [15], where the target extent is modeled by a spatial probability distribution. Furthermore, the set of measurements is preprocessed into associated groups which represent the individual targets. In [22] the target extent is modeled by random matrices and in [16], [17], [18], [20], [19] the approach is combined using PHD and cardinalized PHD-filters. Furthermore, techniques for reducing the number of measurement set partitions, which are essentially based on clustering measurements, are presented in these references. All methods mentioned have in common that they make explicit use of

the target extent. However, scenarios exist where targets generate multiple measurements which are not spatially related in the measurement space.

An example is given by Blind Mobile Localization (BML) [9], [2], [1], where an observer station (OS) tracks the state of an electromagnetic emitter in an urban environment. The boundary conditions of the problem imply that the OS has to determine the location of the mobile terminal by only inspecting the transmitted electromagnetic waves. In urban scenarios the effect of multipath propagation often is inevitable. This is due to physical effects on the electromagnetic wave of the signal such as reflection, diffraction, and scattering. As a consequence, the observer station receives multiple signals that have traveled along different paths. Each of these paths is distinct in either the time of arrival (ToA), azimuth (angle) of arrival (AoA) or the elevation (angle) of arrival (EoA). Hence, the mobile station (MS), which is a point target in the sense of [26], generates several observations, the so-called multipaths. A multipath is defined by a relative time of arrival (RToA), an AoA and an EoA. The distribution of measurements in the measurement space strongly depends on the environment and a measurement function would be discontinuous and difficult to model and calculate. This makes it impossible to find a general distribution of the multipath-measurements in the measurement space, which can be used for the association of targets and multipaths as it is done in [26] and [27], when preprocessing the measurement set.

In [9] a sequential Monte Carlo (SMC)-implementation of the standard Intensity filter (iFilter) [33], [32], which is closely related to the standard PHD-filter [26] and uses the same assumptions, is applied to the problem of BML. For the formulation of the likelihood-function context information of the urban environment is used in terms of a ray-tracing simulation, which predicts a set of multipaths for a given OS-MS constellation (see Figure 1, for details on the formulation of the likelihood-function see [9]). Due to the standard scatterer measurement model of the iFilter, it is assumed that each multipath represents an individual and independent measurement. Therefore, the estimated number of targets is not equal to the true number of targets, but to the number of multipaths which belong to a target. A sophisticated method for state extraction, considering the association possibilities between different multipath-sets and targets, is also presented in [9]. This state extraction scheme needs to be considered since the target generated measurement models of the standard PHD-filter and BML differ. Even though this solution yields satisfying results, it is an approximation, which assumes that each multipath represents an individual target, i.e., the creation of at most one observation per target, which is obviously not given for the application of BML. Taking into account all of the previous considerations a

PHD-filter for targets which generate multiple measurements per sensor-scan without a common distribution in the measurement space is needed.

The PHD-filter derivation using probability generating functionals (PGFLs) can be found in [26], [23], [24], [25] and [35]. A very detailed derivation of the PHD-filter using the PGFL-framework is presented in [21]. There, the PHD-filter is derived by modeling a PGFL, using Bayes theorem and afterwards the update (and prediction) equation of the PHD-filter is obtained by functional differentiation. To derive a PHD-filter for scenarios, which do not fulfill the standard assumptions, PGFLs represent an appropriate approach. In [36] and [26] examples of PGFLs for nonstandard targets are given and the calculation of the respective Gâteaux derivatives using compositions of so-called secular functions with functionals is proposed. In [7] the authors present a general chain rule (GCR) for functional-derivatives. This result is extended to locally convex topological spaces in [6] and closely related to the ideas presented in [36]. It can be used to determine the Gâteaux derivatives of complex PGFLs, e.g., for PGFLs which model target interaction [21, chapter 3]. Furthermore, in [7] a generalized PHD-filter is developed for arbitrary models of target-generated measurements and general clutter processes. The generalized PHD-filter possesses the ability to track targets, which are themselves point scatterers and create multiple measurements per scan, that are not drawn according to a spatial probability distribution in the measurement space.

In [10] the generalized PHD-filter is investigated and approximation conditions are developed. A small numerical evaluation is carried out to demonstrate that the proposed methods are applicable. This work extends the considerations made there by introducing a generalization of the probability of detection for targets that generate multiple measurements per sensor-scan. Furthermore, extensive numerical evaluations are carried out. Especially, the proposed methods are applied to the challenge of BML for the first time and compared to an existing approach.

In this paper, the generalized PHD-filter, using a Poisson-model for the clutter process, is investigated for the purpose of tracking targets with multiple measurements per sensor-scan. Thereby, a spatial distribution of the measurements is not assumed. Two approximations of the update equation of the generalized PHD-filter with Poisson-clutter are presented to reduce the number of partitions and thus the computational effort. To assess the proposed approach two numerical evaluations are carried out. First, a multi-target scenario, where two targets generate multiple correlated measurements, is investigated and different parameterizations of an SMC-implementation of the generalized PHD-filter are applied. The results are compared in terms of the

estimated number of targets, the mean runtime per update, the optimal sub pattern assignment (OSPA) metric and the root mean squared error (RMSE). Second, the generalized PHD-filter is applied to a single-target BML-scenario and it is compared to an adaption of the standard iFilter, presented in [9] in terms of the RMSE and the processing time. A detailed investigation of the different likelihood-functions in the BML-scenario of the two compared approaches closes the numerical evaluation.

This paper is organized as follows. Section II gives an overview of the relation between PGFLs and the PHD-filter. Section III considers the formulation of the problem. In III-A the generalized PHD-filter with Poisson clutter model is presented. Section III-B investigates the computational complexity for scenarios where target measurements are not spatially related. Section IV-A proposes two ways of approximating the update equation of the generalized PHD-filter with Poisson-clutter and without using a distance-criterion in the measurement space. Two numerical evaluations are carried out in Section V. In Section V-A different parameterizations of SMC-implementations of the generalized PHD-filter are applied to a multi-target scenario. The generalized PHD-filter is applied to a BML-scenario and compared to the standard iFilter adaption presented in [10] in Section V-B. Conclusions are drawn and future work is presented in Section VI.

## II. PROBABILITY GENERATING FUNCTIONALS AND THE PHD-FILTER

This section follows the considerations and notation of [21], which is based on [26], [23], [24], [25], [34], [8] and [30]. It has to be pointed out that all the work presented in this section has been presented first in [26], [23], [24], [25], [34], [8] and [30]. However, the notation of this paper is based on [21] and [35] since the authors consider it to be more intuitive.

This section provides background information about the connection between PGFLs and the PHD-filter which are necessary to understand following sections. However, for details the authors refer to [26], [21], [34] or [35], which explains the connection between the PHD- and the Intensity-filter, using PGFLs.

To begin with, let  $\mathcal{X}$  be a separable metric space. A typical choice for  $\mathcal{X}$  is  $\mathbb{R}^d$ ,  $d > 0$ , which is sufficient for the most applications appearing in target tracking. Then the space of sets of points in  $\mathcal{X}$  is defined by

$$E_{\mathcal{X}} := \emptyset \cup \bigcup_{n \geq 1} \mathcal{X}^{(n)}, \quad (1)$$

where  $\mathcal{X}^{(n)}$  is the space of sets of size  $n \in \mathbb{N}$ , that is

$$\mathcal{X}^{(n)} := \{\{x_1, \dots, x_n\} \mid x_i \in \mathcal{X}, i = 1, \dots, n\}. \quad (2)$$

When interpreting  $\mathcal{X}$  as the target state space in a classical multi-target tracking scenario, where the number of present targets are not known,  $E_{\mathcal{X}}$  can be interpreted

as the collection of all possible combinations of target states at a given time-step. It is assumed, that each element  $\varphi \in E_{\mathcal{X}} \setminus \emptyset$  is locally finite, that is each bounded subset of  $\mathcal{X}$  must only contain a finite number of points of  $\varphi$  and simple, i.e.,

$$\forall x_i, x_j \in \varphi, \quad x_i = x_j \Rightarrow i = j. \quad (3)$$

In terms of target tracking this translates to the assumptions that only finitely many targets can be present in a scenario and that no two targets share the same state. A stochastic process in the sense of [34] is defined as a measurable mapping

$$\Phi : (\Omega, \mathcal{F}, \mathbb{P}) \rightarrow (E_{\mathcal{X}}, \mathcal{B}(E_{\mathcal{X}})), \quad (4)$$

where  $(\Omega, \mathcal{F}, \mathbb{P})$  is an arbitrary probability space and  $\mathcal{B}(E_{\mathcal{X}})$  denotes the Borel  $\sigma$ -algebra of  $E_{\mathcal{X}}$ . Note that due to this definition the stochastic model of the point process is defined on the probability space  $(\Omega, \mathcal{F}, \mathbb{P})$ , since  $\Phi$  is defined to be a measurable mapping. The associated counting function for an arbitrary  $B \in \mathcal{B}(\mathcal{X})$  is defined by

$$N(B) : (E_{\mathcal{X}}, \mathcal{B}(E_{\mathcal{X}})) \rightarrow (\mathbb{N}, \mathcal{B}(\mathbb{N})) \\ \varphi \mapsto N_{\varphi}(B) := |B|, \quad (5)$$

which counts the number of elements in  $B$  and is measurable. Then the composition,

$$N(B) \circ \Phi = N_{\Phi(\cdot)}(B) : (\Omega, \mathcal{F}, \mathbb{P}) \rightarrow (\mathbb{N}, \mathcal{B}(\mathbb{N})) \quad (6)$$

is measurable, since the composition of measurable functions is measurable again. It can be interpreted as a counting-function of the outcomes of the stochastic process. In target-tracking for example  $N(B) \circ \Phi$  yields the number of targets in the area  $B \in \mathcal{B}(\mathcal{X})$  for a specific element in the probability space  $(\Omega, \mathcal{F}, \mathbb{P})$ . The intensity measure (first order moment, PHD, etc.) is defined for an arbitrary  $B \in \mathcal{B}(\mathcal{X})$  by the expectation value

$$\mathbb{E}[N_{\Phi(\cdot)}(B)] = \int_{\Omega} N_{\Phi(\omega)}(B) \mathbb{P}(d\omega) = \int_{E_{\mathcal{X}}} N_{\varphi}(B) P_{\Phi}(d\varphi) \quad (7)$$

$$=: \mu_{\Phi}(B), \quad (8)$$

and thus yields the expected number of points in  $B$ . In target tracking  $\mu_{\Phi}(B)$  for  $B \in \mathcal{B}(\mathcal{X})$  denotes the expected number of targets in some area  $B \subseteq \mathcal{X}$ . Therefore, the intensity measure is not a probability density function. Instead, it can be described as a function of subsets of  $\mathcal{X}$  that determines the expected number of elements therein.  $P_{\Phi}$  denotes the pushforward (image) measure of  $\mathbb{P}$ , using the point process  $\Phi$ . For any bounded and Lebesgue-integrable function

$$h : (\mathcal{X}, \mathcal{B}(\mathcal{X})) \rightarrow (\mathbb{R}, \mathcal{B}(\mathbb{R})) \quad (9)$$

the PGFL of the point process  $\Phi$  is defined by

$$G_{\Phi}[h] := \sum_{n \geq 0} \int_{\mathcal{X}^{(n)}} \prod_{i=1}^n h(x_i) P_{\Phi}(d\{x_1, \dots, x_n\}) \quad (10)$$

$$= \sum_{n \geq 0} \frac{1}{n!} \int_{\mathcal{X}^n} \prod_{i=1}^n h(x_i) f_{\Phi}(x_1, \dots, x_n) dx_1 \dots dx_n, \quad (11)$$

where  $f_{\Phi} : \mathcal{X}^n \rightarrow \mathbb{R}$  is the multi-object density of the corresponding Jannossy measure and defined such that

$$\int_B n! P_{\Phi}(d\{x_1, \dots, x_n\}) = \int_B f_{\Phi}(x_1, \dots, x_n) dx_1 \dots dx_n \quad (12)$$

holds for all  $B \in \mathcal{B}(E_X)$ . Equation (11) holds due to the assumed absolute continuity of  $P_{\Phi}$  and the application of the Radon-Nikodym Theorem (for details see [26] or [21, p. 16]).

To illustrate the connection of PGFLs and the PHD-filter, the update equation (the prediction equation is derived analogously) is exemplarily derived using Bayes theorem, the definition of PGFLs and functional differentiation. For details see [26], [21, p. 17–p. 24] or [35].

Let  $X \subseteq \mathbb{R}^d$ ,  $d > 0$  be the target and  $Z \subseteq \mathbb{R}^l$ ,  $l > 0$  be the measurement space. Then

$$E_X = \emptyset \cup \bigcup_{n \geq 1} X^{(n)} \quad (13)$$

and

$$E_Z = \emptyset \cup \bigcup_{n \geq 1} Z^{(n)} \quad (14)$$

are defined analogously to (1). According to the definition of conditional probability, the multi-joint object density is defined on the product space  $E_Z \times E_X$  by

$$\begin{aligned} f_{Z,X} : E_Z \times E_X &\rightarrow \mathbb{R} \\ (Z, X) &\mapsto f_{Z,X}(Z, X) = L_{Z|X}(Z | X) f_X(X), \end{aligned} \quad (15)$$

where  $L_{Z|X} : E_Z \times E_X \rightarrow \mathbb{R}$  denotes the multi-object likelihood-function on  $E_Z \times E_X$ ,  $f_X : E_X \rightarrow \mathbb{R}$  is the distribution of  $X$  on  $E_X$ . In the same way Bayes theorem for point processes is given by

$$\begin{aligned} f_{X|Z} : E_X \times E_Z &\rightarrow \mathbb{R} \\ (X, Z) &\mapsto f_{X|Z}(X | Z) = \frac{L_{Z|X}(Z | X) f_X(X)}{\int_{E_X} \frac{1}{|X'|!} L_{Z|X}(Z | X') f_X(X') dX'}, \end{aligned} \quad (16)$$

where  $f_{X|Z} : E_X \times E_Z \rightarrow \mathbb{R}$  denotes the conditional multi-object density on  $E_X \times E_Z$ . By multiplying (16) with  $(1/|X'|!) \prod_{x \in X'} h(x)$  and integrating over  $E_X$  the PGFL-form of Bayes theorem is obtained by

$$G_{X|Z}[h | Z] = \frac{\int_{E_X} \frac{1}{|X'|!} \prod_{x \in X'} h(x) L_{Z|X}(Z | X') f_X(X') dX'}{\int_{E_X} \frac{1}{|X'|!} L_{Z|X}(Z | X') f_X(X') dX'}. \quad (17)$$

In the following we are interested in an alternative representation of (17). To this end, we first determine the PGFLs of the multi-object likelihood-function and derive afterwards the PGFL of the joint state under the following assumptions (see [26], [35, chapter 5.2]).

- 1) The target process is a Poisson Point Process (PPP) on  $X$  with intensity function  $\mu_S(\cdot)$ .
- 2) Conditioned on the event  $X = \{x_1, \dots, x_n\}$ , the measurement process is the superposition of  $n$  mutually independent, identical, target-oriented measurement-processes and a given PPP clutter process on  $Z$  with intensity function  $\lambda_C(\cdot)$ .
- 3) A target generates at most one measurement in  $Z$ .

First, the PGFL of the multi-object likelihood-function  $L_{Z|X}(Z | X)$  is considered for different cases. If  $X = \emptyset$ , the PGFL is given by

$$\begin{aligned} G_{Z|X}[g | \emptyset] &:= G_{\text{clutter}}[g] \\ &:= \exp \left( \lambda \left( \int_Z c(z) g(z) dz - 1 \right) \right) \end{aligned} \quad (18)$$

due to assumption (2), where  $\lambda \in \mathbb{R}$  denotes the average number of clutter and each false alarm is distributed according to  $c : Z \rightarrow [0, 1]$ . Second, let  $X = \{x\}$ . Then it holds, that

$$\begin{aligned} G_{Z|X}[g | \{x\}] &= \int_{E_Z} \frac{1}{|Z'|!} \prod_{z \in Z'} g(z) L_{Z|X}(Z' | \{x\}) dZ' \\ &= L_{Z|X}(\emptyset | \{x\}) + \int_Z g(z) L_{Z|X}(\{z\} | \{x\}) dz \\ &=: G_{\text{obs}}[g | x], \end{aligned} \quad (19)$$

where (19) is given due to assumption (3) and

$$g : (Z, \mathcal{B}(Z)) \rightarrow (\mathbb{R}, \mathcal{B}(\mathbb{R})) \quad (20)$$

denotes a bounded and Lebesgue integrable test-function. Let  $\hat{L}_{Z|X}$  and  $p_D$  be defined on  $Z \times X$  and  $X$ , respectively such that

$$L_{Z|X}(\{z\} | \{x\}) = p_D(x) \hat{L}_{Z|X}(z | x) \quad (21)$$

and

$$L_{Z|X}(\emptyset | \{x\}) = 1 - p_D(x), \quad (22)$$

where  $x \in X$ ,  $z \in Z$ . This implies

$$G_{\text{obs}}^{\text{PHD}}[g | x] = 1 - p_D(x) + p_D(x) \int_Z g(z) \hat{L}_{Z|X}(z | x) dz, \quad (23)$$

where  $x \in X$ . From now on due to simplicity  $\hat{L}_{Z|X}$  is denoted by  $L_{Z|X}$ . Third, let  $X = \{x_1, \dots, x_n\}$ . Then due to assumption (2) the PGFL is given by

$$G_{Z|X}[g | \{x_1, \dots, x_n\}] = G_{\text{clutter}} \prod_{i=1}^n G_{\text{obs}}^{\text{PHD}}[g | x_i]. \quad (24)$$

The next step is to find an expression for the PGFL of the joint state. It holds that

$$G_{Z,X}[g, h] = \int_{E_X} \frac{1}{|X|!} \prod_{x \in X} h(x) \int_{E_Z} \frac{1}{|Z|!} \prod_{z \in Z} g(z) \quad (25)$$

$$L_{Z|X}(Z | X) f_X(X) dZ dX$$

$$= \int_{E_X} \frac{1}{|X|!} \prod_{x \in X} h(x) G_{\text{clutter}} \prod_{i=1}^n G_{\text{obs}}[g | x] f_X(X) dX \quad (26)$$

$$= G_{\text{clutter}} G_X[h G_{\text{obs}}^{\text{PHD}}[g | \cdot]], \quad (27)$$

where due to assumption (1)  $G_X$  is given by

$$G_X[h] := \exp(\mu(\int_X s(x)h(x)dx - 1)). \quad (28)$$

Equation (25) is given due to the definition of conditional probability and (26) holds since

$$G_{Z|X}[g | x] = \int_{E_Z} \frac{1}{z!} \prod_{z \in Z} g(z) L_{Z|X} dZ \quad (29)$$

and (24). The second factor of (27) denotes a composition of functionals, called branching form of the respective PGFL and holds due to the definition of PGFLs. Note, that (27) is obtained by considering

$$G_{\text{clutter}} \prod_{i=1}^n G_{\text{obs}}[g | \cdot] : X \rightarrow \mathbb{R} \quad (30)$$

as a test-function with respect to  $x \in X$ . In (28)  $\mu$  denotes the average number of targets and  $s : \mathbb{R} \rightarrow [0, 1]$  is the distribution of the targets.

In the following the derivative of a PGFL is needed. Therefore, let  $G$  be a PGFL defined as in (11). Then the Gâteaux derivative of  $G[h]$  with respect to the variation  $\omega$  is defined by

$$\delta G[h; \omega] := \lim_{\epsilon \searrow 0} \frac{G[h + \epsilon \omega] - G[h]}{\epsilon}, \quad (31)$$

where  $\omega$  is a real-valued, bounded and Lebesgue-integrable function on  $X$  (or  $Z$ ). The differentiation with respect to multiple real-valued, bounded and integrable variations  $\omega_1, \dots, \omega_m$  is defined iteratively, that is

$$\delta^m G[h; \omega_1, \dots, \omega_m] = \delta(\delta^{m-1} G[h; \omega_1, \dots, \omega_{m-1}]; \omega_m). \quad (32)$$

In [26] and [35] it is shown that

$$L_{Z|X}(Z | X) = \delta^m G_{Z|X}[g | X; \delta_{z_1}, \dots, \delta_{z_m}]|_{g=0} \quad (33)$$

and thus

$$G_{X|Z}[h | Z] = \frac{\delta^m G_{Z,X}[g, h; \delta_{z_1}, \dots, \delta_{z_m}]|_{g=0}}{\delta^m G_{Z,X}[g, 1; \delta_{z_1}, \dots, \delta_{z_m}]|_{g=0}} \quad (34)$$

holds. Here,  $\delta_a$  denotes Dirac delta at the point  $a$ .

The Gâteaux derivative with respect to the Dirac delta from (33) and (34) has to be investigated carefully, since Dirac delta is not a proper function [40], [12], [14], [38] and thus the ordinary Gâteaux derivative

[13, p. 406] is not defined. However, it can be proven that (31) is well-defined for a large class of PGFLs [11], in the sense that Dirac delta is approximated by a series of test-functions, called approximate identities or Dirac sequences [3, p. 114]. In [11] it is shown that the Gâteaux derivative with respect to the Dirac delta from (33) and (34) can be defined using approximate identities for the class of PGFLs

$$\mathcal{P}_2 \equiv \left\{ \Psi : \mathcal{H} \rightarrow \mathbb{R} \mid \Psi(h) = \sum_{n \geq 0} \frac{a_n}{n!} \cdot \int_{\mathcal{X}^n} \prod_{i=1}^n h(x_i) f_{\Phi}(x_1, \dots, x_n) dx_1 \cdots dx_n \right\}, \quad (35)$$

$$\mathcal{H} \equiv \{h : \mathcal{X} \rightarrow \mathbb{R} \mid h \text{ is bounded and Lebesgue-integrable}\}, \quad (36)$$

$a_n \in [0, 1]$ , where the multi-object density  $f_{\Phi}(x_1, \dots, x_n)$ ,  $x_1, \dots, x_n \in \mathcal{X} \subseteq \mathbb{R}$  is either continuous, bounded and in  $L^1(\mu; \mathcal{X}^n)$  or in  $C_0^0(\mathcal{X}^n)$ , that is a continuous function with compact support,  $n \in \mathbb{N}$ . Furthermore, in [11] and [37] it is shown that many well known tracking filters can be represented by PGFLs from (35).

Finally, the update equation for the first order moment (or PHD)  $\mu_{X|Z}$  is given by an additional functional derivative

$$\mu_{X|Z}(x | z_1, \dots, z_m) = \delta G_{X|Z}[h | Z; \delta_x]|_{h=1}. \quad (37)$$

A computation of (34) and (37) yields the update equation of the PHD-filter

$$\begin{aligned} \mu_{X|Z}(x | z_1, \dots, z_m) = & \mu s(x) \left( (1 - p_D(x)) \right. \\ & \left. + \sum_{z \in Z} \frac{p_D(x) L_{Z|X}(z | x)}{\lambda c(z) + \mu \int_X p_D(x) s(x) \hat{L}_{Z|X}(z | x)} dx \right). \end{aligned} \quad (38)$$

### III. FORMULATION OF THE PROBLEM

#### A. The Generalized PHD-Filter

The previous section shows how to obtain the update equation of the PHD-filter by inspecting PGFLs. When deriving the update equation using PGFLs, essentially three steps can be identified.

- 1) Definition of the PGFL of the multi-object likelihood-function  $G_{Z|X}[g | \{x\}]$  (see (19)–(24))
- 2) Definition of the PGFL of the joint state  $G_{Z,X}$  (see (25)–(28)).
- 3) Functional differentiation to determine the intensity (see (34) and (37)).

In [7] the authors present the GCR, which is a generalization of the fourth chain rule for functional

derivatives from [26]. This can be used to differentiate complex PGFLs. Furthermore, a PHD-filter for general target-generated measurement models and a general clutter process is developed using the GCR. If the clutter is assumed to be Poisson, the update equation of the general PHD-filter for arbitrary number of measurements per target is given by

$$\mu_{X|Z}(x | z_1, \dots, z_m) = \mu_S(x) \left( L_{Z|X}(\emptyset | x) + \frac{\sum_{\pi \in \Pi_{(1:m)}} \left( \sum_{j=1}^{|\pi|} L_{Z|X}(i(\pi_j) | x) \prod_{k=1, k \neq j}^{|\pi|} \eta_{\pi, k} \right)}{\sum_{\pi \in \Pi_{(1:m)}} \prod_{j=1}^{|\pi|} \eta_{\pi, j}} \right), \quad (39)$$

where

$$\eta_{\pi, j} := \mathbb{1}_{\{a:|a|=1\}}(\pi_j) \lambda c(i(\pi_{j,1})) + \mu \int s(x) p_D(x) \cdot L_{Z|X}(i(\pi_{j,1}), \dots, i(\pi_{j,|\pi_j|}) | x) dx, \quad (40)$$

and  $\Pi_{(1:m)}$  denotes the set of all partitions of  $\{\delta_{z_1}, \dots, \delta_{z_m}\}$ , e.g.,  $\Pi_{(1:2)} = \{\{\{\delta_{z_1}\}\}, \{\{\delta_{z_2}\}\}, \{\{\delta_{z_1}, \delta_{z_2}\}\}\}$ . The value of the likelihood-function  $L_{Z|X}(\emptyset | x)$  represents the probability of a non-detection of target  $x$ . The function  $i: \Pi_{(1:m)} \rightarrow \mathcal{P}(Z)$  is defined as  $i(\{\delta_{z_1}, \dots, \delta_{z_m}\}) = (z_1, \dots, z_m)$ , for all  $j \in \{1, \dots, m\}$  and

$$\mathbb{1}_{\{a:|a|=1\}}(\pi) = \begin{cases} 1, & \text{if } |\pi| = 1 \\ 0, & \text{otherwise} \end{cases} \quad (41)$$

defines the indicator function. As mentioned in [7] the probability of detection  $p_D$  in (39) is defined more generally as in the standard PHD-filter. A discussion on this can be found in Section IV-C.

The derivation of (39) can be done analogously to the standard PHD-filter as described in Section II for

$$G_{\text{obs}}[g | x] := L_{Z|X}(\emptyset | x) + \sum_{n \geq 1} \frac{1}{n!} \int_{Z^{(n)}} \prod_{j=1}^n g(z_j) L_{Z|X}(z_1, \dots, z_n | x) dz_1 \dots dz_n \quad (42)$$

instead of (23), using the GCR. The difference between (42) and (23) is that in the second summand of (42) a sum occurs. This is due to the fact that the generalized PHD filter does not assume that a target generates at most one measurement. Instead a target can generate an arbitrary number of measurements and thus all sets of size  $n$ , that is  $Z^{(n)}$  (see definition (1)) need to be considered. Another possible approach for deriving the update equation of the generalized PHD-filter is to use so-called secular functions and the technique of automatic differentiation as it is done in [36].

Note that (39) can handle correlated measurements originating from a specific target, since only the assumption that the measurement process is the superposition of  $n$  mutually independent (conditioned on  $X = \{x_1, \dots, x_n\}$ ) target-oriented measurement-processes is needed for the derivation of the update equation. In particular, the measurements are not assumed to be independent conditioned on a specific target state. Measurements originating from different targets cannot be correlated since in the derivation of the generalized PHD-filter in [7] the corresponding measurement processes need to be mutually independent.

## B. Computational Complexity of the General PHD-Filter

The update equation of the PHD-filter for targets with a general target-generated measurement model (39) and Poisson clutter is highly complex due to the combinatorial sum numerically. The number of partitions is growing exponentially with the number  $n$  of measurements and is given by the Bell number  $B_n$ . The exponential-growth of the Bell number is visualized in Figure 2 and one can see that for an application of (39) approximations are inevitable. In [16], [17], [18], [20], [19] and [39] clustering approaches, which are essentially based on the spatial relation of measurements, are used to reduce the number of partitions. These approximations are possible, if the measurements of a target are spatially related in the measurement space. However, scenarios exist where a target generates multiple measurements per scan which are not spatially related in the measurement space, e.g., BML. For such scenarios, the partitions in equation (39) need to be reduced without using any information about the distribution of measurements in the measurement space.

## IV. APPROXIMATION OF THE UPDATE EQUATION

As mentioned in the previous section an evaluation of all feasible measurement set partitions is not possible due to the exponential-growth of the number of partitions with increasing set size. Moreover, a reduction of the number of partitions by the application of clustering methods is not applicable if measurements that belong to a specific target are not spatially related in the measurement space. To this end, two novel approaches are presented in the following section, which approximate the update equation of the generalized PHD filter, by reducing the number of investigated partitions without assuming an underlying spatial distribution of the measurements belonging to a specific target in the measurement space. Furthermore, a generalized definition of the probability of detection is presented for the generalized PHD filter.

### A. Incorporation of a Priori Information

The first proposed approximation of equation (39) considers available a priori information about the num-

ber of generated measurements per target- and sensor-scan. The idea is to restrict the possible number of generated measurements, that is to assume that a target generates at least  $N_{\min} \in \mathbb{N}$  and at most  $N_{\max} \in \mathbb{N}$  measurements per sensor-scan. Even though it might seem obvious how a restriction of the number of measurements per target will influence the update equation of the generalized PHD-filter, a detailed derivation is carried out in the following to demonstrate how a priori information and specific assumptions can be incorporated via a mathematically correct approach into an existing generalized PHD-filter.

To derive the respective PHD-update equation the general higher order chain rule, presented in [6] is used. As in the previous section let

$$g : (Z, \mathcal{B}(Z)) \rightarrow (\mathbb{R}, \mathcal{B}(\mathbb{R})) \quad (43)$$

and

$$h : (X, \mathcal{B}(X)) \rightarrow (\mathbb{R}, \mathcal{B}(\mathbb{R})) \quad (44)$$

be bounded and Lebesgue-integrable test-functions. First, the PGFL of the joint state is given analogously to equation (27) by

$$G_{Z,X}[g, h] = G_{\text{clutter}} G_X[hG_{\text{obs}}[g | \cdot]] = (\exp \circ f)[g, h], \quad (45)$$

where

$$f[g, h] := \lambda \left( \int c(z)g(z)dz - 1 \right) + \mu \left( \int s(x)h(x)G_{\text{obs}}[g | x]dx - 1 \right) \quad (46)$$

and the approximated PGFL of the likelihood-function  $G_{\text{obs}}[g | \cdot]$ , which incorporates the a priori knowledge on the number of measurements per target is defined by

$$G_{\text{obs}}[g | x] := L_{Z|X}(\emptyset | x) + \sum_{n=N_{\min}}^{N_{\max}} \frac{1}{n!} \int_{Z^n} \prod_{j=1}^n g(z_j) L_{Z|X,n}(z_1, \dots, z_n | x) dz_1 \dots dz_n. \quad (47)$$

Note, that the key to obtain a PGFL-derivable filters with specific target-generated measurement models, only  $G_{\text{obs}}[g | \cdot]$  needs to be adapted. Therefore, incorporating assumptions/information that is scenario specific, can be done by modifying  $G_{\text{obs}}[g | \cdot]$  accordingly. Applying the general higher order chain rule to determine the functional derivative of (45) with respect to impulses yields

$$\begin{aligned} \delta^m G_{Z,X}[g, h; \delta_{z_1}, \dots, \delta_{z_m}] &= \delta^m (\exp \circ f)[g, h; \delta_{z_1}, \dots, \delta_{z_m}] \\ &= \sum_{\pi \in \Pi_{(1:m)}} \delta^{|\pi|} \exp(f[g, h]; \xi_{\pi_1}[g, h], \dots, \xi_{\pi_{|\pi|}}[g, h]) \\ &= \sum_{\pi \in \Pi_{(1:m)}} \exp(f[g, h]) \prod_{j=1}^{|\pi|} \xi_{\pi_j}[g, h], \end{aligned} \quad (48)$$

where

$$\begin{aligned} \xi_{\omega}[g, h] &= \delta^{|\omega|} f[g, h; \omega_1, \dots, \omega_{|\omega|}] \\ &= \mu \int s(x)h(x)\delta^{|\omega|} G_{\text{obs}}[g; \omega_1, \dots, \omega_{|\omega|}] dx. \end{aligned} \quad (49)$$

For the evaluation of (49) the functional derivative of definition (47) has to be considered. Therefore, let  $\omega$  be an arbitrary element of a partition from  $\Pi_{(1:m)}$ . Then, the Gâteaux derivative of the functional is given by

$$\begin{aligned} \delta^{|\omega|} G_{\text{obs}}[g; \omega_1, \dots, \omega_{|\omega|}] &= \sum_{n=N_{\min}}^{N_{\max}} \frac{1}{n!} \cdot n \cdot (n-1) \cdot \dots \cdot (n-|\omega|+1) \\ &\cdot \int_{Z^{n-|\omega|}} \prod_{j=1}^{n-|\omega|} g(z'_j) L_{Z|X}(i(\omega), z'_1, \dots, z'_{n-|\omega|} | x) dz'_1 \dots dz'_{n-|\omega|} \end{aligned} \quad (50)$$

if  $|\omega| < N_{\min}$ . If  $|\omega| \in \{N_{\min}, \dots, N_{\max} - 1\}$  it is given by

$$\begin{aligned} \delta^{|\omega|} G_{\text{obs}}[g; \omega_1, \dots, \omega_{|\omega|}] &= \left( L_{Z|X}(i(\omega) | x) \right. \\ &+ \sum_{n=N_{\min}}^{N_{\max}} \frac{1}{n!} \cdot n \cdot (n-1) \cdot \dots \cdot (n-|\omega|+1) \\ &\cdot \left. \int_{n=N_{\min}}^{N_{\max}} \prod_{j=1}^{n-|\omega|} g(z'_j) L_{Z|X}(i(\omega), z'_1, \dots, z'_{n-|\omega|} | x) dz'_1 \dots dz'_{n-|\omega|} \right) \end{aligned} \quad (51)$$

and if  $|\omega| = N_{\max}$  it is equal to

$$\delta^{|\omega|} G_{\text{obs}}[g; \omega_1, \dots, \omega_{|\omega|}] = L_{Z|X}(i(\omega) | x). \quad (52)$$

If  $|\omega| > N_{\max}$  the derivative is

$$\delta^{|\omega|} G_{\text{obs}}[g; \omega_1, \dots, \omega_{|\omega|}] = 0. \quad (53)$$

Thus,

$$\begin{aligned} \delta^{|\omega|} G_{\text{obs}}[0; \omega_1, \dots, \omega_{|\omega|}] &= \begin{cases} L_{Z|X}(i(\omega) | x), & \text{if } |\omega| \in \{N_{\min}, \dots, N_{\max}\} \\ 0, & \text{otherwise} \end{cases} \end{aligned} \quad (54)$$

$$= 1_A(\omega) L_{Z|X}(i(\omega) | x), \quad (55)$$

where  $A := \{a : |a| \in \{N_{\min}, \dots, N_{\max}\}\}$ . In the following, the short-hand notation from (55) is used. Given the functional derivative of the PGFL of the joint state with respect to impulses the update equation of the corresponding PHD-filter can be determined. It is given by

$$\mu_{X|Z}(x | z_1, \dots, z_m) = \frac{\delta^{m+1} G_{Z,X}[0, 1; \delta_{z_1}, \dots, \delta_{z_m}, \delta_x]}{\delta^m G_{Z,X}[0, 1; \delta_{z_1}, \dots, \delta_{z_m}]} \quad (56)$$

$$= \left( \sum_{\pi \in \Pi_{(1:m)}} \prod_{j=1}^{|\pi|} \xi_{\pi_j}[0, 1] \right)^{-1} \left( \sum_{\pi \in \Pi_{(1:m)}} \delta B_{\pi}[0, 1; \delta_x] \right), \quad (57)$$

where

$$B_{\pi}[g, h] := f[g, h] \cdot \prod_{j=1}^{|\pi|} \xi_{\pi_j}[g, h] \quad (58)$$

and

$$\begin{aligned} \delta B_{\pi}[g, h; \delta_x] &= \mu_S(x) G_{\text{obs}}[g | x] \prod_{j=1}^{|\pi|} \xi_{\pi_j}[g, h] \\ &+ \sum_{j=1}^{|\pi|} \mu_S(x) \delta^{|\pi_j|} G_{\text{obs}}[g; \pi_{j,1}, \dots, \pi_{j,|\pi_j|} | x] \\ &\cdot \prod_{k=1, k \neq j}^{\pi} \xi_{\pi_k}[g, h] \end{aligned} \quad (59)$$

The evaluation of (57) yields the update equation of the approximated generalized PHD-filter with Poisson-clutter. It is given by

$$\begin{aligned} \mu_{X|Z}(x | z_1, \dots, z_m) &= \mu_S(x) \left( L_{Z|X}(\emptyset | x) \right. \\ &\left. + \frac{\sum_{\pi \in \Pi_{(1,m)}} \sum_{j=1}^{|\pi|} 1_A(\pi_j) L_{Z|X}(i(\pi_j) | x) \prod_{k=1, k \neq j}^{|\pi|} \eta_{\pi,k}}{\sum_{\pi \in \Pi_{(1,m)}} \prod_{j=1}^{|\pi|} \eta_{\pi,j}} \right), \end{aligned} \quad (60)$$

where

$$\begin{aligned} \eta_{\pi,j} &:= \xi_{\pi_j}[0, 1] = 1_{\{|a|_a=1\}}(\pi_j) \lambda_C(i(\pi_{j,1})) + \\ &\mu \int s(x) 1_A(\pi_j) p_D(x) L_{Z|X}(i(\pi_j) | x) dx. \end{aligned} \quad (61)$$

Due to the fact that some summands of equation (60) are zero, computational effort can easily be saved. A summand of the sum over all partitions in (60) is zero if for the respective partition  $\pi \in \Pi_{(1,m)}$  holds

$$\exists j \in \{1, \dots, |\pi|\} : |\pi_j| \notin \{1, N_{\min}, \dots, N_{\max}\}, \quad (62)$$

since then either  $1_{\{|a|_a=1\}}(\pi_j) = 0$  or  $1_A(\pi_j) = 0$ . Therefore, the computational effort can be reduced by rejecting the partitions which fulfill condition (62). After rejecting the partitions, equation (39) can be evaluated, since except for the appearance of  $1_A(\cdot) = 0$  it is identical to equation (60).

Note, that partitions are not rejected, if they have a subset, which is of cardinality one. This is independent of  $N_{\min}$  and  $N_{\max}$  and holds since a Poisson-clutter model is chosen. Therefore, clutter is modeled as single measurements in the measurement space. However, more enhanced clutter models could be included. For example, in a BML-scenario the context information, which is available due to a ray-tracer, does not consider cars and other road users. Therefore, typical clutter sources in a BML-scenario can be road users, which reflect the signal emitted by the mobile station and act as new point sources of the reflected electromagnetic wave(s). Thus,

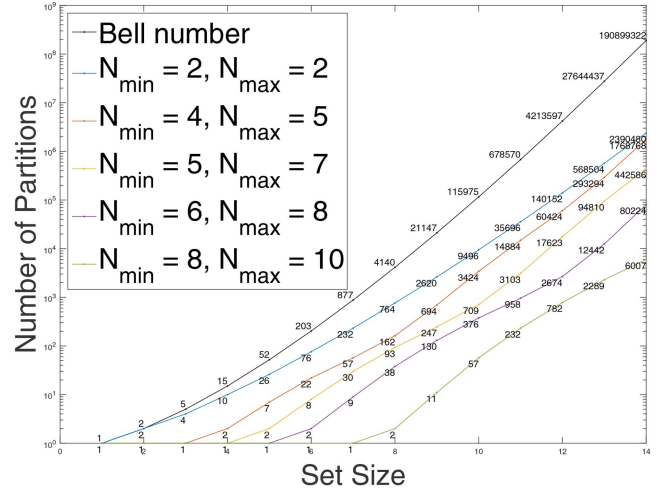


Fig. 2. Comparison of the Bell number and the number of partitions due to approximation (60).

multipaths which are received due to the same clutter source are not independent and hence clutter models which enable multiple measurements per clutter source could enhance data fusion algorithms. Obviously, condition (62) then needs to be adapted.

## B. Evaluation of Significant Summands

In practical applications, the likelihood-function is close to zero or might even be represented by zero for unlikely events due to the numerical resolution of the computer. Therefore, another practical approach of reducing the number of partitions which have to be considered in equation (60) is to evaluate only the terms for which the likelihood-function value is above a specific significance-threshold. To this end, a criterion based on the cardinality of the partition elements is developed to determine those partitions. Let  $\pi \in \Pi_{(1,m)}$  be an arbitrary partition which does not fulfill criterion (62) and  $x \in X$  be an arbitrary target position. Then, if

$$\exists j \in \{1, \dots, |\pi|\} : |\pi_j| > 1 \quad \text{and} \quad L_{Z|X}(i(\pi_j) | x) \leq \tau \quad (63)$$

is fulfilled

$$\sum_{j=1}^{|\pi|} 1_A(\pi_j) L_{Z|X}(i(\pi_j) | x) \prod_{k=1, k \neq j}^{|\pi|} \tilde{\eta}_{\pi,k} \approx 0 \quad (64)$$

approximately holds, where  $\tau > 0$  is a chosen threshold, which is suitable small, for the significance of a partition. Note that  $|\pi_j| > 1$  in (63) has to be fulfilled due to the first summand in  $\tilde{\eta}_{\pi,j}$ , since otherwise it might happen that only the  $j$ th summand of (64) is approximately zero, while the other summands are significantly larger than zero. Hence condition (63) can be used to reduce the number of the considered partitions. If  $\tau = 0$  in (63), “ $\approx$ ” can be replaced by “=” in (64).

Note that for the application of this condition the likelihood-function has to be evaluated for all possible subsets and all particle positions. The number of all

possible subsets is given by the binomial series, e.g., for a set of  $m$  measurements,

$$N_{\text{Subsets}} = \sum_{k=0}^m \binom{m}{k} = 2^m \quad (65)$$

subsets have to be evaluated. However, depending on  $N_{\min}$  and  $N_{\max}$  the application of condition (62) already reduces the number of subsets which have to be considered significantly, that is for  $m > 0$  and  $1 < N_{\min} \leq N_{\max} \leq m$  an application of condition (62) reduces the number of subsets of the measurement set, which have to be considered to

$$N_{\text{Subsets}} = 2^{(N_{\max}+1)-N_{\min}+1}. \quad (66)$$

### C. Generalization of the Probability of Detection

In [7] the authors emphasize that the probability of detection in [7, (27)] is defined more generally than in the standard PHD-filter, where the detection is modeled by a single Bernoulli-process. If targets generate multiple measurements per scan, the detection process can be modeled by a discrete probability distribution over the number of measurements. For (39) and (60) the single-target likelihood function can be formulated by

$$L_{Z|X}(i(\pi_j) | x) = p(|\pi_j|, x) \cdot \hat{L}_{Z|X}(i(\pi_j) | x), \quad (67)$$

where the sensor likelihood function  $\hat{L}_{Z|X}(i(\pi_j) | x)$  is given by

$$\hat{L}_{Z|X}(i(\pi_j) | x) = \tilde{L}(i(\pi_j) | x) \quad (68)$$

and

$$\hat{L}_{Z|X}(\emptyset | x) = 1. \quad (69)$$

Here,  $x \in X$ , where  $X \subseteq \mathbb{R}^d$ ,  $d > 0$  denotes the target space and  $\pi_j \in \pi$ , where  $\pi \in \Pi_{(1:m)} \cup \emptyset$  denotes the set of partitions for a set of measurements of cardinality  $m$ , defined analogously to Section III-A.

For the definition of the generalized probability of detection  $p(\cdot, x)$ ,  $x \in X$  the detection process of the measurements, which are generated by the same target, needs to be investigated. If the detections (each considered as a random variable) of the single measurements are conditionally (conditioned on a specific target) independent and have the same distribution (same detection probability), the detection process can be modeled by a series of Bernoulli-trials. If this assumption is fulfilled, a possible choice for  $p(\cdot, x)$  is the Poisson-distribution, that is

$$p(n, x) = \frac{\lambda^n}{n!} e^{-\lambda}, \quad (70)$$

for all  $n \in \mathbb{N}$  and  $x \in X$ , where the parameter  $\lambda \in \mathbb{R}_{>0}$  is the expected number of measurements per target. If the number of measurements, which are generated by a single target can be restricted to  $N_{\max} \in \mathbb{N}$  the Binomial-

distribution can be used to model the detection process. It is given by

$$p(n, x) = \binom{N_{\max}}{n} q^n (1-q)^{N_{\max}-n}, \quad (71)$$

for all  $n \in \mathbb{N}$  and  $x \in X$ , where  $q \in [0, 1]$  denotes the detection probability of an individual measurement.

Note, that the Binomial-distribution can be considered as a special case of the Poisson-distribution. To this end, let

$$q := \frac{\lambda}{N_{\max}}. \quad (72)$$

Then

$$\lim_{N_{\max} \rightarrow \infty, q \rightarrow 0, N_{\max} q \rightarrow \lambda} \binom{N_{\max}}{n} q^n (1-q)^{N_{\max}-n} = \frac{\lambda^n}{n!} e^{-\lambda}, \quad (73)$$

for all  $n \in \mathbb{N}$  [29, p. 79].

Thus the Poisson-distribution can be used to model the detection process for small detection probabilities of the individual measurements and a large number of trials, that is in scenarios where the target may generate a large number of measurements. The Binomial-distribution can be used if the maximal number of measurements per target  $N_{\max}$  is known. Note, that the two proposed definitions for  $p(\cdot, x)$ ,  $x \in X$  are only valid if the detections of the single measurements belonging to the same target are conditionally independent and identically distributed. If this assumption is not valid, other distributions need to be considered.

## V. NUMERICAL EVALUATION

To verify the applicability of the considerations of Section IV two numerical evaluations are carried out in the following.

### A. Multi-Target Scenario with Correlated Measurements

In this section, a two-target scenario is considered (see Figure 3 (a)), where the targets are moving linearly with a constant speed of 5 m/s (target 1) and 3 m/s (target 2). The trajectory of the first target starts at  $(10, 5)^T$  and is directed to  $(650, 400)^T$ . The second target starts at  $(10, 500)^T$  and is directed to  $(700, 10)^T$ . In each iteration (the scan time is 1 s) two correlated measurements are drawn per target according to a Gaussian-distribution with the following parameters. The mean is given by the position of the target and the covariance matrix is given by  $\Sigma = \begin{pmatrix} R & C \\ C^T & R \end{pmatrix}$ ,  $R = \text{diag}(10, 10)$  and  $C = \text{diag}(5, 5)$ . Since the probability of detection per measurement is  $p_D = 0.8$ , the covariance matrix  $\Sigma$  is restricted according to the size of available measurements per target. Furthermore, two clutter measurements are drawn uniformly per iteration in the field of view, which is given by

$$\text{FOV} := [0, 700] \times [0, 700]. \quad (74)$$

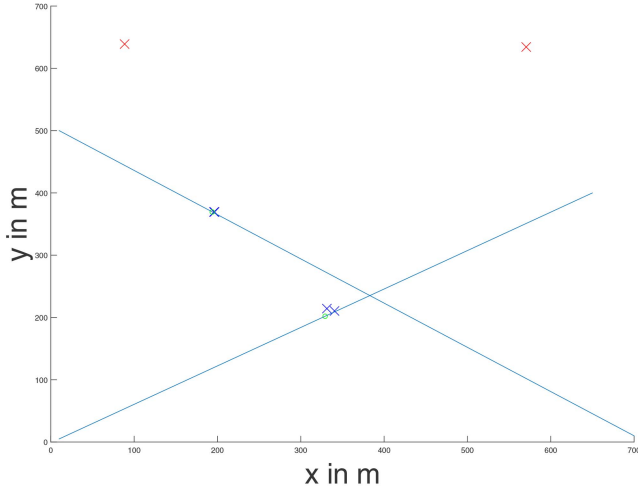


Fig. 3. Visualization of the two-target scenario. Two targets (green circle) are linearly moving with a constant velocity on their trajectory (blue line). In one iteration a target generates two correlated measurements (blue crosses), each with probability of detection  $p_D = 0.8$ . The measurements are drawn around the targets true position according to a Gauss-distribution with covariance matrix  $\Sigma$ . Furthermore, two clutter measurements (red crosses) are generated uniformly over the field of view in each iteration.

$N_{\min}$	$N_{\max}$	$\tau$
1 = —	2 = ●	0.0 = □
2 = - - - -	3 = ●	1.0 = *
	6 = ●	

Fig. 4. Legend for Figures 5–8.

For the evaluation of (60), an SMC-implementation is used. The prediction is the same as for the standard PHD-filter, where the probability of survival is set to  $p_S = 1.0$  for all particles and the single-object transition density is defined by the continuous white-noise acceleration model from [4] with  $\tilde{q} = 1.5$ . To reduce the computational complexity, in each iteration 50 newborn particles are generated around the measurements of the previous iteration. For the initialization 100 particles are uniformly drawn in the field of view. A standard resampling-algorithm (see [33]) is carried out and the maximal number of particles is restricted to 150. For the update of the filter, (60) is implemented and conditions (62) and (63) are used to restrict the number of partitions. The likelihood-function is defined as follows. Let  $Z \subseteq \mathbb{R}^2$  be the measurement space. Then,

$$E_Z := \emptyset \cup \bigcup_{n \geq 1} Z^{(n)} \quad (75)$$

is defined analogously to Section II by the space of sets of points in  $Z$ . The likelihood-function is given by

$$L_{Z|X}(i(\cdot) | \cdot) : E_Z \setminus \emptyset \times \mathbb{R}^4 \rightarrow \mathbb{R}. \quad (76)$$

Let in iteration  $k \in \{1, \dots, 100\}$  be  $m_k \in \{2, \dots, 6\}$  (number of clutter fixed to two, maximum number of measurements per target is two) the number of all received measurements. Let  $X \subseteq \mathbb{R}^4$  be the target state space (position + velocity in 2 dimensions, respectively). Then, for a subset  $z = \{z_1, \dots, z_n\} \in E_Z \setminus \emptyset$ ,  $n \in \{1, \dots, m_k\}$  and  $x \in X$  arbitrary the likelihood-function is defined by

$$L_{Z|X}(i(z) | x) = p(|z|),$$

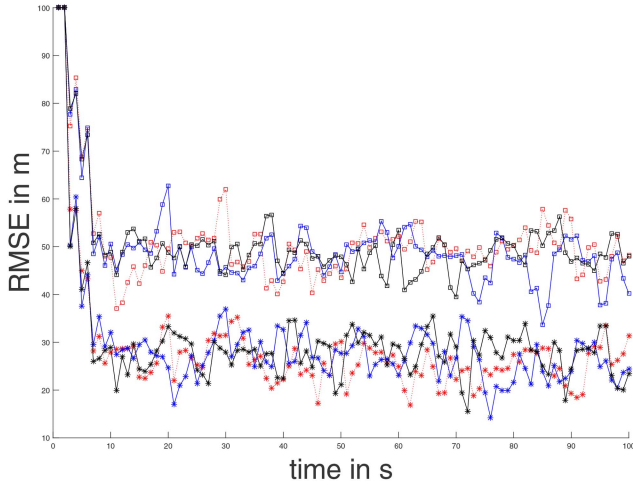
$$\mathcal{N} \left( \begin{pmatrix} z_1 \\ \vdots \\ z_n \end{pmatrix}, \begin{pmatrix} Hx \\ Hx \end{pmatrix}, \begin{pmatrix} R & C & \dots & C \\ C^T & R & \dots & C \\ \vdots & \vdots & \ddots & \vdots \\ C^T & C^T & \dots & R \end{pmatrix} \right), \quad (77)$$

where  $H := \begin{pmatrix} 1 & 0 & 0 & 0 \\ 0 & 1 & 0 & 0 \end{pmatrix}$  and  $p : \mathbb{N} \rightarrow [0, 1]$  defines the probability of observing a set of measurements with the respective number of elements. It is defined by

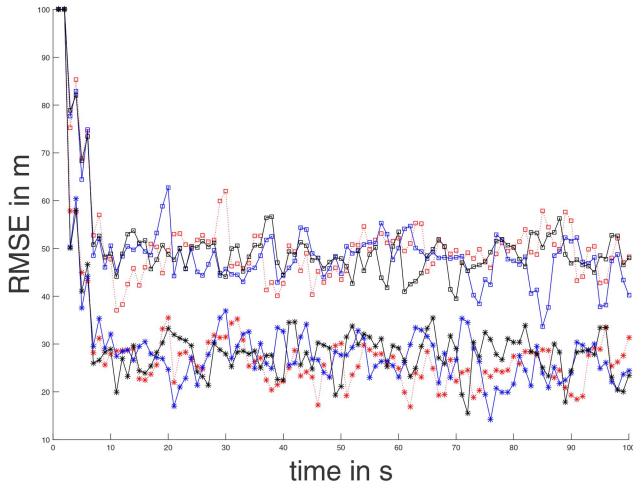
$$p(n) = \begin{cases} 1 - P_D, & \text{if } n = 0 \\ P_D \cdot \binom{2}{n} q^n (1-q)^{2-n}, & \text{if } n > 0, \end{cases} \quad (78)$$

where  $P_D = q = 0.8$ . Note that given a specific target state  $x \in X$  the measurements are not conditionally independent. Since only the mutual independence of the target-oriented measurement processes is needed in the derivation of the generalized PHD-filter, the definition (77) makes sense. The mean number of clutter  $\lambda$  from (40) is set to two and the distribution of clutter  $c : \text{FOV} \rightarrow [0, 1]$  is uniform in the field of view. To extract a state estimate in each iteration, the  $k$ -means algorithm is applied to the set of particles, which were present in the previous iteration. The number of clusters  $k$  is given by the rounded number of estimated target states from the PHD-filter in each iteration. Note that the enhanced state extraction scheme, presented in [31] needs to be modified for applying it to a scenario where several targets generate multiple measurements.

To assess the proposed PHD-filter 100 Monte Carlo runs are performed for different parameterizations of the approximation conditions (63) and (62). Figure 7 visualizes the results of the different parameterizations in terms of the estimated number of targets. It can be seen that the estimated number of targets does not depend on the chosen partition-sizes, that is it does not depend on approximation criterion (63). This is due to the fact that the number of significant partitions with significance threshold  $\tau = 0.0$  (and  $\tau = 1.0$ ) is more or less equal for all three investigated parameterizations  $N_{\min} = 2/N_{\max} = 2$ ,  $N_{\min} = 1/N_{\max} = 3$  and  $N_{\min} = 1/N_{\max} = 6$ . Figure 9 visualizes exemplary for one parametrization the mean number of partitions, where in each Monte Carlo run the mean number of significant partitions is computed



(a) RMSE Target 1



(b) RMSE Target 2

Fig. 5. RMSE with respect to target 1 (a) and target 2 (b). Due to the fact that the generalized PHD-filter over estimates the number of present targets if the significance threshold  $\tau$  is set to 1.0 (see Figure 7) and the fact that the target state extraction is based on the rounded number of estimated targets, the parametrization using  $\tau = 1.0$  perform better in terms of the RMSE than the parametrizations using  $\tau = 0.0$ .

for each time-step over all particles. Furthermore, it can be seen from Figure 7 that the parameterizations with significance threshold  $\tau = 1.0$  have a larger deviation in terms of the estimated number of targets than the parameterizations using the significance threshold  $\tau = 0.0$  and over-estimate the true number of present targets. This yields to a better performance of the parameterizations using the significance threshold  $\tau = 1.0$  in terms of the root mean squared error (RMSE) with respect to the two true target states, which can be seen in Figures 5. This is due to the fact that the target state extraction is done using a  $k$ -means clustering algorithm, where  $k$  is given by the rounded estimated number of targets. Therefore, the over-estimation of the number of targets by the parameterizations with significance threshold  $\tau = 1.0$  yields to a clustering that always estimates at least two clusters. In contrast to that, the parameterizations with significance

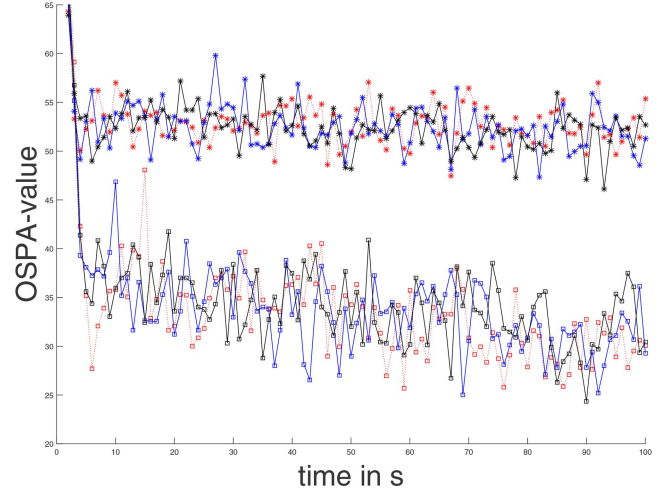


Fig. 6. Mean of the OSPA-values with order  $p = 2$  and cut-off value  $c = 100$ . In terms of the OSPA-metric the parametrizations using  $\tau = 0.0$  perform better compared to those that use  $\tau = 1.0$ , since the over-estimation of the number of targets (see Figure 7) is penalized by the OSPA-metric. The change of the number of investigated partitions does not yield a significant alteration of the results.

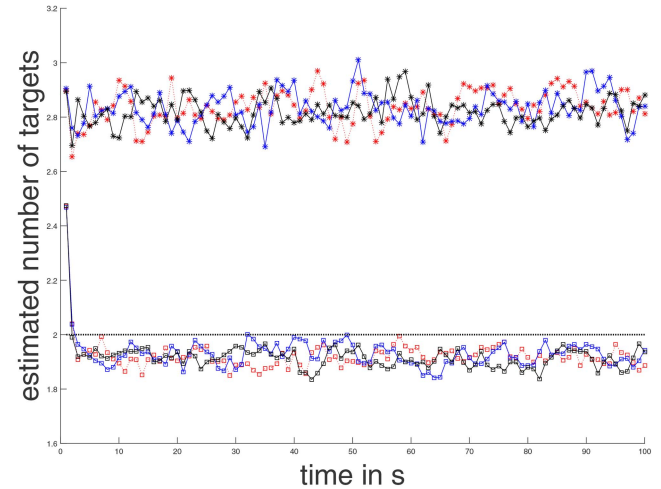


Fig. 7. Estimated number of targets, where the dashed black line shows the true number of present target.

threshold  $\tau = 0.0$  under-estimate the true target number for some iterations and thus the  $k$ -means clustering algorithm estimates only one cluster for these iterations. In iterations, where no estimate for a specific target is produced by the generalized PHD-filter, the squared error is set to  $100^2 \text{ m} = 10000 \text{ m}$ . However, the over-estimation yields to a worse performance of the parameterizations using significance threshold  $\tau = 1.0$  compared to the parameterizations, which use a significance threshold  $\tau = 0.0$ , since each over-estimation is penalized by the OSPA-metric. The result in terms of the mean time consumption per iteration is shown in Figure 8. It can be seen that the parameterizations using the significance threshold  $\tau = 1.0$  are faster compared to the parameterizations using a threshold of  $\tau = 0.0$ . Furthermore, the parameterizations with  $N_{\min} = 2/N_{\max} = 2$  perform bet-

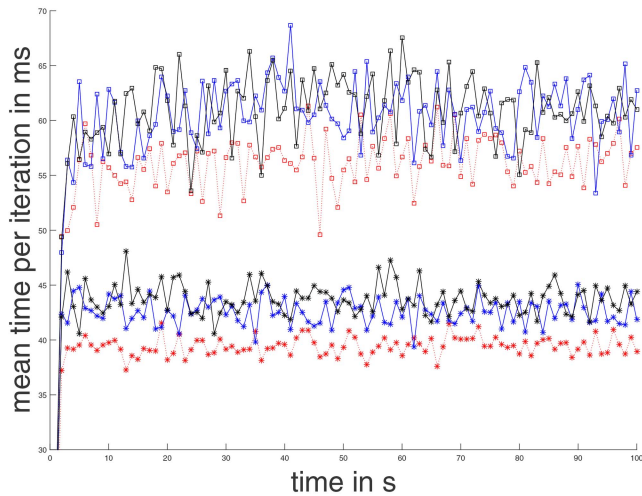


Fig. 8. Comparison of the mean time for updating the generalized PHD-filter of different parametrizations. It can be seen that the more partitions the filter processes and the smaller the significance threshold  $\tau$  is chosen the longer the update takes.

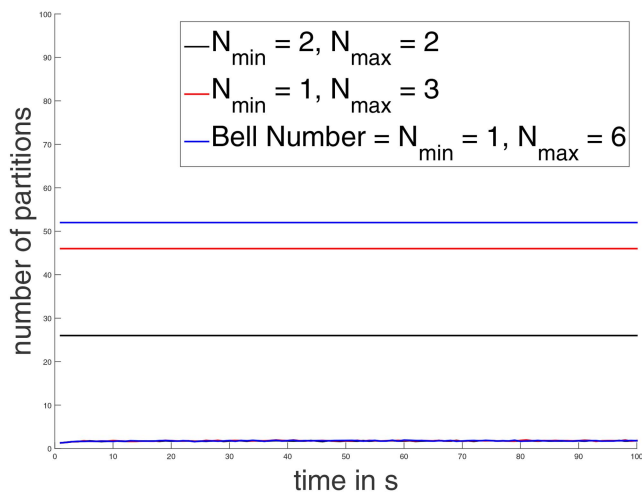


Fig. 9. Mean number of partitions resulting from condition (62) and mean number of partitions due to condition (63) for two parameterizations ( $N_{\min} = 2/N_{\max} = 2$  (black),  $N_{\min} = 1/N_{\max} = 3$  (red)). The number of all partitions is given by the Bell number (blue). For the computation of the mean number of significant partitions in each Monte Carlo run the mean number of significant partitions is computed for each time-step over all particles. Afterwards, the mean of the number of significant partitions is computed over all Monte Carlo runs. The number of significant partitions is almost the same for the two parameterizations.

ter in terms of time consumption than  $N_{\min} = 1/N_{\max} = 3$  and  $N_{\min} = 1/N_{\max} = 6$ . In summary: the less partitions and the larger the significance-threshold is, the faster and worse the algorithm performs.

Also a parameterization without using the two approximation conditions has been investigated in terms of processed time per iteration. Since for this non-approximated SMC generalized PHD-filter one iteration took up to  $5.30 \cdot 10^3$  s, only one MC-run has been performed. Thereby, the mean computation time was  $2.28 \cdot 10^3$  s, which shows, that even if  $N_{\min} = 1$  and  $N_{\max} = 6$  (no approximation in terms of (62) has been made) and

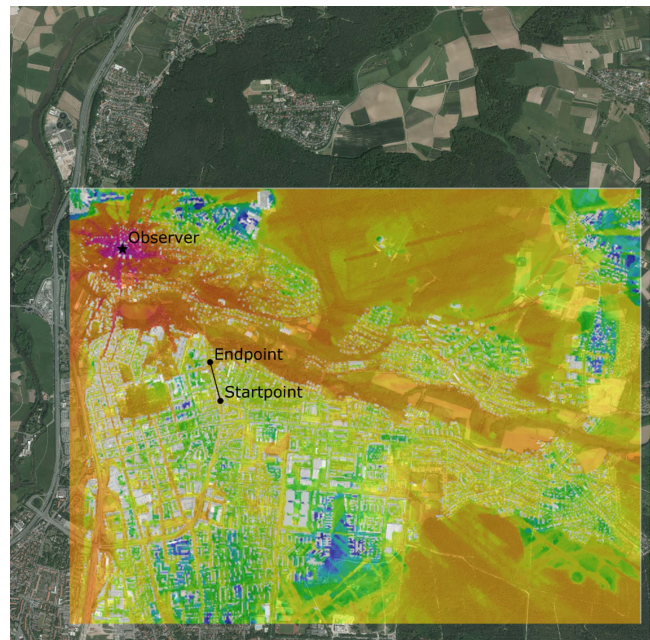


Fig. 10. A single target moves on a linear trajectory with constant speed in an urban environment. At each instance of time multipaths are created using a ray-tracer on a grid and the measurement process is simulated using a Gaussian distributed noise for each multipath—parameter. Furthermore, the detection process is simulated. The colors indicate the received field—strength at the observer (star). Map Data: ©GeoBasis-DE/BKG 2015. Ray-Tracer Visualization: AWE Communications.

$\tau = 0.0$  is chosen, the respective generalized PHD-filter parameterization ( $N_{\min} = 1/N_{\max} = 3, \tau = 0.0$ ) performs about 45 times faster than the standard version, which does not use any approximation condition at all.

All in all, it is numerically shown that the proposed methods of approximation for the generalized PHD-filter can be applied to scenarios where targets generate multiple measurements. It should be noted that the definition of the likelihood-function does depend on the considered scenario and is not part of the numerical evaluation of this work. Furthermore, the following should be kept in mind. The integral of the clutter-intensity  $\lambda c(\cdot)$  yields the number of false measurements (not false targets). Thus  $\lambda$  denotes the mean number of false measurements per iteration. Hence, clutter is defined in terms of elements of the measurement space, not as clutter targets in the target space. Thus, in scenarios where clutter scatterer generate multiple clutter-measurements per scan, enhanced clutter models need to be investigated.

## B. Single Target Blind Mobile Localization Scenario

To demonstrate the connection of the presented approach to the challenge of BML a single-target scenario in a simulated urban environment is presented. For generating multipath-measurements, a database for a fixed OS and a grid of MS locations is generated by using a ray-tracing simulation. The distance between two grid points is set to 10 m. The number of received multipaths

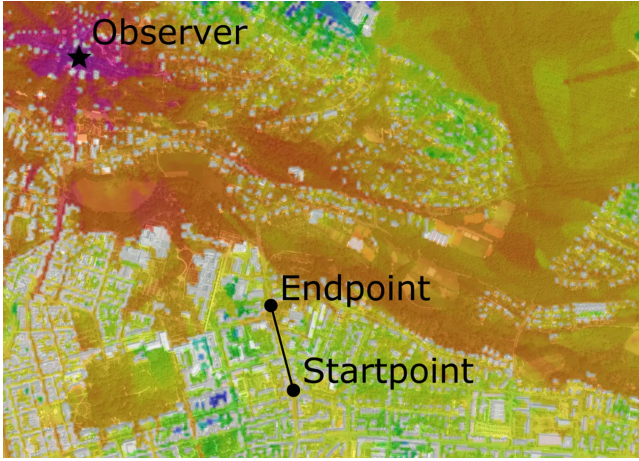


Fig. 11. Zoom of the investigated scenario. Map Data: ©GeoBasis-DE/BKG 2015. Ray-Tracer Visualization: AWE Communications.

is restricted to six and each multipath is characterized by its azimuth (angle) of arrival (AoA), its elevation (angle) of arrival (EoA) and its relative time of arrival (RToA) with respect to the first received multipath. Thus,

$$\mathcal{Z} := [0, 2\pi] \times [-\pi, \pi] \times \mathbb{R}_{>0} \quad (79)$$

and

$$E_{\mathcal{Z}} := \emptyset \cup \bigcup_{n \geq 1} \mathcal{Z}^{(n)} \quad (80)$$

analogously to Section II. Afterwards, a linear ground-truth for the target (that is an electromagnetic emitter), which is moving with a constant velocity of 2.4 m/s, is simulated (see Figure 11). Then, in each time-step the lower left grid point of the box, in which the target is located in, is determined. The multipaths which correspond to the chosen grid point are taken to generate the multipath-measurements, referred to as the true multipaths in the following. First, in each iteration Gaussian-distributed noise is added to the true multipaths, where the standard deviations are set to  $\sigma_{\text{AoA}} = \sigma_{\text{EoA}} = 0.001$  rad for the azimuth and elevation of arrival and  $\sigma_{\text{RToA}} = 1.0/c$  s, where  $c := 299792458$  m/s defines the speed of light. Furthermore, the detection is simulated by a binomial detection process with probability of detection of  $p_D = 0.95$ . No clutter is added to the measurements.

The generalized PHD-filter is implemented including the approximations proposed in (62) and (63), where  $N_{\min} := 3$ ,  $N_{\max} := 6$  and the threshold for significance of a partition  $\tau := 1.0 \cdot 10^{10}$ . The field of view (FOV) of the considered scenario is given by

$$\text{FOV} := [645259.0, 645999.0] \times [5495257.0, 5496747]. \quad (81)$$

Furthermore, the probability of detection is independent of the target's state space, that is  $p(n, x) = p(n)$  for all  $x \in X = \text{FOV} \times \mathbb{R}^2$ ,  $n \in \{1, \dots, 6\}$ . It is modeled by (71), where  $q := p_D := 0.95$ . Then, it is incorporated

into the likelihood-function, which is defined for a hypothetical emitter position  $\xi \in X$  and a set of multipath-measurements  $\mathcal{Z}^K := \{z^k\}_{k=1}^K$ , where  $z^k \in \mathcal{Z}$  (according to the ideas presented in [1]) by

$$p(\{z^k\}_{k=1}^K | \xi) := p(n) \cdot \lambda_{\Phi}^{K-n} \cdot \prod_{j \in I} \mathcal{N}(h_{\xi}^j, z^j, C^j), \quad (82)$$

where

$$h_{\xi} := \{h_{\xi}^k\}_{k=1}^M \quad (83)$$

denotes the set of predicted multipaths with respect to  $\xi$  and the fixed OS coming from the ray-tracer. The occurrence of clutter in a set of multipaths is modeled by

$$\lambda_{\Phi} := \frac{0.1}{\text{FOV}}, \quad (84)$$

which is equal to the clutter density of the generalized PHD-filter. In [chapter 4.4][1] and [2] the probabilistic likelihood-function is defined by the sum over all possible data interpretation, that is all possible associations between measured and predicted multipaths. Therefore, a possible data interpretation is denoted by  $E_{i_1, \dots, i_M}^K$ , where

$$i_j := \begin{cases} 0, & \text{no association, measured} \\ & \text{multipath is not detected} \\ k \in \{1, \dots, K\}, & \text{jth predicted multipath is} \\ & \text{associated with measured} \\ & \text{multipath } k \end{cases} \quad (85)$$

However, due to the computational effort, we only use the best data association, which is determined by applying the Munkres-algorithm [5] to the set of measured and predicted multipaths, using the Mahalanobis-distance with the covariance matrix

$$C^{i_j} = C = \text{diag}[\sigma_{\text{AoA}}^2, \sigma_{\text{EoA}}^2, \sigma_{\text{RToA}}^2] \quad (86)$$

for the construction of the cost matrix. Thus, the index  $i_j$  in (82) denotes the best (global) association for the specific predicted path. The generalized PHD-filter is realized by an SMC-implementation, since the likelihood-function can be computed only point-wisely. The maximal number of particles used by the generalized PHD-filter is given by 700 and particles are only drawn and predicted to grid points, where at least one multipath can be received due to the available database. In each iteration 200 newborn targets are uniformly drawn over the FOV. The single-object transition density is defined by the continuous white-noise acceleration model from [4], with  $\tilde{q} = 1.5$  and the probability of survival  $p_S = 1.0$ . To extract the target states the weighted mean of all particles is computed.

To compare the result of the proposed generalized PHD-filter, the approach proposed in [9] is considered. There, standard PHD and intensity filters (iFilter) are applied to BML. Since the standard PHD and iFilter make the assumption that a target generates at most one measurement per sensor-scan, the integral of the

intensity, that is the estimated number of targets, that are present in the FOV, is equal to the estimated number of measurements. Due to the fact, that one target in BML can emit several multipaths a post-processing is needed for the state-extraction. Thus, in [9] a generalization of the so-called particle grouping from [31] is presented. In the following the generalized mean computation from [9, Section 4.B] together with an SMC-implementation of the iFilter [33] is applied. The likelihood-function of a hypothetical emitter position  $x_i \in X$  and one multipath  $z^k \in \mathcal{Z}^K$ ,  $k \in \{1, \dots, K\}$  is defined by

$$p(z^k | \xi) := \begin{cases} \mathcal{N}(h_\xi^j; z^{i_j}, C^{i_j}), & \text{if } \exists j \in \{1, \dots, M\} \\ & \text{such that } i_j = k \end{cases} \quad (87)$$

$$0, \quad \text{otherwise}$$

The assignment is done via Munkres Algorithm between the set of measured multipaths  $Z$  and the set of predicted multipaths  $h_\xi$  of  $\xi$ . Therefore, the index  $i_j$  denotes the assigned measured multipath  $z^{i_j}$  of the  $j$ th predicted multipath from  $h_\xi$ . The probability of detection is set to  $p^D(x) = 0.9$  for all  $x \in X$  and the detection probability in the space of hypothesis  $\mathcal{S}_\phi$  is defined by  $p^D(\phi) = 0.4$ . The transition probability from  $\mathcal{S}_\phi$  to  $\mathcal{S}$  is set to  $\Psi(x | \phi) = 0.2$ , the transition probability in  $\mathcal{S}_\phi$  is defined as  $\Psi(\phi | \phi) = 0.01$  and the transition probability from  $\mathcal{S}$  to  $\mathcal{S}_\phi$  is given by  $\Psi(\phi | x) = 0.1$ . The number of particles is restricted to 1500. The thresholds for target existence of the standard iFilter and the generalized PHD-filter are set to 0 to make the filter comparable in their RMSE-performance.

To assess both filters with respect to accuracy 100 Monte-Carlo runs of the presented scenario are performed. The results in terms of the RMSE is shown in Figure 12. It can be seen that both filters perform more or less equivalent after iteration 30 (the generalized PHD-filter is slightly better in terms of its RMSE-performance). However, it also can be seen that until iteration 20 the generalized PHD-filter performs worse than the standard iFilter. First, it can be seen that the initialization of the generalized PHD-filter is not as good as the initialization of the standard iFilter. This is essentially due to the fact that the likelihood-function of the generalized PHD-filter is much more restrictive than the likelihood-function of the standard iFilter. This is visualized in Figure 14 (a) and (c) which shows the sum of the likelihood-functions given in (82) and (87), that is

$$\sum_{\pi \in \Pi_{(1,3;6)}^{\mathcal{Z}^K}} p(\pi | \xi), \quad (88)$$

where  $\Pi_{(1,3;6)}^{\mathcal{Z}^K}$  denotes the set of all partitions of  $\mathcal{Z}^K$ , where the subsets of one partition possess cardinality  $c \in \{1, 3, \dots, 6\}$ , that is

$$\Pi_{(1,3;6)}^{\mathcal{Z}^K} := \{ \{ \pi_{z_1}, \dots, \pi_{z_m} \} : \pi_{z_i} \subseteq \mathcal{Z}^K, |\pi_{z_i}| \in \{1, 3, \dots, 6\} \} \quad (89)$$

$$\sum_{k=1}^K p(z^k | \xi) \quad (90)$$

for the standard iFilter and all  $\xi \in X$  respectively. The number of investigated partitions is restricted due to the approximation condition (62), where  $N_{\min} = 3$  and  $N_{\max} = 6$ . For better visualization only values of the likelihood-function, which are larger than  $1 \cdot 10^{10}$  are plotted. It is obvious that the shape of (88) is sharper and therefore more restrictive than (90). This is due to the fact that the likelihood-function in (82) is given by a product of Gaussians. Therefore, partitions with at least one unlikely subset of multipaths (with respect to a hypothetical emitter position) possess a small likelihood-function value. This contrasts the likelihood-function of the standard iFilter, which only assesses single multipaths (see 87). Thus, the time of convergence (until iteration 10–11) of the generalized PHD-filter is longer than the time of convergence of the standard iFilter. Furthermore, it can be seen from Figure 12 that the localization of both filters around iteration 15 gets worse, while the generalized PHD-filter performs worse than the standard iFilter. This is due to the fact, that the likelihood-functions produce ambiguities in terms of the most likely hypothetical emitter position, which is shown in Figures 14 (b) and (d) for iteration 15. Since in some MC-runs a correct initialization of the generalized PHD-filter was not performed until the occurrence of these ambiguities, the generalized PHD-filter performs worse than the standard iFilter. However, the generalized PHD-filter performs better in iteration 20–25, since the restriction cancels out the ambiguities earlier than the likelihood-function of the standard iFilter.

The comparison of both filters in terms of estimated number of targets, that is the integral of the intensity function over FOV is presented in Figure 13. Due to the assumption that one target generates at most one measurement per iteration the standard iFilter estimates the number of multipaths which belong to a target. In contrast to this the generalized PHD-filter estimates after a few iterations the correct number of present targets.

In terms of time consumption the standard iFilter clearly outperforms the generalized PHD-filter: For one MC-run the standard iFilter needs 82614 ms, where the generalized PHD-filter takes 20250085 ms, which shows that it is of factor 245 slower than the standard iFilter.

## VI. CONCLUSION AND FUTURE WORK

In this paper two different ways of approximation for the generalized PHD-filter update from [7] are proposed. In contrast to approximations for extended object and group tracking, the spatial relation of the measurements in the measurement space is not used. The approximations are based on incorporating the a pri-

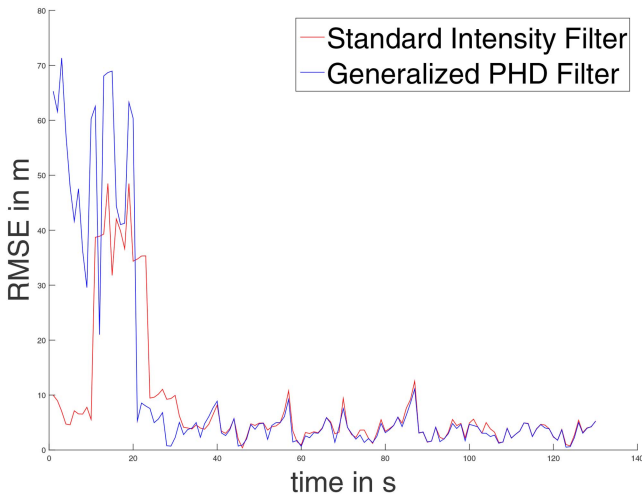


Fig. 12. RMSE of the standard iFilter, which uses an enhanced post-processing scheme for target state extraction and the generalized PHD-filter applying the proposed approximation conditions with  $N_{\min} = 3$ ,  $N_{\max} = 6$  and  $\tau = 1.0 \cdot 10^{10}$ .

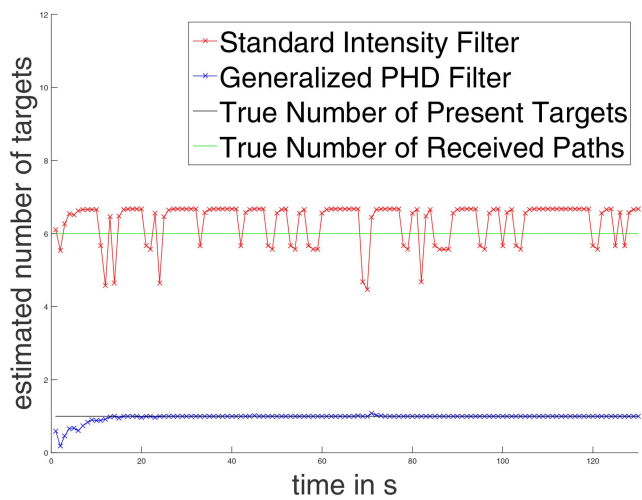
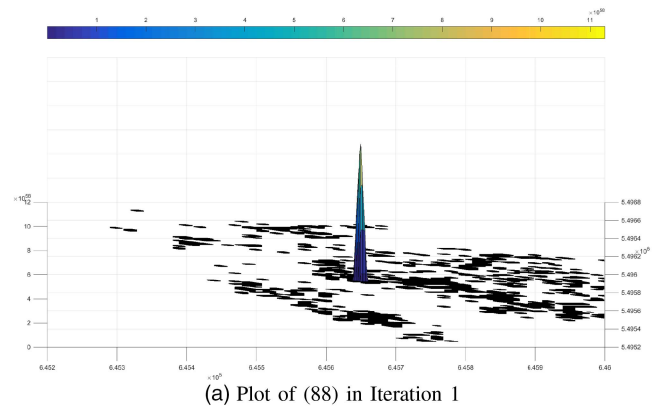
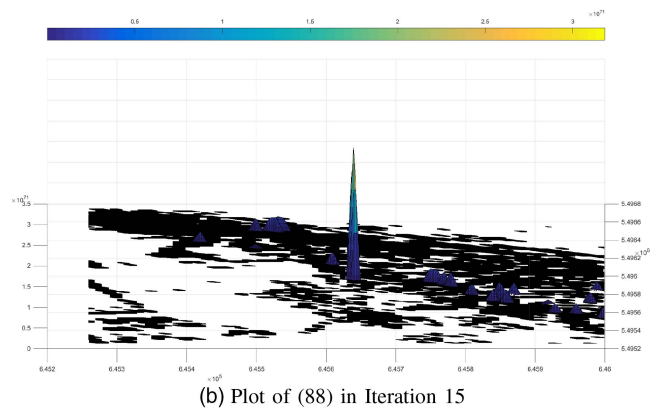


Fig. 13. Estimated number of targets, that is the sum of all particle weights before resampling of the standard iFilter and the generalized PHD-filter. Due to the assumption that one target generates at most one measurement per iteration, which is violated in the considered scenario, the standard iFilter estimates the number of multipaths, which belong to target. The generalized PHD-filter is able to estimate the correct number of present targets.

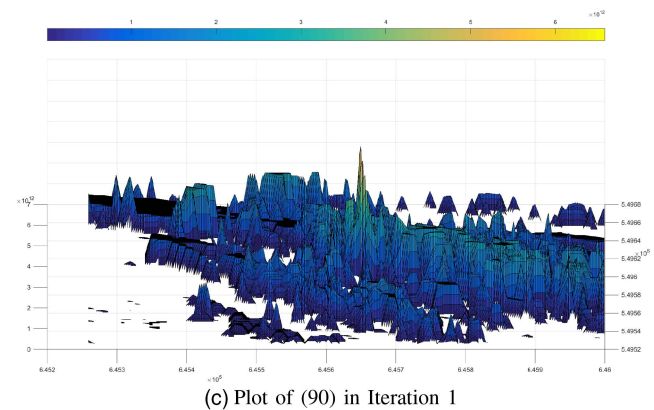
ori knowledge on the number of measurements per target and the significance of a partition in terms of the likelihood-function. Therefore, the proposed approximations can be applied to scenarios, where a spatial distribution of the measurements is not available. Furthermore, the detection process is modeled as a function of target state and number of measurements and the usage of the Binomial- and Poisson-distribution for conditionally independent and identical distributed detection processes of the single measurements is motivated. An example for such a kind of scenario is BML where mobile terminals have to be tracked passively and non-cooperatively in an urban environment (see [9], [1], [2]). Two numerical examples for assessing the pro-



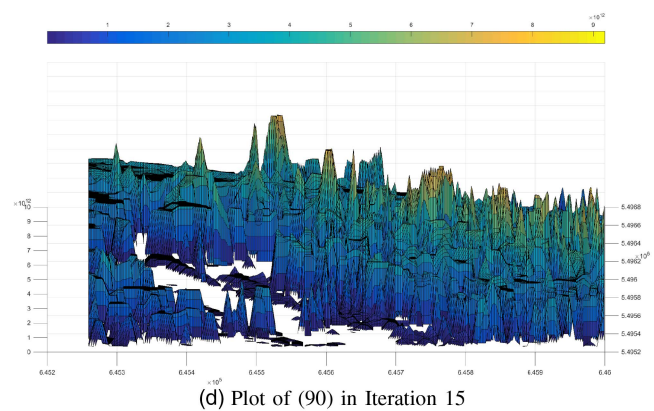
(a) Plot of (88) in Iteration 1



(b) Plot of (88) in Iteration 15



(c) Plot of (90) in Iteration 1



(d) Plot of (90) in Iteration 15

Fig. 14. Visualization of the likelihood-functions (88) and (90) at two instances of time.

posed methods are presented. First, a two-target scenario, where each target generates multiple correlated measurements is used to show the applicability of the

proposed methods and to discuss the number of partitions that have been reduced. Several parameterizations are investigated and compared to each other. Second, a single-target BML-scenario is investigated and the generalized PHD-filter, using the proposed approximations and the generalization of the probability of detection is compared against an adaption of the standard intensity filter in terms of runtime, the estimated number of targets and the RMSE performance.

Future work will investigate improved schemes for state extraction and enhanced clutter modulation.

#### ACKNOWLEDGMENT

The authors would like to thank AWE Communications from Böblingen/Germany for providing a latest version of their ray-tracing simulation “WinProp” to evaluate the developed algorithms in Section V-B.

The authors would also like to thank Stephan Häfner, Martin Käske and Prof. Dr. Reiner Thomä from the Technical University of Ilmenau for providing the simulation of the estimation process used in the numerical evaluation of Section V-B.

This work was supported by the Federal Ministry of Education and Research of Germany (BMBF), within the Project eILT: “Emitter Lokalisierung unter Mehrwegeausbreitungsbedingungen,” <http://eilt.medav.de/>.

#### REFERENCES

- [1] V. Algeier  
*Blind Localization of Mobile Terminals in Urban Scenarios.*  
PhD thesis, TU Ilmenau, 2010.
- [2] V. Algeier, B. Demissie, W. Koch, and R. Thomä  
Track initiation for blind mobile terminal position tracking using multipath propagation.  
*In Proceedings of the 11th International Conference on Information Fusion*, Cologne, Germany, 2008.
- [3] H. W. Alt  
*Lineare Funktionalanalysis.*  
Springer, 2012.
- [4] Y. Bar-Shalom, X. Li, and T. Kirubarajan  
*Estimation with Applications to Tracking and Navigation.*  
Wiley-Interscience, 2001.
- [5] F. Bourgeois and J.-C. Lassalle  
An extension of the Munkres algorithm for the assignment problem to rectangular matrices.  
*Communications of the ACM*, 14(12):802–804, Dec. 1971.
- [6] D. Clark and J. Houssineau  
Faa di bruno’s formula for chain differentials.  
*arXiv Preprint arXiv:1310.2833*, Okt. 2013.
- [7] D. Clark and R. Mahler  
Generalized PHD filter via a general chain rule.  
*In Proceedings of the 15th International Conference on Information Fusion*, Singapore, 2012.
- [8] D. J. Daley and D. Vere-Jones  
*An introduction to the theory of point processes.*,  
volume 2. Springer, 2nd edition edition, 2008.
- [9] C. Degen, F. Govaers, and W. Koch  
Emitter localization under multipath propagation using SMC-intensity filters.  
*In Proceedings of the 16th International Conference on Information Fusion*, Istanbul, Turkey, 2013.
- [10] C. Degen, F. Govaers, and W. Koch  
Tracking targets with multiple measurements per scan.  
*In Proceedings of the 17th International Conference on Information Fusion*, Salamanca, Spain, 2014.
- [11] C. Degen, R. Streit, and W. Koch  
On the functional derivative with respect to the Dirac delta.  
Submitted to the 10th *Workshop on Sensor Data Fusion: Trends, Solutions, and Applications*, Bonn. July 2015.
- [12] P. A. M. Dirac  
The physical interpretation of the quantum dynamics.  
*Proceedings Royal Society*, 113:621–641, 1927.
- [13] E. Engel and R. M. Dreizler  
*Density Functional Theory.*  
Springer, 2011.
- [14] F. G. Friedländer and M. Joshi  
*Introduction to the Theory of Distributions.*  
Cambridge University Press, 2nd edition, 1999.
- [15] K. Gilholm, S. Godsill, S. Maskell, and D. Salmond  
Poisson models for extended target and group tracking.  
*In SPIE Conference 5913: Signal and Data Processing of Small Targets*, 2005.
- [16] K. Grandström  
*Extended Object Tracking using PHD filters.*  
PhD thesis, Linköping University, Sweden, 2012.
- [17] K. Granström, C. Lundquist, and O. Orguner  
Extended target tracking using a gaussian-mixture PHD filter.  
*IEEE Transactions On Aerospace And Electronic Systems*, 48(4):3268–3286, Oct. 2012.
- [18] K. Granström and O. Orguner  
On the reduction of Gaussian inverse wishart mixtures.  
*In Proceedings of the 15th International Conference on Information Fusion*, Singapore, 2012.
- [19] K. Granström and O. Orguner  
A PHD filter for tracking multiple extended targets using random matrices.  
*IEEE Transactions On Aerospace And Electronic Systems*, 60(11):5675–5671, Nov. 2012.
- [20] K. Granström and O. Orguner  
On spawning and combination of extended/group targets modeled with random matrices.  
*IEEE Transactions On Signal Processing*, 61(3):678–692, Feb. 2013.
- [21] J. Houssineau, E. Delande, and D. Clark  
Notes of the summer school on finite set statistics.  
*arXiv preprint arXiv:1308.2586*, Aug. 2013.
- [22] W. Koch and R. Saul  
A Bayesian approach to extended object tracking and tracking of loosely structured target groups.  
*In Proceedings of the 8th International Conference on Information Fusion*, Philadelphia, PA, USA, 2005.
- [23] R. Mahler  
Multitarget filtering via first-order multitarget moments.  
*IEEE Transactions On Aerospace And Electronic Systems*, 39(4):1152–1178, 2003.
- [24] R. Mahler  
Sensor management with non-ideal sensor dynamics.  
*In Proceedings of the 7th International Conference on Information Fusion*, Stockholm, 2004.
- [25] R. Mahler  
PHD filters of higher order in target number.  
*IEEE Transactions On Aerospace And Electronic Systems*, 43(4):1523–1543, 2007.
- [26] R. Mahler  
*Statistical Multisource-Multitarget Information Fusion.*  
Norwood MA: Archtech House, 2007.

- [27] R. Mahler  
PHD filters for nonstandard targets, i: Extended targets.  
In *Proceedings of the 12th International Conference on Information Fusion*, Seattle, WA, USA, 2009.
- [28] L. Mihaylova, A. Y. Carmi, F. Septier, A. Gning, S. K. Pang, and S. Godsill  
Overview of Bayesian sequential Monte Carlo methods for group and extended object tracking.  
*Digital Signal Processing*, 25:1–16, Feb. 2014.
- [29] K. Mosler and F. Schmid  
*Wahrscheinlichkeitsrechnung und schließende Statistik*.  
Springer, 2 edition, 2006.
- [30] J. E. Moyal  
The general theory of stochastic population processes.  
*Acta Mathematica*, 108:1–31, 1962.
- [31] B. Ristic, D. Clark, and B.-N. Vo  
Improved SMC implementation of the PHD-filter.  
In *Proceedings of the 13th International Conference on Information Fusion*, Edinburgh, UK, 2010.
- [32] M. Schikora, W. Koch, R. Streit, and D. Cremers  
Sequential Monte Carlo method for the iFilter.  
In *Proceedings of the 14th International Conference on Information Fusion*, Chicago, IL, USA, 2011.
- [33] M. Schikora, W. Koch, R. Streit, and D. Cremers  
Sequential Monte Carlo method for multi-target tracking with the intensity filter.  
In P. Georgieva, L. Mihaylova, and L. C. Jain, editors, *Advances in Intelligent Signal Processing and Data Mining: Theory and Applications*, volume 410, pages 55–87. Springer, 2012.
- [34] D. Stoyan, W. S. Kendall, and J. Mecke  
*Stochastic geometry and its applications*.  
Wiley, 2nd edition edition, Sep. 1995.
- [35] R. Streit  
The probability generating functional for finite point processes, and its application to the comparison of PHD and intensity filters.  
*Journal of Advances in Information Fusion*, 8(2):119–132, Dec. 2013.
- [36] R. Streit  
A technique for deriving multitarget intensity filters using ordinary derivatives.  
*Journal of Advances in Information Fusion*, 9(1):3–12, June 2014.
- [37] R. Streit, C. Degen, and W. Koch  
The pointillist family of multitarget tracking filters.  
Submitted to IEEE Transaction on Aerospace and Electronic Systems, May 2015. Online available at <http://arxiv.org/abs/1505.08000>; Website retrieved at the 18.06.2015.
- [38] R. S. Strichartz  
*Guide to Distribution Theory and Fourier*.  
World Scientific Publishing Company, 2013.
- [39] A. Swain and D. Clark  
Extended object filtering using spatial independent cluster processes.  
In *Proceedings of the 13th International Conference on Information Fusion*, pages 1–8, Edinburgh, July 2010.
- [40] W. Walter  
*Einführung in die Theorie der Distributionen*.  
B. I.-Wissenschaftsverlag, 1974.



**Christoph Degen** received his Diploma in Mathematics at the Technical University of Kaiserslautern, Germany. Since 2011 he works at the Fraunhofer FKIE in the department for Sensor Data Fusion and Information Processing.

The research of Christoph Degen is focused on the application of finite point processes in target tracking.



**Felix Govaers** received his Diploma in Mathematics and his Ph.D. with the title “Advanced data fusion in distributed sensor applications” in Computer Science, both at the University of Bonn, Germany. Since 2009 he works at Fraunhofer FKIE in the department for Sensor Data Fusion and Information Processing where he now leads the team “Distributed Systems.” The research of Felix Govaers is focused on data fusion for state estimation in sensor networks. This includes track-extraction, processing of delayed measurements as well as the Distributed Kalman filter and track-to-track fusion.



**Johann Wolfgang Koch** (M '00–SM '09–F '11) studied Physics and Mathematics at the Aachen Technical University (RWTH Aachen), Germany, where he earned a Dr. rer. nat. degree in Theoretical Physics. At present, he is head of the department Sensor Data and Information Fusion at Fraunhofer FKIE, a research institute active in network enabled capabilities for defense and security applications. On various topics within target tracking and multisensory fusion, he published a text book, 14 several handbook chapters and more than 200 journal and conference articles. At present, his particular research interests aim at advanced distributed target tracking, linking data fusion and signal processing tightly together, as well as at bridging the gap between the lower and higher levels of information fusion, thus providing better links to decision support systems. For the IEEE Transactions on Aerospace and Electronic Systems he served in various editing positions. Moreover, he is Member of the Board of Governors of the IEEE Aerospace and Electronics Systems Society (AESS), Chair of the Germany Chapter of the AESS, and Member of the Board of Directors of the International Society of Information Fusion, serving as its President in 2013. Since many years, he is active within the NATO Science and Technology Organization (STO), where he worked in research task groups and delivered NATO Lecture Series. At Bonn University, he holds a habilitation degree on Applied Computer Science and teaches on sensor data fusion topics. Moreover, he initiated the series of the annual IEEE AESS workshops Sensor Data Fusion—Trends, Solutions, Applications (SDF 2015: Bonn, October 6–8, 2015).

# An improved measurement model for target tracking under measurement origin uncertainty

VIJI PAUL PANAKKAL  
RAJBABU VELMURUGAN

Single-target tracking using a standard Kalman filter with fixed measurement noise covariance will be effective if the target originated measurement is known. Under measurement origin uncertainty (MOU) the target state is updated in a probabilistic data association (PDA) framework using the set of measurements obtained inside a validation region (gate region). This paper develops a model for validated measurements using a conventional target originated measurement model and a model for measurements with uncertain origin. Using the developed model for validated measurements the measurement noise covariance under measurement origin uncertainty (MOU) is estimated. With this model the multiplicative scalar information reduction factor (IRF) in the computation of Cramér-Rao lower bound (CRLB) with MOU is shown to be due to an additive term in the measurement noise covariance. This additive term is used in the probabilistic data association (PDA) filter for computing the spread of innovation. This leads to a modified measurement noise covariance, innovation covariance and Kalman filter gain resulting in an adaptive iterative PDA (Iter-PDA) filter. Improvements obtained using the proposed approach are demonstrated through Monte Carlo (MC) simulations by comparing with PDA and CRLB. The consistency of the modified filter is checked and found to be within the acceptable limits.

Manuscript received October 13, 2014; revised April 2, 2015; released for publication July 28, 2015.

Refereeing of this contribution was handled by Huimin Chen.

Authors' addresses: V. Panakkal, Central Research Laboratory, Bharat Electronics Ltd., Bangalore, India (e-mail: vijipaulp@bel.co.in). R. Velmurugan, Dept. of Electrical Engineering, Indian Institute of Technology, Bombay, Mumbai, India (e-mail: rajbabu@ee.iitb.ac.in).

1557-6418/15/\$17.00 © 2015 JAIF

## 1. INTRODUCTION

In surveillance systems, measurements can be due to targets of interest, clutter or false alarms. Target tracking in such conditions suffers from measurement origin uncertainty (MOU) in addition to measurement noise. Multiple hypotheses tracking (MHT), the optimal approach for tracking under MOU, [1], [2], uses all measurements  $\mathbf{Z}^k$  up to time  $k$  for data association. The issue with MHT is the maintenance of exponentially increasing number of hypotheses with time [1]. MHT uses pruning and merging of hypotheses to limit the Gaussian components [3], [4]. Sub-optimal approaches such as probabilistic data association (PDA) use only the measurements  $\mathbf{Z}(k)$  obtained at instant  $k$  for updating the predicted target state  $\hat{\mathbf{x}}_i(k | k - 1)$ . Because of the reduced computational effort compared to the optimal approach and due to its robustness towards clutter and missed detection (measurement) PDA is widely used for tracking in clutter [5], [6]. Earlier work exploring different aspects of using PDA in target tracking such as, consistency, maneuver, track initiation-deletion and track bias have appeared in [7], [8], [9], [10], [11]. In this paper the focus is on improving the estimation accuracy under MOU by modeling the uncertainty associated with measurement origin.

PDA uses all the measurements inside a gate area around the predicted state known as validated measurements for state update using the Kalman filter framework. Hence, the posterior state error covariance of the Kalman filter is increased depending on the measurement origin uncertainty. The gate size is determined using the innovation covariance computed using the prediction error covariance and measurement noise covariance. As the state update progresses the filter used in state update attains steady state and the prediction error covariance in Kalman filter reduces. Therefore, for time index  $k = 1, 2, 3$  the gate size computed using the innovation covariance reduces as shown in Fig. 1. The innovation covariance is also used in PDA filter for computing the measurement-to-track association hypotheses probability. In PDA filter, the Kalman filter gain and the innovation covariance corresponding to time instant  $k$  are computed using the parameters available at time  $k - 1$ , i.e., without using measurements from  $k$ th instant. The proposed approach in this paper uses measurements from  $k$ th instant to compute innovation covariance and Kalman filter gain.

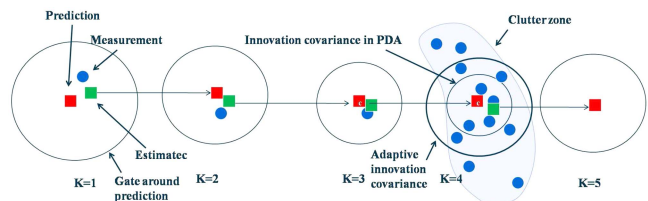


Fig. 1. Instantaneous adaptability of data association filter in clutter and clutter free zones.

In practice targets may move in clutter or clutter free zones and the tracking algorithm should adapt to the situation. As shown in Fig. 1, for time index  $k = 4$  the target enters a clutter zone and the pre-computed innovation covariance does not anticipate a clutter environment. The PDA filter increases the posterior error covariance and anticipates such a situation for the next time instant at  $k = 5$ . The standard PDA implementations provided in [5], [6], [12], [13] lack the instantaneous adaptability to measurement origin uncertainty. The adaptability of PDA filter during target maneuver is addressed in [14] by scaling the process noise covariance using the available data at current time  $k$ . For bearings-only tracking the gain of the extended Kalman filter is modified in [15] for better handling of target maneuver. In the proposed approach, the innovation covariance is adapted instantaneously so that better measurement-to-track association hypotheses probability is obtained. Using the modified innovation covariance the Kalman filter gain with MOU is computed and used for state error covariance update. The innovation covariance is made adaptive by computing the modified measurement noise covariance representing the MOU in addition to the known measurement noise variance.

The method developed in this paper improves the target state estimation accuracy by adaptively adjusting the filter parameters used in state estimation. In the smoothed PDA filter [16], the estimation accuracy of the PDA filter is improved by using measurements from the future. The prior estimates such as predicted target state and innovation covariance can be improved using the smoothed PDA, but with increased computational cost due to the usage of measurements from multiple time instants. For the case of finite resolution sensors the estimation accuracy has been improved compared to PDA in [17] for static and dynamic clutter pattern. In the limiting case of infinite resolution sensors the approach in [17] gives similar estimation accuracy as PDA. In this paper the objective is to model the origin uncertainty and to improve the estimation accuracy compared to PDA even in the case of measurements obtained from sensors having infinite resolution. The estimation accuracy for closely moving targets are improved in iterative JPDA (Iter-JPDA) compared to JPDA by computing better measurement-to-track association probabilities [18], [19] using measurements from the current time frame. The approach presented here also improves the estimation accuracy using measurements from the current time frame. In [20] improved estimation accuracy in the PDA framework has been obtained by modifying the data association probability with an assumption that the target originated measurements will always be closer to the predicted measurements. The approach developed in this paper improves estimation accuracy through better filter parameters obtained by modeling the measurement origin uncertainty. For the case of non-parametric tracking, a measurement sparsity estimation approach is

developed in [21]. Compared to conventional track oriented clutter density estimation the sparsity estimation approach in [21] reports improved track confirmation rate, but the approach does not report estimation accuracy improvements. In parametric form the proposed approach in this paper assumes the spatial density of clutter measurements is known a priori, as in the case of parametric PDA, and assumes that the number of clutter measurements follow a Poisson distribution. In non-parametric form the Poisson parameter is replaced with sample spatial density as in PDA filter.

We compare the mean square error obtained using the proposed approach with the Cramér-Rao lower bound (CRLB) [22]. The CRLB for the unknown parameter estimation is given by the Fisher information matrix (FIM) [23]. The CRLB for a linear dynamic system in the presence of additive white Gaussian noise and MOU has been derived in [9], [24] and observed that a scalar information reduction factor (IRF) exists due to MOU. The sufficient condition for the existence of a scalar IRF in MOU and its wide application is shown in [25], [26]. The exact computation of CRLB with MOU requires higher order integrals to obtain the IRF [9], [24]. A recursive form of CRLB obeying matrix Riccati-like expression is obtained in [27], [28] with an exception that the measurement noise covariance term is multiplied by an IRF. A simplified recursive expression for CRLB is shown in [29], but still requires evaluation of higher order integrals. The tabulated values of IRF given in [27], [30] can be used as an approximation, but for a fixed process and measurement noise ( $\mathbf{Q}$  and  $\mathbf{R}$ ) along with gate size  $\gamma$ . In this paper the information matrix used for the computation of CRLB for linear Gaussian case with MOU has been computed using the modified measurement noise covariance in a recursive form. The derived expression for scalar IRF can be evaluated for any  $\mathbf{Q}$ ,  $\mathbf{R}$  and  $\gamma$  and avoids evaluation of higher order integrals.

The main contribution of this paper is in providing a model for validated measurements to carry out improved data association for target tracking in clutter. Compared to the target originated measurement model the developed model for validated measurements handles the measurement origin uncertainty (MOU). Using the proposed model for validated measurements the adaptive measurement noise covariance in target tracking with MOU is computed. With this adaptive measurement noise covariance other filter parameters are modified and improved target state estimates are obtained. Another contribution of this paper is a method to compute the information reduction factor (IRF) with Monte Carlo (MC) simulations. Using this IRF the CRLB with MOU is computed and the performance of the proposed approach is compared.

The outline of this paper is as follows. In Section 2 we discuss the standard PDA based estimation process for comparison with the proposed approach. The proposed measurement model for validated measurements

to handle MOU is developed in Section 3. Using this measurement model, the modified innovation covariance and Kalman filter gain can be computed. The PDA filter using the proposed model becomes iterative because of the dependency between measurement-to-track association hypothesis probability and the innovation covariance. In Section 4, the recursive form of information matrix update with MOU has been developed. Here we also show that the scalar multiplicative IRF is due to an additive term in the measurement noise covariance computed with MOU. Section 5 gives the simulation results and compares the root mean-square positional error. The filter consistency test results and the variation of IRF for various  $\mathbf{Q}$ ,  $\mathbf{R}$  and  $\lambda$  are also provided. Section 6 provides the conclusion.

## 2. TARGET STATE ESTIMATION USING PDA

Consider the target state transition and measurement model of the form

$$\mathbf{x}_i(k+1) = \mathbf{F}\mathbf{x}_i(k) + \mathbf{w}(k), \quad (1)$$

$$\mathbf{z}_i(k) = \mathbf{H}\mathbf{x}_i(k) + \mathbf{v}(k), \quad (2)$$

where  $k$  is the time index,  $\mathbf{x}_i$  is a state vector of target  $i$ ,  $\mathbf{z}_i$  is the measurement vector,  $\mathbf{w}$  and  $\mathbf{v}$  are zero mean Gaussian noise vectors with covariance  $\mathbf{Q}$  and  $\mathbf{R}$ , respectively. The measurements obtained inside a gate area around the predicted state is referred as validated measurements. The validated measurement set  $\mathbf{Z}(k) = \{\mathbf{z}_j(k)\}_{j=1:m_k}$  obtained at  $k$ th scan consist of  $m_k$  number of measurements and  $\mathbf{Z}^k = \{\mathbf{Z}(k)\}$  denotes the cumulative set of measurements up to time  $k$ . Among the set  $\{\mathbf{z}_j(k)\}_{j=1:m_k}$  the index of target originated measurement is unknown and this causes the measurement origin uncertainty (MOU). The state transition matrix  $\mathbf{F}$  and observation matrix  $\mathbf{H}$  are assumed to be known. The predicted measurement is obtained from the predicted target state as  $\hat{\mathbf{z}}_i(k|k-1) = \mathbf{H}\hat{\mathbf{x}}_i(k|k-1)$ . The error of the predicted measurement is

$$\nu_i(k) = \mathbf{z}_i(k) - \hat{\mathbf{z}}_i(k|k-1),$$

and the corresponding innovation covariance is

$$\mathbf{S}_i(k) = E[\nu_i(k)\nu_i^T(k)]. \quad (3)$$

For single target tracking with measurement origin uncertainty, the joint association hypothesis is defined as

$$\mathbf{A}(j) = \begin{cases} j = 1 : m_k, \mathbf{z}_j(k) \text{ is associated with target and all other measurements are assumed to be from clutter.} \\ j = 0, \text{ No measurement is associated with target, all measurements are assumed to be from clutter.} \end{cases} \quad (4)$$

Measurement index  $j = 0$  indicates no validated measurement is used for association. Therefore,  $\mathbf{A}(0)$  indicates track is associated with predicted measurement  $\hat{\mathbf{z}}(k|k-1)$ . There are  $m_k$  number of measurements

available at scan  $k$  and only one measurement is associated with track. Conventional PDA approach assumes the associated measurement to be target originated. The set of all validated association hypotheses are denoted as  $\mathbf{A} = \{\mathbf{A}(j)\}_{j=0:m_k}$ .

The measurements falling in the validation region  $V(\gamma)$  are only considered for forming the association configuration. Validation region is a region around the predicted target state where the measurements will be available with high probability. The measurements inside the validation region satisfy the condition

$$V_k(\gamma) = [\mathbf{z} : \nu_j(k)\mathbf{S}_i^{-1}(k)\nu_j(k)^T \leq \gamma] \quad (5)$$

where  $\gamma$  is a parameter to control the validation (gate) region and the set of validated measurements at time  $k$  is denoted as  $\mathbf{Z}(k) = \{\mathbf{z}_j(k)\}_{j=1:m_k}$ . The probability of the hypothesis  $\mathbf{A}(j)$  is computed in PDA as

$$\begin{aligned} \beta_j &= p(\mathbf{A}(j) | \mathbf{Z}^k) = p(\mathbf{A}(j) | \mathbf{Z}(k), m_k, \mathbf{Z}^{k-1}), \\ &= \frac{1}{c} p(\mathbf{Z}(k) | \mathbf{A}(j), m_k, \mathbf{Z}^{k-1}) p(\mathbf{A}(j) | m_k, \mathbf{Z}^{k-1}), \\ &= \frac{1}{c} p(\mathbf{Z}(k) | \mathbf{A}(j), m_k, \mathbf{Z}^{k-1}) p(\mathbf{A}(j) | m_k), \end{aligned} \quad (6)$$

where  $c$  is a normalizing constant. The conditioning of  $\mathbf{A}(j)$  on  $\mathbf{Z}^{k-1}$  is considered irrelevant and so the prior for data association  $p(\mathbf{A}(j))$  is uniform in PDA [12]. Hence, the probability of association hypotheses unconditioned (conditioned only on number of measurements) with previous measurements is computed in (6). Because of the un-conditioning of  $\mathbf{A}(j)$  with prior measurements the proposed approach computes the measurement likelihood using innovation covariance unconditioned with any data association hypothesis. In the context of parameter estimation accounting model selection uncertainty the unconditional covariance is computed in [31]. The unconditional covariance improves the precision in estimates by accounting the uncertainty about what model to use [31]. In target tracking under MOU the data association hypothesis  $\mathbf{A}(j)$  assumes measurement  $\mathbf{z}_j$  is originated from target. In the proposed approach the unconditional covariance accounts the uncertainty in  $\mathbf{A}(j)$  and improves the estimation accuracy. The likelihood function of target originated measurement  $\mathbf{z}_j(k)$  is computed in PDA assuming a Gaussian density with mean  $\mathbf{H}\hat{\mathbf{x}}_i(k|k-1)$  and variance  $\mathbf{S}_i(k)$ , i.e. [12]

$$p(\mathbf{Z}(k) | \mathbf{A}(j), \mathbf{Z}^{k-1}) = \begin{cases} V_k^{-m_k+1} P_G^{-1} \mathcal{N}(\mathbf{z}_j(k); \mathbf{H}\hat{\mathbf{x}}_i(k|k-1), \mathbf{S}_i(k)), \\ j = 1, \dots, m_k. \\ V_k^{-m_k} j = 0. \end{cases} \quad (7)$$

where  $V_k$  is the volume of the validation region defined as

$$V_k = c_{n_z} \gamma^{n_z/2} |\mathbf{S}_i(k)|^{1/2}, \quad (8)$$

where  $n_z$  is the dimension of measurement (simulations carried out in this paper are with  $n_z = 2$ ) and  $c_{n_z}$

is the volume of the  $n_z$  dimensional unit hypersphere, and  $c_2 = \pi$ . In contrast to PDA, the proposed approach computes the likelihood given in (7) using a modified innovation covariance  $\mathbf{S}_i^\theta(k)$ , where the term  $\mathbf{S}_i^\theta(k)$  is computed in the proposed approach as unconditional innovation covariance [31]. PDA uses  $\mathbf{S}_i(k)$  in (7) assuming measurement  $\mathbf{z}_j(k)$  is target originated. In the proposed approach the modified innovation covariance  $\mathbf{S}_i^\theta(k)$  is computed using the modified measurement error covariance  $\mathbf{R}_i^\theta(k)$ .

## 2.1 Kalman filter

In the standard Kalman filter for tracking without MOU the prediction and update of error covariance matrices can be summarized as [32], [33]

$$\mathbf{P}_i(k | k-1) = \mathbf{F}\mathbf{P}_i(k-1)\mathbf{F}^T + \mathbf{Q}_i, \quad (9)$$

$$\begin{aligned} \mathbf{P}_i^*(k | k) &= (\mathbf{I} - \mathbf{K}_i(k)\mathbf{H})\mathbf{P}_i(k | k-1)(\mathbf{I} - \mathbf{K}_i(k)\mathbf{H})^T \\ &\quad + \mathbf{K}_i(k)\mathbf{R}\mathbf{K}_i(k)^T, \end{aligned} \quad (10)$$

where  $\mathbf{P}_i^*(k | k)$  denote posterior state error covariance without measurement origin uncertainty. The innovation covariance is computed as

$$\mathbf{S}_i(k) = \mathbf{H}\mathbf{P}_i(k | k-1)\mathbf{H}^T + \mathbf{R}. \quad (11)$$

The Kalman gain  $\mathbf{K}_i(k)$  is computed as

$$\mathbf{K}_i(k) = \mathbf{P}_i(k | k-1)\mathbf{H}^T\mathbf{S}_i^{-1}(k). \quad (12)$$

The updated state estimate is obtained as

$$\tilde{\mathbf{x}}_i(k | k) = \hat{\mathbf{x}}_i(k | k-1) + \mathbf{K}_i(k)\nu_i(k). \quad (13)$$

In standard Kalman filter, the measurement originates from the known target, hence

$$\nu_i(k) = \mathbf{z}_i(k) - \mathbf{H}\hat{\mathbf{x}}_i(k | k-1),$$

can be computed without ambiguity.

## 2.2 Estimation with measurement origin uncertainty (MOU)

In most of the existing approaches to handle measurement origin uncertainty, the posterior target state is obtained as the conditional mean [5] by averaging over all valid association hypotheses. The conditional mean is obtained as the minimum mean square estimate (MMSE) [12]

$$\begin{aligned} \tilde{\mathbf{x}}_i^{(MMSE)}(k | k) &= E[\mathbf{x}_i(k) | \mathbf{Z}^k] \\ &= E[E[\mathbf{x}_i(k) | \mathbf{A}, \mathbf{Z}^k] | \mathbf{Z}^k] \\ &= \sum_{j=0:m_k} E[\mathbf{x}_i(k) | \mathbf{A}(j), \mathbf{Z}^k] P(\mathbf{A}(j) | \mathbf{Z}^k) \\ &= \sum_{j=0:m_k} E[\mathbf{x}_i(k) | \mathbf{A}(j), \mathbf{Z}^k] \beta_j. \end{aligned} \quad (14)$$

The term  $\beta_j = p(\mathbf{A}(j) | \mathbf{Z}^k)$  is computed as [2], [12]

$$\beta_j = \begin{cases} \frac{b}{b + \sum_{j=1}^{m_k} e_j}, & j = 0 \text{ no valid measurement,} \\ \frac{e_j}{b + \sum_{j=1}^{m_k} e_j}, & 1 \leq j \leq m_k. \end{cases} \quad (15)$$

PDA filter in parametric form assumes the number of clutter measurements are obtained from Poisson model defined with parameter  $\lambda$ , where  $\lambda$  is the spatial density of false measurements. Parametric PDA filter computes  $b$  and  $e_j$  as follows

$$\begin{aligned} b &= \lambda \sqrt{2\pi |\mathbf{S}(k)|} \left( \frac{1 - P_d P_G}{P_d} \right), \\ e_j &= \exp(-0.5 \nu_j^T(k) \mathbf{S}^{-1}(k) \nu_j(k)), \end{aligned} \quad (16)$$

where  $|\cdot|$  denotes the determinant, and  $P_d$  is the probability of detection and  $P_G$  is the probability of measurement falling inside the gate. In non-parametric form the Poisson parameter  $\lambda$  is replaced with sample spatial density  $\lambda = m_k/V_k$  as the clutter density.

The proposed approach computes  $b$  and  $e_j$  using (16) by replacing  $\mathbf{S}_i(k)$  with a modified innovation covariance  $\mathbf{S}_i^\theta(k)$  to account for the measurement origin uncertainty. Less than unity value for  $\beta_j$  suggests that the origin of  $j$ th validated measurement is uncertain. The term  $\tilde{\mathbf{x}}_i^{(j)}(k | k) = E[\mathbf{x}_i(k) | \mathbf{A}(j), \mathbf{Z}^k]$  is the updated state estimate conditioned on  $j$ th validated measurement having originated from target. The estimate using  $\mathbf{A}(j)$  is

$$\tilde{\mathbf{x}}_i^{(j)}(k | k) = \hat{\mathbf{x}}_i(k | k-1) + \mathbf{K}_i(k)(\mathbf{z}_j(k) - \mathbf{H}\hat{\mathbf{x}}_i(k | k-1)), \quad (17)$$

where  $\mathbf{K}_i(k)$  is the Kalman gain, and  $\nu_j(k) = \mathbf{z}_j(k) - \mathbf{H}\hat{\mathbf{x}}_i(k | k-1)$  is the corresponding innovation. Given target originated measurement and predicted target state, innovation can be computed without ambiguity. But in (14) target state  $\tilde{\mathbf{x}}_i(k | k)$  is computed with unknown target originated measurement. Using (17) and (14) the estimated target state is

$$\begin{aligned} \tilde{\mathbf{x}}_i^{(MMSE)}(k | k) &= \sum_j \tilde{\mathbf{x}}_i^{(j)}(k | k) \beta_j \\ &= \hat{\mathbf{x}}_i(k | k-1) + \mathbf{K}_i(k) \sum_{j=0:m_k} \nu_j(k) \beta_j(k). \end{aligned} \quad (18)$$

In (18) with index  $j = 0$  the predicted measurement is used for updating the target state. Hence, the measurement prediction error is

$$\begin{aligned} \nu_0(k) &= \mathbf{z}_0(k) - \hat{\mathbf{z}}_i(k | k-1) \\ &= \hat{\mathbf{z}}_i(k | k-1) - \hat{\mathbf{z}}_i(k | k-1) = 0. \end{aligned} \quad (19)$$

Let  $\tilde{\mathbf{z}}_i(k) = \sum_j \bar{\mathbf{z}}_j(k)\beta_j(k)$ . The mean of the estimation error can be computed as

$$\begin{aligned} E(\epsilon_{x,k}) &= E(\mathbf{x}_i(k) - \tilde{\mathbf{x}}_i^{(MMSE)}(k | k)) \\ &= E[\mathbf{x}_i(k) - \hat{\mathbf{x}}_i(k | k-1) - \mathbf{K}_i(k)\tilde{\mathbf{z}}_i(k)] \\ &= E[\epsilon_{x_i,k-1}] - \mathbf{K}_i(k)E[\tilde{\mathbf{z}}_i(k)]. \end{aligned} \quad (20)$$

Therefore, if  $E[\tilde{\mathbf{z}}_i(k)] = 0$  for every  $k$  and  $E[\epsilon_{x_i,k-1}] = 0$  then  $E(\epsilon_{x,k}) = 0$  and the state estimate will be unbiased. PDA assumes only one measurement originated from target. But  $\tilde{\mathbf{z}}_i(k)$  is computed using more than one measurement. On account of this measurement origin uncertainty exists in the computation of  $\tilde{\mathbf{z}}_i(k)$  and the proposed approach attempts to model the measurement origin uncertainty by defining a random variable  $\mathbf{q}_j(k)$ . The proposed approach models the measurement origin uncertainty using  $\mathbf{q}_j(k)$ , so that  $E[\tilde{\mathbf{z}}_i(k)] = 0$  and the target state will remain unbiased. If all measurements are modeled using (2), considering only the target originated case, then the measurement noise covariance is  $\mathbf{R} = E[\mathbf{v}(k)\mathbf{v}(k)^T]$  as in PDA. But only one measurement among the validated measurement might have originated from target. Hence, under measurement origin uncertainty the measurement noise covariance can have two parts. The first part is a fixed known noise covariance  $\mathbf{R}$  for the measurement originated from target and the second part denoted as  $\Sigma(k) = E[\mathbf{q}_j(k)\mathbf{q}_j(k)^T]$  is contributed by the uncertainty in the measurement origin. The uncertainty in measurement origin is computed using the spread of measurements. The random variable  $\mathbf{q}_j(k)$  is used in the next subsection to define the spread of measurements. The modification of the measurement noise covariance affects the innovation covariance, Kalman gain and posterior error covariance as shown in the following sub-sections.

### 3. PROPOSED MEASUREMENT MODEL AND MODIFIED FILTER PARAMETERS

In PDA the target state estimate is obtained using combined innovation  $\tilde{\mathbf{z}}_i(k)$  as given in (18). The combined innovation  $\tilde{\mathbf{z}}_i(k)$  is obtained as

$$\begin{aligned} \tilde{\mathbf{z}}_i(k) &= \sum_j \bar{\mathbf{z}}_j(k)\beta_j(k) \\ &= \sum_{j=0:m_k} (\mathbf{z}_j(k) - \mathbf{H}\hat{\mathbf{x}}_i(k | k-1))\beta_j(k) \\ &= \sum_{j=0:m_k} (\mathbf{z}_j(k)\beta_j(k)) - \mathbf{H}\hat{\mathbf{x}}_i(k | k-1). \end{aligned} \quad (21)$$

Using (21) the target state estimate obtained by (18) can be rewritten as

$$\begin{aligned} \tilde{\mathbf{x}}_i^{(MMSE)}(k | k) &= \hat{\mathbf{x}}_i(k | k-1) \\ &+ \mathbf{K}_i(k) \left( \sum_{j=0:m_k} (\mathbf{z}_j(k)\beta_j(k)) - \mathbf{H}\hat{\mathbf{x}}_i(k | k-1) \right). \end{aligned} \quad (22)$$

In (22) the innovation is computed using the expectation of measurement  $E[\mathbf{z}_j(k)] = \sum_{j=0:m_k} \mathbf{z}_j(k)\beta_j(k)$ . Let the target originated measurement be denoted with index  $i$ ,  $\mathbf{z}_i(k)$ . Therefore, posterior target state computed using (17) with index  $i$  is corresponding to the target originated measurement  $\mathbf{z}_i(k)$ . Comparing the expression for posterior target state in PDA (22) and with the posterior target state obtained with the target originated measurement,  $\mathbf{z}_i(k)$  obtained with measurement index  $i$  in (17)

$$\begin{aligned} \tilde{\mathbf{z}}(k) &= \sum_{j=0:m_k} (\mathbf{z}_j(k)\beta_j(k)) = \mathbf{z}_i(k) \\ &= \mathbf{H}\mathbf{x}_i(k) + \mathbf{v}(k). \end{aligned} \quad (23)$$

If the measurement estimate  $\tilde{\mathbf{z}}(k) = \mathbf{z}_i(k)$  then the PDA estimates computed using (22) is equal to the estimates obtained with known target originated measurement. Hence,  $\tilde{\mathbf{z}}(k)$  is used as an estimate of  $\mathbf{z}_i(k)$  and the error in using validated measurement for updating the state of target instead of the measurement that originated from the target is computed as,  $\mathbf{q}_j(k) = \mathbf{z}_j(k) - \tilde{\mathbf{z}}(k)$ . Substituting for  $\tilde{\mathbf{z}}(k)$  from (23) gives

$$\mathbf{q}_j(k) = \mathbf{z}_j(k) - \sum_{j=0:m_k} \mathbf{z}_j(k)\beta_j(k). \quad (24)$$

Hence, using (23) the modified measurement model for the measurements obtained in the validation region is defined as

$$\begin{aligned} \mathbf{z}_j(k) &= \mathbf{z}_i(k) + \mathbf{q}_j(k) \\ &= \mathbf{H}\mathbf{x}_i(k) + \mathbf{v}(k) + \mathbf{q}_j(k), \end{aligned} \quad (25)$$

where,  $\mathbf{v}(k) \sim \mathcal{N}(\mathbf{v}(k); 0, \mathbf{R})$  and  $\mathbf{q}_j(k) \sim \mathcal{N}(\mathbf{q}_j(k); 0, \Sigma(k))$ . For the target originated measurement, substituting  $j = i$  in (24)

$$\mathbf{q}_i(k) = \mathbf{z}_i(k) - \sum_{j=0:m_k} (\mathbf{z}_j(k)\beta_j(k)). \quad (26)$$

Using (23) in (26), gives  $\mathbf{q}_i(k) = 0$ , accordingly, the modified measurement model given in (25) becomes (2) for the target originated measurement. Under association hypothesis  $\mathbf{A}(0)$  the target originated measurement may not be available inside the validation region and the predicted measurement  $\hat{\mathbf{z}}_i(k | k-1) = \mathbf{H}\hat{\mathbf{x}}_i(k | k-1)$  is used for state update. Hence, under  $\mathbf{A}(0)$  the target originated measurement  $\mathbf{z}_i(k)$  is replaced with  $\hat{\mathbf{z}}_i(k | k-1)$  and (25) becomes

$$\mathbf{z}_j(k) = \hat{\mathbf{z}}_i(k | k-1) + \mathbf{q}_j(k). \quad (27)$$

Using the identity  $\sum_{j=0:m_k} \beta_j(k) = 1$ , the expression for  $\mathbf{q}_j(k)$  is rewritten as

$$\begin{aligned} \mathbf{q}_j(k) &= \mathbf{z}_j(k) - \sum_{j=0:m_k} \mathbf{z}_j(k)\beta_j(k) \\ &= \mathbf{z}_j(k) - \mathbf{H}\hat{\mathbf{x}}_i(k | k-1) \\ &\quad - \sum_{j=0:m_k} (\mathbf{z}_j(k) - \mathbf{H}\hat{\mathbf{x}}_i(k | k-1))\beta_j(k) \\ &= \nu_j(k) - E(\nu_j(k)). \end{aligned} \quad (28)$$

The expression for  $\mathbf{q}_j(k)$  derived in (28) is used in the next subsection for computing  $\Sigma(k)$ . The conventional PDA [12] assumes under hypothesis  $\mathbf{A}(j)$  measurement  $\mathbf{z}_j(k)$  is target originated. The association is carried out under the assumption that at the maximum only one measurement can be originated from target. If  $\mathbf{z}_j(k)$  is target originated then  $\beta_j$  should be equal to one. The proposed model anticipates a non-ideal situation to identify the target originated measurement  $\mathbf{z}_i(k)$  from the set of measurement  $\mathbf{Z}(k) = \{\mathbf{z}_j(k)\}_{j=1:m_k}$ , so has a provision to cater the uncertainties in case none of the  $\beta(j)$  are equal to one. To satisfy  $\mathbf{z}_i(k) = \sum_{j=0:m_k} (\mathbf{z}_j(k)\beta_j(k))$ , the association probability  $\beta_i(k)$  should be equal to one and  $\beta_j(k) = 0$  for all  $j \neq i$ , because  $\sum_{j=0:m_k} \beta_j(k) = 1$ . If,  $\max(\beta_j(k)) = 1$  then there is only one nonzero  $\beta_j(k)$  value ( $\beta_j(k) = p(\mathbf{A}(j) | \mathbf{Z}^k) = 1$ ) and there is no uncertainty in selecting  $\mathbf{A}(j)$ , so  $\Sigma(k) = 0$ . But in practice,  $\max(\beta_j(k)) < 1$  and this implies  $\Sigma(k) \neq 0$  and results in additional terms in measurement error covariance, innovation covariance and posterior target state error covariance. Conventional PDA modifies the posterior target state error covariance with an additional term corresponding to the measurement origin uncertainty. The proposed approach computes the additional additive terms and modifies the measurement error covariance and innovation covariance along with posterior target state error covariance. The additive term used for modifying the measurement error covariance is obtained as,  $\Sigma(k) = E[\mathbf{q}_j(k)\mathbf{q}_j^T(k) | \mathbf{Z}^k]$ . An expression for computing  $\Sigma(k)$  is derived in the next subsection.

### 3.1 Modified measurement error covariance

The modified measurement error covariance is computed using (25) as

$$\begin{aligned} \mathbf{R}^\theta(k) &= E[(\mathbf{z}_j(k) - \mathbf{H}\mathbf{x}_i(k))(\mathbf{z}_j(k) - \mathbf{H}\mathbf{x}_i(k))^T | \mathbf{Z}^k] \\ &= (E[\mathbf{v}(k)\mathbf{v}(k)^T] + E[\mathbf{q}_j(k)\mathbf{q}_j^T(k) | \mathbf{Z}^k]). \end{aligned} \quad (29)$$

In PDA the measurement likelihood is computed using the error covariance  $\mathbf{R}(k)$  conditioned on the hypotheses that the given measurement alone is originated from the target. The modified measurement error covariance  $\mathbf{R}^\theta(k)$  is the unconditional measurement error variance [31]. The unconditional measurement error covariance consists of an additional term. The additional error variance term corresponds to the error in using the validated measurement for updating the target state instead of measurement that originated from the target and this can be obtained using (24) as

$$\begin{aligned} E[\mathbf{q}_j(k)\mathbf{q}_j^T(k) | \mathbf{Z}^k] \\ = E[(\mathbf{z}_j(k) - \tilde{\mathbf{z}}(k))(\mathbf{z}_j(k) - \tilde{\mathbf{z}}(k))^T | \mathbf{Z}^k]. \end{aligned}$$

The first term of the measurement error covariance in (29) is computed as

$$E[\mathbf{v}(k)\mathbf{v}(k)^T] = \mathbf{R}. \quad (30)$$

The second term of the measurement error covariance can be obtained using (28) as

$$\begin{aligned} \Sigma(k) &= E[\mathbf{q}_j(k)\mathbf{q}_j^T(k) | \mathbf{Z}^k] \\ &= E[(\nu_j(k) - E(\nu_j(k))) \\ &\quad (\nu_j(k) - E(\nu_j(k)))^T | \mathbf{Z}^k]. \end{aligned} \quad (31)$$

Using (30) and (31) in (29) the modified measurement error covariance can be computed as

$$\mathbf{R}^\theta(k) = \mathbf{R} + \Sigma(k). \quad (32)$$

Assuming  $\nu_j(k)$  are independent and identically distributed (i.i.d), as shown in [28], the expression for  $\Sigma(k)$  can be obtained from (31) as

$$\begin{aligned} \Sigma(k) &= E[\nu_j(k)\nu_j(k)^T | \mathbf{Z}^k] \\ &\quad - E(\nu_j(k) | \mathbf{Z}^k)E(\nu_j(k) | \mathbf{Z}^k)^T \\ &= \sum_{j=0}^{m_k} \beta_j \nu_j(k)\nu_j(k)^T - \tilde{\mathbf{Z}}(k)\tilde{\mathbf{Z}}(k)^T, \end{aligned} \quad (33)$$

where  $\tilde{\mathbf{Z}}(k) = E(\nu_j(k) | \mathbf{Z}^k)$ . The expectation in (33) is over the measurement error  $\nu_j(k) = \mathbf{z}_j(k) - \mathbf{H}\hat{\mathbf{x}}_i(k | k-1)$  and  $\beta_j \propto p(\nu_j(k))$ . The expression given in (33) is used in PDA filter for computing the posterior error covariance [12], [6]. For the case with  $P_d = 1$  and  $P_G = 1$  in (16), i.e., with  $b = 0$  in (15) results in  $\beta_0 = 0$  and the modified measurement error covariance is obtained as

$$\mathbf{R}^\theta(k) = \mathbf{R} + \Sigma(k). \quad (34)$$

Hence, the modified measurement error covariance  $\mathbf{R}^\theta(k)$  is adaptive with probability of detection  $P_d$  and also with measurement origin uncertainty.

### 3.2 Modified innovation covariance

The modified innovation covariance is computed by substituting  $\mathbf{R}^\theta(k)$  instead of  $\mathbf{R}$  in (11)

$$\mathbf{S}_i^\theta(k) = \mathbf{H}\mathbf{P}_i(k | k-1)\mathbf{H}^T + (1 - \beta_0)\mathbf{R} + \Sigma(k). \quad (35)$$

For  $\beta_0 = 0$  the modified innovation covariance is

$$\mathbf{S}_i^\theta(k) = \mathbf{S}_i(k) + \Sigma(k). \quad (36)$$

where  $\mathbf{S}_i(k)$  is the innovation covariance of target originated measurements and the term  $\Sigma(k)$  is used for computing the spread of innovation in [12]. The modified innovation covariance  $\mathbf{S}_i^\theta(k)$  is used in (16) and (15) to find the data association probabilities in the proposed approach.

### 3.3 Posterior error covariance in PDA

The posterior covariance with measurement origin uncertainty can be obtained from Appendix D.3 of [12] as

$$\mathbf{P}_i(k | k) = E[(\mathbf{x}_i(k) - \tilde{\mathbf{x}}_i(k | k))(\mathbf{x}_i(k) - \tilde{\mathbf{x}}_i(k | k))^T | \mathbf{Z}^k], \quad (37)$$

$$\begin{aligned} \mathbf{P}_i(k | k) &= \beta_0 \mathbf{P}_i(k | k-1) + (1 - \beta_0) \mathbf{P}^*(k | k) \\ &+ \mathbf{K}_i(k) \left( \sum_{j=0}^{m_k} \beta_j \bar{\mathbf{z}}_j \bar{\mathbf{z}}_j^T - \tilde{\mathbf{Z}} \tilde{\mathbf{Z}}^T \right) \mathbf{K}_i(k)^T, \end{aligned} \quad (38)$$

where  $\mathbf{P}^*(k | k)$  is the posterior covariance without measurement origin uncertainty, obtained in (10), and  $\beta_0$  is the probability of updating the target state without having any valid measurement.

#### 3.4 Modified filter gain

The objective in computing gain  $\mathbf{K}$  in Kalman filter is to minimize the estimation error, by minimizing the trace of the posterior error covariance  $\mathbf{P}(k | k)$ . The target index  $i$  is dropped in this section for notational brevity. Substituting the expression for posterior covariance from (10) in (38) gives

$$\begin{aligned} \mathbf{P}(k | k) &= \beta_0 \mathbf{P}(k | k-1) \\ &+ (1 - \beta_0) (\mathbf{I} - \mathbf{K}(k) \mathbf{H}) \mathbf{P}(k | k-1) \\ &\times (\mathbf{I} - \mathbf{K}(k) \mathbf{H})^T + \mathbf{K}(k) \mathbf{R} \mathbf{K}(k)^T \\ &+ \mathbf{K}(k) \left( \sum_{j=0}^{m_k} \beta_j \nu_j \nu_j^T - \tilde{\mathbf{Z}} \tilde{\mathbf{Z}}^T \right) \mathbf{K}(k)^T. \end{aligned} \quad (39)$$

The gain  $\mathbf{K}^\theta$  that minimizes the trace of  $\mathbf{P}(k | k)$  (sum of the mean square errors in the estimates of all the elements of state vector) is obtained by computing the derivative with respect to  $\mathbf{K}$  as

$$\begin{aligned} &\frac{d(\text{trace}\{\mathbf{P}(k | k)\})}{d\mathbf{K}} \\ &= 2(1 - \beta_0) (\mathbf{I} - \mathbf{K}(k | k) \mathbf{H}) \mathbf{P}(k | k-1) (-\mathbf{H})^T \\ &+ 2\mathbf{K}(k | k) ((1 - \beta_0) \mathbf{R} + \sum_{j=0}^{m_k} \beta_j \nu_j \nu_j^T - \tilde{\mathbf{Z}} \tilde{\mathbf{Z}}^T), \end{aligned} \quad (40)$$

and setting this equal to zero. The modified filter gain  $\mathbf{K}^\theta$  is

$$\mathbf{K}^\theta(k) = \frac{(1 - \beta_0) \mathbf{P}(k | k-1) \mathbf{H}^T}{(1 - \beta_0) (\mathbf{H} \mathbf{P}(k | k-1) \mathbf{H}^T + \mathbf{R}) + \sum_{j=0}^{m_k} \beta_j \nu_j \nu_j^T - \tilde{\mathbf{Z}} \tilde{\mathbf{Z}}^T}. \quad (41)$$

The modified gain  $\mathbf{K}^\theta$  obtained in (41) reduces to the standard Kalman gain

$$\mathbf{K}(k) = \frac{\mathbf{P}(k | k-1) \mathbf{H}^T}{\mathbf{H} \mathbf{P}(k | k-1) \mathbf{H}^T + \mathbf{R}} = \frac{\mathbf{P}(k | k-1) \mathbf{H}^T}{\mathbf{S}(k | k)} \quad (42)$$

under no measurement origin uncertainty. The quantity

$$\Sigma(k) = \sum_{j=0}^{m_k} \beta_j \nu_j(k) \bar{\mathbf{z}}_j^T(k) - \tilde{\mathbf{Z}}(k) \tilde{\mathbf{Z}}^T(k),$$

will be zero if  $\beta_j = 1$  for any  $j$ , ( $\sum_{j=0}^{m_k} \beta_j = 1$ ). The target state conditioned on hypothesis  $\mathbf{A}(j)$  denoted as  $\tilde{\mathbf{x}}_i^{(j)}(k | k)$  is computed in (17) is conditioned on only one hypothesis  $\mathbf{A}(j)$ . Hence, the gain  $\mathbf{K}(k)$  used in (17) is the standard Kalman gain. The modified filter gain is used in computing the posterior state error covariance because of the involvement of more than one association hypotheses. The posterior state error covariance computed using modified filter gain  $\mathbf{K}^\theta(k)$  is referred as modified posterior state error covariance denoted by  $\mathbf{P}^\theta(k | k)$ .

The modified posterior state error covariance can be obtained by substituting  $\mathbf{K}^\theta$  obtained by (41) in (39) as

$$\begin{aligned} \mathbf{P}^\theta(k | k) &= \beta_0 \mathbf{P}(k | k-1) + \\ &(1 - \beta_0) ((\mathbf{I} - \mathbf{K}^\theta(k) \mathbf{H}) \mathbf{P}(k | k-1) (\mathbf{I} - \mathbf{K}^\theta(k) \mathbf{H})^T \\ &+ \mathbf{K}^\theta(k) \mathbf{R} \mathbf{K}^\theta(k)^T) \\ &+ \mathbf{K}^\theta(k) \left( \sum_{j=0}^{m_k} \beta_j \nu_j \nu_j^T - \tilde{\mathbf{Z}} \tilde{\mathbf{Z}}^T \right) \mathbf{K}^\theta(k)^T. \end{aligned} \quad (43)$$

#### 3.5 Iterative PDA (Iter-PDA)

The PDA approach uses Kalman filter (KF) framework and in KF the estimation process evolves with time and measurement update. The time update and measurement update steps involved in target tracking under MOU using PDA approach is shown in Fig. 2.

The modified innovation covariance is computed in the proposed approach using modified measurement error covariance  $\mathbf{R}^\theta(k)$  instead of fixed measurement noise variance  $\mathbf{R}$ . The gain used for computing the covariance update in the measurement update step is also modified with the measurement error variance. The difference in the proposed approach compared to conventional PDA approach is shown with bold dotted arrows in Fig. 2. The main difference with conventional PDA is in computing the adaptive data association probabilities and modified filter gain as shown in Fig. 2. The proposed modifications in gain and association probabilities are obtained with dynamic measurement error variance  $\Sigma(k)$ . The modified association probabilities are used for computing the combined target state estimate. The advantage of the proposed technique (Iter-PDA) is shown with Monte Carlo simulations in Sec. 5.

The modified innovation covariance  $\mathbf{S}^\theta(k)$  computed using (35) can be written as

$$\begin{aligned} \mathbf{S}^\theta(k) &= \mathbf{H} \mathbf{P}(k | k-1) \mathbf{H}^T + (1 - \beta_0) \mathbf{R} + \Sigma(k), \\ &= \mathbf{H} \mathbf{P}(k | k-1) \mathbf{H}^T + \mathbf{R}^\theta(k). \end{aligned} \quad (44)$$

Therefore, by modifying the measurement model in Iter-PDA the measurement noise covariance is modified with an additive term  $\Sigma(k)$  corresponding to measurement origin uncertainty. The modified innovation



ties using the iteratively computed maximum a posterior estimates. The proposed approach here computes the association probabilities and innovation covariance by solving (33, 35) and (15, 16) iteratively.

#### 4. CRLB WITH MOU USING MONTE CARLO AVERAGING TECHNIQUE

In target tracking with MOU the tracking performance can be evaluated by comparing how close the mean square error (MSE) is to the theoretical lower bound of the estimation error. This bound obtained as Cramér-Rao lower bound (CRLB) is shown to be the equivalent to the error covariance matrix [23] of the Kalman filter for the linear Gaussian case without MOU. The CRLB with MOU will also provide a mechanism to compare the performance of the proposed approach and PDA approach. In this section a recursive form of CRLB with measurement origin uncertainty is computed for the linear Gaussian case using the measurement model proposed in Sec.3. The difficulty in obtaining the CRLB with MOU is in the computation of information reduction factor (IRF). The approach given in [9], [24] requires computationally intensive numerical integration for the computation of IRF. The other alternative is to use tabulated values given in [27], [30] for a fixed filter parameter case. The approach developed in this section depend on Monte Carlo runs and is applicable to any filter parameters and clutter density.

Let  $\tilde{\mathbf{x}}_i(k|k)$  be an unbiased estimate of  $\mathbf{x}_i(k)$ . The error covariance of  $\tilde{\mathbf{x}}_i(k|k)$  denoted as  $\mathbf{P}_i(k|k)$  has a lower bound referred to as the CRLB on the estimation error and is expressed as [23]

$$\begin{aligned} \mathbf{P}_i(k|k) &= E[(\tilde{\mathbf{x}}_i(k|k) - \mathbf{x}_i(k))(\tilde{\mathbf{x}}_i(k|k) - \mathbf{x}_i(k))^T] \\ &\geq \mathbf{J}^{-1}(k), \end{aligned} \quad (48)$$

where the lower bound  $\mathbf{J}(k)$  is denoted without target index for notational brevity and can be obtained as

$$\begin{aligned} \mathbf{J}(k) &= E\{[\nabla_{\mathbf{x}_i(k)} \log p(\mathbf{x}_i(k), \mathbf{z}_j(k)) \\ &\quad [\nabla_{\mathbf{x}_i(k)} \log p(\mathbf{x}_i(k), \mathbf{z}_j(k))]^T] \\ &= -E\{[\nabla_{\mathbf{x}_i(k)} [\nabla_{\mathbf{x}_i(k)} \log p(\mathbf{x}_i(k), \mathbf{z}_j(k))]^T]. \end{aligned} \quad (49)$$

An unbiased state estimator with covariance matrix equal to CRLB (holding equality in (48)) is statistically efficient [22], [23]. A recursive form of information matrix  $\mathbf{J}(k)$  can be obtained as in [34]

$$\begin{aligned} \mathbf{J}(k+1) &= D^{22}(k) \\ &\quad - D^{21}(k)(\mathbf{J}(k) + D^{11}(k))^{-1}D^{12}(k), \quad (k > 0), \end{aligned} \quad (50)$$

where the terms  $D^{i_1 i_2}(k)$  can be computed as

$$\begin{aligned} D^{11}(k) &= -E\{\nabla_{\mathbf{x}_i(k)}[\nabla_{\mathbf{x}_i(k)} \log p(\mathbf{x}_i(k+1) | \mathbf{x}_i(k))]^T\} \\ D^{21}(k) &= -E\{\nabla_{\mathbf{x}_i(k)}[\nabla_{\mathbf{x}_i(k+1)} \log p(\mathbf{x}_i(k+1) | \mathbf{x}_i(k))]^T\} \\ D^{12}(k) &= -E\{\nabla_{\mathbf{x}_i(k+1)}[\nabla_{\mathbf{x}_i(k)} \log p(\mathbf{x}_i(k+1) | \mathbf{x}_i(k))]^T\} \\ D^{22}(k) &= -E\{\nabla_{\mathbf{x}_i(k+1)}[\nabla_{\mathbf{x}_i(k+1)} \log p(\mathbf{x}_i(k+1) | \mathbf{x}_i(k))]^T\} \\ &\quad - E\{\nabla_{\mathbf{x}_i(k+1)}[\nabla_{\mathbf{x}_i(k+1)} \log p(\mathbf{z}_j(k+1) | \mathbf{x}_i(k+1))]^T\}. \end{aligned} \quad (51)$$

In (51)  $\nabla_{\mathbf{x}_i(k)}$  is the first-order partial derivative operator with respect to  $\mathbf{x}_i(k)$ . The expectation operator is defined as [23]

$$\begin{aligned} &-E\{\nabla_{\mathbf{x}_i(k)}[\nabla_{\mathbf{x}_i(k)} \log p(\cdot)]^T\} \\ &= E\{[\nabla_{\mathbf{x}_i(k)} \log p(\cdot)][\nabla_{\mathbf{x}_i(k)} \log p(\cdot)]^T\}, \end{aligned} \quad (52)$$

and  $D^{12}(k) = [D^{21}(k)]^T$ . Using the state evolution (1) and the modified measurement error covariance (34), the terms inside the expectation of (51) can be evaluated as

$$\begin{aligned} &\nabla_{\mathbf{x}_i(k)} \log p(\mathbf{x}_i(k+1) | \mathbf{x}(k)) \\ &= \nabla_{\mathbf{x}_i(k)} - \frac{1}{2}[[\mathbf{x}_i(k+1) - \mathbf{F}\mathbf{x}_i(k)]^T \mathbf{Q}^{-1}(k) \\ &\quad [\mathbf{x}_i(k+1) - \mathbf{F}\mathbf{x}_i(k)]] \\ &= \mathbf{F}^T \mathbf{Q}^{-1}(k)[\mathbf{x}_i(k+1) - \mathbf{F}\mathbf{x}_i(k)]. \end{aligned} \quad (53)$$

Similarly

$$\begin{aligned} &\nabla_{\mathbf{x}_i(k+1)} \log p(\mathbf{z}_j(k+1) | \mathbf{x}_i(k+1)) \\ &= \nabla_{\mathbf{x}_i(k+1)} - \frac{1}{2}[[\mathbf{z}_j(k+1) - \mathbf{H}\mathbf{x}_i(k+1)]^T \\ &\quad \times (\mathbf{R}^\theta(k+1))^{-1}[\mathbf{z}_j(k+1) - \mathbf{H}\mathbf{x}_i(k+1)]] \\ &= \mathbf{H}^T (\mathbf{R}^\theta(k+1))^{-1}[\mathbf{z}_j(k+1) - \mathbf{H}\mathbf{x}_i(k+1)], \end{aligned} \quad (54)$$

where  $\mathbf{R}^\theta(k+1)$  is the modified measurement error variance and obtained in (34) as

$$\mathbf{R}^\theta(k+1) = \mathbf{R} + \Sigma(k+1). \quad (55)$$

The matrices defined in (51) are computed using (54) and (55) as follows

$$\begin{aligned} D^{11}(k) &= E\{\nabla_{\mathbf{x}(k)}[\nabla_{\mathbf{x}(k)} \log p(\mathbf{x}(k+1) | \mathbf{x}(k))]^T\} \\ &= E\{\mathbf{F}^T \mathbf{Q}^{-1}(k)\mathbf{F}\} = \mathbf{F}^T \mathbf{Q}^{-1}(k)\mathbf{F}, \\ D^{12}(k) &= -\mathbf{F}^T \mathbf{Q}^{-1}(k), \\ D^{22}(k) &= \mathbf{Q}^{-1}(k) + E\{\mathbf{H}^T (\mathbf{R}^\theta(k+1))^{-1}\mathbf{H}\} \\ &= \mathbf{Q}^{-1}(k) + \mathbf{H}^T E\{(\mathbf{R}^\theta(k+1))^{-1}\}\mathbf{H}. \end{aligned} \quad (56)$$

The only term in the computation of  $\mathbf{J}(k+1)$  that depends on measurements is  $D^{22}(k)$ . Using (56) in (50)

the recursive form of  $\mathbf{J}(k+1)$  can be rewritten as

$$\begin{aligned} \mathbf{J}(k+1) &= \mathbf{Q}^{-1}(k) + \mathbf{H}^T E\{(\mathbf{R}^\theta(k+1))^{-1}\} \mathbf{H} \\ &\quad - \mathbf{Q}^{-1}(k) \mathbf{F}(\mathbf{J}(k) + \mathbf{F}^T \mathbf{Q}^{-1}(k) \mathbf{F})^{-1} \mathbf{F}^T \mathbf{Q}^{-1}(k). \end{aligned} \quad (57)$$

The difficulty in computing  $\mathbf{J}(k+1)$  using (57) is the presence of the expectation operator. We use a Monte Carlo approximation of  $\mathbf{J}(k+1)$  as suggested by [23]. The term  $E\{(\mathbf{R}^\theta(k+1))^{-1}\}$  can be obtained, from Appendix A, as

$$\begin{aligned} E\{(\mathbf{R}^\theta(k+1))^{-1}\} &= E\{(\mathbf{R} + \boldsymbol{\Sigma}(k+1))^{-1}\} \\ &= q_2 \mathbf{R}^{-1}, \text{ where } q_2 < 1. \end{aligned} \quad (58)$$

Here  $q_2$  is the scalar information reduction factor (IRF). Substituting (58) in (57), the CRLB with MOU can be obtained as

$$\begin{aligned} \mathbf{J}(k+1) &= \mathbf{Q}^{-1}(k) + \mathbf{H}^T q_2 \mathbf{R}^{-1}(k+1) \mathbf{H} \\ &\quad - \mathbf{Q}^{-1}(k) \mathbf{F}(\mathbf{J}(k) + \mathbf{F}^T \mathbf{Q}^{-1}(k) \mathbf{F})^{-1} \mathbf{F}^T \mathbf{Q}^{-1}(k). \end{aligned} \quad (59)$$

The CRLB for the target state  $\mathbf{x}_i(k)$  can be obtained from the inverse of the information matrix  $\mathbf{J}(k)$  as [22], [23]

$$\text{CRLB}(\mathbf{x}_i(k)) = \mathbf{J}^{-1}(k). \quad (60)$$

A deterministic expression for the CRLB consisting of higher order integrals for evaluating the expectation operation in (58) over all possible validated measurements can be obtained as shown in [27]. One way to avoid the computation of higher order integral is to use the tabulated values for IRF. The tabulated values of IRF given in [27], [30] are for  $q = 1$  and  $\mathbf{R} = \mathbf{I}$ , but for different  $q$  and  $\mathbf{R}$  the IRF values will be different. The values of IRF are shown to depend on  $q$ ,  $\mathbf{R}$ ,  $\lambda$  and  $P_d$  [27], [28]. But, in the simulations carried out in this paper with high clutter density it is observed that the IRF also depends on the time index  $k$  (Fig. 10[a] shows variation of IRF with  $k$ ). The simulation results indicate the information reduction decreases when a filter attains steady state. The RMS positional error provided in the next section are computed using Monte Carlo simulations. Therefore, the CRLB is obtained as an auxiliary result of the simulations. In fact the tracker performance evaluation based on Monte Carlo simulation does not require additional MC runs for the computation of CRLB.

## 5. SIMULATIONS

To compare the proposed approach with PDA, an example scenario having state vector  $\mathbf{x}^T = [x \dot{x}; y \dot{y}]^T$  and initial condition  $\mathbf{x}^T = [200 \ 0; 10000; -15]^T$  is considered [12]. The system evolves according to

$$\mathbf{x}(k+1) = \mathbf{F}\mathbf{x}(k) + \boldsymbol{\Gamma}\mathbf{w}(k), \quad (61)$$

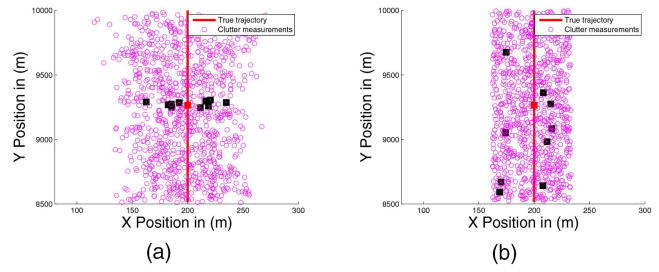


Fig. 3. Scenario in X-Y plane. Clutter measurements obtained from cumulative time instants ( $k = 1$  to 100) are plotted with magenta circles. Clutter measurements at  $k = 50$  are shown with bold black squares. True position at  $k = 50$  is shown with red bold square. (a) Case (i): Clutter measurements are uniformly distributed in a square centered around the correct measurement (b) Case (ii): Clutter measurements are uniformly distributed in surveillance region.

$$\text{where } \boldsymbol{\Gamma} = \begin{bmatrix} T^2/2 & 0 \\ T & 0 \\ 0 & T^2/2 \\ 0 & T \end{bmatrix} \text{ and the time interval } T =$$

1 s. The process noise covariance and state transition matrices are

$$\mathbf{Q} = \begin{bmatrix} \mathbf{Q}_1 & \mathbf{0} \\ \mathbf{0} & \mathbf{Q}_1 \end{bmatrix} q, \quad \mathbf{F} = \begin{bmatrix} \mathbf{F}_1 & \mathbf{0} \\ \mathbf{0} & \mathbf{F}_1 \end{bmatrix}, \quad (62)$$

where

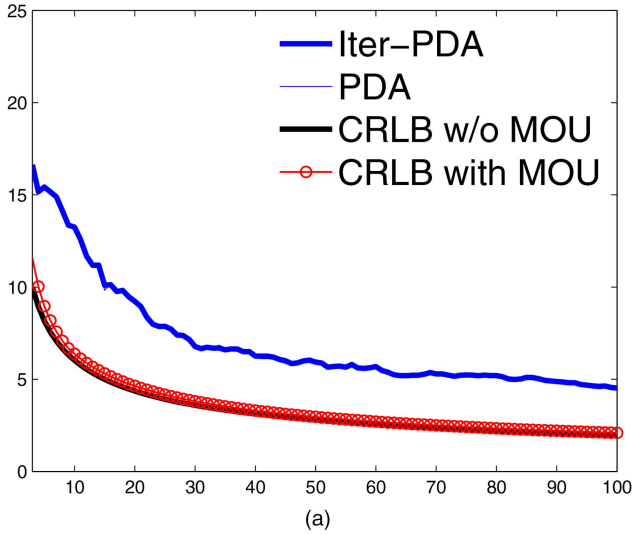
$$\mathbf{Q}_1 = \begin{bmatrix} \frac{T^4}{4} & \frac{T^3}{2} \\ \frac{T^3}{2} & T^2 \end{bmatrix}, \quad \mathbf{F}_1 = \begin{bmatrix} T & 1 \\ 0 & 1 \end{bmatrix}. \quad (63)$$

The process noise is a zero mean white sequence with variance,  $E[\mathbf{w}(k)^2] = q^2$ . Measurement noise is a zero mean white sequence with variance

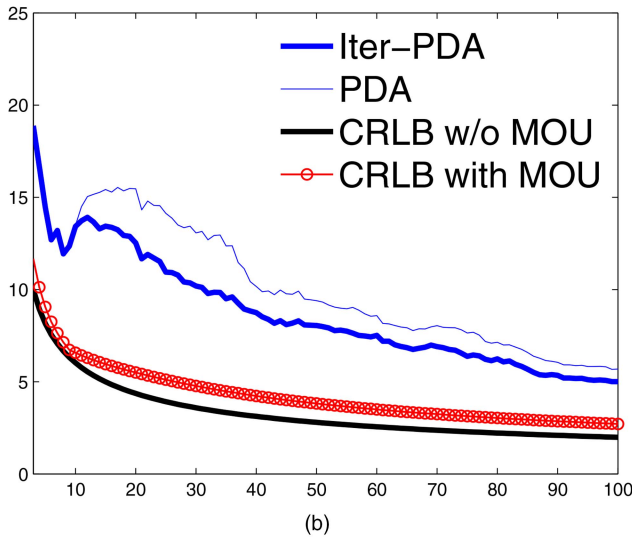
$$\mathbf{R} = \begin{bmatrix} 200 & 0 \\ 0 & 200 \end{bmatrix}.$$

The state error covariance is initialized according to the two-point differencing method [32], [35]. The measurements are assumed to be obtained from target as well as from clutter. The clutter measurements are generated in two ways. In case (i), the clutter points are uniformly distributed in a square having area  $A = 10\pi\gamma|\mathbf{S}(k)|^{1/2}$  and centered around the correct measurement (known in simulation) [12]. In case (ii), clutter measurements are distributed uniformly in a rectangular area covering the surveillance region. The surveillance region is defined by minimum and maximum X-Y coordinates of the trajectory. The scenario is shown in X-Y plane in Fig. 3 for  $q = 0$ . Compared to the case (i) shown in Fig. 3(a), the number of clutter measurements will be lower inside the gate for case (ii) shown in Fig. 3(b), because of the spread of measurements across the surveillance region. Clutter measurements at  $k = 50$  is shown in Fig. 3 to demonstrate the difference in spread of measurements.

The advantage of Iter-PDA will be significantly visible with more clutter points inside the gate. Therefore,



(a)



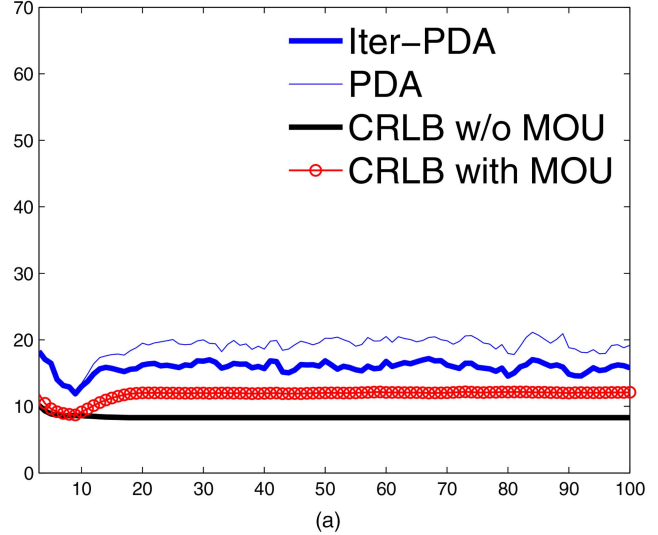
(b)

Fig. 4. RMS positional error (in m) versus time index  $k$ , with conventional and the proposed approach with  $\gamma = 1$  and  $q = 0$  for varying clutter densities (a)  $\lambda = 1e^{-4}$ . (b)  $\lambda = 1e^{-3}$ .

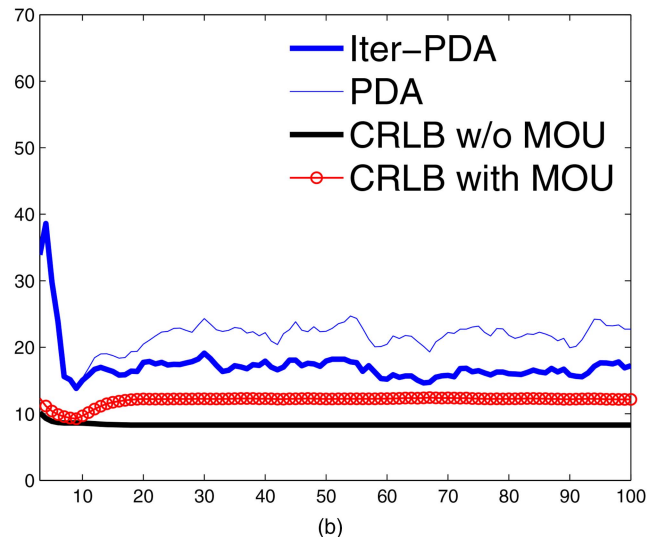
the simulations results with case (i) are provided in Fig. 4 to Fig. 6. The results with case (ii) is provided in Fig. 7. The parameter  $\gamma$  controlling the gate area is defined in Section 2. The average number of clutter points  $\bar{m}_k = \lambda A$  per measurement frame is assumed to be Poisson distributed, where  $\lambda$  is the clutter density. The average number of iterations in Iter-PDA was five. In this section the performance of the Iter-PDA approach and PDA are compared to the CRLB. The CRLB and the information reduction factor (IRF) with MOU are computed for various filter parameters and clutter densities. The IRF variation pattern with  $\lambda$  and time index  $k$  were analyzed using Monte Carlo simulations. The consistency of Iter-PDA filter is also checked and compared with that of PDA under various  $P_d$ ,  $\lambda$  and  $q$ .

### 5.1 Estimation performance

The root mean square (RMS) positional error for 100 Monte Carlo (MC) runs with  $q = 0$  is plotted in



(a)



(b)

Fig. 5. RMS positional error (in m) versus time index  $k$ , with conventional and the proposed approach with  $\gamma = 1$ ,  $\bar{m}_k = 10$  and  $q = 1$  for varying probability of detection (a)  $P_d = 1$ . (b)  $P_d = 0.9$ .

Fig. 4(a), Fig. 4(b) with  $\gamma = 1$ ,  $\lambda = 1e^{-4}$  and  $\lambda = 1e^{-3}$ , respectively. The clutter measurements are introduced at time index  $k = 10$ . The clutter measurements are uniformly distributed in a square centered around the correct measurement as described in case (i). The number of clutter measurements are obtained in parametric form and non-parametric form.

**Parametric form:** The PDA and the proposed Iter-PDA approach computes  $\beta_j$  in parametric form using the known  $\lambda$  values in (15) and (16). As shown in Fig. 4(a) the RMS positional error for the proposed approach (Iter-PDA) and PDA are not significantly different with  $\lambda = 1e^{-4}$ . But, with  $\lambda = 1e^{-3}$  estimation accuracy is improved with Iter-PDA.

**Non-parametric form:** For simulations carried out with  $q = 1$  a higher process error covariance is obtained and this lead to higher  $\mathbf{S}(k)$ , large gate area  $A$  and subsequently to large number of clutter measurements. Hence, instead of keeping  $\lambda$  fixed, the simulations are

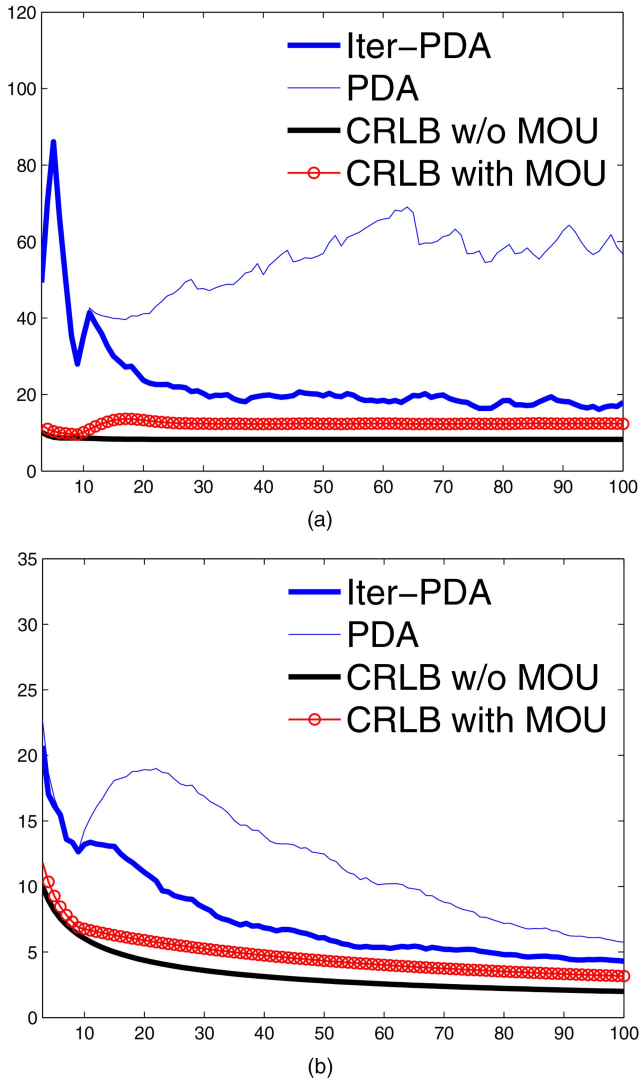


Fig. 6. RMS positional error (in m) versus time index  $k$ , with conventional and the proposed approach with  $\gamma = 1$ , for varying clutter densities, process noise and probability of detection (a)  $\bar{m}_k = 10$ ,  $q = 1$  and  $P_d = 0.7$ . (b)  $\lambda = 1e^{-2}$ ,  $q = 0$  and  $P_d = 1$ .

done with fixed  $\bar{m}_k = A\lambda$  for  $q = 1$  case. Similarly for  $P_d < 1$  the simulations are done with fixed  $\bar{m}_k = A\lambda$ . The PDA and the proposed Iter-PDA approach computes  $\beta_j$  in non-parametric form using the computed  $\lambda$  values ( $\lambda = \bar{m}/A$ ) in (15) and (16).

The RMS positional error with  $\bar{m}_k = 10$  and with  $q = 1$  and  $P_d = 1$ ,  $P_d = 0.9$  are provided in Fig. 5(a) and Fig. 5(b), respectively. Comparing Fig. 4 and Fig. 5 the increase in the CRLB with MOU is significant for  $q = 1$  compared to  $q = 0$ . The RMS positional error in PDA increases more compared to Iter-PDA with  $P_d = 0.9$ . The RMS positional errors for 100 MC runs are provided in Fig. 6(a), for average number of clutter  $\bar{m}_k = 10$  and  $q = 1$  with  $P_d = 0.7$ .

The RMS error in PDA increases with decrease of  $P_d$  as shown in Fig. 5 and Fig. 6(a). The RMS positional error with higher clutter density compared to the results given in Fig. 4, i.e.,  $\lambda = 1e^{-2}$ ,  $q = 0$  and

$P_d = 1$  is provided in Fig. 6(b). Compared to conventional PDA, the proposed approach gives significantly better estimation accuracy with higher amount of clutter as depicted in Fig. 6(b). The estimation accuracy with Iter-PDA is always better than PDA with  $\gamma = 1$ . The sudden increase in error at time instant  $k = 10$  onwards in Fig. 4, Fig. 5 and Fig. 6 is due to the introduction of clutter. The increase in position and velocity errors in Iter-PDA because of the introduction of clutter is low compared to PDA. But with  $\gamma = 2$ ,  $\gamma = 3$  and  $\gamma = 4$  the advantage of Iter-PDA will be visible only with  $\bar{m}_k = 50$  and  $\bar{m}_k = 100$ . Higher value of  $\gamma$  indicates measurement sparseness and so Iter-PDA is unable to extract additional information from measurements. In the proposed approach  $\mathbf{q}_j(k)$  is approximated as a Gaussian random variable with mean zero and variance  $\Sigma_k$ . With higher values of  $\gamma$  the innovation  $\nu_j(k)$  and  $\mathbf{q}_j(k)$  are widely spread around the predicted position. Hence, the approximation  $\mathbf{q}_j(k) \sim \mathcal{N}(\mathbf{q}_j(k); 0, \Sigma(k))$  may not be valid with higher values of  $\gamma$ . Hence, the proposed iterations are done only if the average likelihood is above a threshold, i.e.,  $(1/\bar{m}_k) \sum_{j=m_k} p(z_j(k) | \mathbf{A}(j), \mathbf{Z}^{k-1}) > \delta$ . In this paper  $\delta = 0.1$  has been used for the simulations.

The simulation results for the case (ii), with a uniform clutter pattern, are provided in Fig. 7. Here, the uniform clutter pattern is generated in an area  $A$  covering the entire surveillance region. With  $\lambda = 1e^{-3}$  and  $P_d = 1$  performance of PDA and Iter-PDA are similar. The RMS error obtained without MOU, i.e., by using the correct measurement in the standard Kalman filter based estimation has been carried out. The estimation with correct measurement is carried out to compare the performance of PDA and Iter-PDA against an ideal data association approach. In the absence of actual measurements, i.e., with  $P_d < 1$ , the predicted measurement is used for state update. With  $P_d = 0.7$  the RMS error in position has been improved with Iter-PDA as shown in Fig. 7(a). The RMS positional error has been shown in Fig. 7(b) with  $q = 0.1$ . The RMS error without MOU shows slight increase at  $k = 10$  due to the introduction of  $P_d = 0.7$  from 10th instant. In both cases, Iter-PDA performs better than PDA and the estimation without MOU gives the best result as expected.

## 5.2 Information reduction factor (IRF) with MOU

The value of information reduction factor (IRF)  $q_2$  for various cases of  $q$  and  $\mathbf{R}$  are computed using the simulation scenario described in the previous sub-section with the clutter measurements generated using the case (i). The scalar and matrix IRF obtained with different pattern of measurement noise covariance  $\mathbf{R}$  is summarized in [27]. The objective of this section is to check the scalar nature of IRF  $q_2$  for diagonal measurement noise covariance. The case of measurement noise covariance  $\mathbf{R}$  being a scalar multiple of identity matrix is considered here and the IRF  $q_2(k)$  is shown to be a

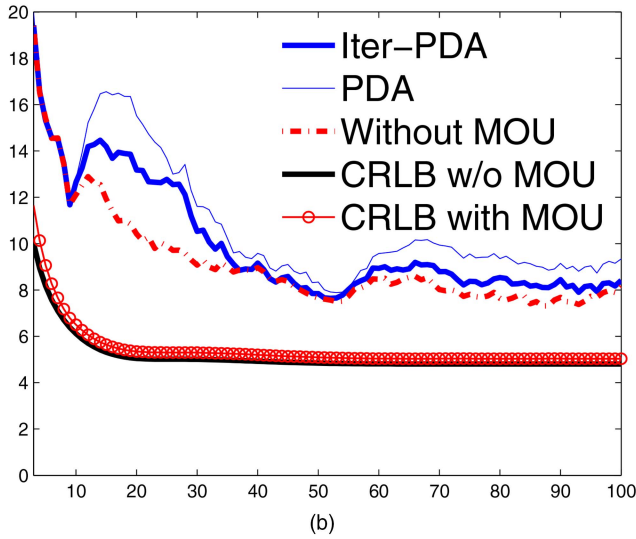
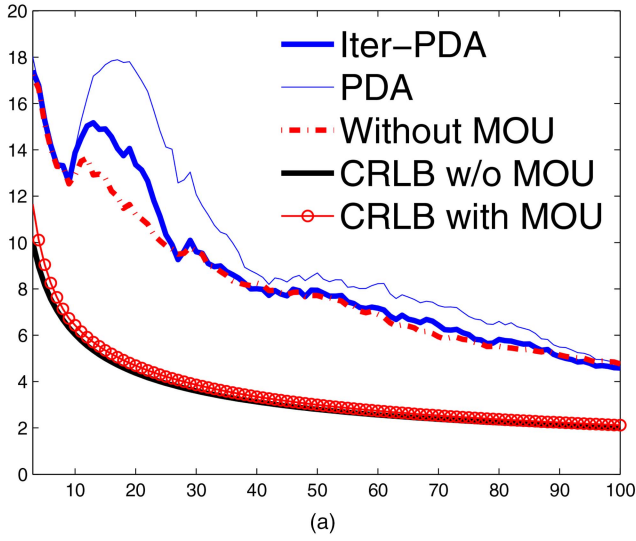


Fig. 7. RMS positional error (in m) versus time index  $k$ , with conventional and the proposed approach with  $\gamma = 1$ ,  $P_d = 0.7$  for varying process noise. Clutter is generated in an area having coordinates covering the entire surveillance region (a)  $q = 0$  (b)  $q = 0.1$ .

scalar for all  $k$ . The IRF  $q_2(k)$  will be a scalar if ratio  $d_{ii}$  of all the diagonal elements of  $\mathbf{R}^{\theta(k)^{-1}}$  and  $\mathbf{R}^{-1}$  are equal. The ratio  $d_{ii}$  is obtained as  $d_{ii}(k) = \frac{\mathbf{R}_{ii}^{\theta(k)^{-1}}}{\mathbf{R}_{ii}^{-1}(k)}$  and for two-dimensional case  $r_{12}(k) = \frac{d_{11(k)}}{d_{22(k)}}$ . For  $r_{12}(k) = 1$ ,  $q_2(k) = d_{11}(k) = d_{22}(k)$ . The IRF  $q_2(k)$  and the ratio  $r_{12}(k)$  are plotted in Fig. 8(a) and Fig. 8(b) with  $\lambda = 1e^{-4}$  and  $\lambda = 1e^{-3}$ , for  $\gamma = 1$ ,  $\mathbf{R} = \begin{bmatrix} 200 & 0 \\ 0 & 200 \end{bmatrix}$  and  $q = 0$ . In Fig. 8,  $r_{12} = 1$  indicates the elements of  $\mathbf{R}^{\theta(k)^{-1}}$  are obtained by multiplying the elements of  $\mathbf{R}(k)^{-1}$  with a scalar. The scalar  $q_2(k)$  is less than one as shown in Fig. 8. In a clutter free zone  $q_2(k) = 1$  and there is no information reduction. The value of  $q_2(k)$  reduces, with increase in clutter density  $\lambda = 1e^{-3}$  as shown in Fig. 8(b).

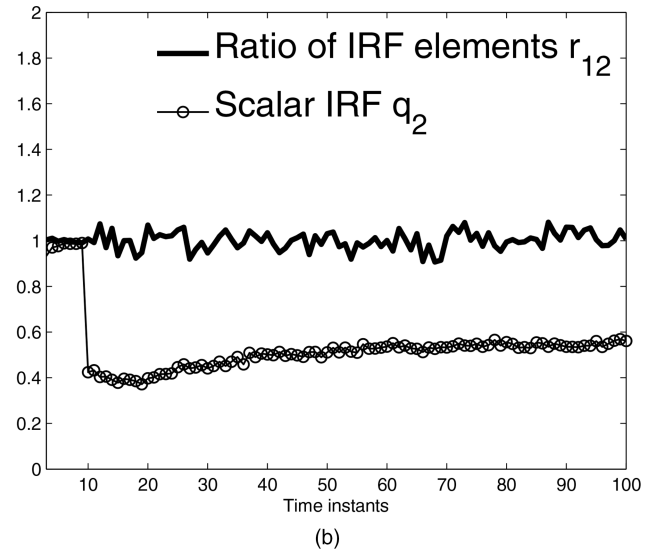
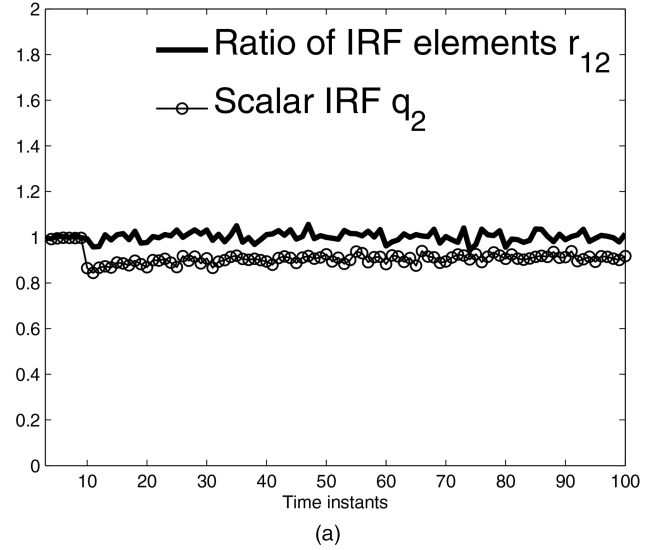


Fig. 8. The ratio of diagonal elements  $r_{12}(k) = d_{11(k)}/d_{22(k)}$  and  $q_2(k)$  versus time index  $k$  with conventional and with the proposed approach with  $\gamma = 1$  for varying clutter densities. (a)  $\lambda = 1e^{-4}$ . (b)  $\lambda = 1e^{-3}$ .

The variation of  $q_2$  with low  $P_d$  and high clutter are analyzed in Fig. 9(a) and Fig. 9(b), respectively. The value of  $q_2(k)$  and  $r_{12}(k)$  are computed with  $\bar{m}_k = 10$ ,  $q = 1$ ,  $P_d = 0.7$  and depicted in Fig. 9(a). Similarly  $q_2(k)$  and  $r_{12}(k)$  for  $\lambda = 1e^{-2}$ ,  $q = 0$ , and  $P_d = 1$  is provided in Fig. 9(b). In all the cases considered here for simulations, the ratio  $r_{12}(k) = 1$  indicates that  $q_2(k)$  is scalar and verifies the results obtained in [9], [24]. For  $\lambda = 1e^{-3}$  and  $\lambda = 1e^{-2}$  the scalar IRF  $q_2$  is not a constant with time  $k$ . The variations are zoomed and shown in Fig. 10(a). In the initial time instants  $q_2$  is low and as filter stabilizes  $q_2$  increases. This suggests that the information loss due to clutter is less as the filter reaches steady state. The variations in trace of posterior state error covariance is plotted in Fig. 10(b). The trace increases rapidly with the introduction of clutter at  $k = 10$  in PDA. In Iter-PDA the raise is nominal and this is due

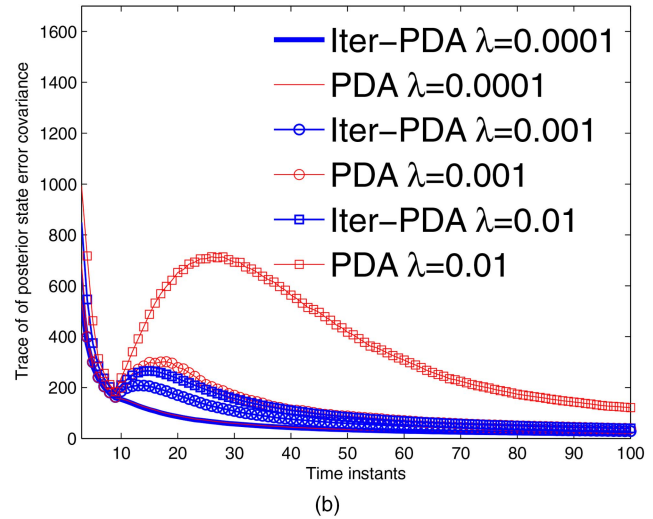
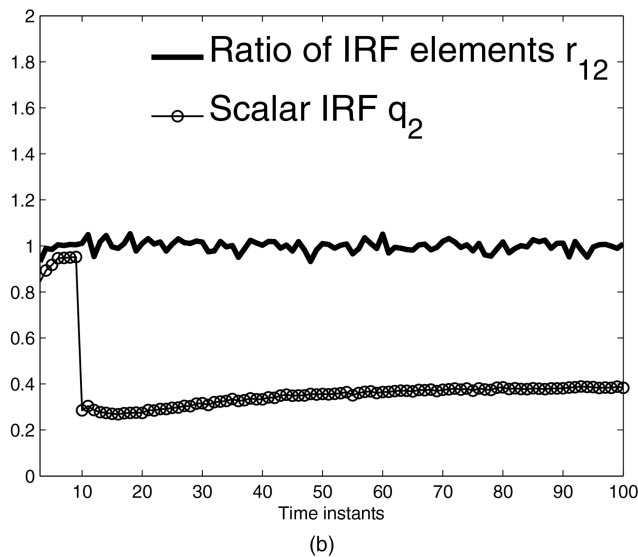
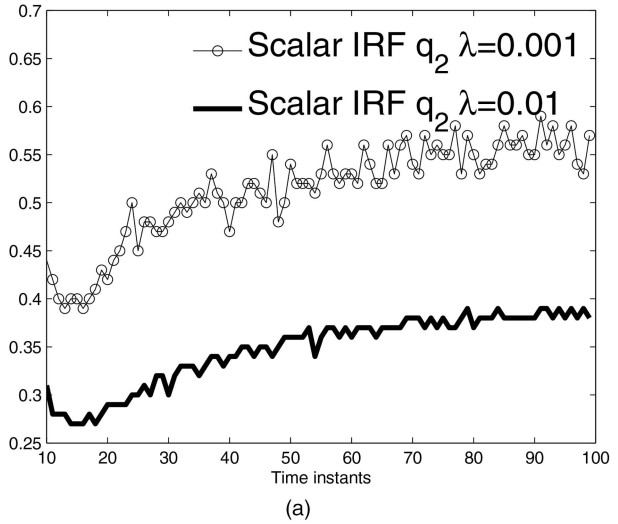
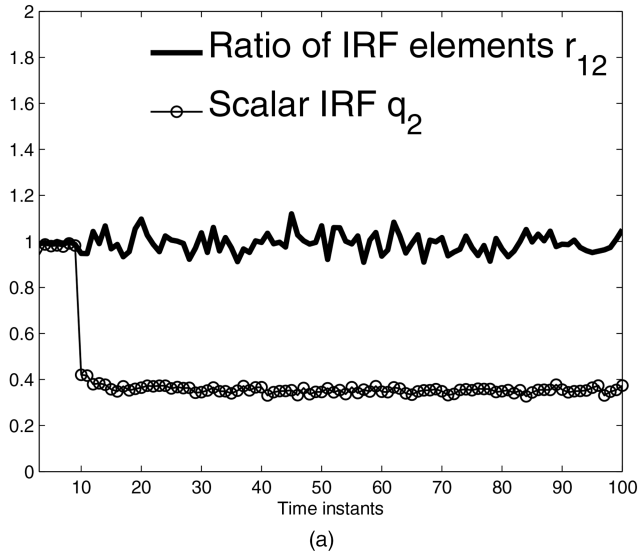


Fig. 9. The ratio of diagonal elements  $r_{12}(k) = d_{11}(k)/d_{22}(k)$  and  $q_2(k)$  versus time index  $k$ , with conventional and proposed approach with  $\gamma = 1$  for varying clutter densities, process noise and probability of detection. (a)  $\bar{m}_k = 10$ ,  $q = 1$ ,  $P_d = 0.7$  (b)  $\lambda = 1e^{-2}$ ,  $q = 0$ ,  $P_d = 1$ .

Fig. 10. (a) Zoomed-in section of  $q_2$  for  $\lambda = 1e^{-3}$  and  $\lambda = 1e^{-2}$ . (b) Trace of the posterior error covariance with  $\lambda = 1e^{-4}$ ,  $\lambda = 1e^{-3}$  and  $\lambda = 1e^{-2}$ .

to the adaptability of Iter-PDA to adjust with clutter by modifying the innovation error covariance.

### 5.3 Consistency of Iter-PDA

The consistency of the proposed Iter-PDA filter is verified using the following three criteria [12], [35]:

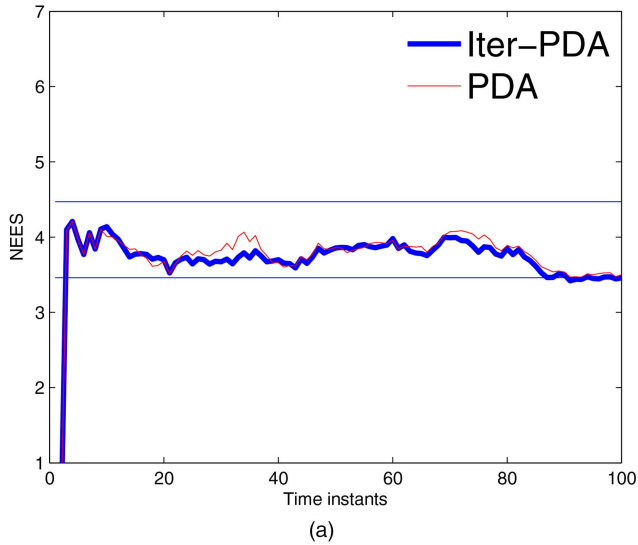
- 1) Normalized state estimation error square (NEES) should be within an acceptable limit.
- 2) Normalized innovation square (NIS) should be within an acceptable limit.
- 3) Innovation should be acceptable as white.

The computation of acceptable limit for the above three criteria are given in [12], [35]. In this section numerical values of NEES, NIS and whiteness of innovation are checked with filter consistency acceptance limits. In [12] PDA filter consistency has been checked

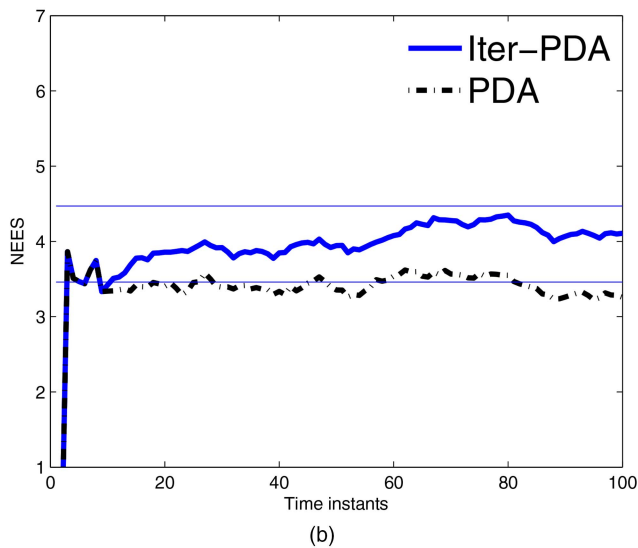
with three clutter densities ( $\lambda = 1e^{-5}$ ,  $\lambda = 1e^{-4}$  and  $\lambda = 4.5e^{-4}$ ) for  $P_d = 1$  and  $q = 0$ . PDA and Iter-PDA give same consistency pattern for the low clutter density cases checked in [12]. In this section consistency of PDA and Iter-PDA are checked with high clutter density ( $\lambda = 1e^{-3}$ ), low  $P_d$  along with process noise  $q = 1$ . The target state vector length  $n_x = 4$ . For  $N = 100$  Monte Carlo (MC) runs, the two sided Chi-square values of NEES with  $\alpha = 0.05$  for  $400(Nn_x)$  degrees of freedom are

$$[\chi_{400}^2(.025), \chi_{400}^2(.975)] = [346.48, 447.63].$$

Dividing the limits by  $N = 100$  the acceptance region will be  $r_1 = 3.46$  and  $r_2 = 4.47$ . The NEES plots with  $\gamma = 1$  (i.e., with 1 sigma gate) and  $\lambda = 1e^{-3}$ ,  $q = 0$ ,  $P_d = 1$  and  $P_d = 0.7$  are provided in Figures 11(a) and 11(b), respectively. With  $P_d = 1$  both PDA and Iter-PDA give similar NEES plots. But with reduced  $P_d$ , NEES plots corresponding to PDA filter cross the boundary while



(a)



(b)

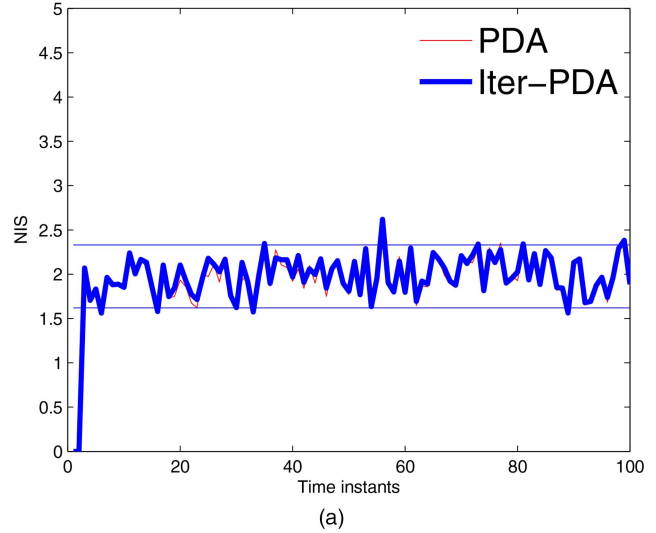
Fig. 11. Normalized state estimation error square (NEES) with  $\gamma = 1$ ,  $q = 0$  and  $\lambda = 1e^{-3}$  for varying probability of detection. (a)  $P_d = 1$  (b)  $P_d = 0.7$

Iter-PDA remains well within the acceptance boundary as shown in Fig. 11(b).

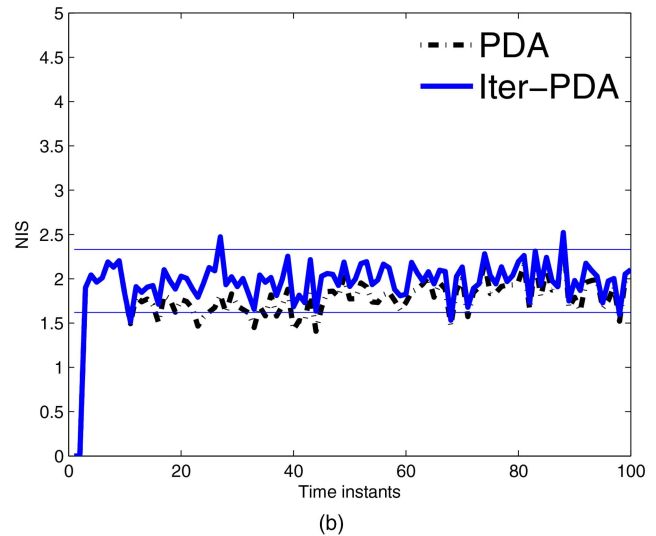
For two-dimensional measurements in X-Y plane,  $n_z = 2$ . For  $N = 100$  Monte Carlo (MC) runs the degree of freedom is  $Nn_z = 200$ . With  $\alpha = 0.05$ , for a two sided interval the Chi-square values for NIS are

$$[\chi_{200}^2(.025), \chi_{200}^2(.975)] = [162.78, 233.99].$$

Dividing the limits by  $N = 100$  the acceptance region will be  $r_1 = 1.62$  and  $r_2 = 2.33$ . The average NIS plots for  $N = 100$  with  $q = 0$  and with  $\gamma = 1$  and  $\lambda = 1e^{-3}$ , for  $P_d = 1$  and  $P_d = 0.7$  are provided in Figures 12(a) and 12(b), respectively. The NIS plots for PDA and Iter-PDA are similar with  $P_d = 1$ . The NIS plots of PDA cross the boundary with reduced  $P_d$  as shown in Fig. 12(b). The auto correlation of the innovation is computed with samples at one time instant apart. The 95 percentage region  $[-1.96\sigma, 1.96\sigma]$  for  $\sigma = 1/\sqrt{N} = 0.1$



(a)



(b)

Fig. 12. Normalized innovation square with  $\gamma = 1$ ,  $q = 0$  and  $\lambda = 1e^{-3}$  for varying probability of detection. (a)  $P_d = 1$  (b)  $P_d = 0.7$ .

is the interval  $[-0.196, 0.196]$ . The innovation is accepted as white if the computed auto correlation is within the acceptance limit. The comparison of whiteness of innovation with  $\gamma = 1$  and  $\lambda = 1e^{-3}$ ,  $q = 0$ , for  $P_d = 1$  and  $P_d = 0.7$  are provided in Figures 13(a) and 13(b), respectively. PDA and Iter-PDA give similar whiteness of innovation with  $P_d = 1$  as shown in Fig. 13(a). With reduced  $P_d$  the auto correlation of the innovation with Iter-PDA is closer to the acceptable limits compared to PDA as shown in Fig. 13(b).

Comparing the NIS values plotted in Fig. 12 the Iter-PDA remains well within the acceptable limits compared to PDA. In Fig. 12(b) the NIS plots corresponding to PDA crosses the lower boundary more often. Lower values of normalized statistic (NEES and NIS) indicate larger covariance. The Iter-PDA adaptively adjusts the state error and innovation covariance, so that the NEES and NIS plots are within acceptable limits.

The results obtained in this section show that the proposed origin uncertainty model improves the esti-

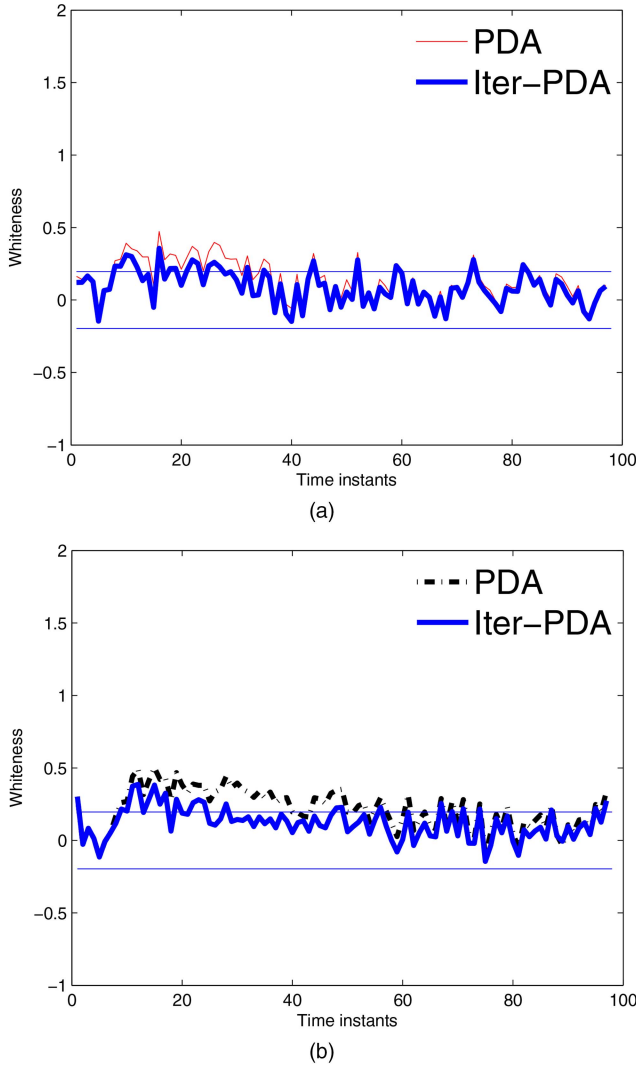


Fig. 13. Innovation auto correlation with  $\gamma = 1$ ,  $q = 0$  and  $\lambda = 1e^{-3}$  for varying probability of detection. (a)  $P_d = 1$  (b)  $P_d = 0.7$ .

mation accuracy. With the proposed modification the error variance and the corresponding error variance obtained as filter parameter are matching, so the consistency of the filter is improved compared to PDA. It is usual practice to compare the estimation accuracy with the theoretical lower bound. But, in case of tracking under MOU the theoretical lower bound i.e., CRLB is difficult to compute because of the numerical complexity in computing the IRF. The simulation results carried out here compute the CRLB under MOU as a by-product of the Monte Carlo runs and present a simple approximate CRLB computation scheme.

## 6. CONCLUSION

The proposed approach in this paper develops a model for validated measurements. Instead of target originated measurement model the proposed approach uses the validated measurement model and enhances the estimation accuracy of PDA filter. Using the developed model for validated measurements the unconditional

measurement error covariance with MOU is computed. The unconditional measurement error covariance with MOU is adaptive with measurement origin uncertainty. With unconditional measurement error covariance the innovation covariance, the Kalman filter gain and the posterior error covariance are modified. The additive term in the measurement noise covariance with MOU computed by the proposed approach vanishes in the absence of MOU and the modified filter parameters reduce to standard Kalman filter parameters.

Monte Carlo simulation results show that the target state estimate obtained using the modified filter parameters are significantly better compared to that obtained using the standard PDA approach under dense clutter scenarios. Under low clutter conditions the proposed Iter-PDA and the standard PDA gives similar performance because the additional measurement noise component is not significant.

The estimation accuracy is compared to CRLB with MOU. The IRF in CRLB with MOU has been obtained in this paper by Monte Carlo (MC) averaging method. Using the Monte Carlo (MC) averaging method the proposed approach is able to compute the CRLB for any given filter characteristic and clutter density. The adaptability of the proposed approach to various clutter conditions has been shown with Monte Carlo simulations.

## ACKNOWLEDGMENT

Authors would like to express sincere thanks to Dr. Ajit T Kalghatgi, Director (R&D) of Bharat Electronics Limited, for the guidance and support to carry out this work. We also thank Mahesh V (Chief scientist CRL) and L. Ramakrishnan (Principal scientist CRL) for the encouragement for the completion of this research work. We are also thankful to the Naval Research Board, DRDO, India, for their support and cooperation. The authors would also like to thank all the reviewers for their helpful suggestions for improving this paper.

## APPENDIX A SCALAR INFORMATION REDUCTION FACTOR

Let  $p_{\Sigma}$  be the probability distribution function of  $\Sigma$ . In the simulations carried in the paper the measurements are in Cartesian coordinates, i.e.  $\mathbf{z}_j(k)$  is of dimension two. The measurement noise in  $x$  and  $y$  components are independent. Hence, it is assumed that  $\mathbf{R}$  is a diagonal matrix. The expected value of modified measurement noise covariance can be computed as

$$\begin{aligned}
 E\{\{\mathbf{R}^{\theta}(k)^{-1}\}\} &= E\{\{\mathbf{R} + \Sigma(k)\}^{-1}\} \\
 &= \frac{1}{\mathbf{R} + \Sigma(1)} p_{\Sigma}(\Sigma(1)) + \frac{1}{\mathbf{R} + \Sigma(2)} p_{\Sigma}(\Sigma(2)) \\
 &\quad + \dots + \frac{1}{\mathbf{R} + \Sigma(k)} p_{\Sigma}(\Sigma(k)) \quad (64)
 \end{aligned}$$

$$\begin{aligned}
\Rightarrow E\{(\mathbf{R}^\theta(k)^{-1})\} &\leq \mathbf{R}^{-1}p_\Sigma(\Sigma(1)) + \mathbf{R}^{-1}p_\Sigma(\Sigma(2)) \\
&\quad + \dots + \mathbf{R}^{-1}p_\Sigma(\Sigma(k)) \\
&= \mathbf{R}^{-1}\sum_k p_\Sigma(\Sigma(k)) = \mathbf{R}^{-1} \\
\Rightarrow E\{(\mathbf{R}^\theta(k)^{-1})\} &\leq \mathbf{R}^{-1}. \tag{65}
\end{aligned}$$

For one dimensional measurements  $\mathbf{R}$  is a scalar,  $\Sigma(k)$  is scalar and (65) holds true. Therefore, expected value of inverse of modified measurement noise covariance can be computed as

$$E\{(\mathbf{R} + \Sigma(k))^{-1}\} = q_2\mathbf{R}^{-1}, \text{ where } q_2 \leq 1. \tag{66}$$

If measurement dimension is more than one ( $n, n > 1$ ), the measurement noise covariance  $\mathbf{R}$  is  $n \times n$ . The additional term  $\Sigma(k)$  is symmetric and positive definite as shown in Appendix D.3 of [12]. Hence,  $\mathbf{R} + \Sigma(k) \leq \mathbf{R}$ . The off-diagonal terms of  $E[\Sigma(k)]$  cancel out because  $\bar{z}_j(k)$  are independent and identically distributed (i.i.d), as shown in [28]. For two-dimensional case with different  $\lambda$ , the ratio of diagonal elements  $r_{12}$  and  $q_2$  are plotted in Fig.8 and Fig.9 using 250 MC runs. Since,  $r_{12} = 1$  the diagonal terms are equal and  $q_2$  is a scalar multiple of  $\mathbf{R}^{-1}$ . Thus, condition (66) is applicable to measurement noise covariance  $\mathbf{R}$  having dimension more than one.

#### APPENDIX B ITERATIVE COMPUTATION OF $\beta_j$ AND $\Sigma(K)$

Using the modified measurement model given in (25) the validated measurements are represented as

$$\mathbf{z}_j(k) = \mathbf{z}_i(k) + \mathbf{q}_j(k), \tag{67}$$

where  $\mathbf{q}_j(k) = \mathbf{z}_j(k) - \sum_{j=0:m_k} \mathbf{z}_j(k)\beta_j(k)$  and the weighted sum of all the measurements are denoted as  $\tilde{\mathbf{z}}(k) = \sum_{j=0:m_k} (\mathbf{z}_j(k)\beta_j(k))$ . The measurement model for validated measurements consists of two parts, the target originated measurement  $\mathbf{z}_i(k)$  and the spread of the measurements

$$\mathbf{q}_j(k) = \mathbf{z}_j(k) - \tilde{\mathbf{z}}(k).$$

Accordingly, the measurement likelihood has two parts one corresponding to target originated and the other corresponding to the uncertainty in target originated measurement. The density of  $\mathbf{q}_j(k)$  is assumed to be Gaussian denoted as  $\mathbf{q}_j(k) \sim \mathcal{N}(\mathbf{q}_j(k); 0, \Sigma_k)$ . The measurement spread is obtained as  $\mathbf{q}_j(k) = \mathbf{z}_j(k) - \sum_{j=0:m_k} (\mathbf{z}_j(k)\beta_j(k))$ . The variance of  $\mathbf{q}_j(k)$  is obtained as the one that maximizes the likelihood. Instead of directly maximizing the measurement likelihood  $\sum_j (p_{\mathbf{z}_j(k)}(\mathbf{A}(j), \mathbf{H}\hat{\mathbf{x}}_i(k|k-1), \mathbf{Z}(k)))$  the proposed approach maximizes log likelihood.

The parameters  $\beta_j$  and  $\Sigma_k$  are computed by minimizing the negative log likelihood. The expectation of log likelihood can be computed as [36]

E-Step:

$$\begin{aligned}
E_{\mathbf{z}_j(k)}[\log(p_{\mathbf{z}_j(k)}(\mathbf{A}(j), \mathbf{H}\hat{\mathbf{x}}_i(k|k-1), \mathbf{Z}(k)))] &= \\
\sum_j \log(p_{\mathbf{z}_j(k)}(\mathbf{A}(j), \mathbf{H}\hat{\mathbf{x}}_i(k|k-1), \mathbf{Z}(k)))\beta_j. &\tag{68}
\end{aligned}$$

Using the modified measurement model given in (25)

$$\begin{aligned}
\mathbf{z}_j(k) - \mathbf{H}\hat{\mathbf{x}}_i(k|k-1) &= \mathbf{z}_i(k) - \mathbf{H}\hat{\mathbf{x}}_i(k|k-1) + \mathbf{q}_j(k) \\
&= \nu_i(k) + \mathbf{q}_j(k). \tag{69}
\end{aligned}$$

Using (69) the log likelihood given in (68) can be obtained as

$$\begin{aligned}
J &= \log(p_{\nu_i(k)}(\mathbf{A}(i), \mathbf{H}\hat{\mathbf{x}}_i(k|k-1), \mathbf{Z}(k))) \\
&\quad + \sum_j (\log p_{\mathbf{q}_j(k)}(\mathbf{A}(j), 0, \mathbf{Z}(k)))\beta_j. \tag{70}
\end{aligned}$$

The term  $\nu_i(k)$  can be rewritten as

$$\begin{aligned}
\nu_i(k) &= \mathbf{z}_i(k) - \mathbf{H}\hat{\mathbf{x}}_i(k|k-1) \\
&= (\mathbf{H}\mathbf{x}_i(k) - \mathbf{H}\hat{\mathbf{x}}_i(k|k-1)) + (\mathbf{z}_i(k) - \mathbf{H}\mathbf{x}_i(k)). \tag{71}
\end{aligned}$$

The first term of (70)  $p_{\nu_i(k)}$  is independent of  $\mathbf{z}_j(k)$  and can be expanded as

$$\begin{aligned}
J_1 &= \log p_{\nu_i(k)}(\mathbf{A}(i), \mathbf{H}\hat{\mathbf{x}}_i(k|k-1), \mathbf{Z}(k)) \\
&= (\mathbf{H}\mathbf{x}_i(k) - \mathbf{H}\hat{\mathbf{x}}_i(k|k-1))(\mathbf{H}\mathbf{P}\mathbf{H}^T)^{-1} \\
&\quad (\mathbf{H}\mathbf{x}_i(k) - \mathbf{H}\hat{\mathbf{x}}_i(k|k-1))^T + \log \det((\mathbf{H}\mathbf{P}\mathbf{H}^T)^{-1}) \\
&\quad + (\mathbf{z}_i(k) - \mathbf{H}\mathbf{x}_i(k))\mathbf{R}^{-1}(\mathbf{z}_i(k) - \mathbf{H}\mathbf{x}_i(k))^T + \log \det(\mathbf{R}). \tag{72}
\end{aligned}$$

The second term depends on  $\mathbf{z}_j(k)$  and can be expanded as

$$\begin{aligned}
J_2 &= \sum_j (\log p_{\mathbf{q}_j(k)}(\mathbf{A}(j), 0, \mathbf{Z}(k)))\beta_j = \\
&\quad \sum_j ((\mathbf{z}_j(k) - \tilde{\mathbf{z}}(k))\Sigma(k)^{-1}(\mathbf{z}_j(k) - \tilde{\mathbf{z}}(k)))^T \\
&\quad + \log \det(\Sigma(k))\beta_j. \tag{73}
\end{aligned}$$

The task of maximizing the measurement likelihood is equivalent to minimizing  $J$ . The first term of  $J_1$  is independent of measurement at  $k$ th instant. For the second term in  $J_1$  (72) maximum likelihood occurs for target originated measurement, i.e. mode of the distribution is at  $\mathbf{z}_i(k)$ . Hence, the sum of likelihood ( $J = J_1 + J_2$ ) is maximum if  $J_2$  (73) also gets maximum at the same point, i.e., at  $\mathbf{z}_i(k)$

$$\mathbf{z}_i(k) = \tilde{\mathbf{z}}(k) = \sum_{j=0:m_k} \mathbf{z}_j(k)\beta_j. \tag{74}$$

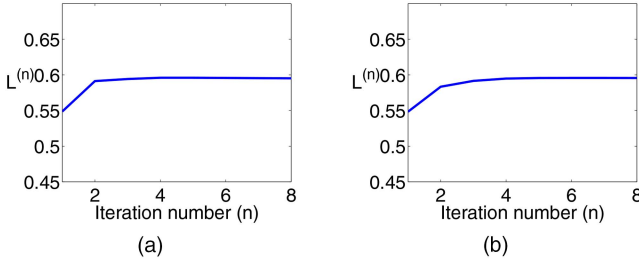


Fig. 14. The expected likelihood versus iteration number  $P_d = 1$ ,  $m_k = 10$  for an arbitrary run. (a)  $q = 0$  (b)  $q = 1$ .

The modified measurement model for the validated measurement set given in (25) satisfy the requirement given in (74). The expression (74) indicates that measurement likelihood will be maximum if the measurement corresponding to target  $i$  is a weighted sum of all the measurements in the validation region. The unknown parameters in  $J$  are  $\beta_j$  and the variance  $\Sigma(k)$  of  $J_2$ . The variance  $\Sigma(k)$  that maximizes  $J_2$  can be obtained by solving  $\nabla_{\Sigma(k)-1} J_2 = 0$

M-Step:

$$\nabla_{\Sigma(k)-1} J_2 = \sum_{j=0:m_k} ((z_j(k) - \tilde{\mathbf{z}}(k))(z_j(k) - \tilde{\mathbf{z}}(k))^T - \Sigma_k) \beta_j$$

Letting  $\nabla_{\Sigma(k)-1} J_2 = 0$

$$\begin{aligned} \implies \Sigma(k) &= \sum_{j=0:m_k} ((z_j(k) - \tilde{\mathbf{z}}(k))(z_j(k) - \tilde{\mathbf{z}}(k))^T) \beta_j \\ &= E[\nu_j(k) \nu_j(k)^T | \mathbf{Z}^k] - E(\nu_j(k) | \mathbf{Z}^k) E(\nu_j(k) | \mathbf{Z}^k)^T \\ &= \sum_{j=0}^{m_k} \beta_j \nu_j(k) \nu_j(k)^T - \tilde{\mathbf{Z}}(k) \tilde{\mathbf{Z}}(k)^T, \end{aligned} \quad (75)$$

where  $\tilde{\mathbf{Z}}(k) = E(\nu_j(k) | \mathbf{Z}^k)$ . By alternating between E-Step (74) and M-Step (75) the iterated  $\beta_j$ 's and  $\Sigma_k$  are obtained. The E-M algorithm and its general form is discussed in [37]. The convergence analysis of E-M algorithms are discussed in [38], [39]. The likelihood  $p_{\mathbf{z}_j(k)}^{(n)}$  at  $n$ th iteration is computed using (76) as

$$\begin{aligned} p_{\mathbf{z}_j(k)}^{(n)}(\mathbf{A}(j), \mathbf{H}\hat{\mathbf{x}}_i(k | k-1), \mathbf{Z}(k)) &= p(\mathbf{Z}(k) | \mathbf{A}(j), \mathbf{Z}^{k-1}) \\ &= \frac{1}{c} \mathcal{N}(\mathbf{z}_j(k); \mathbf{H}\hat{\mathbf{x}}_i(k | k-1), \mathbf{S}_i^{\theta^{(n)}}(k)). \end{aligned} \quad (76)$$

The average variation of the likelihood sum with iterations is computed as

$$L^{(n)} = \frac{1}{k} \sum_k \left( \sum_j \mathcal{N}(\mathbf{z}_j(k); \mathbf{H}\hat{\mathbf{x}}_i(k | k-1), \mathbf{S}_i^{\theta^{(n)}}(k)) \beta_j^n(k) \right). \quad (77)$$

The variations of  $L^{(n)}$  for  $n = 1, \dots, 10$  is plotted in Fig. 14. For  $n = 1$  the proposed approach is same as conventional PDA approach. The variations of expected

likelihood given in Fig. 14(a) shows the likelihood maximization with iterations for  $q = 0$  and  $q = 1$ . The variations are similar in shape and the likelihood values settles at around iteration number 4. Simulations are conducted with other cases with different clutter densities and  $P_d$  and the maximum number of iterations taken for likelihood value settling is found to be around 4.

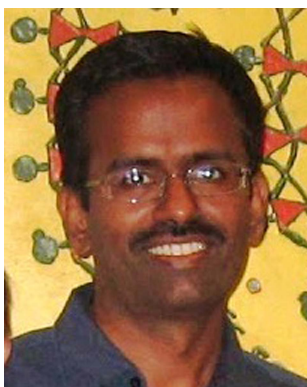
## REFERENCES

- [1] D. B. Reid  
An algorithm for tracking multiple targets,  
*IEEE Trans. on Automatic Control*, vol. 24, pp. 843–853, Dec. 1979.
- [2] S. S Blackman and R. Popoli  
*Design and analysis of modern tracking systems*,  
Artech House, 1993.
- [3] D. Salmond  
Mixture reduction algorithms for point and extended object tracking in clutter,  
*IEEE Trans. on Aerospace and Electronic Systems*, vol. 45, pp. 667–686, 2009.
- [4] J. L. Williams, P. S. Maybeck  
Cost function based Gaussian mixture reduction for target tracking,  
*6th Int. Conf. on Information Fusion*, pp. 1047–1054, 2003.
- [5] Y. Bar-Shalom, F. Daum and J. Huang  
The probabilistic data association filter, estimation in the presence of measurement origin uncertainty,  
*IEEE Control System Magazine*, pp. 82–100, Dec. 2009.
- [6] Y. Bar-Shalom and E. Tse  
Tracking in a cluttered environment with probabilistic data association,  
*Automatica*, vol. 11, pp. 451–460, Nov. 1975.
- [7] Y. Bar-Shalom and A. G. Jaffer  
Adaptive nonlinear filtering for tracking with measurements of uncertain origin,  
*IEEE Con. on Decision and control*, pp. 243–247, Dec. 1972.
- [8] Y. Bar-Shalom and K. Birmiwal  
Variable dimension filter for maneuvering target tracking,  
*IEEE trans. on Aerospace and Electronic Systems*, vol. 18, pp. 621–629, Sept. 1982.
- [9] C. Jauffret and Y. Bar-Shalom  
Track formation with bearing and frequency measurements in clutter,  
*IEEE Trans. on Aerospace and Electronic Systems*, vol. 26, pp. 999–1010, Nov. 1990.
- [10] D. Musicki, R. Evans, and S. Stankovic  
Integrated probabilistic data association,  
*IEEE Trans. Automatic Control*, vol. 39, pp. 1237–1241, 1994.
- [11] R. J. Fitzgerald  
Track biases and coalescence with probabilistic data association,  
*IEEE Trans. on Aerospace and Electronic Systems*, vol. 21, pp. 822–825, Nov. 1985.
- [12] Y. Bar-Shalom and T. E. Fortmann  
*Tracking and data association*,  
Academic press, inc, 1987.
- [13] David F. Crouse, Y. Bar-Shalom, P. Willett and L. Svensson  
The JPDAF in practical systems: Computation and snake oil,  
*Signal and data processing of small targets*, vol. 7698, pp. 1–15, 2010.
- [14] M. Efe, D. Bonvin and P. Brog  
Data association in clutter with an adaptive filter,  
*Proc. Intl. Conf. Info. Fusion*, pp. 1243–1248, 2002.

- [15] S. Koteswara Rao  
Modified gain extended Kalman filter with application to bearings-only passive maneuvering target tracking,  
*IEEE Proceedings—Radar Sonar and Navigations*, vol. 152(4), pp. 239–244, 2005.
- [16] A. S. Rahmathulla, L. Svensson, D. Svensson and P. Willett  
Smoothed probabilistic data association filter,  
*Proc. Intl. Conf. Info. Fusion, Istanbul, Turkey*, pp. 1296–1303, July 2013.
- [17] D. Musicki and R. Evans  
Integrated probabilistic data association—finite resolution,  
*Automatica, Elsevier*, vol. 31(4), pp. 559–570, 1995.
- [18] V. P. Panakkal and R. Velmurugan  
Iterative joint probabilistic data association for avoiding track coalescence and track swap in multi-target tracking,  
*7th IEEE SAM workshop, New Jersey, USA*, pp. 285–288, 2012.
- [19] V. P. Panakkal and R. Velmurugan  
Effective joint probabilistic data association using maximum a posteriori estimates of target states,  
*Proc. Intl. Conf. Info. Fusion, Istanbul, Turkey*, pp. 781–788, July 2013.
- [20] Ni. Longqiang, G. Shesheng and X. Li  
Improved probabilistic data association and its application for target tracking in clutter,  
*Int. Conf. on Electronics, communications and control*, pp. 293–296, 2011.
- [21] T. L. Song and D. Musicki  
Adaptive clutter measurement density estimation for improved target tracking,  
*IEEE Trans. on Aerospace and Electronic Systems*, vol. 47, pp. 1457–1466, Apr. 2011.
- [22] H. Van Trees  
*Detection estimation and modulation theory*, vol. 1, Wiley, 1968.
- [23] B. Ristic, S. Arulampalam, N. Gordon  
*Beyond the Kalman filter, particle filters for tracking applications*, Artech House, 2004.
- [24] T. Kirubarajan and Y. Bar-Shalom  
Low observable target motion analysis using amplitude information,  
*IEEE Tran. on Aerospace and Electronic Systems*, vol. 32, pp. 1367–1384, Oct. 1996.
- [25] P. Willett and Y. Bar-Shalom  
On the CRLB when measurements are of uncertain origin,  
*Proc. 37th IEEE Conf. on Decision and Control, Florida, USA*, pp. 743–747, Dec 1998.
- [26] R. Niu, P. Willett and Y. Bar-Shalom  
Matrix CRLB scaling due to measurements of uncertain origin,  
*IEEE Trans. on Signal Processing*, vol. 49, pp. 1325–1335, July 2001.
- [27] X. Zhang, P. Willett and Y. Bar-Shalom  
Dynamic Cramer-Rao bound for target tracking in clutter,  
*IEEE Tran. on Aerospace and Electronic Systems*, vol. 41, pp. 1154–1167, Oct. 2005.
- [28] X. Zhang, P. Willett and Y. Bar-Shalom  
The Cramer-Rao bound for dynamic target tracking with measurement origin uncertainty,  
*Proc. 41st IEEE Conf. on Decision and Control, Las Vegas, USA*, pp. 3428–3433, Dec 2002.
- [29] Y. Bar-Shalom, X. Zhang and P. Willett  
Simplification of the dynamic Cramer-Rao bound for target tracking in clutter,  
*IEEE Tran. on Aerospace and Electronic Systems*, vol. 47, pp. 1481–1482, Apr. 2011.
- [30] P. Willett  
Issues in target tracking,  
*NATO science and technology organization*, vol. RTO-EN-SET-157, 2012.
- [31] K. P. Burnham and D. R. Anderson  
*Model selection and Multimodel inference, Second edition*, Springer, 2002.
- [32] Y. Bar-Shalom and X. Li  
*Estimation and tracking: Principles, techniques and software*, Artech House, 1993.
- [33] D. Simon  
*Optimal state estimation Kalman,  $H_\infty$  and nonlinear approaches*, Wiley interscience, 2006.
- [34] P. Tichavsky, C. H. Muravchik and A. Nehorai  
Posterior Cramer-Rao bounds for discrete-time nonlinear filtering,  
*IEEE Trans. on Signal Processing*, vol. 46, pp. 1386–1396, May 1998.
- [35] Y. Bar-Shalom, X. Li and T. Kirubarajan  
*Estimation with applications to tracking and navigation*, Artech House, 2001.
- [36] D. Avitzour  
A maximum likelihood approach to data association,  
*IEEE Trans. on Aerospace and Electronic Systems*, vol. 28, pp. 560–566, 1992.
- [37] C. M. Bishop  
*Pattern recognition and machine learning, Chapter 8*, Springer, 2006.
- [38] G. J. McLachlan and T. Krishnan  
*The EM algorithm and extensions*, Wiley & Sons, New York, 1996.
- [39] L. Xu and M. I. Jordan  
On convergence properties of the EM algorithm for Gaussian mixtures,  
*Neural computation*, vol. 8, pp. 129–151, 1996.



**Viji Paul Panakkal** is working as research staff at Central Research Laboratory, BEL, Bangalore, India. His research activities include Radar signal processing, Multi target tracking, and Multi Sensor Data Fusion. He is currently pursuing a Ph.D. degree in Electrical Engineering at Indian Institute of Technology (IIT) Bombay, India.



**Rajbabu Velmurugan** is currently an Associate Professor at the Department of Electrical Engineering, Indian Institute of Technology Bombay, India. He received his Ph.D. degree in electrical engineering from Georgia Institute of Technology, Atlanta. His research interests are in signal processing, statistical signal processing, audio, speech, and image processing. His current focus is on source separation, blind deconvolution, and target tracking problems.

# Bistatic Measurement Fusion from Multistatic Configurations for Air Collision Warning

WENBO DOU  
YAAKOV BAR-SHALOM  
PETER WILLET

A requisite for unmanned aircraft systems (UAS) to operate within a controlled airspace is a capability to sense and avoid collisions with non-cooperative aircraft. Ground-based transmitters and UAS-mounted receivers are preferred due to limitations on UAS. This paper assumes a constant velocity motion of an intruder (target) aircraft and presents a method to estimate the position and velocity of the target so as to predict the closest point of approach. Bistatic range and range rate are assumed the only measurements available. Several configurations are investigated from a parameter observability point of view. It turns out that one needs three transmitters in a general three-dimensional scenario to achieve decent observability of the target motion parameter. With the assumption that the target is at the same altitude as the ownship, one has a two-dimensional scenario in which two transmitters are required in order to have good observability. Simulation results show that the maximum likelihood (ML) estimate of the target parameter using an iterated least squares search can be considered as statistically efficient in both multistatic configurations with good observability for the scenarios considered in this paper. The collision warning can be carried out based on the ML estimate in two different ways. The first approach is to formulate the collision as a hypothesis testing problem using a generalized likelihood function. A second, Bayesian, approach is also presented. The performance of the likelihood based collision warning shows that the multistatic configuration with three transmitters is reliable for collision warning but that the multistatic configuration with two transmitters under the same target and ownship altitude assumption is prone to false alarms. In the configuration with three transmitters, the Bayesian approach yields the similarly reliable collision warning performance as the likelihood-based approach when they use threshold values of the same magnitude.

Manuscript received July 28, 2015; revised October 12, 2015; released for publication November 9, 2015.

Refereeing of this contribution was handled by Benjamin Slocumb.

Supported by ARO Grant W991NF-10-1-0369.

Authors' address: Department of Electrical and Computer Engineering, University of Connecticut, Storrs, CT 06269-4157 (e-mail: {dou, ybs, willett}@engr.uconn.edu.)

---

1557-6418/15/\$17.00 © 2015 JAIF

## 1. INTRODUCTION

Sense-and-Avoid (SAA) capabilities are required for unmanned aircraft systems (UAS) to operate within the national airspace, since the proliferation of UAS has increased the risk of aircraft collision. The air traffic control radar beacon system works well to coordinate cooperative aircraft. Active sensing methods have to be employed for UAS to be functional against non-cooperative targets. The limitations on the size, weight and power of UAS suggest an implementation with ground-based transmitters and UAS-mounted receivers.

There have been numerous works on the UAS collision avoidance problem [1]. Most have emphasized avoidance algorithms [5][13][15], while sensing and estimation methods have been less extensively explored. In [9], a monostatic radar configuration in a two-dimensional (2-D) plane with range and bearing measurements is considered for collision avoidance. In [18], collision warning in a 2-D plane using a monostatic radar with range and azimuth measurements is discussed. A confidence ellipsis at a given time instant is mathematically derived and a confidence corridor is constructed by the regions covered by all confidence ellipses at all time instants within a time interval of interest. A warning decision is based on whether any target aircraft falls within this confidence corridor. The collision warning problem in a multistatic radar configuration has not yet been reported in the literature.

Target localization is possible using a multistatic radar with time of arrival (TOA) measurements [6][10][14][17]. In [14], target localization is considered in a multistatic ultra wideband radar. The problem is formulated as estimation of target position, which is solved using three methods. Taylor series method is shown to have smaller estimation errors than either least-squares or spherical-interpolation method in a system with one transmitter and four receivers. In [10], two methods are presented to estimate the position of a target in a multistatic passive radar. The spherical-intersection method is shown to be better than the spherical-interpolation method in a system with four transmitters and one receiver. In [6], target localization is investigated in a multistatic passive radar system with one receiver when the receiver position is subject to random errors. An approximated maximum likelihood optimization problem is formulated and solved by a semidefinite relaxation combined with bisection method. In [17], target localization based on both time of arrival and angle of arrival measurements in a multistatic radar system is formulated and a weighted least square method is proposed to estimate the target location. TOA measurements can be used to estimate the position but not the velocity, range rate measurements are needed for the velocity.

In our previous work [7][8], a strategy for collision warning in a three-dimensional (3-D) space was pre-

TABLE I  
Target motion parameter observability summary.

Scenario	Sensor configuration	Number of transmitters	Observability
2-D	bistatic	1	marginally observable
2-D	multistatic	2	observable
3-D	bistatic	1	unobservable
3-D	multistatic	2	marginally observable
3-D	multistatic	3	observable

sented, assuming a constant velocity motion of an aircraft of interest (target/intruder), to estimate the position and velocity of the target so as to predict the closest point of approach (CPA). Since an inexpensive system is the goal, only bistatic range and range rate measurements are available. Several configurations listed in Table I are investigated from a parameter observability point of view. In general 3-D scenarios, the target motion parameter is shown to be unobservable in a bistatic configuration (that is: one transmitter and one receiver, not co-located) and a change of course of the receiver (the “observability platform maneuver” that is the saving grace for angle-only target motion analysis (TMA)) merely improves the observability marginally. In a multistatic configuration, one has marginal observability using two transmitters, but good observability with three. In a 2-D scenario which assumes that the target is at the same altitude as the ownship, the target parameter is still only marginally observable in a bistatic configuration. The observability is improved by a small maneuver of the ownship but it is still unappealing. On the other hand, one can have very good observability of the target motion parameter with two transmitters in a 2-D multistatic configuration with the same-altitude assumption, which turns out to be another practically useful configuration in addition to a 3-D multistatic configuration with three transmitters. Simulation results and comparison with the CRLB show that the ML estimate of the target parameter can be considered as statistically efficient in both useful configurations.

The collision warning is formulated as a hypothesis testing problem using a generalized likelihood function. Monte Carlo simulation shows the likelihood-based collision warning algorithm using three transmitters has no missed detection of a collision and has no false alarms when the intruder and ownship altitude separation is beyond 100 m. The likelihood-based collision warning algorithm using two transmitters with the same-altitude assumption has no missed detection of a collision, either. It is, however, prone to false alarms when the CPA angle is near 180°.

This paper extends the previous work [7][8] by (i) taking the physical dimensions of aircraft into consideration in the likelihood-based collision warning algorithm; (ii) investigating the statistical efficiency of the closest point of approach (CPA) time estimate in

the likelihood-based collision warning algorithm; (iii) adding a Bayesian approach for collision warning. Since air collision is deadly, no missed detections can be tolerated. It is also necessary to account for the physical dimensions of aircraft by adding a safety margin to compensate for the errors arising in the point modeling of aircraft. Simulation results show that the likelihood-based collision warning algorithm with a safety margin of 100 m has no missed detections of collision but becomes more conservative with false alarms occurring in more situations.

The likelihood based collision warning algorithm makes decisions by using an estimated CPA time, and Monte Carlo simulations have shown that the CPA time estimate can be considered as unbiased and statistically efficient for the simulated scenarios. The Bayesian approach formulates the CPA distance as a random variable and estimates its probability density function (pdf) as a fitted Rician distribution. Then it defines the collision event by considering the physical dimensions of the aircraft and calculates the probability of collision, based on which a warning decision can be made. The performance of the Bayesian collision warning algorithm is consistent with that of a likelihood-based algorithm.

The remaining sections of this paper are organized as follows. Section 2 describes and formulates the general 3-D problem and considers a special 2-D problem. Section 3 analyzes several possible configurations for collision warning including both 3-D and 2-D scenarios and shows that two of them seem to be practically useful. Section 4 presents the ML estimator based on which two different collision warning algorithms are described in Section 5. Section 6 investigates the efficiency of the ML estimator of the target motion parameter and the efficiency of the CPA time estimate used in the likelihood-based collision warning algorithm, and also shows the performances of both collision warning algorithms and Section 7 draws conclusions.

## 2. PROBLEM FORMULATION

Assume a target of interest (intruder) is moving in 3-D with a constant velocity. The 3-D target position in Cartesian coordinates at time  $k$  is therefore

$$\xi(\mathbf{x}, k) = \mathbf{x}_0 + kT\dot{\mathbf{x}}_0 \quad k = 0, 1, \dots \quad (1)$$

where

$$\mathbf{x} = [\mathbf{x}'_0, \dot{\mathbf{x}}'_0]' = [x, y, z, \dot{x}, \dot{y}, \dot{z}]' \quad (2)$$

is the unknown target motion parameter which is a vector of dimension  $n_x = 6$  consisting of the target’s position  $\mathbf{x}_0$  and velocity  $\dot{\mathbf{x}}_0$  in Cartesian coordinates at time  $k = 0$  (or without loss of generality at any chosen reference time); and  $T$  is the sampling period. There are  $N_{Tx}$  ( $N_{Tx} \geq 1$ ) transmitters at known locations  $\mathbf{u}_i = [x_{u_i}, y_{u_i}, z_{u_i}]'$ ,  $i = 1, \dots, N_{Tx}$ . At time  $k$  ( $k > 0$ ), a moving receiver (the ownship) with known position  $\mathbf{s}(k)$  and velocity  $\dot{\mathbf{s}}(k)$  can obtain measurements consisting of the

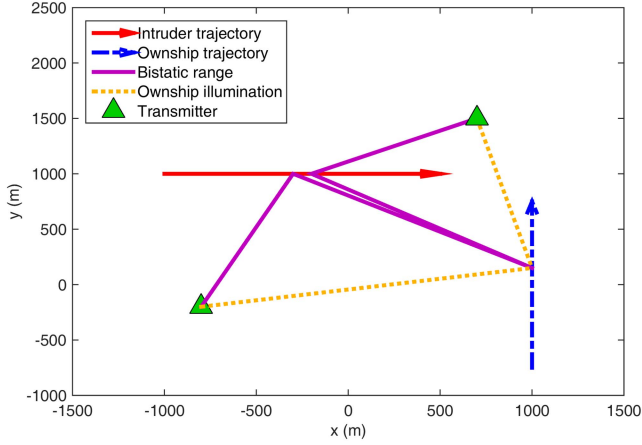


Fig. 1. A multistatic configuration in the X-Y plane. The time differences of arrival (actual measurements) between the direct path (ownship illumination) and the indirect path (bistatic range) multiplied by the speed of light is added to the direct path distance to yield an equivalent bistatic range measurement.

bistatic range [4] illustrated in Figure 1 and the bistatic range rate from the  $i$ th transmitter located at  $\mathbf{u}_i$  given by

$$\mathbf{z}_i(k) = \mathbf{h}_i(\mathbf{x}, k) + \mathbf{w}_i(k) \quad i = 1, \dots, N_{\text{Tx}} \quad (3)$$

where

$$\begin{aligned} \mathbf{h}_i(\mathbf{x}, k) &= \begin{bmatrix} r_i(k) \\ \dot{r}_i(k) \end{bmatrix} \\ &= \begin{bmatrix} \|\boldsymbol{\xi}(\mathbf{x}, k) - \mathbf{s}(k)\| + \|\boldsymbol{\xi}(\mathbf{x}, k) - \mathbf{u}_i\| \\ \frac{[\boldsymbol{\xi}(\mathbf{x}, k) - \mathbf{s}(k)]' [\dot{\mathbf{x}}_0 - \dot{\mathbf{s}}(k)]}{\|\boldsymbol{\xi}(\mathbf{x}, k) - \mathbf{s}(k)\|} + \frac{[\boldsymbol{\xi}(\mathbf{x}, k) - \mathbf{u}_i]' \dot{\mathbf{x}}_0}{\|\boldsymbol{\xi}(\mathbf{x}, k) - \mathbf{u}_i\|} \end{bmatrix} \end{aligned} \quad (4)$$

and  $\mathbf{w}_i(k)$  are the measurement noises, assumed to be independent and identically distributed zero-mean white Gaussian sequences with known covariance matrix

$$R_i = \begin{bmatrix} \sigma_r^2 & 0 \\ 0 & \sigma_{\dot{r}}^2 \end{bmatrix} \quad (5)$$

The measurement function comprising all the measurements at time  $k$  is

$$\mathbf{z}(k) = \mathbf{h}(\mathbf{x}, k) + \mathbf{w}(k) \quad k = 1, \dots \quad (6)$$

where

$$\mathbf{z}(k) = [\mathbf{z}_1(k)' \dots \mathbf{z}_{N_{\text{Tx}}}(k)']' \quad (7)$$

$$\mathbf{h}(\mathbf{x}, k) = [\mathbf{h}_1(\mathbf{x}, k)' \dots \mathbf{h}_{N_{\text{Tx}}}(\mathbf{x}, k)']' \quad (8)$$

$$\mathbf{w}(k) = [\mathbf{w}_1(k)' \dots \mathbf{w}_{N_{\text{Tx}}}(k)']' \quad (9)$$

and

$$R(k) = E[\mathbf{w}(k)\mathbf{w}(k)'] = \begin{bmatrix} R_1 & \mathbf{0} & \dots & \mathbf{0} \\ \mathbf{0} & R_2 & \dots & \mathbf{0} \\ \vdots & \vdots & \ddots & \vdots \\ \mathbf{0} & \mathbf{0} & \dots & R_{N_{\text{Tx}}} \end{bmatrix} \quad (10)$$

Since both intruder and ownship are moving, it is important to avoid any collision between them. The goal

is thus to estimate the target parameter  $\mathbf{x}$  based on  $N$  frames of measurements, and to deliver a warning long enough and confidently enough before a possible collision occurs so as to predict the CPA and, presumably, to do something about it if needed.

## 2.1. Parameter Observability

We need to check the observability of the target motion parameter (2) to see whether there is sufficient information in the data. Observability requires the invertibility of the Fisher information matrix (FIM), which is given by [3]

$$J = E\{[\nabla_{\mathbf{x}} \ln \Lambda(\mathbf{x}; \mathbf{Z})][\nabla_{\mathbf{x}} \ln \Lambda(\mathbf{x}; \mathbf{Z})]'\}_{\mathbf{x}=\mathbf{x}_t} \quad (11)$$

where  $\Lambda(\mathbf{x}; \mathbf{Z})$  is the likelihood function of the parameter based on the measurement set

$$\mathbf{Z} = \mathbf{z}(k)_{k=1}^N \quad (12)$$

and  $\mathbf{x}_t$  is the true value of the target motion parameter. In a simulated scenario,  $\mathbf{x}_t$  is known. However, in a real scenario where  $\mathbf{x}_t$  is unknown and needs to be estimated, the FIM is evaluated at the estimate.

Since the measurement noises are assumed to be white, we have

$$\Lambda(\mathbf{x}; \mathbf{Z}) = \prod_{k=1}^N p(\mathbf{z}(k) | \mathbf{x}) \quad (13)$$

where

$$\begin{aligned} p(\mathbf{z}(k) | \mathbf{x}) &= |2\pi R(k)|^{-1/2} \\ &\cdot \exp\left(-\frac{1}{2}[\mathbf{z}(k) - \mathbf{h}(\mathbf{x}, k)]' R(k)^{-1} [\mathbf{z}(k) - \mathbf{h}(\mathbf{x}, k)]\right) \end{aligned} \quad (14)$$

The gradient of the log-likelihood function is

$$\nabla_{\mathbf{x}} \ln \Lambda(\mathbf{x}; \mathbf{Z}) = -\sum_{k=1}^N [\nabla_{\mathbf{x}} \mathbf{h}(\mathbf{x}, k)' R(k)^{-1} [\mathbf{z}(k) - \mathbf{h}(\mathbf{x}, k)]] \quad (15)$$

Substituting (15) into (11) yields

$$\begin{aligned} J &= \sum_{k=1}^N [\nabla_{\mathbf{x}} \mathbf{h}(\mathbf{x}, k)' R(k)^{-1} [\nabla_{\mathbf{x}} \mathbf{h}(\mathbf{x}, k)']]_{\mathbf{x}=\mathbf{x}_t} \\ &= \sum_{k=1}^N \sum_{i=1}^{N_{\text{Tx}}} [\nabla_{\mathbf{x}} \mathbf{h}_i(\mathbf{x}, k)' R_i^{-1} [\nabla_{\mathbf{x}} \mathbf{h}_i(\mathbf{x}, k)']]_{\mathbf{x}=\mathbf{x}_t} \end{aligned} \quad (16)$$

If  $J$  is not invertible, then the target motion parameter is unobservable. Otherwise, the size of confidence region for the true target position [3] can be used to distinguish between marginal observability and good observability. In this paper, marginal and good observability are distinguished from each other by the length of the longest semiaxis of 99.9999% probability region. In the application of air collision warning, one could say that the observability is good if the longest semiaxis is, say, less than 100 meters and that the observability is marginal if the longest semiaxis is, say, more than

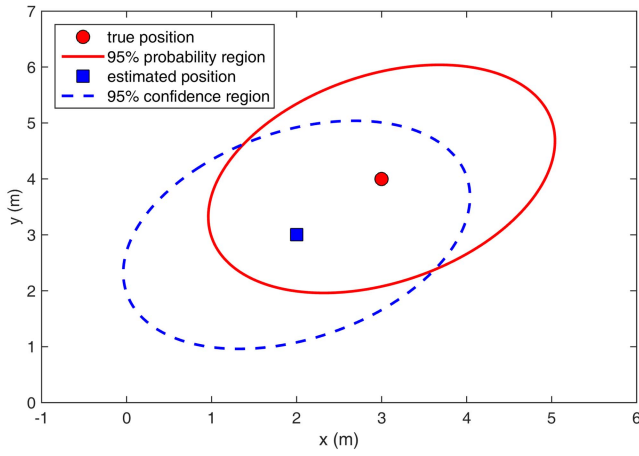


Fig. 2. Confidence region and probability region in the X-Y plane. If an estimate is inside 95% probability region around the truth, then the truth must be inside 95% confidence region around this estimate.

100 meters. Mathematically, the length of the longest semiaxis is proportional to the square root of largest eigenvalue of the covariance matrix in (20).

## 2.2. Confidence Region in the General Case

Suppose one has an unbiased and statistically efficient estimate  $\hat{\mathbf{x}}$ , that is

$$E[\hat{\mathbf{x}}] = \mathbf{x}_t \quad (17)$$

$$P \triangleq E[(\hat{\mathbf{x}} - \mathbf{x}_t)(\hat{\mathbf{x}} - \mathbf{x}_t)'] = J^{-1} \quad (18)$$

where  $J^{-1}$  is the Cramer Rao lower bound (CRLB). The 3-D target position estimate at an arbitrary time  $t$  is

$$\hat{\mathbf{x}}_p(t) = \begin{bmatrix} 1 & 0 & 0 & t & 0 & 0 \\ 0 & 1 & 0 & 0 & t & 0 \\ 0 & 0 & 1 & 0 & 0 & t \end{bmatrix} \hat{\mathbf{x}} \triangleq \Phi_p(t)\hat{\mathbf{x}} \quad (19)$$

and the corresponding covariance is

$$P_p(t) = \Phi_p(t)P\Phi_p(t)' \quad (20)$$

If one further assumes  $\hat{\mathbf{x}}$  is Gaussian, that is,

$$\hat{\mathbf{x}} \sim \mathcal{N}(\mathbf{x}_t, P) \quad (21)$$

then, because of linear transformation in (19)

$$\hat{\mathbf{x}}_p(t) \sim \mathcal{N}(\mathbf{x}_p(t), P_p(t)) \quad (22)$$

The normalized estimation error squared (NEES) for the target position  $\mathbf{x}_p(t)$  at  $t$ , defined as

$$\epsilon_p(t) = [\mathbf{x}_p(t) - \hat{\mathbf{x}}_p(t)]' P_p^{-1}(t) [\mathbf{x}_p(t) - \hat{\mathbf{x}}_p(t)] \quad (23)$$

is chi-square distributed with  $n_x/2$  degrees of freedom, that is,

$$\epsilon_p(t) \sim \chi_{n_x/2}^2 \quad (24)$$

Let  $g$  be such that

$$P\{\epsilon_p(t) \leq g^2\} = 1 - Q \quad (25)$$

where  $Q$  is a small tail probability. Given the predicted target position  $\hat{\mathbf{x}}_p(t)$ , the  $100(1 - Q)\%$  confidence region [2] for the true position  $\mathbf{x}_p(t)$  is defined to be within the ellipsoid given by

$$[\mathbf{x}_p(t) - \hat{\mathbf{x}}_p(t)]' P_p^{-1}(t) [\mathbf{x}_p(t) - \hat{\mathbf{x}}_p(t)] = g^2 \quad (26)$$

Alternatively, given the true position  $\mathbf{x}_p(t)$ , (26) is also defined to be the  $100(1 - Q)\%$  probability region for the predicted target position  $\hat{\mathbf{x}}_p(t)$ . These two regions as shown in Figure 2 have identical geometrical sizes since they can be represented by the same equation as in (26). If either region is large, one has marginal observability of the target position; if any one of the regions is small, one has good observability of the target position.

## 2.3. Confidence Region When Intruder and Ownship at Same Altitude

If the intruder's altitude  $z$  is assumed to be known and is equal to that of the ownship, then the 2-D X-Y plane at the altitude  $z$  is of interest and everything related to the target can be considered restricted to this 2-D space. Specifically, the target parameter to be estimated becomes

$$\mathbf{x}^{2D} = [x, y, \dot{x}, \dot{y}]' \quad (27)$$

Correspondingly, the 2-D target position at an arbitrary time  $t$  is

$$\mathbf{x}_p^{2D}(t) = \begin{bmatrix} 1 & 0 & t & 0 \\ 0 & 1 & 0 & t \end{bmatrix} \mathbf{x}^{2D} \quad (28)$$

The confidence region for the true target position around its estimate is now an ellipse given by (26).

## 3. SCENARIOS AND OBSERVABILITY ANALYSIS

From (26), the size of the confidence region for the true target position around the predicted position is the same as that of the probability region for the predicted target position around the true position. Since it is more convenient for an observability analysis to obtain the probability region for the predicted target position with the true target motion parameter assumed available than to estimate the true target parameter and obtain the confidence region for it, in this section several scenarios are simulated with the knowledge of the true target motion parameter and the probability region of the estimate in each scenario is obtained without performing any estimation.

A radar system, which consists of three transmitters on the ground and one receiver mounted on an unmanned aircraft system (UAS)—the ownship—is used to warn of a possible collision between the UAS (ownship) and an intruder aircraft. The transmitters are located at (0 m, 1000 m, 0 m), (0 m, -1000 m, 0 m) and (1000 m, 0 m, 0 m) in Cartesian coordinates, and

TABLE II  
Scenario specifications. The last column reflects the results from Section 3.

Scenario	Transmitters used	UAS motion	Target altitude	Collision	Semixis lengths of 99.9999% probability region (m)
1	Tx1	CV	Unknown	Yes	$3 \times 10^9$ , 2020, 62
2	Tx1	two-segment CV	Unknown	Yes	6468, 1660, 109
3	Tx1 and Tx2	CV	Unknown	Yes	1542, 50, 41
4	Tx1 and Tx2	two-segment CV	Unknown	Yes	1402, 51, 41
5	Tx1, Tx2 and Tx3	CV	Unknown	Yes	50, 42, 11
6	Tx1, Tx2 and Tx3	CV	Unknown	No	48, 43, 12
7	Tx1	CV	Known	Yes	2600, 81
8	Tx1	two-segment CV	Known	Yes	301, 25
9	Tx1 and Tx2	CV	Known	Yes	40, 8

are denoted by Tx1, Tx2 and Tx3, respectively. The UAS is moving at an altitude of 1500 m.

Eight collision scenarios and one non-collision scenario listed in the Table II, differing in the number of transmitters, the motion of the UAS and the dimensionality of target parameter are studied here. Scenarios with the “known target altitude” assumption are referred to as 2-D scenarios. The rest are 3-D scenarios. Two motions of UAS are considered. In a constant velocity (CV) motion, the UAS starts moving from the point  $(-4500 \text{ m}, 0 \text{ m}, 1500 \text{ m})$  at time  $t = 0 \text{ s}$  with a constant velocity  $\dot{\mathbf{x}}_0 = [50 \text{ m/s}, 0 \text{ m/s}, 0 \text{ m/s}]'$ . In a two-segment CV motion, the UAS starts with a constant velocity  $[43 \text{ m/s}, -25 \text{ m/s}, 0 \text{ m/s}]'$  from the point  $(-4306 \text{ m}, 752 \text{ m}, 1500 \text{ m})$  at time  $t = 0 \text{ s}$  for 27 s and then executes a  $5^\circ/\text{s}$  coordinated turn for 6 s before changing to another velocity  $[50 \text{ m/s}, 0 \text{ m/s}, 0 \text{ m/s}]'$  when it arrives at the location  $(-2850 \text{ m}, 0 \text{ m}, 1500 \text{ m})$ . In all the collision scenarios, the intruder aircraft starts from the position  $(4500 \text{ m}, 0 \text{ m}, 1500 \text{ m})$  at time  $t = 0 \text{ s}$  with a constant velocity  $\dot{\mathbf{x}}_0 = [-50 \text{ m/s}, 0 \text{ m/s}, 0 \text{ m/s}]'$  and will collide with the UAS at time  $t = 90 \text{ s}$ . In the non-collision scenario, the altitude of the intruder aircraft is assumed to be 1600 m, which is 100 m higher than in the collision scenarios, and the CPA occurs at time  $t = 90 \text{ s}$ . Bistatic range and range rate measurements are made from the ownship every 1 s over a period of 60 s, which is 30 s before the CPA time. The noise standard deviations for the range and range rate measurements are assumed to be 8.66 m and 1 m/s, respectively, at all times.

Figures 3 and 4 visualize all the 3-D scenarios and plots the 99.9999% probability region, the lengths of the semiaxes of which are also shown in Table II, around the collision point or the target CPA in each scenario.

In Scenario 1, the FIM is nearly singular with a condition number<sup>1</sup> of 18.8. The large probability region (which implies a large confidence region) indicates the target parameter is practically unobservable and even an efficient estimator is useless in such a situation.

<sup>1</sup>The condition number is  $\log_{10}(\lambda_{\max}/\lambda_{\min})$ , where  $\lambda_{\max}$  and  $\lambda_{\min}$  are the largest and smallest eigenvalues of the FIM.

In Scenario 2, the FIM is not ill-conditioned. The ellipsoid is much smaller than in the first scenario, which indicates the change of course in the ownship trajectory improves the observability. However, the size of the probability (or confidence) region is still quite large so that even an efficient estimator remains practically useless.

Compared with the 3-D bistatic configuration (Scenarios 1 and 2), adding a second transmitter in Scenarios 3 and 4 reduces the target localization uncertainty, although the size of the probability region is still too large to be useful. Comparison between Figures 3(c) and 3(d) indicates that the further reduction of the localization uncertainty resulting from the change of course in the ownship trajectory in the multistatic configuration is not as significant as in the bistatic.

As shown in Figures 4(a) and 4(b), the addition of a third transmitter into the multistatic configuration has significantly improved observability, which makes the localization practically useful. Therefore, one needs three transmitters in a 3-D multistatic configuration to build up an efficient estimator based on which a useful collision warning algorithm can be designed.

Figure 5 visualizes all the 2-D scenarios and plots the 99.9999% probability region around the collision point in each scenario. Compared with 3-D scenarios, the knowledge of target altitude in a 2-D scenario results in a significant reduction in the uncertainty. In Scenario 7, the size of the probability region is still too large to be useful. In Scenario 8, the probability region could be useful, however, it is due to the change of course of the ownship and this maneuver action itself could lead a safety situation to a dangerous collision. In Scenario 9, adding a second transmitter reduces the target localization uncertainty significantly. The size of this region is practically useful. Therefore, with the knowledge of the target altitude one needs two transmitters in a multistatic configuration to build up an efficient estimator based on which a useful collision warning algorithm can be designed.

In the sequel, collision warning is only considered in those two practically useful configurations—3 transmitters in general 3-D scenarios and 2 transmitters with

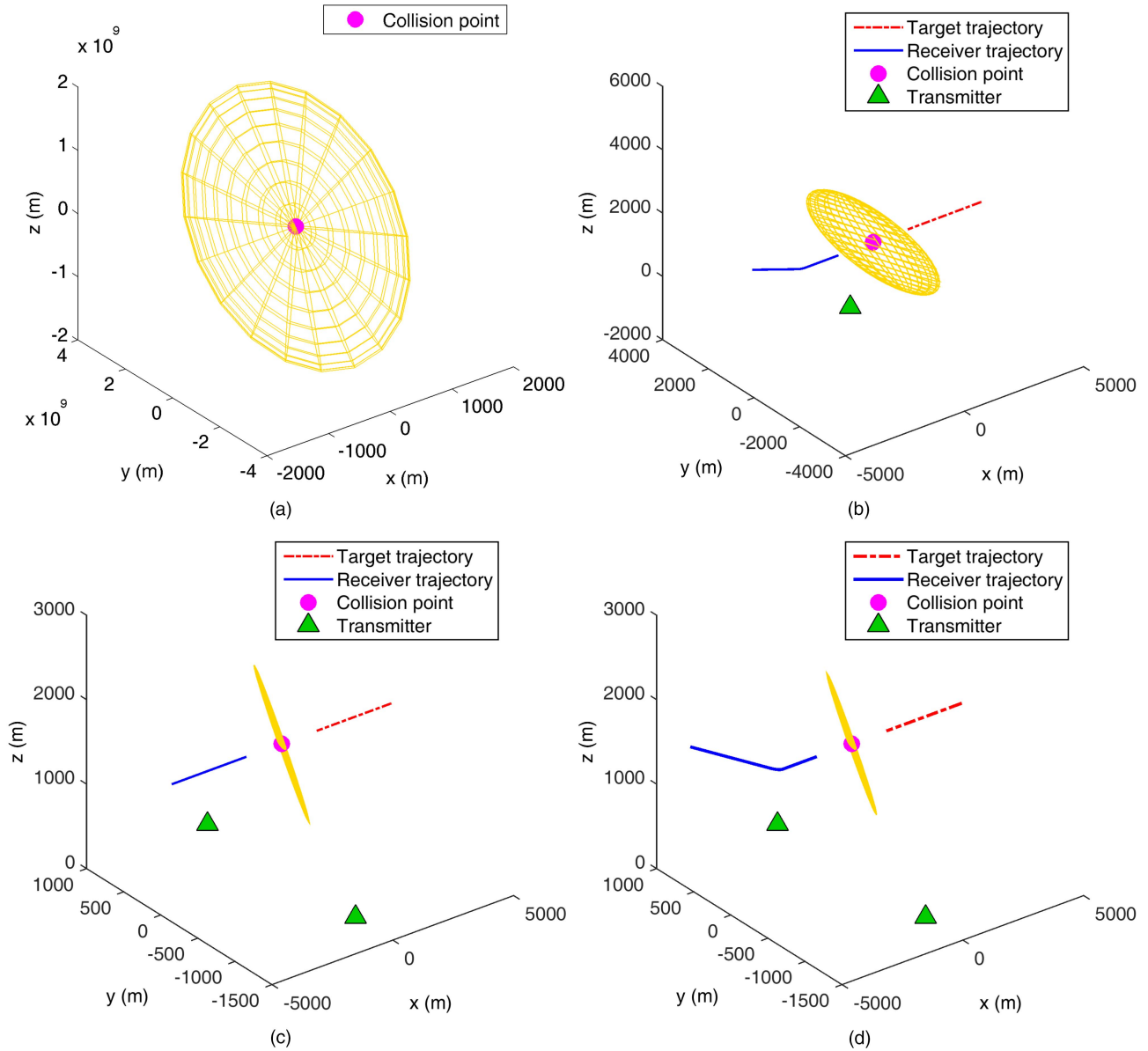


Fig. 3. 99.9999% (ellipsoidal) probability region around the collision point in Scenarios 1 to 4. The target motion parameter is practically unobservable in Scenario 1. The target motion parameter is marginally observable in Scenarios 2, 3 and 4. (a) Scenario 1. (b) Scenario 2. (c) Scenario 3. (d) Scenario 4.

known target altitude in 2-D scenarios, corresponding where to Scenarios 5, 6 and 9.

#### 4. THE MAXIMUM LIKELIHOOD ESTIMATOR

The ML estimate of the target motion parameter  $\mathbf{x}$  in (2) is

$$\hat{\mathbf{x}}_{\text{ML}} = \arg \max_{\mathbf{x}} \Lambda(\mathbf{x}; \mathbf{Z}) \quad (29)$$

where  $\Lambda(\mathbf{x}; \mathbf{Z})$  is given in (13). The ILS technique [2] was used to find the ML estimate in this case. If we set (15) to zero, we will notice that there is no closed-form solution. Using a first order series expansion about an estimate  $\hat{\mathbf{x}}^j$  at the end of the  $j$ th iteration leads to an iterative scheme and the  $(j + 1)$ th estimate is

$$\hat{\mathbf{x}}^{j+1} = \hat{\mathbf{x}}^j + [(H^j)'R^{-1}H^j]^{-1}(H^j)'R^{-1}[\mathbf{z} - \mathbf{h}(\hat{\mathbf{x}}^j)] \quad (30)$$

$$\mathbf{z} = [\mathbf{z}(1)', \mathbf{z}(2)', \dots, \mathbf{z}(N)']' \quad (31)$$

$$\mathbf{h}(\hat{\mathbf{x}}^j) = [\mathbf{h}(\hat{\mathbf{x}}^j, 1), \mathbf{h}(\hat{\mathbf{x}}^j, 2), \dots, \mathbf{h}(\hat{\mathbf{x}}^j, N)]' \quad (32)$$

$$R = \begin{bmatrix} R(1) & \mathbf{0} & \dots & \mathbf{0} \\ \mathbf{0} & R(2) & \dots & \mathbf{0} \\ \vdots & \vdots & \ddots & \vdots \\ \mathbf{0} & \mathbf{0} & \dots & R(N) \end{bmatrix} \quad (33)$$

and

$$H^j = \begin{bmatrix} [\nabla_{\mathbf{x}} \mathbf{h}(\mathbf{x}, 1)']'|_{\mathbf{x}=\hat{\mathbf{x}}^j} \\ [\nabla_{\mathbf{x}} \mathbf{h}(\mathbf{x}, 2)']'|_{\mathbf{x}=\hat{\mathbf{x}}^j} \\ \vdots \\ [\nabla_{\mathbf{x}} \mathbf{h}(\mathbf{x}, N)']'|_{\mathbf{x}=\hat{\mathbf{x}}^j} \end{bmatrix} \quad (34)$$

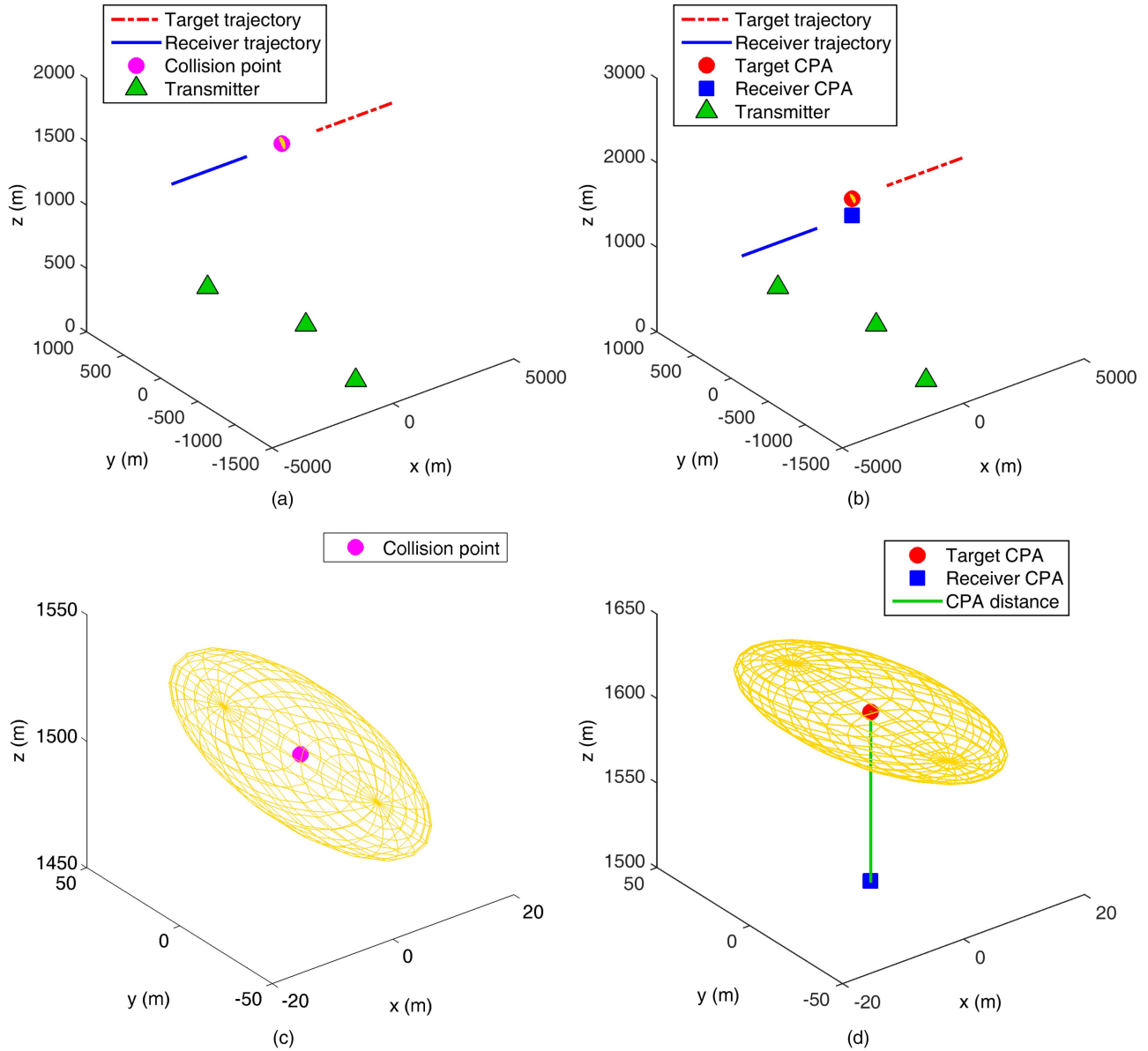


Fig. 4. 99.9999% (ellipsoidal) probability region around the collision point or the target CPA in Scenarios 5 and 6. The target motion parameter observability is good in both scenarios. (a) Scenario 5. (b) Scenario 6. (c) Scenario 5 magnified. (d) Scenario 6 magnified.

An initial estimate can be obtained by solving (3) with the noise set to zero based on the measurements for two transmitters at two different time instants.

The ML estimate of the target parameter  $\mathbf{x}_{2D}$  in (27) in a 2-D scenario can be found using the ILS technique in the same manner.

This paper assumes that a fixed number  $N$  of frames of measurements are processed together using a batch approach. Therefore, there is no need to use a recursive algorithm for sequential update. One can sequentially process the measurements using a recursive estimator as more and more measurements are received. For example, the probability region considered in this paper will become smaller and smaller as more and more measurements are used in the target parameter estimation. The decision on collision warning can be made earlier before

$N$  frames of measurements become available. However, since the problem is highly nonlinear, a recursive estimator would be by necessity suboptimal, either due to linearization or using a particle filter. We will consider this in the future: This is a topic for future investigation.

## 5. COLLISION WARNING APPROACHES

### 5.1. Collision Warning via Hypothesis Testing Based on a Generalized Likelihood Function

The collision event at time  $t$  ( $t$  to be determined) is defined by equating the true target position  $\mathbf{x}_p(t)$  to the ownship position, namely,

$$\{\text{Collision at } t\} \triangleq \{\mathbf{x}_p(t) = \mathbf{s}(t)\} \quad (35)$$

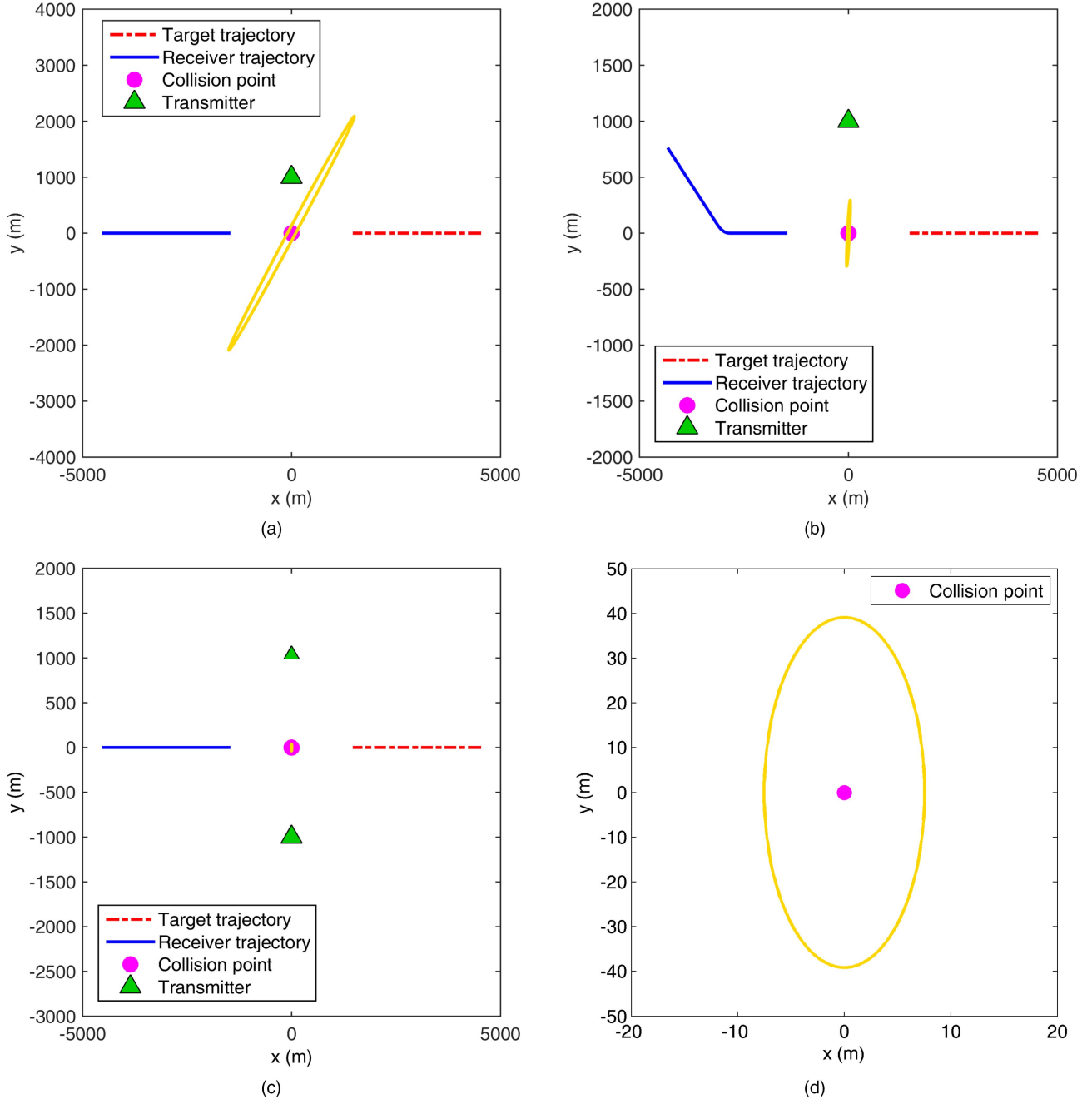


Fig. 5. 99.9999% (elliptic) probability region around the collision point in 2-D scenarios. The target motion parameter is marginally observable in Scenarios 7 and 8. The target motion parameter observability is good in Scenario 9. (a) Scenario 7. (b) Scenario 8. (c) Scenario 9. (d) Scenario 9 magnified.

Following [2], the likelihood function of collision is the pdf of the predicted target position to time  $t$  (the “observation” based on which the collision warning can be made) conditioned on (35)

$$\begin{aligned}
 \Lambda[\mathbf{x}_p(t) = \mathbf{s}(t); \hat{\mathbf{x}}_p(t)] &= p[\hat{\mathbf{x}}_p(t) | \mathbf{x}_p(t) = \mathbf{s}(t)] \\
 &= \mathcal{N}[\hat{\mathbf{x}}_p(t); \mathbf{s}(t), P_p(t)] = |2\pi P_p(t)|^{-1/2} \\
 &\quad \cdot \exp\left(-\frac{1}{2}[\hat{\mathbf{x}}_p(t) - \mathbf{s}(t)]' P_p^{-1}(t) [\hat{\mathbf{x}}_p(t) - \mathbf{s}(t)]\right)
 \end{aligned} \tag{36}$$

where  $\hat{\mathbf{x}}_p(t)$  is given by (19). The use of the covari-

ance  $P_p(t)$  in (36) is justified based on the discussion presented in Section 6, which validates the efficiency of (29).

Since the time  $t$  in (36) is not known, we estimate the CPA time as

$$\hat{t}_{\text{CPA}} = \arg \max_t \Lambda[\mathbf{x}_p(t) = \mathbf{s}(t); \hat{\mathbf{x}}_p(t)] \tag{37}$$

The CPA time estimate is found by using the Quasi-Newton method with a cubic line search procedure. The search starts with an initial value, which can be obtained using (58) by considering the estimated target parameter

as deterministic. For the purpose of simulations, the MATLAB function “fminunc” is used.

The collision warning can be formulated as a hypothesis testing problem as follows. The two hypotheses are, based on (37)

$$H_0 : \mathbf{x}_p(\hat{t}_{\text{CPA}}) = \mathbf{s}(\hat{t}_{\text{CPA}}) \quad (38)$$

$$H_1 : \mathbf{x}_p(\hat{t}_{\text{CPA}}) \neq \mathbf{s}(\hat{t}_{\text{CPA}}) \quad (39)$$

The (generalized<sup>2</sup>) likelihood function for  $H_0$  is

$$\begin{aligned} \Lambda[H_0; \hat{\mathbf{x}}_p(\hat{t}_{\text{CPA}})] &= \mathcal{N}[\hat{\mathbf{x}}_p(\hat{t}_{\text{CPA}}); \mathbf{s}(\hat{t}_{\text{CPA}}), P_p(\hat{t}_{\text{CPA}})] \\ &= \mathcal{N}[\mathbf{s}(\hat{t}_{\text{CPA}}); \hat{\mathbf{x}}_p(\hat{t}_{\text{CPA}}), P_p(\hat{t}_{\text{CPA}})] \end{aligned} \quad (40)$$

For a given level of significance, say 0.0001% (assuming this is the desired confidence to avoid collision,  $Q = 10^{-6}$  in (25)), there are two equivalent procedures to determine whether  $H_0$  should be rejected.

Procedure 1: one computes

$$\epsilon = [\hat{\mathbf{x}}_p(\hat{t}_{\text{CPA}}) - \mathbf{s}(\hat{t}_{\text{CPA}})]' P_p^{-1}(\hat{t}_{\text{CPA}}) [\hat{\mathbf{x}}_p(\hat{t}_{\text{CPA}}) - \mathbf{s}(\hat{t}_{\text{CPA}})] \quad (41)$$

and

$$\epsilon_{\text{th}} = F_{\chi^2}^{-1}(1 - Q, n_{\text{dof}}) \quad (42)$$

where  $F_{\chi^2}^{-1}$  is the inverse of the cumulative distribution function (cdf) of a chi-square random variable with  $n_{\text{dof}}$  degrees of freedom. If

$$\epsilon > \epsilon_{\text{th}} \quad (43)$$

then  $\mathbf{s}(\hat{t}_{\text{CPA}})$  is outside the 99.9999% confidence region centered at  $\hat{\mathbf{x}}_p(\hat{t}_{\text{CPA}})$ , then one can say that collision is unlikely ( $< 0.0001\%$ ). Otherwise a collision warning is issued.

Procedure 2: one computes

$$\epsilon = [\hat{\mathbf{x}}_p(\hat{t}_{\text{CPA}}) - \mathbf{s}(\hat{t}_{\text{CPA}})]' P_p^{-1}(\hat{t}_{\text{CPA}}) [\hat{\mathbf{x}}_p(\hat{t}_{\text{CPA}}) - \mathbf{s}(\hat{t}_{\text{CPA}})] \quad (44)$$

and estimates the probability of collision as

$$P_c = 1 - F_{\chi^2}(\epsilon, n_{\text{dof}}) \quad (45)$$

where  $F_{\chi^2}$  is the cdf of a chi-square random variable with  $n_{\text{dof}}$  degrees of freedom. If

$$P_c > 0.0001\% \quad (46)$$

then a collision warning is alerted.

These two procedures are equivalent because of the invertibility of the cdf of the chi-square distribution.

So far, both the target and the ownship have been modeled as points of zero size. If one takes the physical dimensions of both the target and the ownship into consideration, a safety margin  $\Delta d$  (which would, typically, be more than the sum of the target and ownship sizes) is needed in the decision making. In this case, the definition of the collision event in (35) will be modified to be

$$\{\text{Collision at } t\} \triangleq \{\|\mathbf{x}_p(t) - \mathbf{s}(t)\| \leq \Delta d\} \quad (47)$$

<sup>2</sup>This is a generalized likelihood function because it relies on  $\hat{t}_{\text{CPA}}$ , which is an estimate.

and the hypotheses in (38) and (39) will be modified as

$$H_0 : \|\mathbf{x}_p(t) - \mathbf{s}(t)\| \leq \Delta d \quad (48)$$

$$H_1 : \|\mathbf{x}_p(t) - \mathbf{s}(t)\| > \Delta d \quad (49)$$

Therefore,  $H_0$  in (48) is rejected at a level of 0.0001% if  $\mathbf{s}(\hat{t}_{\text{CPA}})$  is outside the 99.9999% confidence region centered at  $\hat{\mathbf{x}}_p(\hat{t}_{\text{CPA}})$  and

$$\Delta d < \min_{\mathbf{x}} \|\mathbf{s}(\hat{t}_{\text{CPA}}) - \mathbf{x}\| \quad (50)$$

subject to

$$\begin{aligned} &[\hat{\mathbf{x}}_p(\hat{t}_{\text{CPA}}) - \mathbf{x}]' P_p^{-1}(\hat{t}_{\text{CPA}}) [\hat{\mathbf{x}}_p(\hat{t}_{\text{CPA}}) - \mathbf{x}] \\ &= F_{\chi^2}^{-1}(0.999999, n_{\text{dof}}) \end{aligned} \quad (51)$$

that is, the minimum distance between  $\mathbf{s}(\hat{t}_{\text{CPA}})$  and any point on the surface of the 99.9999% confidence region is larger than  $\Delta d$ .

Equivalently, in a similar way to (44)–(46), one can also estimate the probability of collision as

$$P_c = 1 - F_{\chi^2}(\epsilon_{\text{min}}, n_{\text{dof}}) \quad (52)$$

where

$$\epsilon_{\text{min}} = \min_{\mathbf{x}} [\hat{\mathbf{x}}_p(\hat{t}_{\text{CPA}}) - \mathbf{x}]' P_p^{-1}(\hat{t}_{\text{CPA}}) [\hat{\mathbf{x}}_p(\hat{t}_{\text{CPA}}) - \mathbf{x}] \quad (53)$$

subject to

$$\|\mathbf{s}(\hat{t}_{\text{CPA}}) - \mathbf{x}\| \leq \Delta d \quad (54)$$

## 5.2. Collision Warning Based on a Bayesian Approach

In the Bayesian approach instead of using  $\hat{t}_{\text{CPA}}$  as “the collision time,” the approach accounts for  $t_{\text{CPA}}$  as a random variable. Since the CPA distance  $d_{\text{CPA}}$  (the distance between the target and the ownship at the CPA time) is a function of the CPA time,  $d_{\text{CPA}}$  is also a random variable. One can define the collision event based on  $d_{\text{CPA}}$  and estimate the probability of collision based on an estimated pdf of  $d_{\text{CPA}}$ .

1) CPA distance as a function of the target parameter:

Under the assumption that both the target and the ownship are moving with constant velocities, the CPA time is when the target and the ownship are closest to each other, that is

$$\begin{aligned} t_{\text{CPA}} &= \arg \min_t \|\mathbf{x}_p(t) - \mathbf{s}(t)\| \\ &= \arg \min_t \|(\mathbf{x}_0 + t\dot{\mathbf{x}}_0) - (\mathbf{s}_0 + t\dot{\mathbf{s}}_0)\| \\ &= \arg \min_t \|(\mathbf{x}_0 + t\dot{\mathbf{x}}_0) - (\mathbf{s}_0 + t\dot{\mathbf{s}}_0)\|^2 \\ &= \arg \min_t d^2 \end{aligned} \quad (55)$$

Taking the derivative of  $d^2$  with respect to  $t$  and setting it to zero

$$\frac{dD}{dt} = 2[(\mathbf{x}_0 + t\dot{\mathbf{x}}_0) - (\mathbf{s}_0 + t\dot{\mathbf{s}}_0)]' [\dot{\mathbf{x}}_0 - \dot{\mathbf{s}}_0] = 0 \quad (56)$$

the CPA time is obtained as

$$t_{\text{CPA}} = -\frac{[\mathbf{x}_0 - \mathbf{s}_0]'[\dot{\mathbf{x}}_0 - \dot{\mathbf{s}}_0]}{\|\dot{\mathbf{x}}_0 - \dot{\mathbf{s}}_0\|^2} \quad (57)$$

and the CPA distance is therefore a function of the target parameter  $\mathbf{x}$  in (2)

$$\begin{aligned} d_{\text{CPA}} &= f(\mathbf{x}) = \|\mathbf{x}_p(t_{\text{CPA}}) - \mathbf{s}(t_{\text{CPA}})\| \\ &= \|\mathbf{x}_0 - \mathbf{s}_0 - \frac{[\mathbf{x}_0 - \mathbf{s}_0]'[\dot{\mathbf{x}}_0 - \dot{\mathbf{s}}_0]}{\|\dot{\mathbf{x}}_0 - \dot{\mathbf{s}}_0\|^2}(\dot{\mathbf{x}}_0 - \dot{\mathbf{s}}_0)\| \end{aligned} \quad (58)$$

In the above,  $\|\cdot\|$  is the Cartesian norm.

2) Estimation of the probability density of  $d_{\text{CPA}}$ :

Assuming a diffuse (non-informative) prior density for the target parameter  $\mathbf{x}$ , as in [2], the posterior density of  $\mathbf{x}$  conditioned on  $\hat{\mathbf{x}}_{\text{ML}}$ , given by (29), is approximated as

$$p[\mathbf{x} | \hat{\mathbf{x}}_{\text{ML}}] = \mathcal{N}[\mathbf{x}; \hat{\mathbf{x}}_{\text{ML}}, J^{-1}] \quad (59)$$

This Gaussian approximation is reasonable as Section 6 shows that the ML estimate can be considered as unbiased and statistically efficient, that is, (17) and (18) hold.

One possible way of estimating the density of  $d_{\text{CPA}}$  is to draw  $N_s$  samples of  $\mathbf{x}$  from (59), obtain  $N_s$  samples of  $d_{\text{CPA}}$  and fit a density based on these samples. In this paper, we estimate the pdf of  $d_{\text{CPA}}$  as a Rician distribution. The validity of fitting the Rician distribution is confirmed in Section 6. The Rician distribution with noncentrality parameter  $\nu \geq 0$  and scale parameter  $\sigma > 0$  has the density function

$$p_{d_{\text{CPA}}}(x | \nu, \sigma) = \frac{x}{\sigma^2} \exp\left(-\frac{x^2 + \nu^2}{2\sigma^2}\right) I_0\left(\frac{x\nu}{\sigma^2}\right), \quad x > 0 \quad (60)$$

where  $I_0(\cdot)$  is the zero-order modified Bessel function of the first kind. Based on the  $N_s$  samples of  $d_{\text{CPA}}$ , the ML estimates  $\nu^{\text{ML}}$  and  $\sigma^{\text{ML}}$  can be obtained using the method presented in [12].

3) Decision making:

One can define the collision event as

$$\{\text{Collision}\} = \{d_{\text{CPA}} \leq d_{\text{min}}\} \quad (61)$$

where  $d_{\text{min}}$  is the minimum distance between the aircraft for which a collision will not occur, that is, one believe that a collision occurs if the estimated  $d_{\text{CPA}}$  is less than  $d_{\text{min}}$  by taking the aircraft dimensions into account. Therefore, the probability of collision is

$$\begin{aligned} P_c &= P(\{\text{Collision}\}) = P(\{d_{\text{CPA}} \leq d_{\text{min}}\}) \\ &= \int_0^{d_{\text{min}}} p_{d_{\text{CPA}}}(x | \nu^{\text{ML}}, \sigma^{\text{ML}}) dx \end{aligned} \quad (62)$$

The integration in (62) is evaluated using the MATLAB function ‘‘cdf.’’ The average computational time in a single run, including the target parameter estimation, sampling, Rician distribution parameter estimation and the integration (62), is around 0.6 s. This computation is

performed in MATLAB 2015a on a Windows machine equipped with a 2.40 GHz Intel Core 2 Quad CPU with 4 GB RAM. Consequently, we feel it is not unreasonable to claim that it would be real-time feasible with a dedicated processor and code in machine language.

If  $P_c$  is smaller than, say, 0.0001%, the collision is unlikely and no warning will be issued. Otherwise, a warning will be given.

## 6. SIMULATION RESULTS

### 6.1. Efficiency of ML Estimator of the Target Parameter

Under the hypothesis  $H_x$  that the ML estimator (29) is unbiased and efficient, that is, the mean of the estimation error is zero and the estimation errors match the covariance given by the CRLB as in (18), the NEES for the target parameter

$$\epsilon_x = \tilde{\mathbf{x}}' J \tilde{\mathbf{x}} \quad (63)$$

is chi-square distributed with  $n_x$  degrees of freedom. The sample average NEES from  $N$  Monte Carlo runs would be

$$\bar{\epsilon}_x = \frac{1}{N} \sum_{i=1}^N \epsilon_x^i \quad (64)$$

where  $\epsilon_x^i$  is a sample from  $i$ th Monte Carlo run. The quantity  $N\bar{\epsilon}_x$  is chi-square distributed with  $Nn_x$  degrees of freedom. Therefore, for a given level of significance  $\alpha$ ,  $H_x$  cannot be rejected if

$$\bar{\epsilon}_x \in \left[ \frac{L_x}{N}, \frac{U_x}{N} \right] \quad (65)$$

where  $L_x$  and  $U_x$  are the  $100\alpha/2$  and  $100(2 - \alpha)/2$  percentile points of a chi-square random variable with  $Nn_x$  degrees of freedom.

The sample averages of the NEES for the 6-D target parameter ( $n_x = 6$ ) in Scenario 5 from 100 Monte Carlo runs based on the CRLB evaluated at the truth and at the estimate are calculated. The values are 6.2576 and 6.2207, which can be considered practically identical. Both values fall inside the two-sided 60% probability region [5.70, 6.29], which means that one can accept the null hypothesis  $H_x$  at a high significance level of 40%, i.e., we allow a probability of making a type I (reject  $H_x$  when it is true) error that is 40% in this case. In addition, the likelihood function (13) is exponential, which is a necessary, although not sufficient, condition for the MLE to be efficient [16]. This strongly affirms the acceptability of the CRLB as the actual covariance of the 3-D estimator in Scenario 5. The same reasoning was used in [11] to demonstrate the statistical efficiency of composite position measurements from passive sensors for a variety of geometries.

The sample averages of the NEES for the 4-D target parameter ( $n_x = 4$ ) in Scenario 9 from 100 Monte Carlo runs based on the CRLB evaluated at the truth and at the estimate are also calculated. The values are

3.9209 and 3.9199, which can also be considered practically identical. Both values fall inside the two-sided 30% probability region [3.885, 4.103] (i.e., the alternative hypothesis  $H_1$  (“not efficient”) is rejected at a rather high significance level of 70%), which confirms the acceptability of the CRLB as the actual covariance of the 2-D estimator in Scenario 9. Therefore, the unbiasedness and efficiency of the ML estimator is verified in both scenarios considered in this paper.

Simulation results also show that the collision warning algorithm based on the CRLB covariance provides reliable performance by comparing the CRLB-based error probability of  $10^{-5}$  with  $10^5$  Monte Carlo runs. The number of missed collision detections in this case was 2 in  $10^5$  runs. If one considers the following hypothesis test

$$H_0 : P_{\text{FA}} = 10^{-5} \quad (66)$$

$$H_1 : P_{\text{FA}} > 10^{-5} \quad (67)$$

then, based on the Poisson approximation with parameter  $\lambda$  of the binomial distribution of the number of missed detections in  $10^5$  runs ( $H_0 : \lambda = 1$ ;  $H_1 : \lambda > 1$  with  $10^5$  runs), the probability of getting no more than 2 missed collision detections is 0.9197, i.e., we can accept  $H_0$  at a level of significance of 8%. (The outcome is to the left of the 8% tail.) With  $10^5$  runs and the threshold set for  $P_{\text{FA}} = 10^{-4}$  (then  $H_0 : \lambda = 10$ ), we obtained 5 missed collision detections, i.e., in this case  $H_0$  can be accepted at a level of significance of 93% (unusually high).

## 6.2. Efficiency of the CPA Time Estimate

Based on (36), the CPA time estimate  $\hat{t}_{\text{CPA}}$  in (37) is a function of the target parameter estimate  $\hat{\mathbf{x}}$ , denoted as

$$\hat{t}_{\text{CPA}} = g[\hat{\mathbf{x}}] \quad (68)$$

Unfortunately, the function  $g$  has no closed-form expression, therefore, we estimate the variance of  $\hat{t}_{\text{CPA}}$  using the unscented transformation technique [3] as follows:

Firstly, by the method of moment matching, the Gaussian density  $\mathcal{N}(\hat{\mathbf{x}}; \mathbf{x}_t, P)$  of the  $n_x$ -dimensional  $\hat{\mathbf{x}}$  (centered at the true value  $\mathbf{x}_t$ ; this is in view of the unbiasedness and efficiency discussed in the previous subsection) is replaced by a  $(2n_x + 1)$ -point probability mass function (pmf)

$$p(\hat{\mathbf{x}}) = \sum_{i=-n_x}^{n_x} w^i \delta(\hat{\mathbf{x}} - \hat{\mathbf{x}}^i) \quad (69)$$

where  $\delta(\cdot)$  is the Dirac delta function. The sigma points of the pmf are

$$\hat{\mathbf{x}}^i = \mathbf{x}_t + \text{sgn}(i)a[P]_{|i|}^{1/2} \quad i = -n_x, \dots, n_x; \quad a \in \mathbb{R} \quad (70)$$

where  $[P]_i^{1/2}$  is the  $i$ th column of the Cholesky factor of  $P$  defined by

$$\sum_{i=1}^{n_x} [P]_i^{1/2} ([P]_i^{1/2})' = P \quad (71)$$

and the signum function is defined as

$$\text{sgn}(i) \triangleq \begin{cases} -1 & i < 0 \\ 0 & i = 0 \\ 1 & i > 0 \end{cases} \quad (72)$$

The point masses are [3]

$$w^i = \begin{cases} \frac{1}{2a^2} & |i| = 1, \dots, n_x \\ \frac{a^2 - n_x}{a^2} & i = 0 \end{cases} \quad (73)$$

which sum up to unity. With the sigma points and point masses specified above, the pmf (69) has the same mean and covariance matrix as the Gaussian pdf  $\mathcal{N}(\hat{\mathbf{x}}; \mathbf{x}_t, P)$  regardless of the value of  $a$ . A reasonable choice of  $a$  is  $\sqrt{n_x + 2}$ , so we use that in this paper. In a simulated scenario, the true value of the parameter is known. However, in a real scenario where the true value of the parameter is unknown and needs to be estimated, the sigma points of  $\hat{\mathbf{x}}$  need to match the moments of  $\mathcal{N}(\hat{\mathbf{x}}, P)$  with  $P$  evaluated at the estimate.

Secondly, a sigma point of  $\hat{t}_{\text{CPA}}$  corresponding to  $\hat{\mathbf{x}}^i$  can be obtained as

$$\hat{t}^i = g[\hat{\mathbf{x}}^i] \quad (74)$$

Lastly, the pdf of  $\hat{t}_{\text{CPA}}$  is approximated by the pmf

$$p(\hat{t}_{\text{CPA}}) = \sum_{i=-n_x}^{n_x} w^i \delta(\hat{t}_{\text{CPA}} - \hat{t}^i) \quad (75)$$

which has mean

$$\bar{t} = \sum_{i=-n_x}^{n_x} w^i \hat{t}^i \quad (76)$$

and variance

$$\sigma_t^2 = \sum_{i=-n_x}^{n_x} w^i (\hat{t}^i - \bar{t})^2 \quad (77)$$

If we assume that  $\hat{t}_{\text{CPA}}$  is a Gaussian random variable with mean  $t_{\text{CPA}}$  and variance  $\sigma_t^2$ , then under the hypothesis  $H_t$  that the estimator (37) is unbiased and efficient, the NEES for the CPA time

$$\epsilon_t = \frac{(t_{\text{CPA}} - \hat{t}_{\text{CPA}})^2}{\sigma_t^2} \quad (78)$$

is chi-square distributed with 1 degree of freedom. The sample average NEES from  $N$  Monte Carlo runs would be

$$\bar{\epsilon}_t = \frac{1}{N} \sum_{i=1}^N \epsilon_t^i \quad (79)$$

where  $\epsilon_t^i$  is a sample from  $i$ th Monte Carlo run. The quantity  $N\bar{\epsilon}_t$  is chi-square distributed with  $N$  degrees of

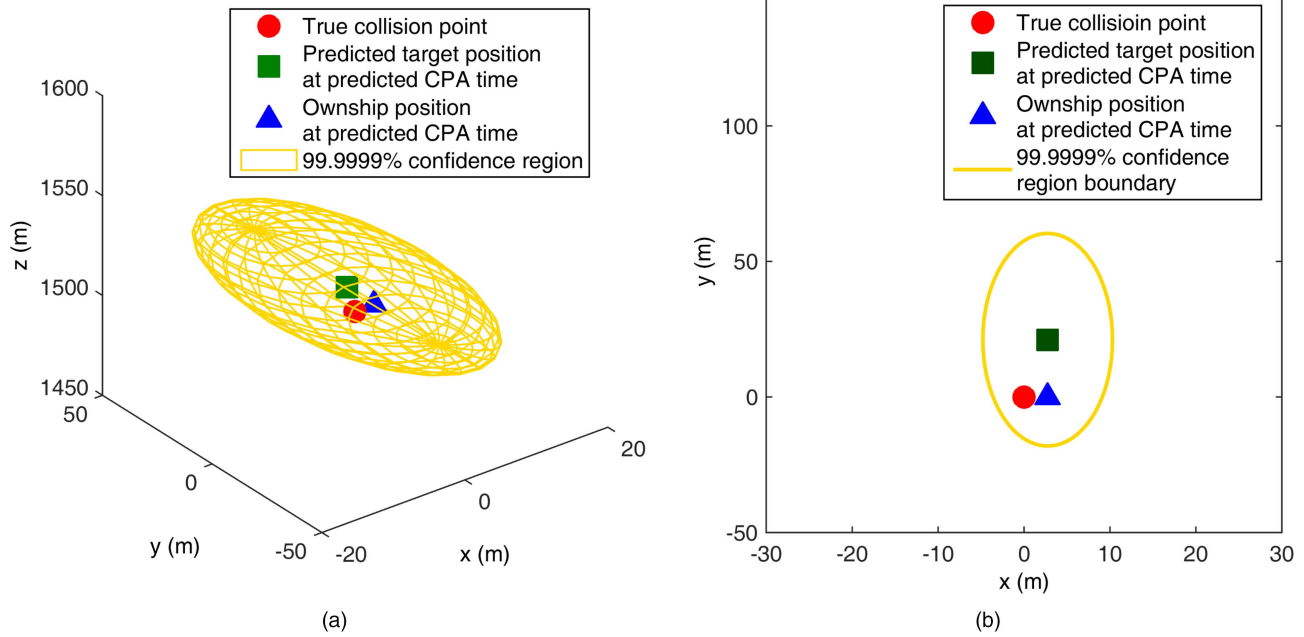


Fig. 6. Collision warning is “on” in a single run in Scenarios 5 and 9. (a) Scenario 5. (b) Scenario 9.

freedom. Therefore, for a given level of significance  $\alpha$ ,  $H_t$  cannot be rejected if

$$\bar{\epsilon}_t \in \left[ \frac{L_t}{N}, \frac{U_t}{N} \right] \quad (80)$$

where  $L_t$  and  $U_t$  are the  $100\alpha/2$  and  $100(2 - \alpha)/2$  percentile points of a chi-square random variable with  $N$  degrees of freedom.

The sample averages of the NEES for the CPA time estimate in Scenario 5 from 100 Monte Carlo runs based on the true value and the estimate of the target parameter are calculated. The values are 1.0914 and 1.0950, which can be considered practically identical. Both values fall inside the two-sided 60% probability region [0.879, 1.117], which confirms the unbiasedness and efficiency of the CPA time estimate in Scenario 5 for the 3-D case. The sample averages of the NEES for the CPA time estimate in Scenario 9 from 100 Monte Carlo runs based on the true value and the estimate of the target parameter are calculated. The values are 0.8753 and 0.8737, which can also be considered practically identical. Both values fall inside the two-sided 60% probability region, which confirms the unbiasedness and efficiency of the CPA time estimate in Scenario 9 for the 2-D case.

### 6.3. Collision Warning Based on the Generalized Likelihood Function

The collision warning is “on” for all 100 runs in Scenario 5 and 9 with the target and the ownship modeled as points, that is, at the predicted CPA time the ownship is inside the confidence region of the true target around its predicted position as illustrated in Figure 6(a) and 6(b). The collision warning is “off” for all 100 runs in Scenario 6, that is, at the predicted CPA

time the ownship is outside the confidence region of the true target around its predicted position as illustrated in Figure 7(a).

Taking the physical dimensions of the aircraft into consideration and using a safety margin of 100 m, the collision warning is “on” for all 100 runs in Scenario 5 and 9. However, the collision warning is “on” for all 100 runs in Scenario 6, that is, false alarms occur. Although at the predicted CPA time the ownship is outside the confidence region of the true target around its predicted position, the minimum distance between the ownship and the ellipsoid is less than the safety margin as illustrated in Figure 7(b).

The term “CPA angle” is defined as the angle formed by the target velocity vector and the ownship velocity vector at the CPA time when they are projected on a plane at the same altitude. Therefore, the CPA angle is  $180^\circ$  in Scenarios 5, 6 and 9.

The performance of the 3-D likelihood-based collision warning algorithm is further evaluated by varying the target and ownship altitude separation<sup>3</sup> from 0 to 300 m in steps of 50 m and the CPA angle from  $180^\circ$  to  $135^\circ$  in steps of  $15^\circ$  one parameter at a time in Scenario 5. From Figure 8(a), the 3-D likelihood based collision warning algorithm has no missed detections of a collision in 100 runs. There are some false alarms when the intruder and ownship altitude separation is 50 m and the number of false alarms increases slightly with the CPA angle decreasing. There are no false alarms when the intruder and ownship altitude separation is beyond 100 m.

<sup>3</sup>1000 ft ( $\approx 300$  m) is a global standard for vertical separation

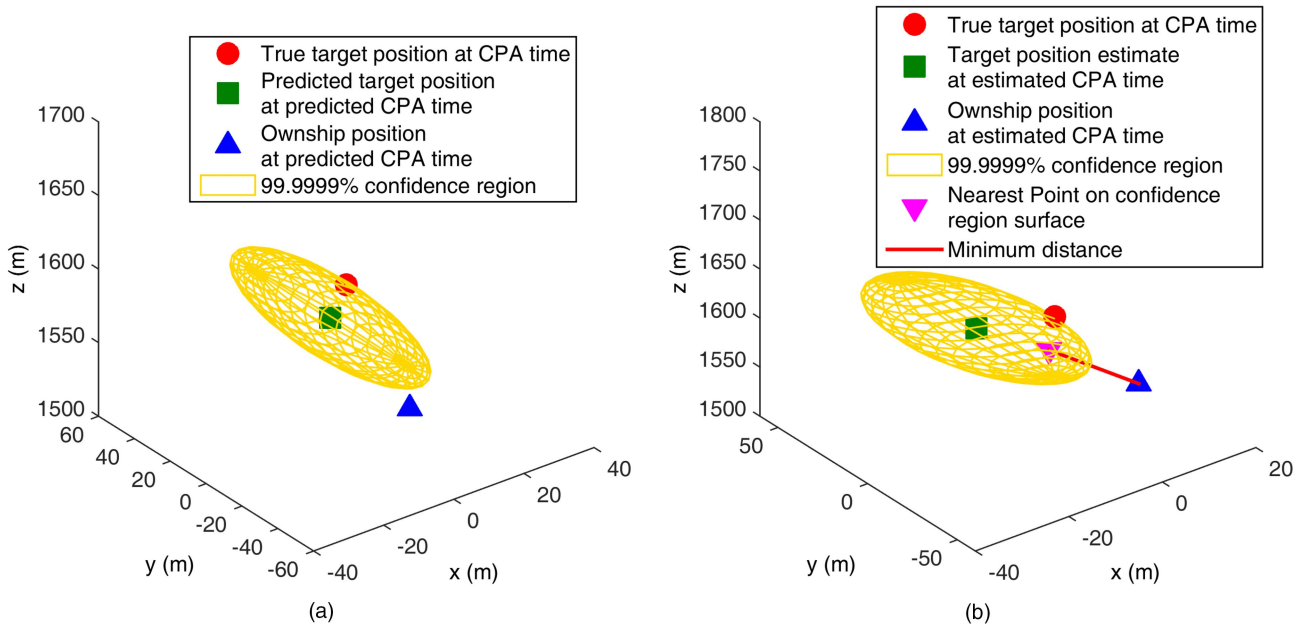


Fig. 7. Collision warning decisions in a single run in Scenario 6. Collision warning is “off” without a safety margin but is “on” with a safety margin of 100 m. (a) Without a safety margin. (b) With a safety margin of 100 m.

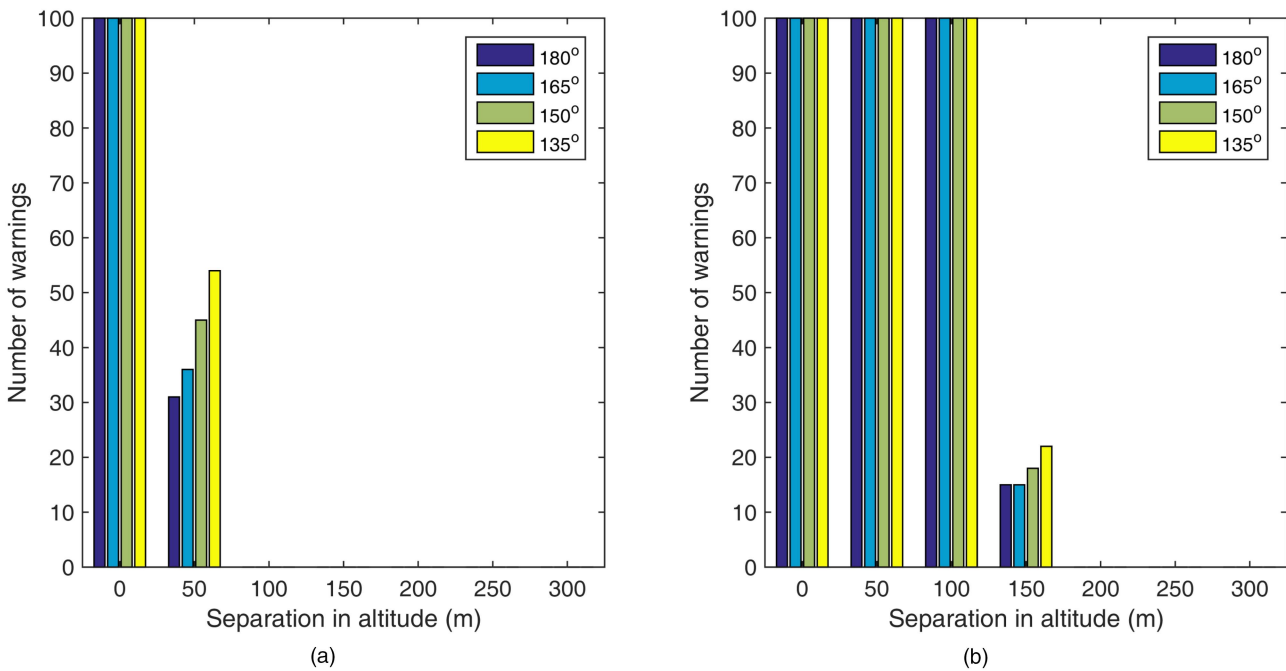


Fig. 8. The number of warnings in 100 runs using the 3-D likelihood based collision warning algorithm. (a) Without a safety margin. (b) With a safety margin of 100 m.

Figure 9(a) shows the histogram of the logarithm of the estimated probability of collision in 10,000 runs from scenarios with different CPA angles when there is a collision (the target and ownship altitude separation is 0 m). The estimated probability of collision has a similar distribution for different CPA angles, which is also observed at other levels of altitude separation. More than 95% of the time, the probability of collision is estimated to be larger than 10%. Since the probability of collision is always estimated to be larger than

0.0001%, there are no missed detections, which confirms the results shown in Figure 8(a). As the separation in altitude increases from 0 to 50 m, the estimated probability of collision gets much smaller as shown in Figure 9(b). Similar phenomena are also observed at other CPA angles. False alarms occur about 30% of the time when the estimated probability of collision is larger than 0.0001%. When the intruder and ownship altitude separation is beyond 100 m, the estimated probability is always less than  $10^{-16}$  and hence

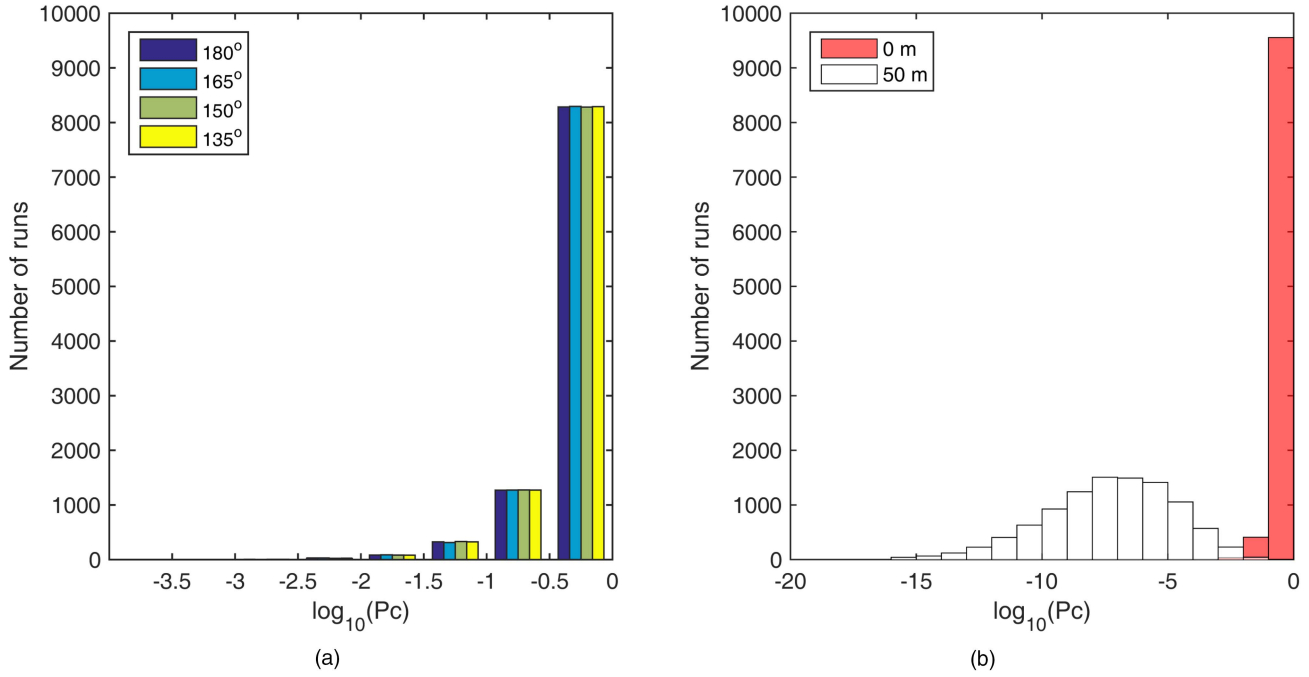


Fig. 9. The histogram of  $\log_{10}P_c$  in 10000 runs using the 3-D likelihood based collision warning algorithm. (a) Separation in altitude is 0 m. (b) CPA angle is  $180^\circ$ .

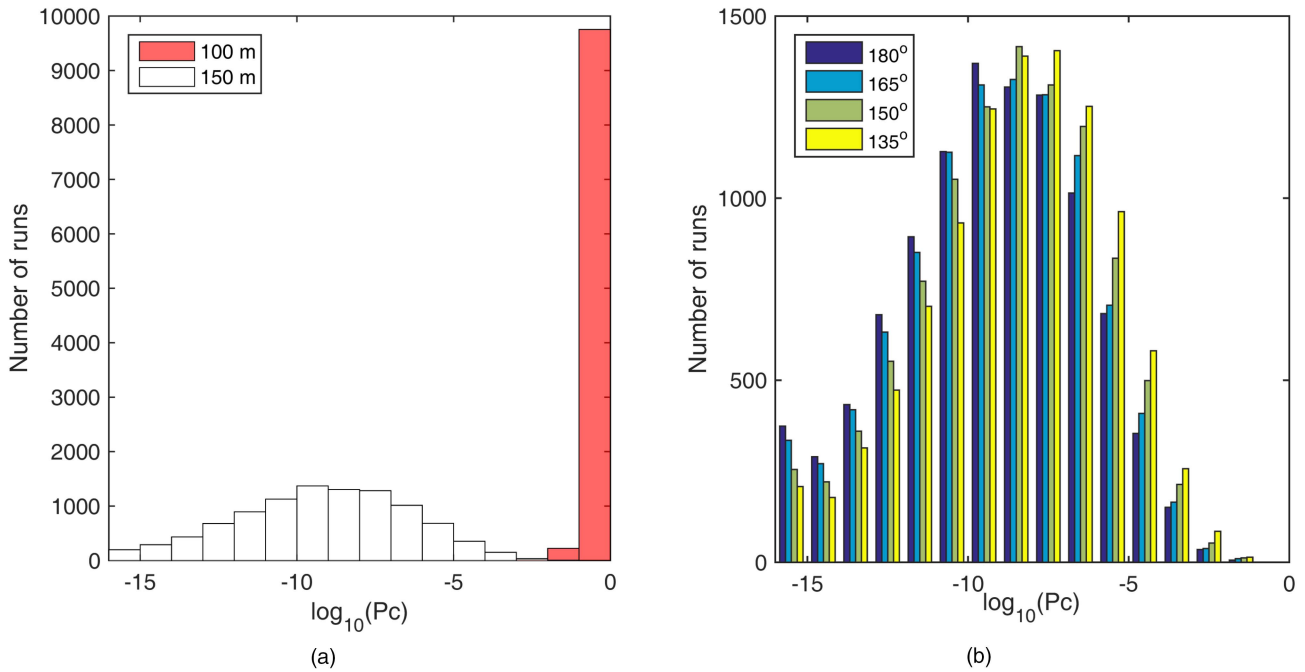


Fig. 10. The histogram of  $\log_{10}P_c$  in 10000 runs using the 3-D likelihood based collision warning algorithm with a safety margin of 100 m. (a) CPA angle is  $180^\circ$ . (b) Separation in altitude is 150 m.

the corresponding distributions are not shown in Figure 9(b).

With a safety margin of 100 m, from Figure 8(b), the 3-D likelihood based collision warning algorithm has no missed detections of a collision. However, it becomes more conservative and there are always false alarms when the intruder and ownship altitude separation is below 100 m, which is not surprising because of a safety

margin of same distance. The number of false alarms starts to decrease at 150 m altitude separation.

When the altitude separation is 0 or 50 m, it turns out that the estimated probability of collision is always 1 in 10,000 Monte Carlo runs. When the altitude separation is 100 m, the estimated probability of collision is not always unity: see Figure 10(a) for the distribution of its logarithm. When the separation is 150 m, the estimated

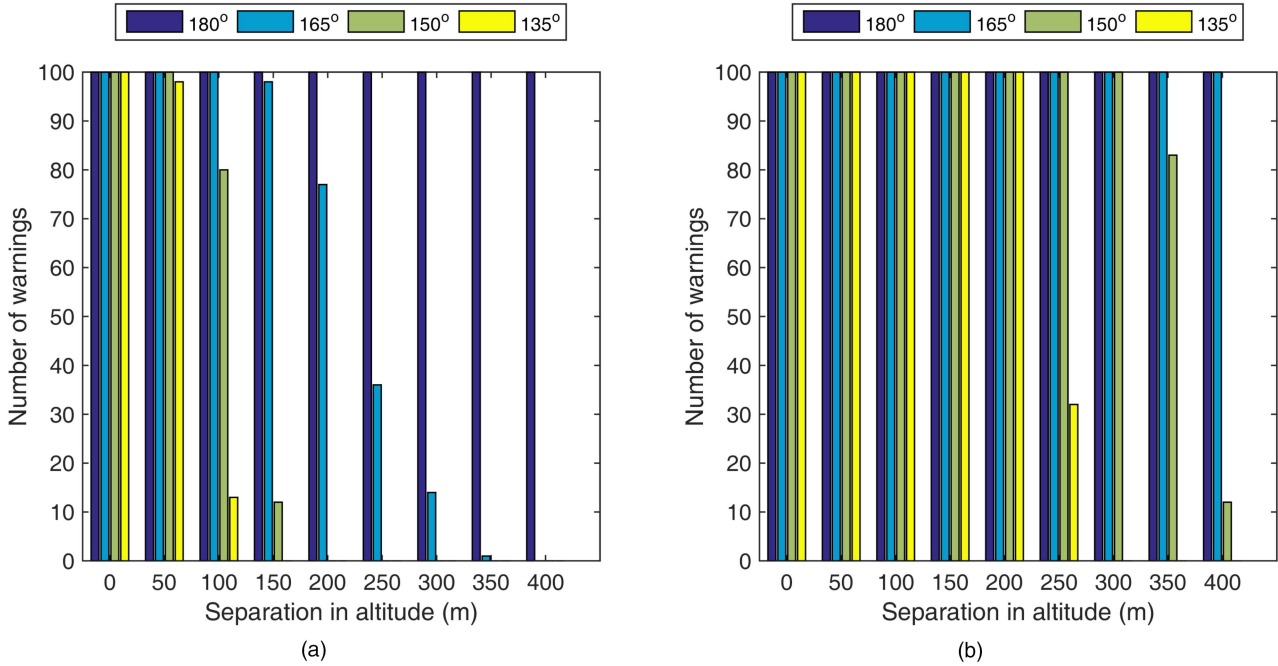


Fig. 11. The number of warnings in 100 runs using the 2-D likelihood based collision warning algorithm. (a) Without a safety margin. (b) With a safety margin of 100 m.

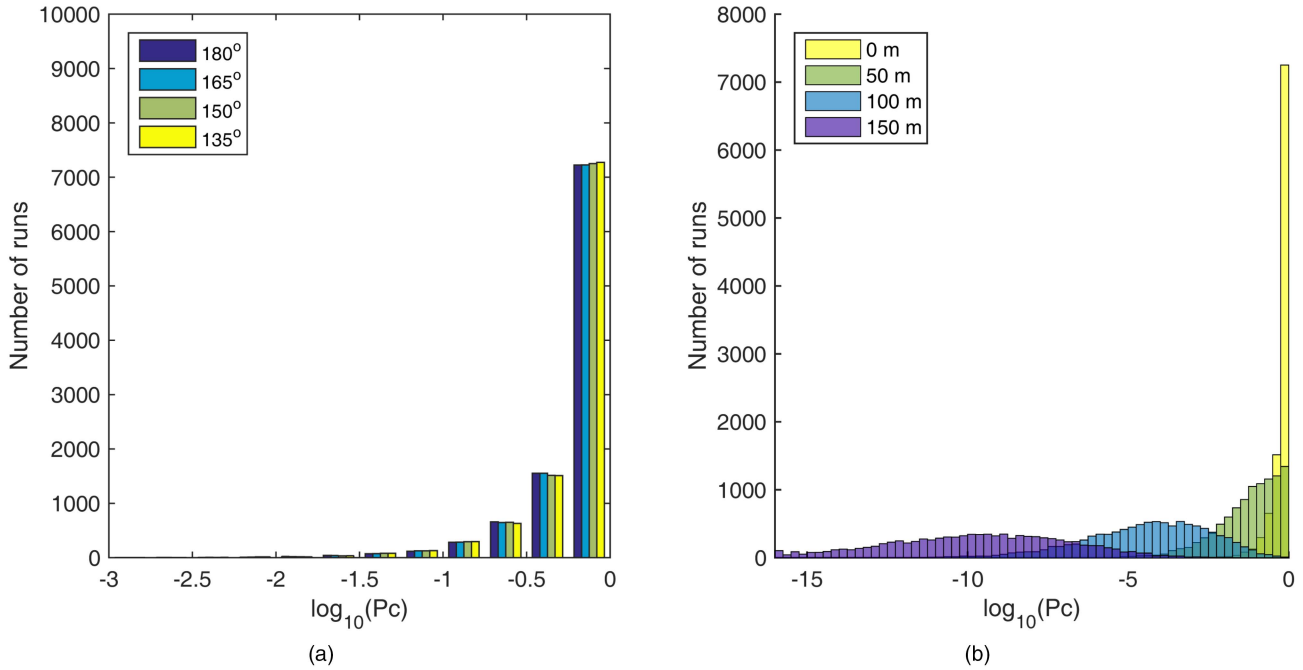


Fig. 12. The histogram of  $\log_{10} P_c$  in 10000 runs using the 2-D likelihood based collision warning algorithm. (a) Separation in altitude is 0 m. (b) CPA angle is 150°.

probability of collision becomes much smaller. The similar distributions are also observed at other CPA angles as illustrated in Figure 10(b). It is estimated to be less than 0.0001% for more than 90% of the time. When the intruder and ownship altitude separation is beyond 200 m, the estimated probability is always less than  $10^{-16}$ .

The performance of the 2-D likelihood based collision warning algorithm is evaluated in the same manner. Figure 11(a) shows that there are no missed detections of collisions in 100 runs, which is the same as in the 3-D scenarios. The estimated probability of collision is very close to 1 for most of the time in 10000 runs and its distribution is similar at different CPA angles as indi-

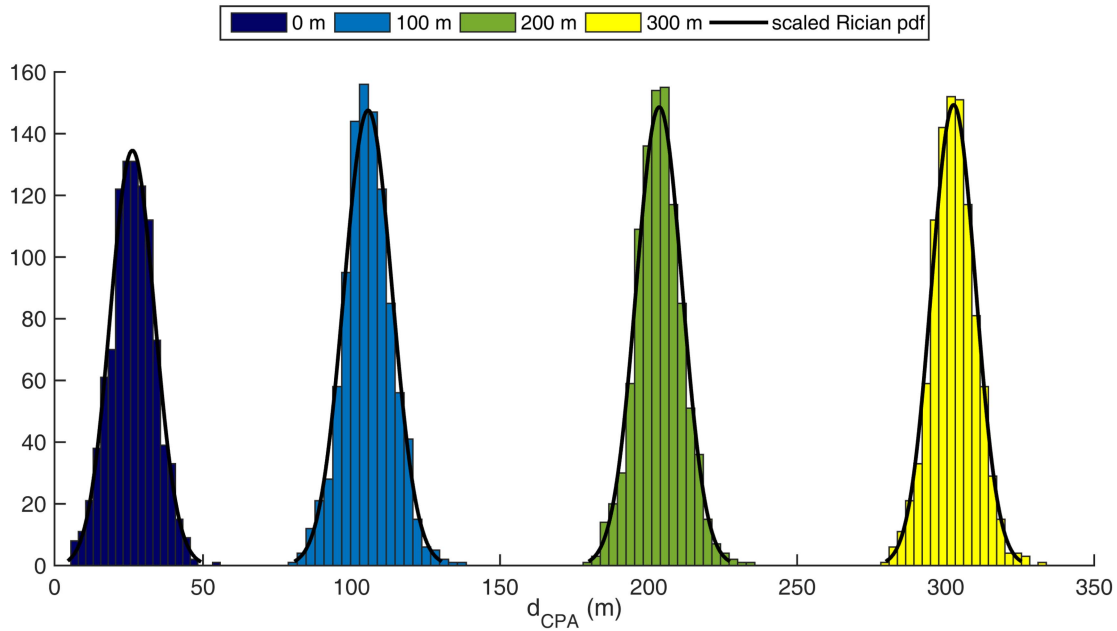


Fig. 13. The histograms of  $d_{CPA}$  with fitted Rician distributions when the CPA angle is  $180^\circ$ .

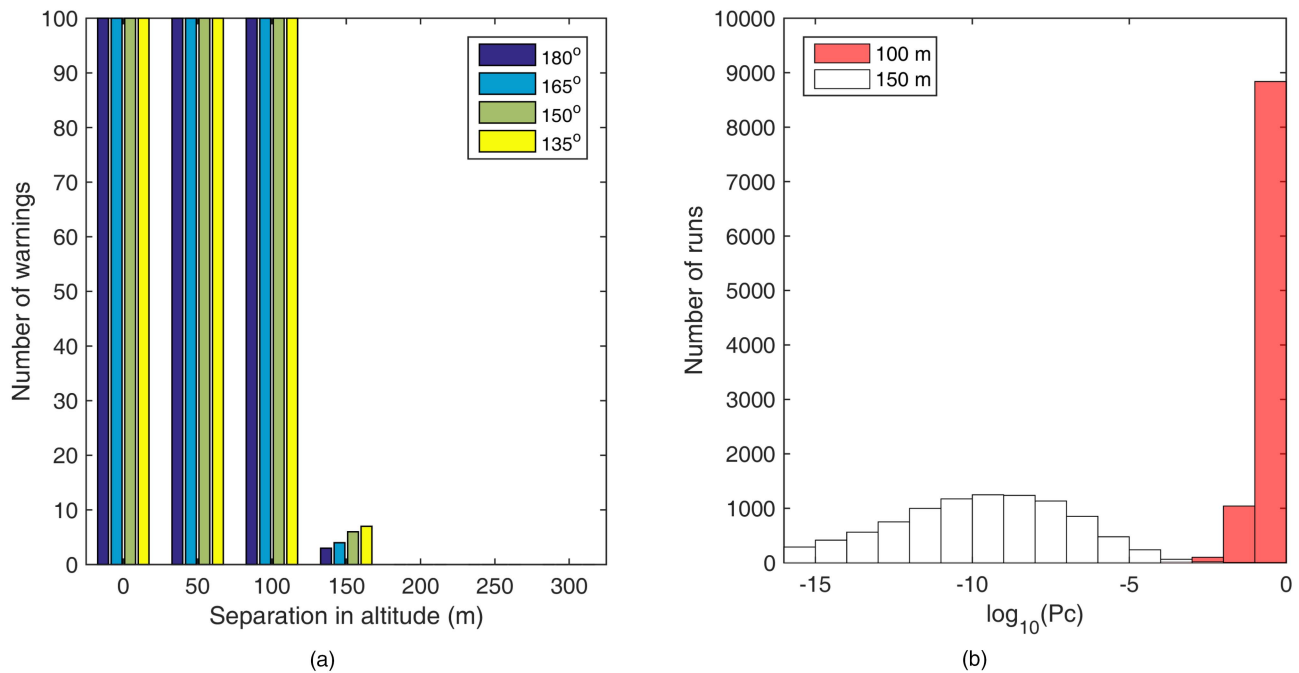


Fig. 14. Performance of the 3-D Bayesian collision warning algorithm with  $d_{min} = 100$  m. (a) Histogram of the number of warnings in 100 runs. (b) Histogram of  $\log_{10}P_c$  in 10000 runs with CPA angle  $180^\circ$ .

cated in Figure 12(a). The CPA angle has a pronounced effect on false alarms in the 2-D case. Recall that in the 2-D scenarios it is (conservatively) assumed that the intruder is at the same altitude as the ownship, which is not true when the altitude separation is not zero. When the CPA angle is close to  $180^\circ$ , the collision is very likely to occur based on the same altitude assumption, and, consequently, the false alarm rate is therefore very high. At other CPA angles, as the altitude separation increases, the number of false alarms decreases and the

estimated probability of collision becomes smaller as indicated in Figure 12(b).

With a safety margin of 100 m, there are no missed detections of collisions. However, there are more false alarms because of both the same altitude assumption and the safety margin.

Based on the above observations, we submit that 3-D estimation with at least 3 transmitters is the only one reliable configuration for collision warning and that 2-D estimation with 2 transmitters is prone to false alarms

when the CPA angle is  $180^\circ$  even if there is more than 400 m altitude separation.

#### 6.4. Collision Warning Based on the Bayesian Approach

The one-sample Kolmogorov-Smirnov test fails to reject the hypothesis that 1000 samples of  $d_{CPA}$  comes from a Rician distribution with parameters that are ML estimates based on the same 1000 samples in all 100 Monte Carlo runs in each of the 3-D scenarios that are used to evaluate the likelihood based collision warning algorithm in previous subsection. The fitted Rician distributions with the corresponding histograms of  $d_{CPA}$  at different levels of altitude separations at  $180^\circ$  CPA angle are shown in Figure 13. As shown in the previous subsection, 2-D collision warning with 2 transmitters under the same altitude assumption is unreliable because it is prone to false alarm, therefore the Bayesian approach is considered only in the multistatic configuration with 3 transmitters in this paper. It turned out that the hypothesis that the pdf of  $d_{CPA}$  is Rician is no longer valid in the 2D scenarios when the same altitude assumption does not hold. Nevertheless, it is possible to estimate the probability of collision by fitting a kernel distribution instead of a Rician distribution in those 2-D scenarios.

The performance of 3-D Bayesian collision warning algorithm with  $d_{min} = 100$  m is shown in Figure 14, which is very similar to that of 3-D likelihood based collision warning algorithm with a safety margin 100 m. There are no missed detections of a collision but there are always false alarms when the intruder and ownship altitude separation is below 100 m. The number of false alarms starts to decrease at 150 m altitude separation and becomes zero when the altitude separation is beyond 200 m.

Comparing Figure 14(b) and 10(a), the estimated probability of collision from the 3-D Bayesian algorithm has a similar distribution to that from the 3-D likelihood based algorithm. As the altitude separation increases, the estimated probability of collision is getting smaller. When the altitude separation is 0 or 50 m, it turns out the estimated probability of collision is always 1 in 10,000 Monte Carlo runs. When the intruder and ownship altitude separation is beyond 200 m, the estimated probability is always less than  $10^{-16}$ .

## 7. CONCLUSIONS

The ability to sense and avoid non-cooperative targets is essential for UAS to perform routine tasks when they are not alone in the airspace. We investigated several configurations with bistatic range and range rate measurements for collision warning. It turned out that a multistatic configuration is needed to provide good observability of the target, which is useful for collision warning. The minimum number of the transmitters required is three in a 3-D scenario and two in a 2-D scenario. We also implemented an ML estimator in both

types of scenarios using the ILS technique and showed that the estimator can be considered as statistically efficient through Monte Carlo simulations for the scenarios considered. Based on the ML estimator, the collision warning was approached in two different ways. The first method is formulating the collision as a hypothesis testing problem using a generalized likelihood function, where the efficiency of the CPA time is also verified. The second method is a Bayesian formulation focusing on the time of CPA modeled as a random variable. Only the multistatic configuration with three transmitters is reliable for collision warning because the multistatic configuration with two transmitters based on the same target and ownship altitude assumption turns out to be prone to false alarms. When the minimum distance in the Bayesian approach is the same as the safety margin in the likelihood based approach, both algorithms yield very similar collision warning performance.

## ACKNOWLEDGEMENT

Stimulating discussions with Melissa Meyer and Robert Coury are gratefully acknowledged. This work is supported by ARO W991NF-10-1-0369.

## REFERENCES

- [1] B. M. Albaker, and N. A. Rahim  
A survey of collision avoidance approaches for unmanned aerial vehicles.  
In *International Conference for Technical Postgraduates*, Dec. 2009.
- [2] Y. Bar-Shalom, X.-R. Li, and T. Kirubarajan  
*Estimation with Applications to Tracking and Navigation: Theory, Algorithms and Software*.  
New York: Wiley, 2001.
- [3] Y. Bar-Shalom, P. K. Willett, and X. Tian  
*Tracking and Data Fusion: A Handbook of Algorithms*.  
Storrs, CT: YBS Publishing, 2011.
- [4] S. S. Blackman, and R. Popoli  
*Design and Analysis of Modern Tracking Systems*.  
Artech House, 1999.
- [5] C. Carbone, U. Ciniglio, F. Corrado, and S. Luongo  
A novel 3D geometric algorithm for aircraft autonomous collision avoidance.  
In *Proceedings of 45th IEEE Conference on Decision and Control*, Dec. 2006, 1580–1585.
- [6] B. K. Chalise, Y. D. Zhang, M. G. Amin, and B. Himed  
Target localization in a multi-static passive radar system through convex optimization.  
*Signal Processing*, 102, 0 (2014), 207–215.
- [7] W. Dou, P. K. Willett, and Y. Bar-Shalom  
Fusion of range-only measurements from multistatic configurations for air collision warning.  
In *Proceedings of IEEE Aerospace Conference*, March 2015.
- [8] W. Dou, P. K. Willett, and Y. Bar-Shalom  
Configuration selection for fusion of measurements from multistatic radars for air collision warning.  
In *Proceedings of 18th International Conference on Information Fusion*, July 2015.
- [9] Y. K. Kwag, and C. H. Chung  
UAV based collision avoidance radar sensor.  
In *IEEE International Geoscience and Remote Sensing Symposium*, July 2007, 639–642.

- [10] M. Malanowski, and K. Kulpa  
Two methods for target localization in multistatic passive radar.  
*IEEE Transactions on Aerospace and Electronic Systems*, 48, 1 (Jan. 2012), 572–580.
- [11] R. W. Osborne, III and Y. Bar-Shalom  
Statistical efficiency of composite position measurements from passive sensors.  
*IEEE Transactions on Aerospace and Electronic Systems*, 49, 4 (Oct. 2013), 2799–2806.
- [12] J. Sijbers, A. J. den Dekker, P. Scheunders, D. Van Dyck  
Maximum-likelihood estimation of Rician distribution parameters.  
*IEEE Transactions on Medical Imaging*, 17, 3 (June 1998), 357–361.
- [13] D. Sislak, M. Rehak, M. Pechoucek, D. Pavilicek and M. Uller  
Negotiation-based approach to unmanned aerial vehicles.  
In *IEEE 2006 Workshop on Distributed Intelligent Systems*, June 2006, 279–284.
- [14] M. Švecová, D. Kocur, R. Zetik, and J. Rovňáková,  
Target localization by a multistatic UWB radar.  
In *Proceedings of 20th International Conference Radioelektronika*, April 2010.
- [15] C. J. Tomlin, J. Lygeros, and S. S. Sastry  
A game theoretic approach to controller design for hybrid systems.  
*Proceedings of the IEEE*, 88, 7 (July 2000), 949–970.
- [16] H. L. Van Trees, K. L. Bell, and Z. Tian  
*Detection Estimation and Modulation Theory, 2nd Edition, Part I, Detection, Estimation, and Filtering Theory*.  
New York: Wiley, 2013.
- [17] J.-H. Wen, J.-S. Li, C.-Y. Yang, C.-H. Chen, and H.-C. Chen  
Localization scheme of multistatic radars system based on the information of measured signal.  
In *Proceedings of 9th International Conference on Broadband and Wireless Computing, Communication and Applications*, Nov. 2014, 462–466.
- [18] P. R. Williams  
Aircraft collision avoidance using statistical decision theory.  
In *Proceedings of SPIE 1694, Sensors and Sensor Systems for Guidance and Navigation II*, July 1992.



**Wenbo Dou** is a graduate student in the Department of Electrical and Computer Engineering at the University of Connecticut. He received the Bachelor of Engineering in Electrical and Electronic Engineering with First Class Honors from Nanyang Technological University in 2011. His current research interests are bias estimation, acoustic signal based multi-target localization and tracking, data fusion and machine learning.

**Yaakov Bar-Shalom** was born on May 11, 1941. He received the B.S. and M.S. degrees from the Technion, Israel Institute of Technology, in 1963 and 1967 and the Ph.D. degree from Princeton University in 1970, all in electrical engineering. From 1970 to 1976 he was with Systems Control, Inc., Palo Alto, California. Currently he is Board of Trustees Distinguished Professor in the Dept. of Electrical and Computer Engineering and Marianne E. Klewin Professor in Engineering at the University of Connecticut. He is also Director of the ESP (Estimation and Signal Processing) Lab. His current research interests are in estimation theory, target tracking and data fusion. He has published over 500 papers and book chapters in these areas and in stochastic adaptive control. He coauthored the monograph *Tracking and Data Association* (Academic Press, 1988), the graduate texts *Estimation and Tracking: Principles, Techniques and Software* (Artech House, 1993; translated into Russian, MG TU Bauman, Moscow, Russia, 2011), *Estimation with Applications to Tracking and Navigation: Algorithms and Software for Information Extraction* (Wiley, 2001), the advanced graduate texts *Multitarget-Multisensor Tracking: Principles and Techniques* (YBS Publishing, 1995), *Tracking and Data Fusion* (YBS Publishing, 2011), and edited the books *Multitarget-Multisensor Tracking: Applications and Advances* (Artech House, Vol. I, 1990; Vol. II, 1992; Vol. III, 2000). He has been elected Fellow of IEEE for “contributions to the theory of stochastic systems and of multi-target tracking.” He has been consulting to numerous companies and government agencies, and originated the series of Multitarget-Multisensor Tracking short courses offered via UCLA Extension, at Government Laboratories, private companies and overseas. During 1976 and 1977 he served as Associate Editor of the *IEEE Transactions on Automatic Control* and from 1978 to 1981 as Associate Editor of *Automatica*. He was Program Chairman of the 1982 American Control Conference, General Chairman of the 1985 ACC, and Co-Chairman of the 1989 IEEE International Conference on Control and Applications. During 1983–87 he served as Chairman of the Conference Activities Board of the IEEE Control Systems Society and during 1987–89 was a member of the Board of Governors of the IEEE CSS. He was a member of the Board of Directors of the International Society of Information Fusion (1999–2004) and served as General Chairman of FUSION 2000, President of ISIF in 2000 and 2002 and Vice President for Publications in 2004–13. In 1987 he received the IEEE CSS Distinguished Member Award. Since 1995 he is a Distinguished Lecturer of the IEEE AESS and has given numerous keynote addresses at major national and international conferences. He is co-recipient of the M. Barry Carlton Award for the best paper in the *IEEE Transactions on Aerospace and Electronic Systems* in 1995 and 2000 and recipient of the 1998 University of Connecticut AAUP Excellence Award for Research. In 2002 he received the J. Mignona Data Fusion Award from the DoD JDL Data Fusion Group. He is a member of the Connecticut Academy of Science and Engineering. In 2008 he was awarded the IEEE Dennis J. Picard Medal for Radar Technologies and Applications, and in 2012 the Connecticut Medal of Technology. He has been listed by academic.research.microsoft (top authors in engineering) as #1 among the researchers in Aerospace Engineering based on the citations of his work.





**Peter Willett** has been a faculty member in the Electrical and Computer Engineering Department at the University of Connecticut since 1986. Since 1998 he has been a Professor, and since 2003 an IEEE Fellow. His primary areas of research have been statistical signal processing, detection, machine learning, communications, data fusion, and tracking. He is editor-in-chief of *IEEE Signal Processing Letters*, 2014–2016. He was editor-in-chief for *IEEE Transactions on Aerospace and Electronic Systems* from 2006–2011, and AESS Vice President for Publications 2012–2014. He was associate editor for *IEEE Transactions on Aerospace and Electronic Systems* (for Data Fusion and Target Tracking), ISIF's *Journal of Advances in Information Fusion* and *IEEE Transactions on Systems, Man, and Cybernetics* (A and B). He is remains associate editor-in-chief for the IEEE AES Magazine. He is a member of the IEEE AESS Board of Governors and of the IEEE Signal Processing Society's Sensor-Array and Multichannel (SAM) technical committee (and is now Chair).

# Early Fusion and Query Modification in Their Dual Late Fusion Forms

LESZEK KALICIAK  
HANS MYRHAUG  
AYSE GOKER  
DAWEI SONG

**In this paper, we prove that specific widely used models in Content-based Image Retrieval for information fusion are interchangeable. In addition, we show that even advanced, non-standard fusion strategies can be represented in dual forms. These models are often classified as representing early or late fusion strategies. We also prove that the standard Rocchio algorithm with specific similarity measurements can be represented in a late fusion form.**

Manuscript received December 4, 2014; revised February 25, 2015 and May 11, 2015; released for publication May 13, 2015.

Refereeing of this contribution was handled by Alexander Toet.

Authors' addresses: L. Kaliciak, H. Myrhaug, and A. Goker, AmbieSense Ltd, 7 Queens Gardens, Aberdeen, AB15 4YD, UK, (e-mail: {leszek, hans, ayse}@ambiesense.com). D. Song, Tianjin University, The Open University, Walton Hall, Milton Keynes, Buckinghamshire, MK7 6AA, UK, (e-mail: dawei.song@open.ac.uk).

1557-6418/15/\$17.00 © 2015 JAIF

## I. INTRODUCTION

Fusion strategies<sup>1</sup> play an important role in many areas of research, including text Information Retrieval (IR), Content-based Image Retrieval (CBIR), Computer Vision, Geospatial Information Systems, Business Intelligence, Bioinformatics—to name a few. In CBIR and Computer Vision, the most widely used fusion schemes are early and late fusion strategies. They are important because they allow us to combine various notions of visual information, textual information, etc. at the representation level or system decision level.

In general, Content-based Image Retrieval is usually based on the Vector Space Model. It represents information objects as multidimensional vectors. A user query is also represented as a vector which can be an image (referred to as visual example) or text. It often contains two types of information—visual and textual. When the user submits his/her query, the similarity measurement is applied to compute the relevance scores denoting the similarities between the query and images in the data collection. The images are then ranked according to the relevance scores and the top  $n$  images are presented to the user.

Based on the experimental results, researchers have hinted at the potential interchangeability of specific fusion schemes [14]. In this paper, we mathematically prove that this interchangeability is directly related to the interaction between early fusion operators and similarity measurements. Thus, we validate the hypotheses (interchangeability of specific fusion approaches) that stem from experimental observations and show the equivalence of particular fusion models. In addition, we also derive equivalent, dual forms of the Rocchio query modification model.

This journal paper is an extension and a follow-up of our previous papers [9], [10]. Here, we enrich the original publication with specific non-standard early fusion strategies and show that even advanced models based on the early and late fusion strategies can be interchangeable. We also devote an entire section to proving that the standard Rocchio query modification model [20], [1], [34] has a dual form—which would differ with respect to the similarity measure. The late fusion analogues to the Rocchio algorithm had so far been considered as separate, different techniques [22], [12]. Section related to hybrid relevance feedback model is based on another conference publication [10].

The rest of this paper is organized as follows: Section 2 presents the background and related work on the early and late fusion schemes. Section 3 shows the relationships between various models representing different fusion strategies with examples. An interesting finding which presents dual late fusion forms of the standard Rocchio query modification model can be found in Section 4. Finally, conclusions and information on future work are provided in Section 5.

<sup>1</sup>In this paper, terms “fusion strategies,” “fusion schemes,” “fusion methods,” and “fusion techniques” will be used interchangeably.

## II. BACKGROUND AND RELATED WORK

Different features (i.e. various visual, textual) in CBIR represent complementary yet correlated aspects of the same multimedia objects. This, in turn, presents an opportunity to utilize this complementarity by combining the feature spaces in order to improve their performance. Fusion strategies are the main tools that can be used to accomplish the aforementioned task [5], [3]. Early fusion strategy combines the feature spaces at the representation level (fusion of representations) whereas late fusion strategy combines them at the decision level (fusion of relevance scores). Thus, for example, one can combine visual and textual features in the first round retrieval. It is also possible to combine them in the context of user relevance feedback [10], [8], [6]. Moreover, search by multiple visual examples also requires combination of features corresponding to these visual examples. Many current state-of-the-art CBIR systems combine various visual features (often local and global) to achieve the best performance (e.g. [17]).

The most widely used early fusion technique is concatenation of visual and textual representations. In fact, some researchers implicitly assume concatenation to be synonymous with an early fusion strategy. Other recently proposed models incorporate the tensor product to combine visual and textual systems [30]. The tensor product represents a useful fusion technique as it takes into account all the combinations of different features' dimensions. It has also other applications in IR, for example, to model semantic (verb-noun pairs) composition [31]. The main drawback of the early fusion approach is the well-known curse of dimensionality. Later in the paper we show that the curse of dimensionality can be avoided if the equivalent late fusion form is known.

In the case of the late fusion, the most widely used method is the arithmetic mean of the scores, their sum (referred to as CombSUM in the literature), or their weighted linear combination. One of the best performing systems on the ImageCLEF2007 data collection, XRCE [17], utilizes both early—concatenation of features and late—an average of relevance scores fusion strategies for comparison purposes. Another common combination method, referred to as CombPROD in the literature, is the squared geometric mean of the relevance scores—their product. It has been argued, that the major drawback of the late fusion approaches is their inability to capture the correlation between different modalities [18]. However, in the paper we show that in some cases the late fusion can be represented in the form of an early fusion.

Early and late fusion strategies can be also considered in the context of classification, e.g. image categorization [4]. In the case of classification, late fusion is performed differently, as a weighted voting strategy from the outputs of different classifiers [21], [24]. Some

fusion strategies in CBIR can be also classified as intermediate fusion [4]. They simultaneously learn individual classifier and combination classifier weights [33], and this process happen at various levels of learning. In this paper, however, our focus is on the similarity-based image retrieval.

Thus, in general, most literature on fusion strategies in Content-based Image Retrieval utilize either concatenation or a linear combination of relevance scores in their models (e.g. [29]). Others have used both for experimental comparison [27], [28] and conclude that both strategies generate similar results (slightly better performance of a late fusion) or are in favour of an early fusion strategy (e.g. [25]). All of them, however, treat these fusion strategies as separate, individual data combination approaches.

In this paper, we aim to prove that specific widely used standard and non-standard fusion models in CBIR are equivalent. All presented models are based on early and late fusion strategies, and represent counterexamples showing that these strategies should not always be considered as separate.

## III. RELATIONSHIPS BETWEEN FUSION STRATEGIES

The most widely used fusion models in Content-based Image Retrieval are based on the early and late fusion schemes. We are going to show, that specific combinations of similarity measures and individual scores (late fusion) can be represented as similarities computed on pre-tensored or pre-concatenated individual representations (early fusion), and vice versa.

Some of the best performing similarity measurements in information retrieval in general are: cosine similarity and metrics from the Minkowski family of distances (Euclidean, Manhattan, etc.). In particular, Euclidean distance is often utilized in visual search [11], while textual search often uses cosine similarity [35]. Moreover, late fusion is most often represented as a product of relevance scores, their sum, or their weighted linear combination [18], [29]. The early fusion, on the other hand, is usually represented by concatenation of feature spaces [31], [29].

Thus, in this section, we are going to investigate the interactions between these similarity measurements and early fusion operators. We are going to reveal the relationships between concatenation and tensor product with the following similarity measurements:

- inner product<sup>2</sup>
- cosine similarity
- weighted cosine similarity (can be used to change the importance of different feature spaces)
- Euclidean metric

We also investigate the interactions of the aforementioned early fusion operators with a combination

---

<sup>2</sup>In this paper, terms “inner product” and “dot product” will be used interchangeably.

of Euclidean distance and cosine similarity. That is because often cosine similarity performs best in text IR (Information Retrieval) while Euclidean distance gives the best performance in CBIR. Therefore, we may want to utilize different similarity measurements for different feature spaces. Interestingly, we can combine these different similarity measurements in such a way, that this combination will correspond to the feature fusion at the representation level. Further, we explore the interactions with the Minkowski family of distances, which encompasses a wide range of various metrics and similarity measurements. The discovered relationships are supported by examples.

For the clarity of the formulas, in this section we assume that the visual and textual features were normalized. This is not a necessary assumption as analogous relationships can be found for representations that were not normalized.

Table I presents the notation used in the paper.

A. Interactions of early fusion operators (concatenation, tensor product) with the dot product

1) We can start by making a few simple observations. Let us employ a standard inner product as the similarity measurement. Let  $d$  be a vector representation of a multimedia document. We can check that

$$\langle d_1^v \oplus d_1^t \mid d_2^v \oplus d_2^t \rangle = \langle d_1^v \mid d_2^v \rangle + \langle d_1^t \mid d_2^t \rangle \quad (1)$$

where  $\langle \cdot \mid \cdot \rangle$  denotes an inner product,  $\oplus$  is the direct product (concatenation of vectors) and  $d_i^v, d_i^t$  are the visual and textual image representations of the  $i$ th image, for example. We can assume that  $d_1^v, d_1^t$  denote the visual and textual query representations (query by visual example) and  $d_2^v, d_2^t$  denote the visual and textual representations of an image from the image collection. We would measure these similarities for all the images in the data collection and use the relevance scores to rank the images.

From the above equation we can see, that concatenation of vectors is equivalent to addition of measurements (scores) performed on individual feature spaces.

To clarify, concatenation ( $\oplus$ ) of two  $n$  and  $m$  dimensional vectors produces a new  $n + m$  dimensional vector, for example

$$(a, b) \oplus (c, d, e) = (a, b, c, d, e) \quad (2)$$

2) Tensor product ( $\otimes$ ) of two  $n$  and  $m$  dimensional vectors generates an  $n \cdot m$  dimensional vector or an  $n$  by  $m$  dimensional matrix. For example

$$(a, b) \otimes (c, d, e) = (ac, ad, ae, bc, bd, be) \quad (3)$$

or

$$(a, b) \otimes (c, d, e) = \begin{pmatrix} ac & ad & ae \\ bc & bd & be \end{pmatrix} \quad (4)$$

It has been shown that the tensor product can be useful when combining the representations as it takes

TABLE I  
Overview of the notation used in the paper.

Symbol	Meaning
$d_1^v, d_1^t$	Visual and textual vector representations of the query, respectively
$d_2^v, d_2^t$	Visual and textual vector representations of an arbitrary image from an image collection, respectively
$\oplus$	Vector concatenation (early fusion operator)
$\otimes$	Tensor product (early fusion operator)
$\langle \cdot \mid \cdot \rangle$	Similarity measurement—inner product (dot product), $s_{in}(\cdot, \cdot)$
$s_c(\cdot, \cdot)$	Similarity measurement—cosine similarity
$s_e(\cdot, \cdot)$	Similarity measurement—Euclidean metric
$s_b(\cdot, \cdot)$	Similarity measurement—Bhattacharya similarity
$s_p(\cdot, \cdot)$	Similarity measurements—Minkowski family of distances
$s_{in}(\cdot, \cdot)$	Similarity measurement—inner product (dot product)
$\  \cdot \ $	Vector norm
$Q_d$	an arbitrary document vector from the data collection
$Q_m$	modified query vector
$Q_o$	original query vector
$D_j$	related document vector
$D_k$	non-related document vector
$a$	original query weight
$b$	related documents' weights
$c$	non-related documents' weights
$D_r$	set of related documents
$D_{nr}$	set of non-related documents
$(\cdot)^T$	transpose operator
$A$	observable
$M$	density matrix
$\langle A \rangle = tr(MA)$	predicted mean value of the measurement
$P = p^T p$	projector onto a subspace
$Pr$	probability of the projection

into account all of the combinations of vectors' dimensions and gives good discrimination in terms of similarity measurements [13]. Assuming that the systems were prepared independently, we have

$$\langle d_1^v \otimes d_1^t \mid d_2^v \otimes d_2^t \rangle = \langle d_1^v \mid d_2^v \rangle \cdot \langle d_1^t \mid d_2^t \rangle \quad (5)$$

where  $\otimes$  denotes the tensor operator.

From the above equation it turns out that the inner product of the tensor products is a product of the measurements (scores) performed on individual feature spaces. One of the implications of this observation is that there is no need for performing the tensor operation.

B. Interactions of early fusion operators (concatenation, tensor product) with the cosine similarity

One of the best performing similarity measures in text IR is the cosine similarity ( $s_c$ )

$$s_c(d_1, d_2) = \frac{\langle d_1 \mid d_2 \rangle}{\|d_1\| \cdot \|d_2\|} \quad (6)$$

The following equations hold

$$\begin{aligned}
\|d_1^v \otimes d_1^t\| &= \\
&= \sqrt{\langle d_1^v \otimes d_1^t | d_1^v \otimes d_1^t \rangle} = \\
&= \sqrt{\langle d_1^v | d_1^v \rangle \cdot \langle d_1^t | d_1^t \rangle} = \\
&= \|d_1^v\| \cdot \|d_1^t\| = \\
&= 1 = \|d_2^v \otimes d_2^t\| \tag{7}
\end{aligned}$$

and

$$\begin{aligned}
\|d_1^v \oplus d_1^t\| &= \\
&= \sqrt{\langle d_1^v \oplus d_1^t | d_1^v \oplus d_1^t \rangle} = \\
&= \sqrt{\langle d_1^v | d_1^v \rangle + \langle d_1^t | d_1^t \rangle} = \\
&= \sqrt{\|d_1^v\|^2 + \|d_1^t\|^2} = \\
&= \sqrt{2} = \|d_2^v \oplus d_2^t\| \tag{8}
\end{aligned}$$

Therefore, we get

$$s_c(d_1^v \otimes d_1^t, d_2^v \otimes d_2^t) = s_c(d_1^v, d_2^v) \cdot s_c(d_1^t, d_2^t) \tag{9}$$

$$s_c(d_1^v \oplus d_1^t, d_2^v \oplus d_2^t) = \frac{1}{2}(s_c(d_1^v, d_2^v) + s_c(d_1^t, d_2^t)) \tag{10}$$

Here, the square root of the similarity between the tensored representations is the geometric mean of the scores computed independently and the similarity between the concatenated representations is the arithmetic mean of individual scores.

Let us assume, that a model incorporates cosine similarity as a measurement used in combining the sub-systems (i.e. visual features or visual and textual features). Then, the concatenation or tensor operation produces the same effect as incorporation of the CombSUM or CombPROD late fusion methods, respectively.

C. Interactions of an early fusion operator (concatenation) with the weighted cosine similarity

If we utilize weighted combinations (with  $r_1, r_2$  denoting the weights, the importance of visual and textual representations, for example), then we get<sup>3</sup>

$$\begin{aligned}
s_c(r_1 d_1^v \oplus r_2 d_1^t, r_1 d_2^v \oplus r_2 d_2^t) &= \\
&= \frac{1}{r_1^2 + r_2^2} (r_1^2 s_c(d_1^v, d_2^v) + r_2^2 s_c(d_1^t, d_2^t)) \tag{11}
\end{aligned}$$

<sup>3</sup>Similar observations can be made for other similarity measurements. Here, we only present the weighted combinations for the cosine similarity.

PROOF Because

$$\begin{aligned}
\|(r_1 d^v) \oplus (r_2 d^t)\| &= \\
&= \sqrt{\langle (r_1 d^v) \oplus (r_2 d^t) | (r_1 d^v) \oplus (r_2 d^t) \rangle} = \\
&= \sqrt{\langle r_1 d^v | r_1 d^v \rangle + \langle r_2 d^t | r_2 d^t \rangle} = \\
&= \sqrt{r_1^2 \langle d^v | d^v \rangle + r_2^2 \langle d^t | d^t \rangle} = \\
&= \sqrt{r_1^2 \|d^v\|^2 + r_2^2 \|d^t\|^2} = \\
&= \sqrt{r_1^2 + r_2^2}
\end{aligned}$$

we get

$$\begin{aligned}
s_c(r_1 d_1^v \oplus r_2 d_1^t, r_1 d_2^v \oplus r_2 d_2^t) &= \\
&= \frac{\langle r_1 d_1^v \oplus r_2 d_1^t | r_1 d_2^v \oplus r_2 d_2^t \rangle}{r_1^2 + r_2^2} = \\
&= \frac{\langle r_1 d_1^v | r_1 d_2^v \rangle + \langle r_2 d_1^t | r_2 d_2^t \rangle}{r_1^2 + r_2^2} = \\
&= \frac{1}{r_1^2 + r_2^2} \left( r_1^2 \frac{\langle d_1^v | d_2^v \rangle}{\|d_1^v\| \|d_2^v\|} + r_2^2 \frac{\langle d_1^t | d_2^t \rangle}{\|d_1^t\| \|d_2^t\|} \right) = \\
&= \frac{1}{r_1^2 + r_2^2} (r_1^2 s_c(d_1^v, d_2^v) + r_2^2 s_c(d_1^t, d_2^t))
\end{aligned}$$

D. Interactions of early fusion operators (concatenation, tensor product) with the Euclidean metric

We can also find the relationships for Euclidean metric

$$s_e(d_1, d_2) = \sqrt{\langle d_1 - d_2 | d_1 - d_2 \rangle}. \tag{12}$$

Thus

$$s_e(d_1^v \oplus d_1^t, d_2^v \oplus d_2^t) = \sqrt{s_e^2(d_1^v, d_2^v) + s_e^2(d_1^t, d_2^t)} \tag{13}$$

and

$$\begin{aligned}
s_e(d_1^v \otimes d_1^t, d_2^v \otimes d_2^t) &= \\
&= \sqrt{s_e^2(d_1^v, d_2^v) + s_e^2(d_1^t, d_2^t) - \frac{1}{2}s_e^2(d_1^v, d_2^v)s_e^2(d_1^t, d_2^t)} \tag{14}
\end{aligned}$$

PROOF (1) From the fact that

$$s_e(d_1, d_2) = \sqrt{\|d_1\|^2 + \|d_2\|^2 - 2\langle d_1 | d_2 \rangle}$$

and

$$\|d_1 \oplus d_2\| = \sqrt{2}$$

we can show that

$$\begin{aligned}
s_e(d_1^v \oplus d_1^t, d_2^v \oplus d_2^t) &= \\
&= \sqrt{\|d_1^v \oplus d_1^t\|^2 + \|d_2^v \oplus d_2^t\|^2 - 2\langle d_1^v \oplus d_1^t | d_2^v \oplus d_2^t \rangle} = \\
&= \sqrt{4 - 2(\langle d_1^v | d_2^v \rangle + \langle d_1^t | d_2^t \rangle)} = \\
&= \sqrt{2 - 2\langle d_1^v | d_2^v \rangle + 2 - 2\langle d_1^t | d_2^t \rangle} = \\
&= \sqrt{s_e^2(d_1^v, d_2^v) + s_e^2(d_1^t, d_2^t)}
\end{aligned}$$

(2) Notice that

$$\begin{aligned}
s_e^2(d_1^v, d_2^v) \cdot s_e^2(d_1^t, d_2^t) &= \\
&= (2 - 2\langle d_1^v | d_2^v \rangle) \cdot (2 - 2\langle d_1^t | d_2^t \rangle) = \\
&= 2(2 - 2\langle d_1^v | d_2^v \rangle) + \\
&\quad + 2(2 - 2\langle d_1^t | d_2^t \rangle) - 2(2 - 2\langle d_1^v | d_2^v \rangle \langle d_1^t | d_2^t \rangle) = \\
&= 2s_e^2(d_1^v, d_2^v) + 2s_e^2(d_1^t, d_2^t) - 2s_e^2(d_1^v \otimes d_1^t, d_2^v \otimes d_2^t)
\end{aligned}$$

E. Interactions of early fusion operators (concatenation, tensor product) with the Bhattacharya similarity

Similarly, for the Bhattacharya similarity

$$s_b(d_1, d_2) = -\ln \left( \sum_i \sqrt{(d_1)_i \cdot (d_2)_i} \right) \quad (15)$$

we get

$$s_b(d_1^v \otimes d_1^t, d_2^v \otimes d_2^t) = s_b(d_1^v, d_2^v) + s_b(d_1^t, d_2^t) \quad (16)$$

and

$$\begin{aligned}
s_b(d_1^v \oplus d_1^t, d_2^v \oplus d_2^t) &= \\
&= -\ln(e^{-s_b(d_1^v, d_2^v)} + e^{-s_b(d_1^t, d_2^t)}) \quad (17)
\end{aligned}$$

PROOF Let us denote

$$\sqrt{d} = \left( \sqrt{d_1}, \sqrt{d_2}, \dots, \sqrt{d_n} \right)$$

Then

$$\begin{aligned}
s_b(d_1^v \otimes d_1^t, d_2^v \otimes d_2^t) &= \\
&= -\ln \left( \sum_k \sqrt{(d_1^v \otimes d_1^t)_k \cdot (d_2^v \otimes d_2^t)_k} \right) = \\
&= -\ln \left( \left\langle \sqrt{d_1^v \otimes d_1^t} \mid \sqrt{d_2^v \otimes d_2^t} \right\rangle \right) = \\
&= -\ln \left( \left\langle \sqrt{d_1^v} \otimes \sqrt{d_1^t} \mid \sqrt{d_2^v} \otimes \sqrt{d_2^t} \right\rangle \right) = \\
&= -\ln \left( \left\langle \sqrt{d_1^v} \mid \sqrt{d_2^v} \right\rangle \cdot \left\langle \sqrt{d_1^t} \mid \sqrt{d_2^t} \right\rangle \right) = \\
&= - \left( \ln \left\langle \sqrt{d_1^v} \mid \sqrt{d_2^v} \right\rangle + \ln \left\langle \sqrt{d_1^t} \mid \sqrt{d_2^t} \right\rangle \right) = \\
&= - \left( \ln \sum_i \sqrt{(d_1^v)_i \cdot (d_2^v)_i} + \ln \sum_j \sqrt{(d_1^t)_j \cdot (d_2^t)_j} \right) = \\
&= s_b(d_1^v, d_2^v) + s_b(d_1^t, d_2^t)
\end{aligned}$$

For the concatenation, we have

$$\begin{aligned}
s_b(d_1^v \oplus d_1^t, d_2^v \oplus d_2^t) &= \\
&= -\ln \left( \sum_k \sqrt{(d_1^v \oplus d_1^t)_k \cdot (d_2^v \oplus d_2^t)_k} \right) = \\
&= -\ln \left( \left\langle \sqrt{d_1^v \oplus d_1^t} \mid \sqrt{d_2^v \oplus d_2^t} \right\rangle \right) = \\
&= -\ln \left( \left\langle \sqrt{d_1^v} \oplus \sqrt{d_1^t} \mid \sqrt{d_2^v} \oplus \sqrt{d_2^t} \right\rangle \right) = \\
&= -\ln \left( \left\langle \sqrt{d_1^v} \mid \sqrt{d_2^v} \right\rangle + \left\langle \sqrt{d_1^t} \mid \sqrt{d_2^t} \right\rangle \right) = \\
&= -\ln \left( e^{\ln \langle \sqrt{d_1^v} \mid \sqrt{d_2^v} \rangle} + e^{\ln \langle \sqrt{d_1^t} \mid \sqrt{d_2^t} \rangle} \right) = \\
&= -\ln(e^{-s_b(d_1^v, d_2^v)} + e^{-s_b(d_1^t, d_2^t)})
\end{aligned}$$

F. Interactions of early fusion operators (concatenation, tensor product) with the Euclidean Metric. Interpretation of non-linear combinations of cosine similarity and Euclidean distance

Sometimes it might be beneficial to utilize different similarity measures for different feature spaces [7] (i.e. Euclidean metric for visual features and cosine similarity for textual space). Interestingly, we can fuse the scores in such a way, that their combination would correspond to (for example) measuring the Euclidean distance between the concatenated or tensored representations

$$\begin{aligned}
s_e(d_1^v \oplus d_1^t, d_2^v \oplus d_2^t) &= \\
&= \sqrt{s_e^2(d_1^v, d_2^v) - 2s_c(d_1^t, d_2^t) + 2} \quad (18)
\end{aligned}$$

$$\begin{aligned}
s_e(d_1^v \otimes d_1^t, d_2^v \otimes d_2^t) &= \\
&= \sqrt{s_e^2(d_1^v, d_2^v)s_e^2(d_1^t, d_2^t) - 2s_c(d_1^t, d_2^t) + 2} \quad (19)
\end{aligned}$$

PROOF Stems from the fact that

$$\begin{aligned}
s_e^2(d_1^t, d_2^t) &= \\
&= 2 - 2\langle d_1^t | d_2^t \rangle = \\
&= 2 - 2 \frac{\langle d_1^t | d_2^t \rangle}{\|d_1^t\| \|d_2^t\|} = \\
&= 2 - 2s_c(d_1^t, d_2^t)
\end{aligned}$$

and (5), (13).

G. Interactions of early fusion operators (concatenation, tensor product) with the Minkowski Family of Distances

Minkowski family of distances include widely utilized Manhattan and Euclidean metrics. Manhattan distance, for example, was utilized in [15] to query the CBIR system by multiple visual examples. In this aforementioned paper, individual scores corresponding to visual examples were aggregated. It is interesting to know,

that if one concatenated the representations corresponding to visual examples and utilized Manhattan metric, then the influence of these fusion methods on the retrieval performance would be exactly the same.

Minkowski family of distances is represented by the formula

$$s_p(d_1, d_2) = \left( \sum_{i=1}^n |d_1^i - d_2^i|^p \right)^{1/p} \quad (20)$$

where  $p \in \mathbb{N}$ .

For the fractional values of  $p \in (0, 1)$ , the formula is not a metric in the mathematical sense. However, it has been shown [16], that the similarity measure with fractional values of  $p$  works well in CBIR.

We are going to show, that

$$s_p(d_1^v \oplus d_1^t, d_2^v \oplus d_2^t) = (s_p^p(d_1^v, d_2^v) + s_p^p(d_1^t, d_2^t))^{1/p} \quad (21)$$

PROOF

$$\begin{aligned} s_p(d_1^v \oplus d_1^t, d_2^v \oplus d_2^t) &= \\ &= \|d_1^v \oplus d_1^t - d_2^v \oplus d_2^t\|_p = \\ &= \|(d_1^v - d_2^v) \oplus (d_1^t - d_2^t)\|_p = \\ &= (\|d_1^v - d_2^v\|_p^p + \|d_1^t - d_2^t\|_p^p)^{1/p} = \\ &= (s_p^p(d_1^v, d_2^v) + s_p^p(d_1^t, d_2^t))^{1/p} \end{aligned}$$

where

$$\|d\|_p = (d_1^p + d_2^p + \dots + d_n^p)^{1/p}$$

Here, the representations do not have to be normalized.

Hence, in these cases the early and late fusion approaches are interchangeable. The fusion of representations is then, in fact, the fusion of similarities computed independently on visual and textual feature spaces. This is, in our opinion, an interesting finding.

#### H. Advanced Early Fusion and Interchangeability

The following section is based on and contains excerpts from [10].

Even advanced, non-standard early fusion can in some cases be represented as a late fusion. The hybrid CBIR relevance model introduced in [10] can be considered as a dual form fusion. The model is based on the tensor product of co-occurrence matrices representing visual and textual subspaces of queries and feedback images. It was proven that this advanced measurement performed on the combined representations is equivalent to the non-trivial combination of measurements performed on individual feature spaces. Knowledge of this interchangeability makes the models easy to implement and significantly faster (computations performed on individual feature spaces).

Modern retrieval systems allow the users to interact with the system in order to narrow down and refine the search [18], [10]. This interaction takes the form of implicit or explicit feedback. The representations of the

images in the feedback set are often aggregated or concatenated (or co-occurrence matrices may be aggregated to represent i.e. probability distribution matrix). The information extracted from the feedback set is utilized to expand the query or re-rank the top images returned in the first round of the retrieval.

The proposed hybrid relevance feedback model was inspired by the measurement used in quantum mechanics, which is based on an expectation value, predicted mean value of the measurement

$$\langle A \rangle = \text{tr}(\rho A) \quad (22)$$

where  $\text{tr}$  denotes the trace operator,  $\rho$  represents a density matrix of the system and  $A$  is an observable. We can also represent an observable  $A$  as a density matrix (corresponding to the query or an image in the collection). For more information on the analogies between quantum mechanics and information retrieval the curious reader is referred to [23].

We are going to use the tensor operator  $\otimes$  to combine the density matrices corresponding to visual and textual feature spaces. In quantum mechanics, the tensor product of density matrices of different systems represents a density matrix of the combined system (see [32]).

Thus, the proposed measurement is represented by

$$\text{tr}((M_1 \otimes M_2) \cdot ((a^T \cdot a) \otimes (b^T \cdot b))) \quad (23)$$

where  $M_1, M_2$  represent density matrices (co-occurrence matrices) of the query and images in the feedback set corresponding to visual and textual spaces respectively,  $a$  and  $b$  denote row vectors representing visual and textual information for an image from the data collection,<sup>4</sup> and  $T$  is the transpose operation on matrices. We would perform this measurement on all the images in the collection, thus re-scoring the data collection based on the user feedback.

Assuming that the systems were prepared independently (otherwise we would have to try to model a concept analogous to entanglement [2]), we get

$$\begin{aligned} \text{tr}((M_1 \otimes M_2) \cdot ((a^T \cdot a) \otimes (b^T \cdot b))) &= \\ &= \text{tr}((M_1 \cdot (a^T \cdot a)) \otimes (M_2 \cdot (b^T \cdot b))) = \\ &= \text{tr}(M_1 \cdot (a^T \cdot a)) \cdot \text{tr}(M_2 \cdot (b^T \cdot b)) = \\ &= \langle M_1 | a^T \cdot a \rangle \cdot \langle M_2 | b^T \cdot b \rangle \end{aligned} \quad (24)$$

where  $\langle \cdot | \cdot \rangle$  denotes an inner product operating on a vector space.

Let  $q_v, q_t$  denote the visual and textual representations of the query,  $c^i, d^i$  denote visual and textual representations of the images in the feedback set,  $r_1, r_2$  denote the weighting factors (constant, importance of query and feedback density matrices respectively), and  $n$  denote the number of images in the feedback set. Then, we define  $M_1$  and  $M_2$  as weighted combinations of co-occurrence matrices (a subspace generated by the

<sup>4</sup>For the clarity of formulas  $a = d_2^v, b = d_2^t$ .

query vector and vectors from the feedback set).<sup>5</sup> Here,  $D_q^v, D_q^t, D_f^v$ , and  $D_f^t$  represent co-occurrence matrices of query and feedback images corresponding to visual and textual features respectively.

$$\begin{aligned} M_1 &= r_1 \cdot D_q^v + \frac{r_2}{n} \cdot D_f^v = \\ &= r_1 \cdot q_v^T \cdot q_v + \sum_i \left( \frac{r_2}{n} \cdot (c^i)^T \cdot c^i \right) \end{aligned} \quad (25)$$

and

$$\begin{aligned} M_2 &= r_1 \cdot D_q^t + \frac{r_2}{n} \cdot D_f^t = \\ &= r_1 \cdot q_t^T \cdot q_t + \sum_i \left( \frac{r_2}{n} \cdot (d^i)^T \cdot d^i \right) \end{aligned} \quad (26)$$

The common way of co-occurrence matrix generation is to multiply the term-document matrix by its transpose (rows of the matrix represent the documents  $d_1, \dots, d_m$ ), that is  $D = M^T \cdot M$ . Notice, that this is equivalent to  $D = \sum_{i=1}^n d_i^T \cdot d_i$ .

This observation, due to the properties of an inner product, will allow us to further simplify our model

$$\begin{aligned} \langle M_1 \otimes M_2 | (a^T \cdot a) \otimes (b^T \cdot b) \rangle &= \\ &= \langle M_1 | a^T \cdot a \rangle \cdot \langle M_2 | b^T \cdot b \rangle = \\ &= \langle r_1 \cdot q_v^T \cdot q_v + \sum_i \left( \frac{r_2}{n} \cdot (c^i)^T \cdot c^i \right) | a^T \cdot a \rangle \cdot \\ &= \left\langle r_1 \cdot q_t^T \cdot q_t + \sum_i \left( \frac{r_2}{n} \cdot (d^i)^T \cdot d^i \right) | b^T \cdot b \right\rangle = \\ &= \left( \langle r_1 \cdot q_v^T \cdot q_v | a^T \cdot a \rangle + \sum_i \frac{r_2}{n} \langle (c^i)^T \cdot c^i | a^T \cdot a \rangle \right) \cdot \\ &= \left( \langle r_1 \cdot q_t^T \cdot q_t | b^T \cdot b \rangle + \sum_i \frac{r_2}{n} \langle (d^i)^T \cdot d^i | b^T \cdot b \rangle \right) = \\ &= \left( r_1 \cdot \langle q_v | a \rangle^2 + \frac{r_2}{n} \cdot \sum_i \langle c^i | a \rangle^2 \right) \cdot \\ &= \left( r_1 \cdot \langle q_t | b \rangle^2 + \frac{r_2}{n} \cdot \sum_i \langle d^i | b \rangle^2 \right) \end{aligned} \quad (27)$$

Notice that the model breaks down into the weighted combinations of individual measurements. The squares of the inner products come from the correlation matrices and can play an important role in the measurement. Later in the paper, we are going to justify this claim.

We can consider a variation of the aforementioned model, where just like in the original one  $M_1 = r_1 \cdot D_q^v + (r_2/n) \cdot D_f^v$  and  $M_2 = r_1 \cdot D_q^t + (r_2/n) \cdot D_f^t$ . We can decompose (eigenvalue decomposition) the density ma-

<sup>5</sup>Co-occurrence matrices are quite often utilized in the Information Retrieval (IR) field. Because they are Hermitian and positive-definite, they can be thought of as density matrices (probability distribution).

trices  $M_1, M_2$  to estimate the bases<sup>6</sup> ( $p_i^v, p_j^t$ ) of the subspaces generated by the query and the images in the feedback set. Now, let us consider the measurement

$$\langle P_1 \otimes P_2 | (a^T a) \otimes (b^T b) \rangle \quad (28)$$

where  $P_1, P_2$  are the projectors onto visual and textual subspaces generated by query and the images in the feedback set ( $\sum_i (p_i^v)^T p_i^v, \sum_j (p_j^t)^T p_j^t$ ), and  $a, b$  are the visual and textual representations of an image from the data set. Because the tensor product of the projectors corresponding to visual and textual Hilbert spaces ( $H_1, H_2$ ) is a projector onto the tensored Hilbert space<sup>7</sup> ( $H_1 \otimes H_2$ ), the model can be interpreted as probability of relevance context, the probability that vector  $a \otimes b$  was generated within the subspace (representing the relevance context) generated by  $M_1 \otimes M_2$ . Hence

$$\begin{aligned} \langle P_1 \otimes P_2 | (a^T a) \otimes (b^T b) \rangle &= \\ &= \langle P_1 | a^T a \rangle \cdot \langle P_2 | b^T b \rangle = \\ &= \left\langle \sum_i (p_i^v)^T p_i^v | a^T a \right\rangle \cdot \left\langle \sum_j (p_j^t)^T p_j^t | b^T b \right\rangle = \\ &= \sum_i \langle p_i^v | a \rangle^2 \cdot \sum_j \langle p_j^t | b \rangle^2 = \\ &= \sum_i Pr_i^v \cdot \sum_j Pr_j^t = \\ &= \|(\langle p_1^v | a \rangle, \dots, \langle p_n^v | a \rangle) \otimes (\langle p_1^t | b \rangle, \dots, \langle p_n^t | b \rangle)\|^2 \end{aligned} \quad (29)$$

where  $Pr$  denotes the projection probability and  $\|\cdot\|$  represents vector norm.

We can see that this measurement is equivalent to the weighted combinations of all the probabilities of projections for all the images involved. In quantum mechanics, the square of the absolute value of the inner product between the initial state and the eigenstate is the probability of the system collapsing to this eigenstate. In our case, the square of the absolute value of the inner product can be interpreted as a particular contextual factor influencing the measurement.

#### IV. QUERY MODIFICATION AND LATE FUSION

Query reformulation techniques are often used in multimedia retrieval to narrow down the search based

<sup>6</sup>It has been highlighted [19] that the orthogonal decomposition may not be the best option for visual spaces because the receptive fields that result from this process are not localized, and the vast majority do not at all resemble any known cortical receptive fields. Thus, in the case of visual spaces, we may want to utilize decomposition methods that produce non-orthogonal basis vectors.

<sup>7</sup>A Hilbert space is a vector space with an inner product operation on elements of the vector space. It is a generalization of the notion of a Euclidean space. Hence, Hilbert spaces allow us to utilize a wider variety of mathematical tools to model various phenomena in IR, for example. This generalization can also often encompass many different models operating in Euclidean space, thus unifying various approaches.

on the user feedback. We are going to show, that the Rocchio query modification algorithm [26] can be represented as a late fusion, a combination of a number of individual relevance scores. This interesting finding shows that the same effect can be achieved by either modifying the query or combining individual relevance scores.

The late fusion analogues to the Rocchio algorithm have been considered as separate, different techniques [22], [12]. We show that one of the standard query modification algorithms, the Rocchio model, also has its dual late fusion form representations.

Rocchio algorithm modifies the query so that it moves closer to the centroid of relevant documents and further away from the centroid of irrelevant ones

$$Q_m = (a \cdot Q_o) + \left( b \cdot \frac{1}{|D_r|} \cdot \sum_{D_j \in D_r} D_j \right) - \left( c \cdot \frac{1}{|D_{nr}|} \cdot \sum_{D_k \in D_{nr}} D_k \right) \quad (30)$$

where

- $Q_m$ —modified query vector
- $Q_o$ —original query vector
- $D_j$ —related document vector
- $D_k$ —non-related document vector
- $a$ —original query weight
- $b$ —related documents' weights
- $c$ —non-related documents' weights
- $D_r$ —set of related documents
- $D_{nr}$ —set of non-related documents

We will show, that the modification of the query can be interpreted as a weighted combination of the measurements (scores, similarities) between a query and a document from the data collection and between a query and each document from the feedback set. In this section, for the clarity of the formulas, we assume that all vectors were normalized to unit vectors and  $Q_d$  denotes an arbitrary document vector from the data collection.

#### A. Inner Product

After modifying the query, we need to re-compute the scores. Thus, we would get

$$\begin{aligned} \langle Q_m | Q_d \rangle &= \\ &= a \langle Q_o | Q_d \rangle + \frac{b}{|D_r|} \sum_{D_j \in D_r} \langle D_j | Q_d \rangle - \\ &\quad \frac{c}{|D_{nr}|} \sum_{D_k \in D_{nr}} \langle D_k | Q_d \rangle \end{aligned} \quad (31)$$

PROOF

$$\begin{aligned} \langle Q_m | Q_d \rangle &= \\ &= \left\langle aQ_o + b \frac{1}{|D_r|} \sum_{D_j \in D_r} D_j - c \frac{1}{|D_{nr}|} \sum_{D_k \in D_{nr}} D_k | Q_d \right\rangle = \\ &= \langle aQ_o | Q_d \rangle + \\ &\quad + \left\langle \frac{b}{|D_r|} \sum_{D_j \in D_r} D_j | Q_d \right\rangle - \left\langle \frac{c}{|D_{nr}|} \sum_{D_k \in D_{nr}} D_k | Q_d \right\rangle = \\ &= a \langle Q_o | Q_d \rangle + \frac{b}{|D_r|} \sum_{D_j \in D_r} \langle D_j | Q_d \rangle - \\ &\quad - \frac{c}{|D_{nr}|} \sum_{D_k \in D_{nr}} \langle D_k | Q_d \rangle \end{aligned}$$

Hence, the query modification with the inner product as a similarity measurement can be represented in a specific late fusion form.

#### B. Cosine Similarity

For the cosine similarity, we get

$$\begin{aligned} s_c(Q_m, Q_d) &= \frac{1}{\|Q_m\|} \left( as_c(Q_o, Q_d) + \right. \\ &\quad \left. + \frac{b}{|D_r|} \sum_j s_c(D_j, Q_d) - \frac{c}{|D_{nr}|} \sum_k s_c(D_k, Q_d) \right) \end{aligned} \quad (32)$$

$$\begin{aligned} \|Q_m\|^2 &= a^2 + c^2 + \\ &\quad + \frac{2ab}{|D_r|} \sum_j s_c(Q_o, D_j) - \frac{2ac}{|D_{nr}|} \sum_k s_c(Q_o, D_k) - \\ &\quad \frac{2bc}{|D_r| \cdot |D_{nr}|} \sum_j \sum_k s_c(D_j, D_k) \end{aligned} \quad (33)$$

PROOF

$$\begin{aligned} s_c(Q_m, Q_d) &= \frac{\langle Q_m | Q_d \rangle}{\|Q_m\| \cdot \|Q_d\|} = \\ &= \frac{1}{\|Q_m\|} \left( as_c(Q_o, Q_d) + \right. \\ &\quad \left. + \frac{b}{|D_r|} \sum_j s_c(D_j, Q_d) - \frac{c}{|D_{nr}|} \sum_k s_c(D_k, Q_d) \right) \end{aligned}$$

where

$$\begin{aligned} \|Q_m\|^2 &= \langle Q_m | Q_m \rangle = \\ &= \left\langle aQ_o + \frac{b}{|D_r|} \sum_j D_j - \frac{c}{|D_{nr}|} \sum_k D_k | aQ_o + \right. \\ &\quad \left. + \frac{b}{|D_r|} \sum_j D_j - \frac{c}{|D_{nr}|} \sum_k D_k \right\rangle = \end{aligned}$$

$$\begin{aligned}
&= a^2 \langle Q_o | Q_o \rangle + \frac{2ab}{|D_r|} \sum_j \langle Q_o | D_j \rangle - \\
&\quad - \frac{2ac}{|D_{nr}|} \sum_k \langle Q_o | D_k \rangle - \frac{2bc}{|D_r| \cdot |D_{nr}|} \sum_j \sum_k \langle D_j | D_k \rangle + \\
&\quad + \frac{c^2}{|D_{nr}|^2} \sum_k \sum_k \langle D_k | D_k \rangle = \\
&= a^2 + c^2 + \frac{2ab}{|D_r|} \sum_j s_c(Q_o, D_j) - \frac{2ac}{|D_{nr}|} \sum_k s_c(Q_o, D_k) - \\
&\quad - \frac{2bc}{|D_r| \cdot |D_{nr}|} \sum_j \sum_k s_c(D_j, D_k)
\end{aligned}$$

Hence, the query modification with the cosine similarity as a similarity measurement can be represented in a specific late fusion form.

### C. Euclidean Distance

For the Euclidean distance

$$\begin{aligned}
s_e^2(Q_m, Q_d) &= \\
&= a^2 + c^2 + 2ab - 2ac - 2bc - 2a - 2b - 2c + 1 - \\
&\quad \frac{ab}{|D_r|} \sum_j s_e(Q_o, D_j) + \frac{ac}{|D_{nr}|} \sum_k s_e(Q_o, D_k) + \\
&\quad + \frac{bc}{|D_r| \cdot |D_{nr}|} \sum_j \sum_k s_e(D_j, D_k) + \\
&\quad + as_e(Q_o, Q_d) + \\
&\quad + \frac{b}{|D_r|} \sum_j s_e(D_j, Q_d) + \frac{c}{|D_{nr}|} \sum_k s_e(D_k, Q_d) \quad (34)
\end{aligned}$$

PROOF Based on the previous observation (for cosine similarity), we get

$$\begin{aligned}
s_e^2(Q_m, Q_d) &= \\
&= a^2 + c^2 + \frac{2ab}{|D_r|} \sum_j \langle Q_o | D_j \rangle - \\
&\quad \frac{2ac}{|D_{nr}|} \sum_k \langle Q_o | D_k \rangle - \frac{2bc}{|D_r| \cdot |D_{nr}|} \sum_j \sum_k \langle D_j | D_k \rangle + \\
&\quad + 1 - 2a \langle Q_o | Q_d \rangle - \frac{2b}{|D_r|} \sum_j \langle D_j | Q_d \rangle \\
&\quad - \frac{2c}{|D_{nr}|} \sum_k \langle D_k | Q_d \rangle = \\
&= a^2 + c^2 + 1 + \frac{2ab}{|D_r|} |D_r| - \frac{2ab}{|D_r|} |D_r| + \\
&\quad + \frac{2ab}{|D_r|} \sum_j \langle Q_o | D_j \rangle + \frac{2ac}{|D_{nr}|} |D_{nr}| - \frac{2ac}{|D_{nr}|} |D_{nr}| + \\
&\quad - \frac{2ac}{|D_{nr}|} \sum_k \langle Q_o | D_k \rangle + \frac{2bc}{|D_r| \cdot |D_{nr}|} |D_r| \cdot |D_{nr}| - \\
&\quad - \frac{2bc}{|D_r| \cdot |D_{nr}|} |D_r| \cdot |D_{nr}| - \frac{2bc}{|D_r| \cdot |D_{nr}|} \sum_j \sum_k \langle D_j | D_k \rangle +
\end{aligned}$$

$$\begin{aligned}
&+ 2a - 2a - 2a \langle Q_o | Q_d \rangle + \\
&+ \frac{2b}{|D_r|} |D_r| - \frac{2b}{|D_r|} |D_r| - \frac{2b}{|D_r|} \sum_j \langle D_j | Q_d \rangle + \\
&+ \frac{2c}{|D_{nr}|} |D_{nr}| - \frac{2c}{|D_{nr}|} |D_{nr}| - \frac{2c}{|D_{nr}|} \sum_k \langle D_k | Q_d \rangle = \\
&= a^2 + c^2 + 2ab - 2ac - 2bc - 2a - 2b - 2c + 1 - \\
&\quad - \frac{ab}{|D_r|} \sum_j s_e(Q_o, D_j) + \frac{ac}{|D_{nr}|} \sum_k s_e(Q_o, D_k) + \\
&\quad + \frac{bc}{|D_r| \cdot |D_{nr}|} \sum_j \sum_k s_e(D_j, D_k) + \\
&\quad + as_e(Q_o, Q_d) + \frac{b}{|D_r|} \sum_j s_e(D_j, Q_d) + \\
&\quad + \frac{c}{|D_{nr}|} \sum_k s_e(D_k, Q_d)
\end{aligned}$$

Hence, the query modification with the Euclidean distance as a similarity measurement can be represented in a specific late fusion form.

### D. Hybrid Relevance Feedback and Rocchio Algorithm

We can also tensor or concatenate the modified query vectors in order to generate hybrid models. Then ( $v, t$  indexes denote visual and textual representations respectively)

$$\begin{aligned}
\langle Q_m^v \otimes Q_m^t | Q_d^v \otimes Q_d^t \rangle &= \\
&= \langle Q_m^v | Q_d^v \rangle \langle Q_m^t | Q_d^t \rangle = \\
&= (a \langle Q_o^v | Q_d^v \rangle + \frac{b}{|D_r|} \sum_{D_j \in D_r} \langle D_j^v | Q_d^v \rangle - \\
&\quad \frac{c}{|D_{nr}|} \sum_{D_k \in D_{nr}} \langle D_k^v | Q_d^v \rangle) \cdot \\
&\quad (a \langle Q_o^t | Q_d^t \rangle + \frac{b}{|D_r|} \sum_{D_j \in D_r} \langle D_j^t | Q_d^t \rangle - \\
&\quad \frac{c}{|D_{nr}|} \sum_{D_k \in D_{nr}} \langle D_k^t | Q_d^t \rangle) \quad (35)
\end{aligned}$$

and for concatenation

$$\begin{aligned}
\langle Q_m^v \oplus Q_m^t | Q_d^v \oplus Q_d^t \rangle &= \\
&= \langle Q_m^v | Q_d^v \rangle + \langle Q_m^t | Q_d^t \rangle = \\
&= a (\langle Q_o^v | Q_d^v \rangle + \langle Q_o^t | Q_d^t \rangle) + \\
&\quad + \frac{b}{|D_r|} \sum_{D_j \in D_r} (\langle D_j^v | Q_d^v \rangle + \langle D_j^t | Q_d^t \rangle) - \\
&\quad \frac{c}{|D_{nr}|} \sum_{D_k \in D_{nr}} (\langle D_k^v | Q_d^v \rangle + \langle D_k^t | Q_d^t \rangle) \quad (36)
\end{aligned}$$

TABLE II  
Summary of the findings.

Early fusion interacting with the similarity	Late fusion equivalent
$s_{in}(d_1^v \oplus d_1^t, d_2^v \oplus d_2^t)$	$s_{in}(d_1^v   d_2^v) + s_{in}(d_1^t   d_2^t)$
$s_{in}(d_1^v \otimes d_1^t, d_2^v \otimes d_2^t)$	$s_{in}(d_1^v   d_2^v) \cdot s_{in}(d_1^t   d_2^t)$
$s_c(d_1^v \otimes d_1^t, d_2^v \otimes d_2^t)$	$s_c(d_1^v, d_2^v) \cdot s_c(d_1^t, d_2^t)$
$s_c(d_1^v \oplus d_1^t, d_2^v \oplus d_2^t)$	$\frac{1}{2}(s_c(d_1^v, d_2^v) + s_c(d_1^t, d_2^t))$
$s_c(r_1 d_1^v \oplus r_2 d_1^t, r_1 d_2^v \oplus r_2 d_2^t)$	$\frac{(r_1^2 s_c(d_1^v, d_2^v) + r_2^2 s_c(d_1^t, d_2^t))}{r_1^2 + r_2^2}$
$s_e(d_1^v \oplus d_1^t, d_2^v \oplus d_2^t)$	$\sqrt{s_e^2(d_1^v, d_2^v) + s_e^2(d_1^t, d_2^t)}$
$s_e(d_1^v \otimes d_1^t, d_2^v \otimes d_2^t)$	$\sqrt{s_e^2(d_1^v, d_2^v) + s_e^2(d_1^t, d_2^t) - \frac{1}{2}s_e^2(d_1^v, d_2^v)s_e^2(d_1^t, d_2^t)}$
$s_b(d_1^v \otimes d_1^t, d_2^v \otimes d_2^t)$	$s_b(d_1^v, d_2^v) + s_b(d_1^t, d_2^t)$
$s_b(d_1^v \oplus d_1^t, d_2^v \oplus d_2^t)$	$-\ln(w_1 + w_2)$ $w_1 = e^{-s_b(d_1^v, d_2^v)}$ $w_2 = e^{-s_b(d_1^t, d_2^t)}$
$s_e(d_1^v \oplus d_1^t, d_2^v \oplus d_2^t)$	$\sqrt{s_e^2(d_1^v, d_2^v) - 2s_e(d_1^t, d_2^t) + 2}$
$s_e(d_1^v \otimes d_1^t, d_2^v \otimes d_2^t)$	$\sqrt{s_e^2(d_1^v, d_2^v)s_e(d_1^t, d_2^t) - 2s_e(d_1^t, d_2^t) + 2}$
$s_p(d_1^v \oplus d_1^t, d_2^v \oplus d_2^t)$	$(s_p^p(d_1^v, d_2^v) + s_p^p(d_1^t, d_2^t))^{1/p}$
$tr(M_1 \otimes M_2) \cdot ((a^T \cdot a) \otimes (b^T \cdot b))$	$(r_1 \cdot \langle q_v   a \rangle^2 + \frac{r_2}{n} \cdot \sum_i \langle c^i   a \rangle^2) \cdot (r_1 \cdot \langle q_t   b \rangle^2 + \frac{r_2}{n} \cdot \sum_i \langle d^i   b \rangle^2)$
$\langle P_1 \otimes P_2   (a^T a) \otimes (b^T b) \rangle$	$\ (\langle p_1^v   a \rangle, \dots, \langle p_n^v   a \rangle) \otimes (\langle p_1^t   b \rangle, \dots, \langle p_n^t   b \rangle)\ ^2$
$\langle Q_m   Q_d \rangle$	$a \langle Q_o   Q_d \rangle + \frac{b}{ D_r } \sum_{D_j \in D_r} \langle D_j   Q_d \rangle - \frac{c}{ D_{nr} } \sum_{D_k \in D_{nr}} \langle D_k   Q_d \rangle$
$s_c(Q_m, Q_d)$	$\frac{1}{\ Q_m\ } \left( a s_c(Q_o, Q_d) + \frac{b}{ D_r } \sum_j s_c(D_j, Q_d) - \frac{c}{ D_{nr} } \sum_k s_c(D_k, Q_d) \right)$
$\ Q_m\ ^2$	$a^2 + c^2 + \frac{2ab}{ D_r } \sum_j s_c(Q_o, D_j) - \frac{2ac}{ D_{nr} } \sum_k s_c(Q_o, D_k) - \frac{2bc}{ D_r  \cdot  D_{nr} } \sum_j \sum_k s_c(D_j, D_k)$
$s_e^2(Q_m, Q_d)$	$a^2 + c^2 + 2ab - 2ac - 2bc - 2a - 2b - 2c + 1 -$ $\frac{ab}{ D_r } \sum_j s_e(Q_o, D_j) + \frac{ac}{ D_{nr} } \sum_k s_e(Q_o, D_k) + \frac{bc}{ D_r  \cdot  D_{nr} } \sum_j \sum_k s_e(D_j, D_k) +$ $a s_e(Q_o, Q_d) + \frac{b}{ D_r } \sum_j s_e(D_j, Q_d) + \frac{c}{ D_{nr} } \sum_k s_e(D_k, Q_d)$

We can use other similarity measures

$$s_c(Q_m^v \otimes Q_m^t, Q_d^v \otimes Q_d^t) = s_c(Q_m^v, Q_d^v) \cdot s_c(Q_m^t, Q_d^t) \quad (37)$$

$$s_c(Q_m^v \oplus Q_m^t, Q_d^v \oplus Q_d^t) = \frac{1}{2}(s_c(Q_m^v, Q_d^v) + s_c(Q_m^t, Q_d^t)) \quad (38)$$

$$s_e(Q_m^v \otimes Q_m^t, Q_d^v \otimes Q_d^t) = \sqrt{s_e^2(Q_m^v, Q_d^v) + s_e^2(Q_m^t, Q_d^t) - \frac{1}{2}s_e^2(Q_m^v, Q_d^v)s_e^2(Q_m^t, Q_d^t)} \quad (39)$$

$$s_e(Q_m^v \oplus Q_m^t, Q_d^v \oplus Q_d^t) = \sqrt{s_e^2(Q_m^v, Q_d^v) + s_e^2(Q_m^t, Q_d^t)} \quad (40)$$

$$s_e(Q_m^v \otimes Q_m^t, Q_d^v \otimes Q_d^t) = \sqrt{s_e^2(Q_m^v, Q_d^v) - 2s_c(Q_m^t, Q_d^t) + 2} \quad (41)$$

$$s_e(Q_m^v \otimes Q_m^t, Q_d^v \otimes Q_d^t) =$$

$$= \sqrt{s_e^2(Q_m^v, Q_d^v)s_e(Q_m^t, Q_d^t) - 2s_c(Q_m^t, Q_d^t) + 2} \quad (42)$$

where the last formula would be a suggested combination choice (Euclidean distance for measuring the similarity between visual representations and cosine similarity for textual representations).

Thus, the standard Rocchio query modification algorithm can be represented as a late fusion, a combination of individual similarity measurements. This late fusion strategy is equivalent to the standard query modification approach.

Table II presents the summary of all the findings. Figures 1 to 11 in the Appendix show examples related to concatenation operator interacting with the inner product, tensor product interacting with the inner product, concatenation operator interacting with the cosine similarity, tensor product interacting with the cosine

similarity, weighted concatenation operator interacting with the cosine similarity, concatenation operator interacting with the Euclidean distance, tensor product interacting with the Euclidean distance, concatenation operator interacting with the Bhattacharya similarity, concatenation operator interacting with the Euclidean distance for visual features and cosine similarity for text, tensor product interacting with the Euclidean distance for visual features and cosine similarity for text, and concatenation operator interacting with the Minkowski Family of Distances, respectively.

## V. CONCLUSIONS AND FUTURE WORK

Fusion strategies are widely utilized in many areas of research, including Information Retrieval. Findings presented in this paper are universal and also apply to other areas of research. Here, however, we focus on the application of fusion strategies to Content-based Image Retrieval (CBIR).

In this paper, we have investigated some interesting interactions between widely used similarity measurements and widely used operators related to early fusion strategy. We have shown that these interactions between specific similarity measurements and specific early fusion strategies have resulted in combinations of representations at the decision level (late fusion strategy). In other words, we have mathematically proved that specific combinations of early fusion strategies and specific similarity measurements are equivalent to particular combinations of measurements (i.e. relevance scores) computed on individual feature spaces.

We have also shown that the query modification method with specific similarity measurements (classic Rocchio algorithm) can be interpreted as weighted combinations of individual similarity measurements. What this means is that the same effect can be achieved by either modifying the query or combining individual relevance scores. The existing late fusion analogues to the Rocchio algorithm have been considered as separate, different techniques. However, we have seen that the Rocchio model also have its dual late fusion form representations.

For future work we plan to search for other combinations of various operators and similarity measures that could interact in such a way as to represent late fusion. We have discovered that even advanced early fusion can be represented as specific combinations of similarity measurements. We will be also investigating whether the late fusion is capable of capturing the correlation between feature spaces or the interaction between the early fusion operators and the similarity measurements de-correlates features.

## ACKNOWLEDGMENT

This work has been partially funded by the EC FP7 OPENi project no. 317883 on Internet of Services (<http://www.openi-ict.eu/>). The motivation of the project

is to provide cloud-based applications and services for mobile users. The AmbieSense work is focused on providing advanced search facilities for large-scale multimedia and social media applications in the cloud.

## VI. APPENDIX

EXAMPLE 1. Concatenation with the inner product.

Query visual representation:  $\left(\frac{\sqrt{2}}{2}, \frac{\sqrt{2}}{2}\right)$

Query textual representation:  $\left(\frac{\sqrt{2}}{2}, 0, \frac{\sqrt{2}}{2}\right)$

Arbitrary image from the collection (visual): (1,0)

Arbitrary image from the collection (text): (1,0,0)

$$L = \left\langle \left(\frac{\sqrt{2}}{2}, \frac{\sqrt{2}}{2}\right) \oplus \left(\frac{\sqrt{2}}{2}, 0, \frac{\sqrt{2}}{2}\right) \mid (1,0) \oplus (1,0,0) \right\rangle =$$

$$\left\langle \frac{\sqrt{2}}{2}, \frac{\sqrt{2}}{2}, \frac{\sqrt{2}}{2}, 0, \frac{\sqrt{2}}{2} \mid 1,0,1,0,0 \right\rangle = \sqrt{2}$$

$$R = \left\langle \left(\frac{\sqrt{2}}{2}, \frac{\sqrt{2}}{2}\right) \mid (1,0) \right\rangle + \left\langle \left(\frac{\sqrt{2}}{2}, 0, \frac{\sqrt{2}}{2}\right) \mid (1,0,0) \right\rangle =$$

$$\frac{\sqrt{2}}{2} + \frac{\sqrt{2}}{2} = \sqrt{2}$$

$$L = R$$

Therefore the concatenation with the inner product as a similarity measurement can be represented in a late fusion form. This means that these specific early and late fusion strategies must produce the same ranking of images.

EXAMPLE 2. Tensor product with the inner product.

Query visual representation:  $\left(\frac{\sqrt{2}}{2}, \frac{\sqrt{2}}{2}\right)$

Query textual representation:  $\left(\frac{\sqrt{2}}{2}, 0, \frac{\sqrt{2}}{2}\right)$

Arbitrary image from the collection (visual): (1,0)

Arbitrary image from the collection (text): (1,0,0)

$$L = \left\langle \left(\frac{\sqrt{2}}{2}, \frac{\sqrt{2}}{2}\right) \otimes \left(\frac{\sqrt{2}}{2}, 0, \frac{\sqrt{2}}{2}\right) \mid (1,0) \otimes (1,0,0) \right\rangle =$$

$$\left\langle \frac{1}{2}, 0, \frac{1}{2}, \frac{1}{2}, 0, \frac{1}{2} \mid 1,0,0,0,0,0 \right\rangle = \frac{1}{2}$$

$$R = \left\langle \left(\frac{\sqrt{2}}{2}, \frac{\sqrt{2}}{2}\right) \mid (1,0) \right\rangle \cdot \left\langle \left(\frac{\sqrt{2}}{2}, 0, \frac{\sqrt{2}}{2}\right) \mid (1,0,0) \right\rangle =$$

$$\frac{\sqrt{2}}{2} \cdot \frac{\sqrt{2}}{2} = \frac{1}{2}$$

$$L = R$$

Therefore the tensor product with the inner product as a similarity measurement can be represented in a late fusion form. This means that these specific early and late fusion strategies must produce the same ranking of images.

EXAMPLE 3. Concatenation with the cosine similarity.

Query visual representation:  $\left(\frac{\sqrt{2}}{2}, \frac{\sqrt{2}}{2}\right)$

Query textual representation:  $\left(\frac{\sqrt{2}}{2}, 0, \frac{\sqrt{2}}{2}\right)$

Arbitrary image from the collection (visual): (1,0)

Arbitrary image from the collection (text): (1,0,0)

$$L = s_c \left( \left(\frac{\sqrt{2}}{2}, \frac{\sqrt{2}}{2}\right) \oplus \left(\frac{\sqrt{2}}{2}, 0, \frac{\sqrt{2}}{2}\right), (1,0) \oplus (1,0,0) \right) =$$

$$\frac{\sqrt{2}}{\sqrt{\frac{1}{2} + \frac{1}{2} + \frac{1}{2} + \frac{1}{2}} \cdot \sqrt{1+1}} = \frac{\sqrt{2}}{2}$$

$$R = \frac{1}{2} \cdot \left( s_c \left( \left( \frac{\sqrt{2}}{2}, \frac{\sqrt{2}}{2} \right), (1,0) \right) + s_c \left( \left( \frac{\sqrt{2}}{2}, 0, \frac{\sqrt{2}}{2} \right), (1,0,0) \right) \right) =$$

$$\frac{1}{2} \cdot \left( \frac{\frac{\sqrt{2}}{2}}{1+1} + \frac{\frac{\sqrt{2}}{2}}{1+1} \right) = \frac{\sqrt{2}}{2}$$

$$L = R$$

Therefore the concatenation with the cosine similarity as a similarity measurement can be represented in a late fusion form. This means that these specific early and late fusion strategies must produce the same ranking of images.

EXAMPLE 4. Tensor product with the cosine similarity.

$$\text{Query visual representation: } \left( \frac{\sqrt{2}}{2}, \frac{\sqrt{2}}{2} \right)$$

$$\text{Query textual representation: } \left( \frac{\sqrt{2}}{2}, 0, \frac{\sqrt{2}}{2} \right)$$

$$\text{Arbitrary image from the collection (visual): } (1,0)$$

$$\text{Arbitrary image from the collection (text): } (1,0,0)$$

$$L = s_c \left( \left( \frac{\sqrt{2}}{2}, \frac{\sqrt{2}}{2} \right) \otimes \left( \frac{\sqrt{2}}{2}, 0, \frac{\sqrt{2}}{2} \right), (1,0) \otimes (1,0,0) \right) =$$

$$s_c \left( \left( \frac{1}{2}, 0, \frac{1}{2}, \frac{1}{2}, 0, \frac{1}{2} \right), (1,0,0,0,0,0) \right) = \frac{1}{1+1} = \frac{1}{2}$$

$$R = s_c \left( \left( \frac{\sqrt{2}}{2}, \frac{\sqrt{2}}{2} \right), (1,0) \right) \cdot s_c \left( \left( \frac{\sqrt{2}}{2}, 0, \frac{\sqrt{2}}{2} \right), (1,0,0) \right) =$$

$$\frac{\frac{\sqrt{2}}{2}}{\sqrt{\frac{1}{2} + \frac{1}{2} \cdot \sqrt{1}}} \cdot \frac{\frac{\sqrt{2}}{2}}{\sqrt{\frac{1}{2} + \frac{1}{2} \cdot \sqrt{1}}} = \frac{\sqrt{2}}{2} \cdot \frac{\sqrt{2}}{2} = \frac{1}{2}$$

$$L = R$$

Therefore the tensor product with the cosine similarity as a similarity measurement can be represented in a late fusion form. This means that these specific early and late fusion strategies must produce the same ranking of images.

EXAMPLE 5. Weighted concatenation with the cosine similarity.

$$\text{Query visual representation: } \left( \frac{\sqrt{2}}{2}, \frac{\sqrt{2}}{2} \right)$$

$$\text{Query textual representation: } \left( \frac{\sqrt{2}}{2}, 0, \frac{\sqrt{2}}{2} \right)$$

$$\text{Arbitrary image from the collection (visual): } (1,0)$$

$$\text{Arbitrary image from the collection (text): } (1,0,0)$$

$$L = s_c \left( 2 \cdot \left( \frac{\sqrt{2}}{2}, \frac{\sqrt{2}}{2} \right) \oplus 4 \cdot \left( \frac{\sqrt{2}}{2}, 0, \frac{\sqrt{2}}{2} \right), \right.$$

$$\left. 2 \cdot (1,0) \oplus 4 \cdot (1,0,0) \right) =$$

$$s_c \left( \left( \sqrt{2}, \sqrt{2}, 2\sqrt{2}, 0, 2\sqrt{2} \right), (2,0,4,0,0) \right) =$$

$$\frac{2\sqrt{2}+8\sqrt{2}}{\sqrt{2+2+8+8 \cdot \sqrt{4+16}}} = \frac{10\sqrt{2}}{\sqrt{20 \cdot \sqrt{20}}} = \frac{\sqrt{2}}{2}$$

$$R =$$

$$\frac{1}{4+16} \cdot \left( 4s_c \left( \left( \frac{\sqrt{2}}{2}, \frac{\sqrt{2}}{2} \right), (1,0) \right) \right.$$

$$\left. + 16s_c \left( \left( \frac{\sqrt{2}}{2}, 0, \frac{\sqrt{2}}{2} \right), (1,0,0) \right) \right) =$$

$$\frac{1}{20} \cdot \left( 4\frac{\sqrt{2}}{2} + 16\frac{\sqrt{2}}{2} \right) = \frac{\sqrt{2}}{2}$$

$$L = R$$

Therefore the weighted concatenation with the cosine as a similarity measurement can be represented in a late fusion form. This means that these specific early

and late fusion strategies must produce the same ranking of images.

EXAMPLE 6. Concatenation with the Euclidean distance.

$$\text{Query visual representation: } \left( \frac{\sqrt{2}}{2}, \frac{\sqrt{2}}{2} \right)$$

$$\text{Query textual representation: } \left( \frac{\sqrt{2}}{2}, 0, \frac{\sqrt{2}}{2} \right)$$

$$\text{Arbitrary image from the collection (visual): } (1,0)$$

$$\text{Arbitrary image from the collection (text): } (1,0,0)$$

$$L = s_e \left( \left( \frac{\sqrt{2}}{2}, \frac{\sqrt{2}}{2} \right) \oplus \left( \frac{\sqrt{2}}{2}, 0, \frac{\sqrt{2}}{2} \right), (1,0) \oplus (1,0,0) \right) =$$

$$s_e \left( \left( \frac{\sqrt{2}}{2}, \frac{\sqrt{2}}{2}, \frac{\sqrt{2}}{2}, 0, \frac{\sqrt{2}}{2} \right), (1,0,1,0,0) \right) =$$

$$\sqrt{\left( \frac{\sqrt{2}}{2} - 1 \right)^2 + \frac{1}{2} + \left( \frac{\sqrt{2}}{2} - 1 \right)^2 + \frac{1}{2}} = \sqrt{4 - 2\sqrt{2}}$$

$$R = \sqrt{s_e^2 \left( \left( \frac{\sqrt{2}}{2}, \frac{\sqrt{2}}{2} \right), (1,0) \right) + s_e^2 \left( \left( \frac{\sqrt{2}}{2}, 0, \frac{\sqrt{2}}{2} \right), (1,0,0) \right)} =$$

$$\sqrt{\left( \frac{\sqrt{2}}{2} - 1 \right)^2 + \left( \frac{\sqrt{2}}{2} \right)^2 + \left( \frac{\sqrt{2}}{2} - 1 \right)^2 + \left( \frac{\sqrt{2}}{2} \right)^2} = \sqrt{4 - 2\sqrt{2}}$$

$$L = R$$

Therefore the concatenation with the Euclidean distance as a similarity measurement can be represented in a late fusion form. This means that these specific early and late fusion strategies must produce the same ranking of images.

EXAMPLE 7. Tensor product with the Euclidean distance.

$$\text{Query visual representation: } \left( \frac{\sqrt{2}}{2}, \frac{\sqrt{2}}{2} \right)$$

$$\text{Query textual representation: } \left( \frac{\sqrt{2}}{2}, 0, \frac{\sqrt{2}}{2} \right)$$

$$\text{Arbitrary image from the collection (visual): } (1,0)$$

$$\text{Arbitrary image from the collection (text): } (1,0,0)$$

$$L = s_e \left( \left( \frac{\sqrt{2}}{2}, \frac{\sqrt{2}}{2} \right) \otimes \left( \frac{\sqrt{2}}{2}, 0, \frac{\sqrt{2}}{2} \right), (1,0) \otimes (1,0,0) \right) =$$

$$s_e \left( \left( \frac{1}{2}, 0, \frac{1}{2}, \frac{1}{2}, 0, \frac{1}{2} \right), (1,0,0,0,0,0) \right) = \sqrt{\frac{1}{4} + \frac{1}{4} + \frac{1}{4} + \frac{1}{4}} = 1$$

$$R^2 = s_e^2 \left( \left( \frac{\sqrt{2}}{2}, \frac{\sqrt{2}}{2} \right), (1,0) \right) + s_e^2 \left( \left( \frac{\sqrt{2}}{2}, 0, \frac{\sqrt{2}}{2} \right), (1,0,0) \right) -$$

$$\frac{1}{2}s_e^2 \left( \left( \frac{\sqrt{2}}{2}, \frac{\sqrt{2}}{2} \right), (1,0) \right) \cdot s_e^2 \left( \left( \frac{\sqrt{2}}{2}, 0, \frac{\sqrt{2}}{2} \right), (1,0,0) \right) =$$

$$2 - \sqrt{2} + 2 - \sqrt{2} - \frac{1}{2}(2 - \sqrt{2})^2 = 1$$

$$R = \sqrt{1} = 1$$

$$L = R$$

Therefore the tensor product with the Euclidean distance as a similarity measurement can be represented in a late fusion form. This means that these specific early and late fusion strategies must produce the same ranking of images.

EXAMPLE 8. Concatenation with the Bhattacharya similarity.

$$\text{Query visual representation: } \left( \frac{\sqrt{2}}{2}, \frac{\sqrt{2}}{2} \right)$$

$$\text{Query textual representation: } \left( \frac{\sqrt{2}}{2}, 0, \frac{\sqrt{2}}{2} \right)$$

$$\text{Arbitrary image from the collection (visual): } (1,0)$$

Arbitrary image from the collection (text):  $(1, 0, 0)$

$$L = s_b \left( \left( \frac{\sqrt{2}}{2}, \frac{\sqrt{2}}{2} \right) \oplus \left( \frac{\sqrt{2}}{2}, 0, \frac{\sqrt{2}}{2} \right), (1, 0) \oplus (1, 0, 0) \right) =$$

$$s_b \left( \left( \frac{\sqrt{2}}{2}, \frac{\sqrt{2}}{2}, \frac{\sqrt{2}}{2}, 0, \frac{\sqrt{2}}{2} \right), (1, 0, 1, 0, 0) \right) =$$

$$-\ln \left( \sqrt{\frac{\sqrt{2}}{2}} + \sqrt{\frac{\sqrt{2}}{2}} \right) = -\ln(2 \cdot 2^{-1/4}) = -\ln(2^{3/4})$$

$$R = s_b \left( \left( \frac{\sqrt{2}}{2}, \frac{\sqrt{2}}{2} \right), (1, 0) \right) + s_b \left( \left( \frac{\sqrt{2}}{2}, 0, \frac{\sqrt{2}}{2} \right), (1, 0, 0) \right) =$$

$$-\ln \left( e^{\ln \left( \sqrt{\frac{\sqrt{2}}{2}} \right)} + e^{\ln \left( \sqrt{\frac{\sqrt{2}}{2}} \right)} \right) = -\ln \left( 2 \sqrt{\frac{\sqrt{2}}{2}} \right) =$$

$$-\ln(2^{3/4})$$

$$L = R$$

Therefore the concatenation with the Bhattacharya similarity as a similarity measurement can be represented in a late fusion form. This means that these specific early and late fusion strategies must produce the same ranking of images.

EXAMPLE 9. Concatenation with the Euclidean distance for visual features and cosine similarity for text.

Query visual representation:  $\left( \frac{\sqrt{2}}{2}, \frac{\sqrt{2}}{2} \right)$

Query textual representation:  $\left( \frac{\sqrt{2}}{2}, 0, \frac{\sqrt{2}}{2} \right)$

Arbitrary image from the collection (visual):  $(1, 0)$

Arbitrary image from the collection (text):  $(1, 0, 0)$

$$L = s_e \left( \left( \frac{\sqrt{2}}{2}, \frac{\sqrt{2}}{2} \right) \oplus \left( \frac{\sqrt{2}}{2}, 0, \frac{\sqrt{2}}{2} \right), (1, 0) \oplus (1, 0, 0) \right) =$$

$$s_e \left( \left( \frac{\sqrt{2}}{2}, \frac{\sqrt{2}}{2}, \frac{\sqrt{2}}{2}, 0, \frac{\sqrt{2}}{2} \right), (1, 0, 1, 0, 0) \right) =$$

$$\sqrt{4 - 2\sqrt{2}}$$

$$s_e \left( \left( \frac{\sqrt{2}}{2}, \frac{\sqrt{2}}{2} \right), (1, 0) \right) = \sqrt{2 - \sqrt{2}}$$

$$s_c \left( \left( \frac{\sqrt{2}}{2}, 0, \frac{\sqrt{2}}{2} \right), (1, 0, 0) \right) = \frac{\sqrt{2}}{2}$$

$$R = \sqrt{2 - \sqrt{2} - \sqrt{2} + 2} = \sqrt{4 - 2\sqrt{2}}$$

$$L = R$$

Therefore the concatenation with the above similarity measurements can be represented in a late fusion form. This means that these specific early and late fusion strategies must produce the same ranking of images.

EXAMPLE 10. Tensor product with the Euclidean distance for visual features and cosine similarity for text.

Query visual representation:  $\left( \frac{\sqrt{2}}{2}, \frac{\sqrt{2}}{2} \right)$

Query textual representation:  $\left( \frac{\sqrt{2}}{2}, 0, \frac{\sqrt{2}}{2} \right)$

Arbitrary image from the collection (visual):  $(1, 0)$

Arbitrary image from the collection (text):  $(1, 0, 0)$

$$L = s_e \left( \left( \frac{\sqrt{2}}{2}, \frac{\sqrt{2}}{2} \right) \otimes \left( \frac{\sqrt{2}}{2}, 0, \frac{\sqrt{2}}{2} \right), (1, 0) \otimes (1, 0, 0) \right) =$$

$$s_e \left( \left( \frac{1}{2}, 0, \frac{1}{2}, \frac{1}{2}, 0, \frac{1}{2} \right), (1, 0, 0, 0, 0, 0) \right) = \sqrt{\frac{1}{4} + \frac{1}{4} + \frac{1}{4} + \frac{1}{4}} = 1$$

$$s_e \left( \left( \frac{\sqrt{2}}{2}, \frac{\sqrt{2}}{2} \right), (1, 0) \right) = \sqrt{2 - \sqrt{2}}$$

$$s_c \left( \left( \frac{\sqrt{2}}{2}, 0, \frac{\sqrt{2}}{2} \right), (1, 0, 0) \right) = \frac{\sqrt{2}}{2}$$

$$R = \sqrt{(2 - \sqrt{2}) \cdot \frac{\sqrt{2}}{2} - \sqrt{2} + 2} = 1$$

$$L = R$$

Therefore the tensor product with the above similarity measurements can be represented in a late fusion form. This means that these specific early and late fusion strategies must produce the same ranking of images.

EXAMPLE 11. Concatenation with the Minkowski Family of Distances.

Query visual representation:  $d_1^v = (1, 3, 4)$

Query textual representation:  $d_1^t = (12, 1, 4, 2)$

Arbitrary image from the collection (visual):

$d_2^v = (0, 3, 5)$

Arbitrary image from the collection (text):

$d_2^t = (11, 0, 3, 1)$

$s_{p=1/4}(d_1^v, d_2^v) =$

$$(|1 - 0|^{1/4} + |3 - 3|^{1/4} + |4 - 5|^{1/4})^4 = 2^4 = 16$$

$s_{p=1/4}(d_1^t, d_2^t) =$

$$(|12 - 11|^{1/4} + |1 - 0|^{1/4} + |4 - 3|^{1/4} + |2 - 1|^{1/4})^4 = 4^4 = 256$$

Therefore, the right-hand side of the equation becomes

$$R = (s_{p=1/4}^{1/4}(d_1^v, d_2^v) + s_{p=1/4}^{1/4}(d_1^t, d_2^t))^4 =$$

$$(16^{1/4} + 256^{1/4})^4 = (2 + 4)^4 = 1296$$

For the left-hand side, we have

$$L = s_{p=1/4}(d_1^v \oplus d_1^t, d_2^v \oplus d_2^t) =$$

$$s_{p=1/4}((1, 3, 4, 12, 1, 4, 2), (0, 3, 5, 11, 0, 3, 1)) =$$

$$(1 + 0 + 1 + 1 + 1 + 1 + 1)^4 = 1296$$

Thus,  $L = R$ .

Therefore concatenation operation with the above similarity measurements can be represented in a late fusion form. This means that this specific early and late fusion strategy must produce the same ranking of images.

## REFERENCES

- [1] [http://www.courses.ischool.berkeley.edu/i240/s11/Lectures/Lecture\\_15.ppt](http://www.courses.ischool.berkeley.edu/i240/s11/Lectures/Lecture_15.ppt)  
Berkeley—lecture notes.
- [2] P.D. Bruza, K. Kitto, D. Nelson, C.L. McEvoy  
Entangling words and meaning.  
*Proceedings of the 2nd Quantum Interaction Symposium*, 118–124, 2008.
- [3] D. Borth, R. Ji, T. Chen, T. Breuel, S. Chang  
Large-scale visual sentiment ontology and detectors using adjective noun pairs.  
*Proceedings of the 21st ACM International Conference on Multimedia*, 223–232, 2013.
- [4] N. Bhowmik, V. R. Gonzalez, V. Gouet-Brunet, H. Pedrini, G. Bloch  
Efficient fusion of multidimensional descriptors for image retrieval.  
*IEEE International Conference on Image Processing*, 5766–5770, 2014.

- [5] J. C. Caicedo  
Multimodal information spaces for content-based image retrieval.  
In *Proceedings of the Third BCS-IRSG conference on Future Directions in Information Access*, 110–116, 2009.
- [6] Y.C. Chang, H.H. Chen  
Increasing relevance and diversity in photo retrieval by result fusion.  
*Working Notes of CLEF 2008*, 2008.
- [7] Z. Chen, W. Liu, F. Zhang, M. J. Li and H. J. Zhang  
Web mining for web image retrieval.  
*Journal of the American Society for Information Science and Technology*, 52(10):831–839, 2001.
- [8] A. Depeursinge, H. Muller  
Fusion techniques for combining textual and visual information retrieval.  
*ImageCLEF, The Springer International Series on Information Retrieval*, 32:95–114, 2010.
- [9] L. Kaliciak, H. Myrhaug, A. Goker, D. Song  
On the duality of specific early and late fusion strategies.  
*Information Fusion (FUSION), 17th International Conference on*, 1–8, 2014.
- [10] L. Kaliciak, D. Song, N. Wiratunga, J. Pan  
Combining visual and textual systems within the context of user feedback.  
*The 19th International Conference on Multimedia Modeling*, 7732(1):445–455, 2013.
- [11] A. Kumar, J. Kim, W. Cai, M. Fulham, D. Feng  
Content-based medical image retrieval: a survey of applications to multidimensional and multimodality data.  
*Journal of Digital Imaging*, vol. 26, 1025–1039, 2013.
- [12] V. Lavrenko, W. B. Croft  
Relevance models in information retrieval.  
In *Croft and Lafferty*, 13:11–56, 2003.
- [13] Y.Li, H. Cunningham  
Geometric and quantum methods for information retrieval.  
*SIGIR Forum*, 42(2):22–32, 2008.
- [14] F. Lingensfeller, J. Wagner, E. Andre  
A systematic discussion of fusion techniques for multimodal affect recognition tasks.  
*ICMI*, 19–26, 2011.
- [15] H. Liu  
A framework for understanding user interaction with content-based image retrieval: model, interface and users.  
PhD Thesis. [kmi.open.ac.uk/people/alumni/haiming-liu](http://kmi.open.ac.uk/people/alumni/haiming-liu), 2010.
- [16] H. Liu, D. Song, S. Rueger, R. Hu, V. Uren  
Comparing dissimilarity measures for content-based image retrieval.  
*The 4th Asia Information Retrieval Symposium*, 44–50, 2008.
- [17] T. Mensink, G. Csurka, F. Perronnin  
LEAR and XRCE’s participation to visual concept detection task—ImageCLEF 2010.  
*CLEF 2010—Conference on Multilingual and Multimodal Information Access evaluation*, 77–80, 2006.
- [18] T. Mensink, J. Verbeek, G. Csurka  
Weighted transmedia relevance feedback for image retrieval and auto-annotation.  
*Technical Report Number 0415*, 2011.
- [19] B.A. Olshausen, D.J. Field  
Emergence of simple-cell receptive field properties by learning a sparse code for natural images.  
*Nature*, 381:607–609, 1996.
- [20] A. Popescu-Belis, R. Stiefelhagen  
A probabilistic model for user relevance feedback on image retrieval.  
*Lecture Notes in Computer Science*, 5237:260–271, 2008.
- [21] D. Picard, N. Thome, and M. Cord  
An efficient system for combining complementary kernels in complex visual categorization tasks.  
*Proceedings of 17th IEEE International Conference on Image Processing*, 3877–3880, 2010.
- [22] E. Rabinovich, O. Rom, O. Kurland  
Utilizing relevance feedback in fusion-based retrieval.  
In *Proceedings of the 37th International ACM SIGIR Conference on Research and Development in Information Retrieval*, 313–322, 2014.
- [23] C.J. van Rijsbergen  
The geometry of information retrieval.  
*Cambridge University Press*, 2004.
- [24] V. Risojevic and Z. Babic  
Fusion of global and local descriptors for remote sensing image classification.  
*IEEE Geoscience and Remote Sensing Letters*, 10(4):836–840, 2013.
- [25] S. Robertson, H. Zaragoza, M. Taylor  
Simple BM25 extension to multiple weighted fields.  
In *Proceedings of the Thirteenth ACM International Conference on Information and Knowledge Management*, 42–49, 2004.
- [26] J. Rocchio  
Relevance feedback in information retrieval.  
*The Smart Retrieval System-Experiments in Automatic Document Processing*, 313–323, 1971.
- [27] S. Cees, M. Worring, A. Smeulders  
Early versus late fusion in semantic video analysis.  
In *Proceedings of the 13th Annual ACM International Conference on Multimedia*, 399–402, 2005.
- [28] S. Cees, M. Worring, J. C. Gemert, J. M. Geusebroek, A. Smeulders  
The challenge problem for automated detection of 101 semantic concepts in multimedia.  
In *Proceedings of the 13th Annual ACM International Conference on Multimedia*, 421–430, 2006.
- [29] C. Vogt, and C. W. Garrison  
Fusion via a linear combination of scores.  
*Information Retrieval*, 1(3):151–173, 1999.
- [30] J. Wang, D. Song, L. Kaliciak  
Tensor product of correlated text and visual features: a quantum theory inspired image retrieval framework.  
*AAAI-Fall 2010 Symposium on Quantum Information for Cognitive, Social, and Semantic Processes*, 109–116, 2010.
- [31] D. Widdows  
Semantic vector products: Some initial investigations.  
*Proceedings of the 2nd Quantum Interaction Symposium*, 2008.
- [32] [www.quantum.umb.edu/Jacobs/QMT/QMT\\_AppendixA.pdf](http://www.quantum.umb.edu/Jacobs/QMT/QMT_AppendixA.pdf)  
Combining systems: the tensor product and partial trace.
- [33] W. Zhang, Z. Qin, and T. Wan  
Image scene categorization using multi-bag-of-features.  
*Proceedings of International Conference on Machine Learning and Cybernetics*, 4:1804–1808, 2011.
- [34] Z. Ye, B. He, X. Huang, and H. Lin  
Revisiting Rocchio’s relevance feedback algorithm for probabilistic models.  
*Lecture Notes in Computer Science*, 6458:151–161, 2010.
- [35] S. Xie, and L. Yang  
Using corpus and knowledge-based similarity measure in maximum marginal relevance for meeting summarization.  
*Acoustics, Speech and Signal Processing*, 4985–4988, 2008.



**Leszek Kaliciak** works as a Research Scientist within the field of Image and Multimedia Retrieval at AmbieSense Ltd. He researches and develops products and services for image retrieval, mobile applications, and cloud. His research interests include image processing and multimedia retrieval, and information fusion. He is a member of ECIR, SIGIR, AIRS, and ACM Transactions on Multimedia Computing, Communications and Applications. He is leading the image retrieval development for AmbieSense on several projects. For instance, he is currently working on the OPENi EU project where he is researching, developing, and optimizing new and novel search and information fusion technologies for cloud service provision.

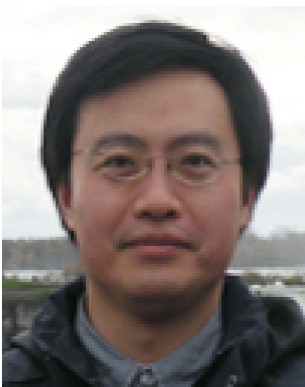


**Hans Myrhaug** is a specialist in mobile technologies, ubiquitous solutions provision, and co-founder of AmbieSense Ltd. Apart from being the CTO of AmbieSense he also led the application development work of the 14 mill Euro webinos Integrated Project with 70+ people involved across 22 partners. He was also the Coordinator of the AmbieSense EU project, which was a 5.7 mill Euro international project with 50+ people involved throughout the project, with 8 project partners, and several sub-contractors. Its successful completion led to the establishment of AmbieSense, the company, offering software and hardware products. He worked as Project Coordinator and research scientist for the applied research institute SINTEF ICT in Norway, prior to spinning out AmbieSense as a business. He has more than 18 years experience in international research and innovation creating a range of wireless and ubiquitous solutions and services based on wireless sensors, miniaturized devices, search, and the cloud, including more recently also a high-end software camera. As CTO he heads the research and development activities of AmbieSense Ltd across technologies such as software, hardware, and cloud.



**Ayse Goker** has over 20 years' research and development experience in areas including context-learning algorithms, multimedia and social media, web user logs, personalization and mobile information systems. Her work involves a strong user-centered approach to algorithm and search-system design, development and evaluation. Goker has been involved in the webinos and the Social Sensor Integrated Projects. Social Sensor is enabling real-time multimedia indexing and search in the Social Web, with partners such as Yahoo, Alcatel-Lucent, Deutsche Welle, IBM, and ITI-Certh. She has been an entrepreneur and pioneer in context-aware information retrieval systems since the early 1990s. She holds a lifelong Enterprise Fellowship from the Royal Society of Edinburgh and Scottish Enterprise for her contributions to the AmbieSense EU project, which subsequently commercialized as AmbieSense Ltd. She is also Professor of Computational Systems, School of Computing, Robert Gordon University, chairing the Digital Technologies Theme at IDEAS research center.

**Dawei Song** obtained his PhD from the Chinese University of Hong Kong in year 2000. He worked as a Research Scientist at the Distributed Systems Technology Center, Australia, and as a Professor of Computing at the Robert Gordon University in Scotland. He currently works at the Open University in Milton Keynes, England, and the Tianjin University in Tianjin, China. His major research interests include information retrieval models, web and enterprise search systems, biomedical information retrieval, text-based knowledge discovery from biomedical resources, and management and search of complex data (multimedia and biological structures). He has been a Principal Investigator of a number of prestigious research projects funded by the UK's Engineering and Physical Sciences Research Council, and has received twice the IBM Innovation Awards in 2006 and 2007. He is a professional member of ACM, and the Secretary of the Information Retrieval Specialists Group of the British Computer Society (BCS). He is a Steering Committee Member of the Asian Information Retrieval Symposium (AIRS). He is on editorial board of the International Journal of Computer Processing of Languages. He has served as a guest editor for the ACM Transactions on Asian Language Information Processing, and as a Programme Committee member for a number of well-respected conferences such as ACM SIGIR, CIKM, and ECIR. He has published papers on respected journals such as ACM transactions on Information Systems, Journal of American Society for Information Science and Technology, Decision Support Systems, IEEE Transactions on Knowledge and Data Engineering, and top conferences such as ACM SIGIR and CIKM.



# Fusion of Asynchronous Passive Measurements

RICHARD W. OSBORNE, III  
YAAKOV BAR-SHALOM  
PETER WILLETT

The use of angular information in the form of line-of-sight (LOS) measurements from passive sensors for the purposes of target localization and tracking has been extensively studied. Previous work has shown that the formation of fused *composite* measurements from a minimum number of LOS measurements (two) is statistically efficient, and therefore, the Cramér-Rao Lower Bound (CRLB) provides a valid measurement noise covariance for the resulting composite measurement. If the LOS measurements are not synchronized, however, the formation of composite measurements is not possible from two LOS observations. In this paper, two methods are presented for forming composite measurements when LOS observations are obtained asynchronously. It is demonstrated that the minimum number of LOS measurements required from two asynchronous sensors is four, and that both methods provide a statistically efficient estimate for track initialization.

Manuscript received October 23, 2015; released for publication December 30, 2015.

Refereeing of this contribution was handled by William Blair.

Authors' address: University of Connecticut, Storrs, CT 06269-4157. (e-mail: {rosborne,ybs,willett}@engr.uconn.edu).

R. Osborne and Y. Bar-Shalom were supported by ARO Grant W911NF-10-1-0369, and P. Willett was supported under ONR contract N000014-13-1-0231.

1557-6418/15/\$17.00 © 2015 JAIF

## 1. INTRODUCTION

Target localization and tracking algorithms often make use of passive sensors, these being for stealthy surveillance of a region. The main disadvantage of using such sensors is that they generally provide only line-of-sight (LOS) measurements, and without providing range measurements, a single passive sensor cannot fully localize a target. The angular measurements could be directly used in nonlinear tracking filters, or composite measurements can be obtained by fusing multiple angular measurements, with the resulting composite measurements passed to the tracking filter.

The fused composite measurements can provide full Cartesian position (and possibly velocity) estimates to take advantage of the ensuing linear measurement equation. If the state equation is linear, then one can use linear filters. The use of *S-D* assignment algorithms for association of angular measurements from passive sensors can be found in [4], [8]. In the present paper we will assume that the angular measurements have been correctly associated and will focus on the formation of composite measurements and their use in track initialization. The composite measurements could continue to be used in a linear tracking filter, or the angular measurements could be used directly in a nonlinear (EKF) filter, such as in [9], where tracking boost phase missiles with LOS measurements was examined.

Prior work on target localization through angular measurements includes [3], [5], [6], [10]–[12]. Application of Taylor-series estimation to the problem of target localization is presented in [5] and extended in [11]. In both papers, though the statistics of the estimation errors are examined, neither the CRLB nor the statistical efficiency of the procedure is investigated.

In [10], equations are derived for the covariance-based uncertainty ellipsoids, circular error probability regions, and geometric dilution of precision, along with their relation to the particular localization scheme and received signal characteristics. However, the CRLB and the statistical efficiency of the estimation scheme are not considered.

LOS measurements to “beacons” with known location have been used to determine the position and attitude of a sensor (camera) in [3]. In this formulation, the LOS angle measurements to the beacons are taken by the sensor at an unknown location and the angles are with respect to the unknown attitude of the sensor. Thus, the estimation of the sensor location and attitude has to be done simultaneously. Observability conditions and the CRLB were derived for this problem.

An investigation of the CRLB of the initial state estimate of a boost phase object using LOS measurements from geosynchronous satellites is considered in [12]. That paper, however, focused only on the behavior of the CRLB, and not on whether any estimation scheme meets the CRLB.

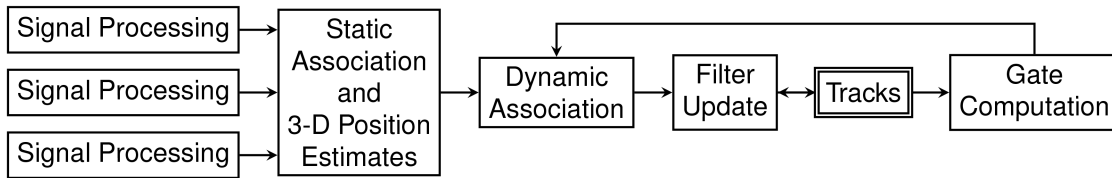


Fig. 1. Type III multisensor information processing configuration.

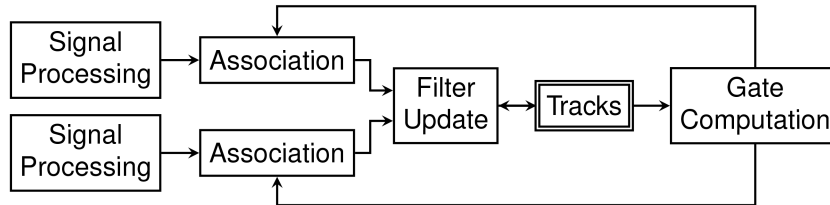


Fig. 2. Type IV multisensor information processing configuration.

The ML estimation for bearing-only target localization (triangulation) was considered in [6]. In that paper, examples in two dimensions with bearing-only measurements show that the ML estimator is unbiased and efficient only when a significant number of measurements are utilized.

None of the previously mentioned papers provided a comparison of linear and nonlinear tracking filters using angular and composite measurements. Furthermore, these papers did not examine the particular difficulties of utilizing asynchronous measurements.

In [7] the statistical efficiency of composite measurements was examined for passive sensors which provide LOS measurements. In that work, it was shown via statistical tests that the minimum number of measurements (two) provide a composite measurement with a resulting estimation error that was consistent with the Cramér-Rao Lower Bound (CRLB) of the resulting parameter estimation problem. Demonstration that the estimator in question was statistically efficient (i.e., the estimator met the CRLB) was of particular interest since the CRLB can be easily calculated and can then be used as a measurement noise covariance for linear tracking filters which utilize the resulting composite measurement.

One particular limitation of the method outlined in [7] is the need for the sensors to be perfectly synchronized. The present work expands the method of [7] for use with asynchronous passive sensors and again demonstrates the statistical efficiency of the approach. Additionally, an alternative track initialization scheme using interpolated LOS measurements is examined, and it is demonstrated that both methods are statistically efficient and the performance difference between them is statistically insignificant.

Section 2 provides an overview of the relevant data fusion configurations (Type III and Type IV—see [2]). Section 3 formulates the problem by illustrating the requirements for observability and outlining the method of forming composite measurements. Section 4 provides

simulation results and Section 5 summarizes the paper and presents conclusions.

## 2. MULTISENSOR TRACKING CONFIGURATIONS

As defined in [2], there are four general configurations of information processing for multisensor tracking. The Type I configuration refers to single sensor tracking and provides a baseline for comparison of multisensor tracking configurations. The Type II configuration refers to single sensor tracking followed by track-to-track association and fusion. There exist a number of subsets of this configuration depending on possible levels of feedback and memory. Of particular interest to this paper, however, are the Type III and Type IV configurations.

### 2.1. Type III Multisensor Configuration

The Type III multisensor configuration is illustrated in Figure 1. In this configuration, each (passive) sensor performs individual signal processing to generate (LOS) measurements. The measurements are then passed on to a fusion center where the measurements are associated and combined into full three-dimensional (3D) position measurements, referred to as *supermeasurements* or *composite measurements*. The composite measurements can then undergo “dynamic association,” i.e., the association of measurements to existing tracks (or, alternatively, to form new tracks). The use of composite measurements allows the tracking filter to behave as a single sensor tracker would.

### 2.2. Type IV Multisensor Configuration

The Type IV multisensor configuration is the fully centralized multisensor tracking configuration and illustrated in Figure 2. In this configuration, each sensor performs individual signal processing to generate measurements, and each measurement is passed to a fusion center which will then perform the association of mea-

measurements to tracks followed by track update (as well as formation/termination of new/old tracks).

### 3. PROBLEM FORMULATION

Assume we have  $N_s$  sensors with known position  $\mathbf{s}_i = [x_i, y_i, z_i]'$ ,  $i = 1, 2, \dots, N_s$ , in Cartesian coordinates. Each sensor provides line-of-sight (LOS) measurements, where the LOS measurement at time  $t_n$  (not necessarily the same across sensors) is to a target at the unknown position  $\mathbf{x}_p(t_n) = [x(t_n), y(t_n), z(t_n)]'$ , in the same Cartesian coordinates. The measurement from sensor  $i$  and at time  $t_n$  is

$$\mathbf{z}_i(t_n) = h(\mathbf{x}_p(t_n), \mathbf{s}_i) + w_i(t_n) \quad (1)$$

where  $w_i(t_n)$  is zero-mean white Gaussian measurement noise with covariance matrix  $R_i$  and

$$\begin{aligned} h(\mathbf{x}_p(t_n), \mathbf{s}_i) &= \begin{bmatrix} \alpha_i(t_n) \\ \epsilon_i(t_n) \end{bmatrix} \\ &= \begin{bmatrix} \tan^{-1} \left( \frac{y(t_n) - y_i}{x(t_n) - x_i} \right) \\ \tan^{-1} \left( \frac{z(t_n) - z_i}{\sqrt{(x(t_n) - x_i)^2 + (y(t_n) - y_i)^2}} \right) \end{bmatrix} \end{aligned} \quad (2)$$

Furthermore, it will be assumed that, in the asynchronous case, the measurements are provided to the fusion center with a time stamp at which the measurement was taken. This time stamp will be assumed to be known perfectly.

For a more detailed overview of the LOS measurement fusion in the synchronous case, see [7]. The procedure for the synchronous case is to utilize Iterated Least Squares (closely related to the Gauss-Newton method) with two LOS measurements to obtain a maximum likelihood (ML) estimate of the full 3D position of the target. We assume that there is no data association uncertainty between the two measurements (i.e., it is known perfectly that they belong to the same target).

For the asynchronous case, modifications are needed to account for each measurement being taken at a different time. Assuming that the measurements are taken a short time interval apart (so that the target does not have time to maneuver), the target will be well-modeled by a constant velocity motion model. In order to fit a constant velocity motion model to the target, a six dimensional state vector must be estimated, consisting of the target's position and velocity at a particular point in time. There exists, however, a subtle unobservability for this problem that will necessitate the use of more measurements than at first seems necessary.

#### 3.1. Incomplete Observability of the Target State with Three LOS Measurements

Since each LOS measurement (1) is a two dimensional vector, three such measurements should be the

minimum required to solve for a constant velocity target's state, i.e., we have six equations (observations from (2)) and six unknowns (target position and velocity in 3D space). The estimation of the constant velocity target's state at a particular point in time, however, is basically equivalent to finding three positions along the LOS vectors (one position along each vector), such that the three positions are appropriately spaced to match the constant velocity model and the three time stamps. Given three sensors with one LOS from each, the target parameter vector is fully observable (provided the sensors are not positioned on a straight line). If multiple LOS measurements are provided by the same sensor, however, there is a lack of full observability when three LOS measurements are provided if the trajectory is coplanar with the line connecting the two sensors. This incomplete observability will be demonstrated by illustrating some of the multiple solutions obtained when given two LOS measurements from one sensor and one from a second sensor.

Figure 3 depicts three possible trajectories which are found to fit the same three LOS observations provided by two sensors. In addition to the true target which was simulated to generate the observations, there are two other ghost targets (only two are shown here; there are many possible), traveling in different directions with different constant speeds, that could have produced the same observations. Since the target's state is thus unobservable with three LOS measurements, the *minimum number of observations* which can form composite measurements from two asynchronous sensors is *four*.

#### 3.2. Formation of Composite Measurements from Asynchronous LOS

Due to the issues with observability of the six dimensional target state, a single composite measurement will be formed from a batch of four asynchronous LOS measurements. Similar to [7], the formation of the composite measurement will be done via Iterated Least Squares (ILS) [1] using the ML criterion.

We will assume that the batch of measurements provided to the fusion center is

$$\mathbf{z} = [\mathbf{z}_1(t_1)', \mathbf{z}_2(t_2)', \mathbf{z}_3(t_3)', \mathbf{z}_4(t_4)']' \quad t_1 < t_2 < t_3 < t_4 \quad (3)$$

where  $\mathbf{z}_i(t_n)$  is given by (1).<sup>1</sup>

The composite measurement will consist of the target's state

$$\mathbf{x}(t_f) = [x(t_f), y(t_f), z(t_f), \dot{x}(t_f), \dot{y}(t_f), \dot{z}(t_f)]' \quad (4)$$

<sup>1</sup>The notation of (3) would seem to suggest that four sensors are used, however, any order of measurements from two to four sensors would be valid. In fact, in later simulations, the measurements will be assumed to come from two sensors at alternating times, i.e.,  $[z_1(t_1), z_2(t_2), z_1(t_3), z_2(t_4)]$ .

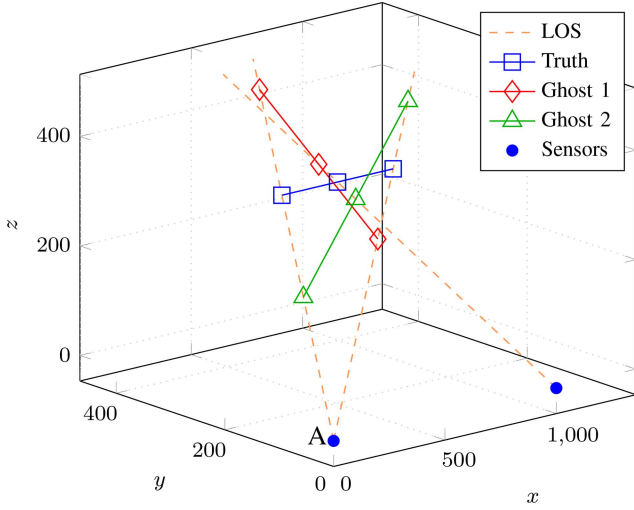


Fig. 3. Three possible target trajectories that fit three identical LOS observations. The speeds of these targets are 250 m/s (Truth), 146.6 m/s (Ghost 1), and 498.5 m/s (Ghost 2). The two LOS from A and one LOS from B allow additional possible (ghost) trajectories.

at a particular “fusion time”  $t_f$ . The ILS estimate (after the  $j$ th iteration) of the target state (4) is

$$\hat{\mathbf{x}}_{\text{ILS}}^{j+1} = \hat{\mathbf{x}}_{\text{ILS}}^j + [(H^j)'R^{-1}H^j]^{-1}(H^j)'R^{-1} \cdot [\mathbf{z} - \mathbf{h}(\hat{\mathbf{x}}_{\text{ILS}}^j)] \quad (5)$$

where

$$\mathbf{h}(\hat{\mathbf{x}}_{\text{ILS}}^j) \triangleq \begin{bmatrix} h(F(t_1, t_f), \hat{\mathbf{x}}_{\text{ILS}}^j, \mathbf{s}_1) \\ h(F(t_2, t_f), \hat{\mathbf{x}}_{\text{ILS}}^j, \mathbf{s}_2) \\ h(F(t_3, t_f), \hat{\mathbf{x}}_{\text{ILS}}^j, \mathbf{s}_3) \\ h(F(t_4, t_f), \hat{\mathbf{x}}_{\text{ILS}}^j, \mathbf{s}_4) \end{bmatrix} \quad (6)$$

$$F(t_n, t_f) \triangleq \begin{bmatrix} 1 & 0 & 0 & t_n - t_f & 0 & 0 \\ 0 & 1 & 0 & 0 & t_n - t_f & 0 \\ 0 & 0 & 1 & 0 & 0 & t_n - t_f \\ 0 & 0 & 0 & 1 & 0 & 0 \\ 0 & 0 & 0 & 0 & 1 & 0 \\ 0 & 0 & 0 & 0 & 0 & 1 \end{bmatrix} \quad (7)$$

$$R = \begin{bmatrix} R_1 & 0 & 0 & 0 \\ 0 & R_2 & 0 & 0 \\ 0 & 0 & R_3 & 0 \\ 0 & 0 & 0 & R_4 \end{bmatrix} \quad (8)$$

and  $H^j$  is the Jacobian matrix of the measurements (given below) evaluated at the  $j$ th ILS estimate.

By using the transition matrix (7), the target state (4) is predicted to the time of each measurement in (3), and (6) provides the predicted LOS observation for use in forming the necessary residuals for the ILS iteration (5).

The Jacobian matrix is

$$H = [H_1' \quad H_2' \quad H_3' \quad H_4']' \quad (9)$$

where<sup>2</sup>

$$H_i = \begin{bmatrix} \frac{\partial \alpha_i}{\partial x} & \frac{\partial \alpha_i}{\partial y} & \frac{\partial \alpha_i}{\partial z} & \frac{\partial \alpha_i}{\partial \dot{x}} & \frac{\partial \alpha_i}{\partial \dot{y}} & \frac{\partial \alpha_i}{\partial \dot{z}} \\ \frac{\partial \epsilon_i}{\partial x} & \frac{\partial \epsilon_i}{\partial y} & \frac{\partial \epsilon_i}{\partial z} & \frac{\partial \epsilon_i}{\partial \dot{x}} & \frac{\partial \epsilon_i}{\partial \dot{y}} & \frac{\partial \epsilon_i}{\partial \dot{z}} \end{bmatrix} \quad (10)$$

The necessary partial derivatives with respect to the position terms of (4) are

$$\frac{\partial \alpha_i}{\partial x} = -\frac{\Delta y_i}{(\Delta x_i)^2 + (\Delta y_i)^2} \quad (11)$$

$$\frac{\partial \alpha_i}{\partial y} = \frac{\Delta x_i}{(\Delta x_i)^2 + (\Delta y_i)^2} \quad (12)$$

$$\frac{\partial \alpha_i}{\partial z} = 0 \quad (13)$$

$$\frac{\partial \epsilon_i}{\partial x} = -\frac{(\Delta x_i)(\Delta z_i)}{\sqrt{(\Delta x_i)^2 + (\Delta y_i)^2} \|\mathbf{x} - \mathbf{s}_i\|^2} \quad (14)$$

$$\frac{\partial \epsilon_i}{\partial y} = -\frac{(\Delta y_i)(\Delta z_i)}{\sqrt{(\Delta x_i)^2 + (\Delta y_i)^2} \|\mathbf{x} - \mathbf{s}_i\|^2} \quad (15)$$

$$\frac{\partial \epsilon_i}{\partial z} = \frac{\sqrt{(\Delta x_i)^2 + (\Delta y_i)^2}}{\|\mathbf{x} - \mathbf{s}_i\|^2} \quad (16)$$

where  $\|\cdot\|$  denotes the Euclidean norm,

$$\begin{bmatrix} \Delta x_i \\ \Delta y_i \\ \Delta z_i \end{bmatrix} \triangleq \begin{bmatrix} 1 & 0 & 0 & \Delta t_n & 0 & 0 \\ 0 & 1 & 0 & 0 & \Delta t_n & 0 \\ 0 & 0 & 1 & 0 & 0 & \Delta t_n \end{bmatrix} \mathbf{x} - \mathbf{s}_i \quad (17)$$

and

$$\Delta t_n \triangleq t_n - t_f \quad (18)$$

The partial derivatives with respect to the velocity terms of (4) are

$$\frac{\partial \alpha_i}{\partial \dot{x}} = \Delta t_n \frac{\partial \alpha_i}{\partial x} \quad (19)$$

$$\frac{\partial \alpha_i}{\partial \dot{y}} = \Delta t_n \frac{\partial \alpha_i}{\partial y} \quad (20)$$

$$\frac{\partial \alpha_i}{\partial \dot{z}} = \Delta t_n \frac{\partial \alpha_i}{\partial z} \quad (21)$$

$$\frac{\partial \epsilon_i}{\partial \dot{x}} = \Delta t_n \frac{\partial \epsilon_i}{\partial x} \quad (22)$$

$$\frac{\partial \epsilon_i}{\partial \dot{y}} = \Delta t_n \frac{\partial \epsilon_i}{\partial y} \quad (23)$$

$$\frac{\partial \epsilon_i}{\partial \dot{z}} = \Delta t_n \frac{\partial \epsilon_i}{\partial z} \quad (24)$$

### 3.3. Initial Solution

In order to perform the numerical search via ILS, an initial estimate  $\hat{\mathbf{x}}_{\text{ILS}}^0$  is required. Since four LOS measurements are needed to form the composite measurement, the initialization will be done by forming two Cartesian measurements from pairs of LOS, as if they

<sup>2</sup>The time argument  $t_f$  has been omitted for simplicity, but note that the partial derivatives are taken with respect to the elements of (4).

were taken synchronously. Since the initialization needs only to be approximate, the error introduced by (incorrectly) assuming pairs of LOS measurements are taken synchronously will be corrected by refinement in subsequent updates.

In this case, each pair of LOS measurements will form a Cartesian position as

$$\begin{bmatrix} x^0 \\ y^0 \\ z^0 \end{bmatrix} = \begin{bmatrix} \frac{y_2 - y_1 + x_1 \tan \alpha_1 - x_2 \tan \alpha_2}{\tan \alpha_1 - \tan \alpha_2} \\ \frac{\tan \alpha_1 (y_2 + \tan \alpha_2 (x_1 - x_2)) - y_1 \tan \alpha_2}{\tan \alpha_1 - \tan \alpha_2} \\ z_1 + \tan \epsilon_1 \left| \frac{(y_1 - y_2) \cos \alpha_2 + (x_2 - x_1) \sin \alpha_2}{\sin(\alpha_1 - \alpha_2)} \right| \end{bmatrix} \quad (25)$$

The two Cartesian positions formed from (25) can then be differenced to provide an approximate initial velocity estimate. This procedure is analogous to two-point differencing [1] and will provide a full six-dimensional state estimate to initialize the ILS algorithm.

#### 3.4. Formation of Composite Measurements from Interpolated Asynchronous LOS

As an alternative to the above method of forming full composite measurements by explicitly fitting to a constant velocity model, one could form the composite measurement by utilizing interpolated asynchronous LOS measurements and two-point differencing.

In the interpolation method, the successive LOS measurements from one sensor are interpolated to the time of a measurement from the second sensor, i.e., the interpolated measurement is

$$\hat{\mathbf{z}}_i(t_n) = \mathbf{z}_i(t_{n-1}) + \frac{t_n - t_{n-1}}{t_{n+1} - t_{n-1}} [\mathbf{z}_i(t_{n+1}) - \mathbf{z}_i(t_{n-1})] \quad (26)$$

where  $t_n$  in this case would be the time of the measurement from the second sensor, and  $t_{n-1}$  and  $t_{n+1}$  are the times of the two measurements from the first sensor. This interpolated LOS and the second sensor's LOS measurement can then provide a composite position measurement using the method of [7]. This can be repeated using a different set of LOS measurements to obtain a composite position measurement at another time. Two-point differencing is then performed on the two composite position measurements, and the resulting state estimate and covariance are predicted to the fusion time  $t_f$ .

In later sections, comparisons are made between this interpolation method and the full asynchronous LOS composite measurement method of Subsection 3.2. In order to use the same number of asynchronous LOS measurements (four) in both the interpolation method and the composite measurement method, the first use of (26) will involve  $[\mathbf{z}_1(t_1), \mathbf{z}_2(t_2), \mathbf{z}_1(t_3)]$ , and the second

will involve  $[\mathbf{z}_2(t_2), \mathbf{z}_1(t_3), \mathbf{z}_2(t_4)]$ . The use of the middle two LOS measurements in both composite measurements will result in correlated errors, but the two-point differencing will be carried out assuming uncorrelated errors.

#### 3.5. Cramér-Rao Lower Bound

The Cramér-Rao Lower Bound (CRLB) provides a lower bound on the estimation error obtainable from an unbiased estimator, where

$$E\{(x - \hat{x})(x - \hat{x})'\} \geq J^{-1} \quad (27)$$

where  $J$  is the Fisher Information Matrix (FIM),  $x$  is the true value to be estimated, and  $\hat{x}$  is the estimate.

The FIM is

$$J = E\{[\nabla_{\mathbf{x}} \ln \Lambda(\mathbf{x})][\nabla_{\mathbf{x}} \ln \Lambda(\mathbf{x})]'\} \Big|_{\mathbf{x}=\mathbf{x}_{true}} \quad (28)$$

where  $\Lambda(\mathbf{x})$  is the likelihood function of the parameter vector to be estimated, and the FIM is evaluated at the true parameter vector.<sup>3</sup>

The gradient of the log-likelihood function is

$$\nabla_{\mathbf{x}} \lambda(\mathbf{x}) = \sum_{i=1}^{N_s} H_i' R_i^{-1} (\mathbf{z}_i(t_i) - h(F(t_f, t_i) \mathbf{x}, \mathbf{s}_i)) \quad (29)$$

which, when plugged into (28) gives

$$J = \sum_{i=1}^{N_s} H_i' (R_i^{-1})' H_i \Big|_{\mathbf{x}=\mathbf{x}_{true}} \quad (30)$$

$$= H'(R^{-1})' H \Big|_{\mathbf{x}=\mathbf{x}_{true}} \quad (31)$$

The resulting CRLB,  $J^{-1}$ , evaluated at the final estimate  $\hat{\mathbf{x}}_{ILS}$ , can be used as an (estimated) measurement noise covariance matrix for the resulting composite measurement. This allows  $\hat{\mathbf{x}}_{ILS}$  to be used as a linear measurement, avoiding the need to use LOS measurements directly in a nonlinear tracking filter.

## 4. SIMULATION RESULTS

In order to examine the fusion of asynchronous LOS measurements in Type III multisensor tracking configurations, a nearly constant velocity target was simulated. The motion model used was a constant velocity (CV) motion model [1].

The target's initial state was

$$\mathbf{x}(t_0) = [-4000 \quad 4000 \quad 500 \quad 100 \quad 0 \quad 0] \quad (32)$$

Two sensors were assumed to be positioned at

$$\mathbf{s}_1 = [0 \quad 0 \quad 0]' \quad (33)$$

$$\mathbf{s}_2 = [2000 \quad y_2 \quad 0]' \quad (34)$$

<sup>3</sup>The strict definition of the FIM requires it to be evaluated at the true parameter, however, evaluation at the estimate (referred to as the *observed* Fisher information) generally yields a very good approximation.

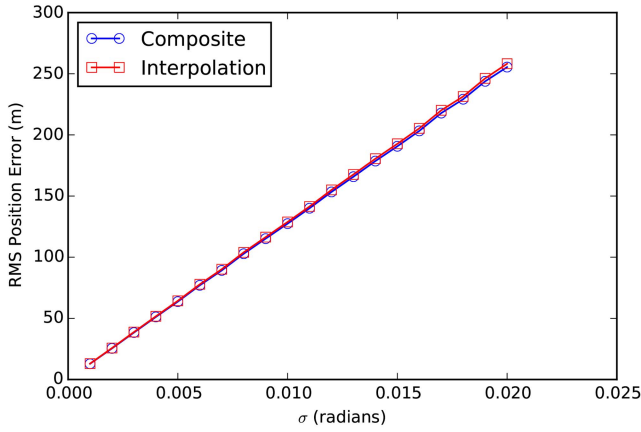


Fig. 4. RMS position error (over 10,000 Monte Carlo runs) of initial track state for various measurement noise standard deviations and  $y_2 = 8,000$ .

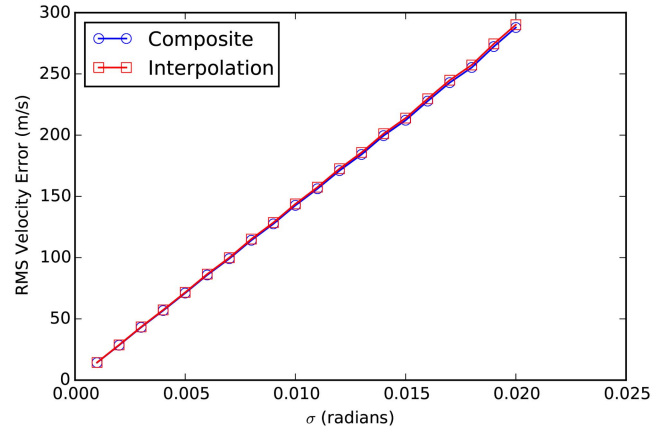


Fig. 5. RMS velocity error (over 10,000 Monte Carlo runs) of initial track state for various measurement noise standard deviations and  $y_2 = 8,000$ .

where two sensor-target geometries are tested by using  $y_2 = 0$  or  $y_2 = 8000$ . When  $y_2 = 0$ , the target trajectory is coplanar with the line connecting the sensors, demonstrating in a practical fashion that the fourth LOS measurement provides observability for the problem described in Subsection 3.1.

The two sensors are assumed to provide measurements at a sampling interval of  $T = 1$  s, however, Sensor 2 provides measurements offset  $T/2$  after Sensor 1; meaning there is one LOS measurement provided every  $T/2$ , as opposed to two LOS measurements provided every  $T$ .

With synchronous measurements, the Type III configuration could provide composite measurements of the target position in Cartesian space once every second, formed in the same manner as in [7]. With asynchronous measurements, the Type III configuration will provide composite measurements of the target position *and velocity* at the time of the final LOS observation in the batch; but only one composite measurement will be generated at intervals of  $2T$  (since four LOS measurements are needed).

Two methods of initializing target tracks using a batch of four LOS measurements will be compared. The formation of composite position and velocity estimates described in Section 3.2 can be used, with the CRLB covariance used as the initial track covariance. Alternatively, the method of Section 3.4—a combination of interpolation of the LOS measurements and two-point differencing [1]—will be used.

Figure 4 shows the RMS position error of the initial track state for both initialization methods. The measurement noise standard deviation is varied from 1 mrad to 20 mrad,  $y_2 = 8000$ , and 10,000 Monte Carlo runs are performed. The two methods perform nearly identically.

Figure 5 shows the RMS velocity error of the initial track state for both initialization methods. Once again, the velocity error is nearly identical for both methods.

Figure 6 shows the normalized estimation error squared (NEES) for the two initialization methods. The

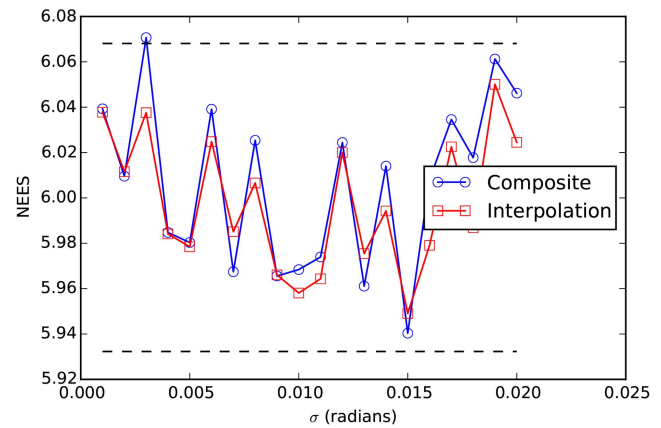


Fig. 6. Normalized estimation error squared (NEES) over 10,000 Monte Carlo runs, with  $y_2 = 8,000$ .

NEES provides a way of evaluating the consistency of the estimation errors with the covariances provided by each estimation method. The dashed line of the figure shows the 95% probability region for the NEES, demonstrating that the estimate errors are commensurate with their corresponding calculated covariances. In the case of the composite measurement, the covariance is provided by the CRLB. In the case of the interpolation method, the covariance is given by the two-point differencing procedure [1], where the measurement noise covariance for each of the two composite position measurements is given by the CRLB as outlined in [7]. Note that, since an interpolated measurement is used, the measurement noise covariance of the interpolated measurement is not equal to the single LOS measurement noise covariance. Due to the interpolation (and the fact that, in this case, the interpolation is performed at the midpoint between two measurements), the measurement noise covariance of the interpolated LOS measurements is half that of an individual measurement. The fact that the measurement noises in the interpolations are correlated, however, will be neglected.

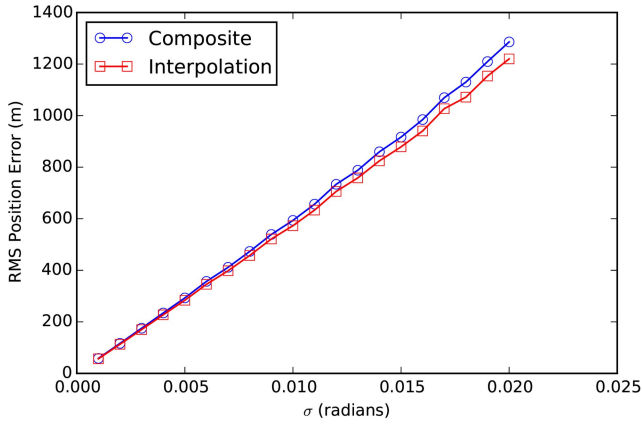


Fig. 7. RMS position error (over 10,000 Monte Carlo runs) of initial track state for various measurement noise standard deviations and  $y_2 = 0$ .

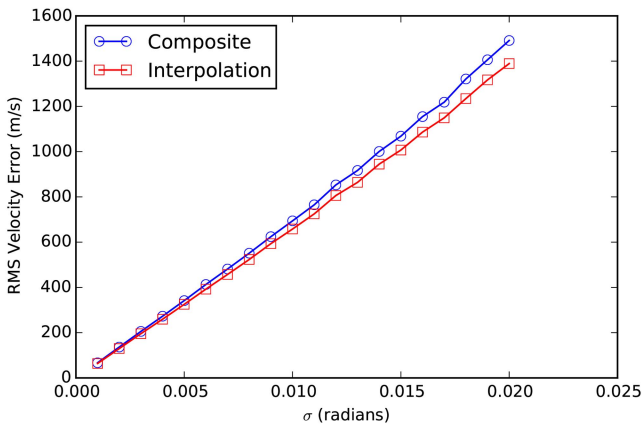


Fig. 8. RMS velocity error (over 10,000 Monte Carlo runs) of initial track state for various measurement noise standard deviations and  $y_2 = 0$ .

The method which fuses all four LOS measurements into a composite position and velocity estimate provides a consistent covariance using the CRLB, demonstrating that the estimator is statistically efficient with a batch of four LOS measurements. The interpolation method, however, also provides consistency, in spite of the fact that the interpolation measurement noises are assumed uncorrelated.

Figures 7–8 show the RMSE position and velocity error when  $y_2 = 0$ . In this case, there appears to be a slight improvement in performance when using interpolated measurements. In order to test this, the statistical significance of the error difference was examined. The squared error of each element of the state (position and velocity in  $x$ ,  $y$ , and  $z$ ) was normalized by its respective error covariance and averaged over the Monte Carlo runs. This provides a statistical test involving a chi-square random variable (similar to the NEES), where a non-zero mean in the difference of the errors (i.e., a significant improvement in one method over the other) will manifest as a value outside of the  $1 - \alpha$  probability region. For the average over 10,000 Monte Carlo runs and

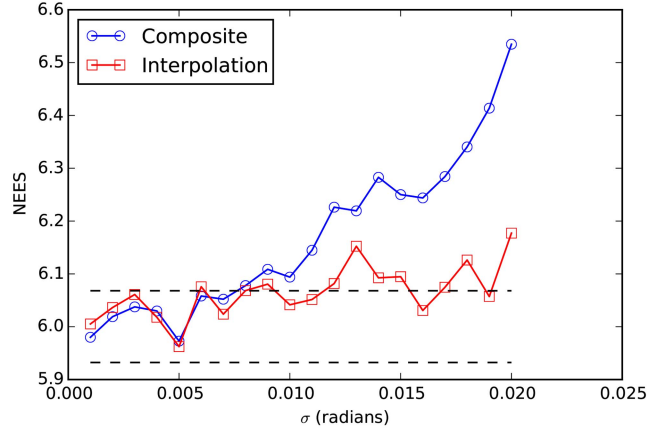


Fig. 9. Normalized estimation error squared (NEES) over 10,000 Monte Carlo runs, with  $y_2 = 0$ .

$\alpha = 0.05$ , this value is 1.02. The maximum normalized squared difference of the errors over all measurement noise values and dimensions was 0.021, well below the threshold required to reject the hypothesis that there is no statistically significant difference in accuracy.

Figure 9 shows the NEES for the case where  $y_2 = 0$ . For this more difficult geometry, where the target trajectory is coplanar with the line connecting the sensors, the statistical efficiency breaks down for the composite measurement method when the measurement noise standard deviation increases. The interpolation method, however, is more resistant to the difficulties imposed by the marginally observable geometry. The correlations introduced by the interpolation method work in our favor in the marginally observable case by reinforcing a solution that is skewed towards the middle two measurements. This in turn reinforces a more “straight line” solution over the ML solution’s fit to the four noisy data points.

Following track initialization, the track maintenance phase can be carried out either in the Type III configuration (where batches of measurements are fused into full composite measurements of position and velocity) or the Type IV configuration where the track is updated one measurement at a time (in a nonlinear tracking filter). For the examples considered here, the choice of fusion configuration for the track maintenance phase made no significant difference in tracking performance over the course of the target’s trajectory. It should be noted, however, that when the track maintenance phase was examined, both types of track updates (Type III and Type IV) were performed on identically initialized tracks. This ensures that the effect of the style of track update was examined independently of the track initialization method.

In order to test the above track initialization methods for accelerating targets (but retaining the assumption of a CV target), the simulations were repeated for targets

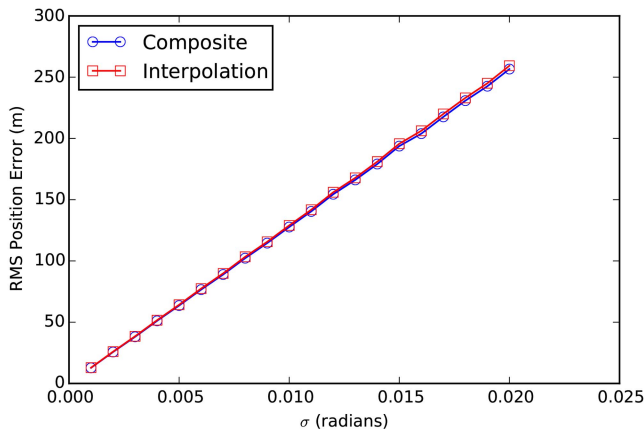


Fig. 10. RMS position error (over 10,000 Monte Carlo runs) of initial track state for  $y_2 = 8,000$  and a target with  $1 \text{ m/s}^2$  acceleration.

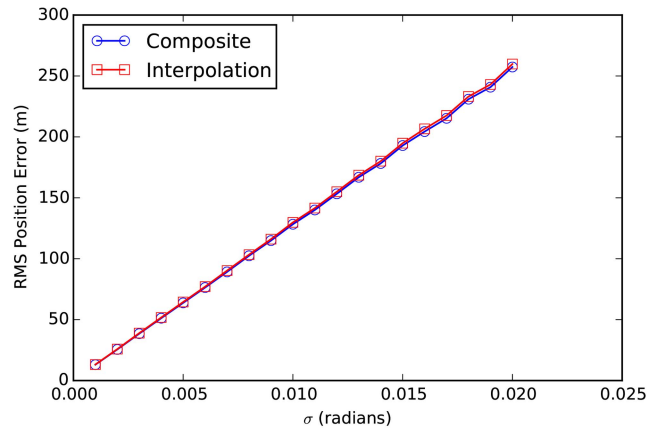


Fig. 13. RMS position error (over 10,000 Monte Carlo runs) of initial track state for  $y_2 = 8,000$  and a target with  $10 \text{ m/s}^2$  acceleration.

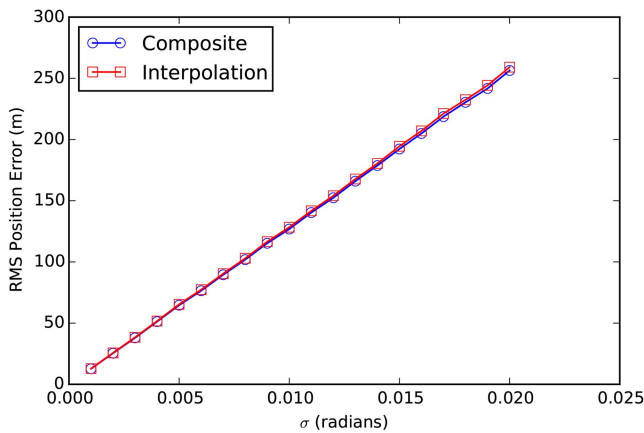


Fig. 11. RMS position error (over 10,000 Monte Carlo runs) of initial track state for  $y_2 = 8,000$  and a target with  $2 \text{ m/s}^2$  acceleration.

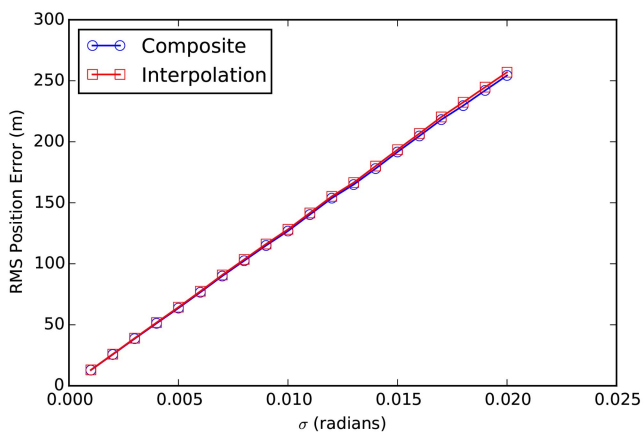


Fig. 12. RMS position error (over 10,000 Monte Carlo runs) of initial track state for  $y_2 = 8,000$  and a target with  $5 \text{ m/s}^2$  acceleration.

which had constant accelerations of  $1 \text{ m/s}^2$ ,  $2 \text{ m/s}^2$ ,  $5 \text{ m/s}^2$  and  $10 \text{ m/s}^2$ .

Figures 10–13 show the RMSE position error for the various accelerating targets. There is no significant change in the RMSE position error over this range of accelerations. The RMSE velocity errors (not included

here) show similar results.

Figures 14–17 show the NEES for the accelerating targets. When the acceleration is large enough, the errors from neglecting the acceleration component can have a significant impact on the statistical consistency for the smaller levels of measurement noise. When the measurement noise is large enough (or if the target was further away), the cross-range measurement error would mask the errors that are a result of neglecting the acceleration. In such cases (small levels of cross-range errors), the target model used in the initialization method would need to account for the acceleration. Using a constant acceleration model, however, would require more measurements in order to estimate the acceleration of the target in addition to the position and velocity.

## 5. CONCLUSIONS

The use of angular measurements for target localization and tracking has been widely studied, including the formation of fused composite measurements to avoid the need for nonlinear filtering. Previous research into the formation of composite Cartesian position measurements from LOS measurements demonstrated that the maximum likelihood (ML) estimate obtained via the ILS algorithm was able to provide a statistically efficient estimate using only two LOS measurements. This allowed the CRLB to be used as the measurement noise covariance for the purposes of target tracking with the fused composite measurements. This procedure required the measurements to be synchronized, however, which may be an unrealistic assumption for real systems.

This paper presented two methods of forming fused composite measurements from four *asynchronous* LOS measurements, and demonstrated that four LOS measurements are the minimum required from two asynchronous sensors to do so. In addition to forming a composite position and velocity estimate directly from the four asynchronous LOS measurements, an alternative

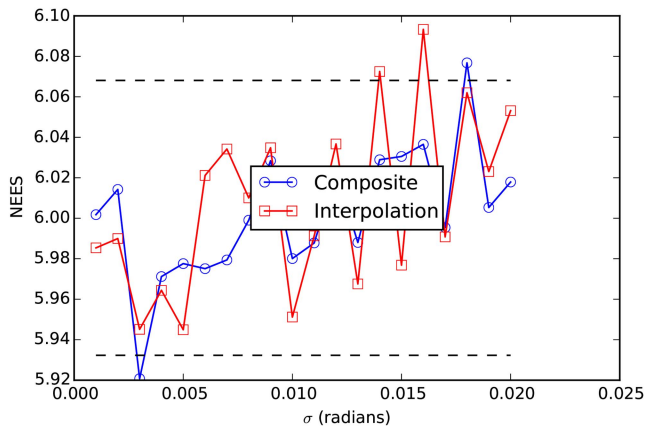


Fig. 14. Normalized estimation error squared (NEES) over 10,000 Monte Carlo runs, with  $y_2 = 8,000$  and a target with  $1 \text{ m/s}^2$  acceleration.

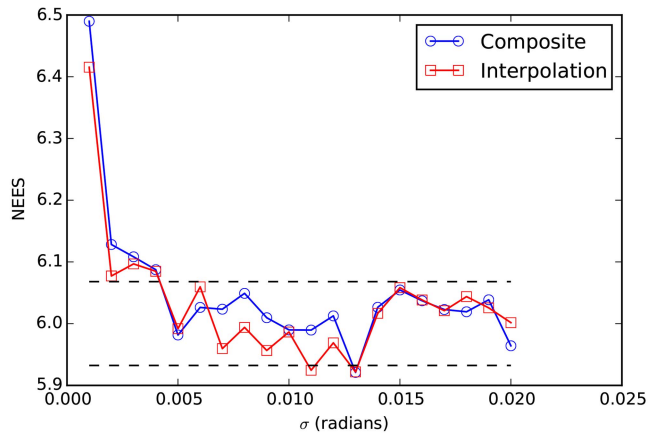


Fig. 16. Normalized estimation error squared (NEES) over 10,000 Monte Carlo runs, with  $y_2 = 8,000$  and a target with  $5 \text{ m/s}^2$  acceleration.

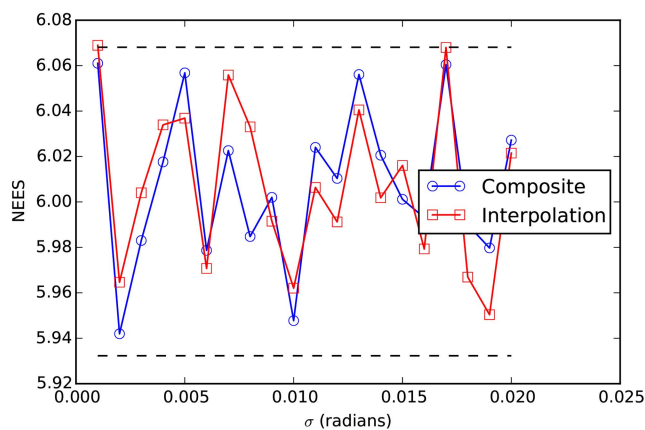


Fig. 15. Normalized estimation error squared (NEES) over 10,000 Monte Carlo runs, with  $y_2 = 8,000$  and a target with  $2 \text{ m/s}^2$  acceleration.

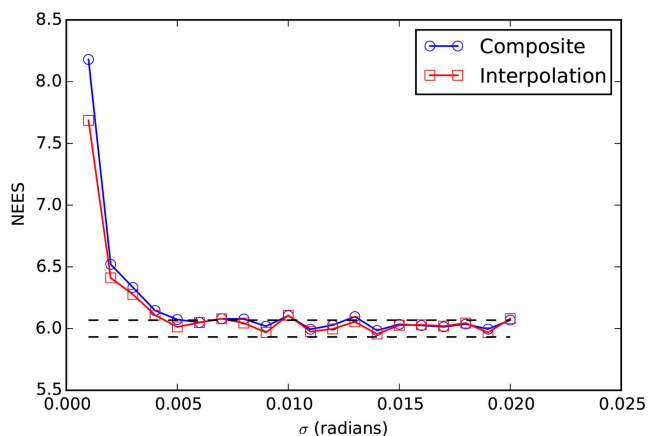


Fig. 17. Normalized estimation error squared (NEES) over 10,000 Monte Carlo runs, with  $y_2 = 8,000$  and a target with  $10 \text{ m/s}^2$  acceleration.

involving interpolating successive LOS measurements was presented. The resulting composite measurements were then compared to the ML method. Both methods provide a way to initialize tracks, and the difference in their accuracies were found to be statistically insignificant. Furthermore, both methods generally provide a statistically consistent error covariance. The interpolation method proved to provide a more consistent error covariance in the marginally observable case of a target trajectory which is coplanar with the line connecting the two sensors. The consistency of the error covariance could also break down for large target accelerations (in comparison to the cross-range error of the sensors). In such cases, the acceleration would need to be estimated as well, at the expense of requiring more measurements from the sensors.

#### REFERENCES

- [1] Y. Bar-Shalom, X.-R. Li, and T. Kirubarajan *Estimation with Applications to Tracking and Navigation: Theory, Algorithms and Software*. J. Wiley and Sons, 2001.
- [2] Y. Bar-Shalom, P. K. Willett, and X. Tian *Tracking and Data Fusion*. YBS Publishing, 2011.
- [3] J. L. Crassidis, R. Alonso, and J. L. Junkins *Optimal Attitude and Position Determination from Line-of-Sight Measurements*, *Journal of the Astronautical Sciences*, vol. 48(2), pp. 391–408, 2000.
- [4] S. Deb, M. Yeddanapudi, K. R. Pattipati, and Y. Bar-Shalom *A Generalized S-Dimensional Algorithm for Multisensor Multitarget State Estimation*, *Aerospace and Electronic Systems, IEEE Transactions on*, vol. 33, no. 2, pp. 523–538, 1997.
- [5] W. H. Foy *Position-Location Solutions by Taylor-Series Estimation*, *Aerospace and Electronic Systems, IEEE Transactions on*, vol. 12(2), pp. 187–194, Mar. 1976.
- [6] M. Gavish and A. J. Weiss *Performance Analysis of Bearing-Only Target Location Algorithms*, *Aerospace and Electronic Systems, IEEE Transactions on*, vol. 28(3), pp. 817–828, Jul. 1992.
- [7] R. W. Osborne, III and Y. Bar-Shalom *Statistical Efficiency of Composite Position Measurements from Passive Sensors*, *Aerospace and Electronic Systems, IEEE Transactions on*, vol. 49, no. 4, pp. 2799–2806, Oct. 2013.

- [8] R. L. Popp, K. R. Pattipati, and Y. Bar-Shalom  
m-Best S-D Assignment Algorithm with Application to  
Multitarget Tracking,  
*Aerospace and Electronic Systems, IEEE Transactions on*,  
vol. 37, no. 1, pp. 22–39, Jan. 2001.
- [9] R. Tharmarasa, T. Kirubarajan, N. Nandakumaran, and Y. Bar-Shalom  
Profile-Free Launch Point Estimation for Ballistic Targets  
Using Passive Sensors,  
*Journal of Advances in Information Fusion*, vol. 7(1), pp.  
46–60, Jun. 2012.
- [10] D. J. Torrieri  
Statistical Theory of Passive Location Systems,  
*Aerospace and Electronic Systems, IEEE Transactions on*,  
vol. 20(2), pp. 183–198, Mar. 1984.
- [11] M. Wax  
Position Location from Sensors with Position Uncertainty,  
*Aerospace and Electronic Systems, IEEE Transactions on*,  
vol. 19(5), pp. 658–662, Sep. 1983.
- [12] Y. Zhao, D. Yi, Y. Li, and Q. Zhang  
CRLB of Initial State Estimation for Boost Phase Object  
Based on 8-State Gravity Turn Model Using Space-Based  
Observations,  
in *2010 2nd International Conference on Signal Processing  
Systems (ICSPS)*, vol. 1, Dalian, China, Jul. 2010, pp. 781–  
789.



**Richard W. Osborne, III** obtained his B.S., M.S., and Ph.D. degrees in electrical engineering from the University of Connecticut in 2004, 2007, and 2012, respectively. From 2012–2014 he was an Assistant Research Professor in the Electrical Engineering department at the University of Connecticut, Storrs, CT. From 2014–2015 he was a Senior Research Engineer at BAE Systems, Inc. in Burlington, MA, and since 2015, he has been a Senior Research Engineer at United Technologies Research Center in East Hartford, CT. His academic interests include adaptive target tracking, information/sensor fusion, perception/computer vision, and other aspects of estimation.

**Yaakov Bar-Shalom** was born on May 11, 1941. He received the B.S. and M.S. degrees from the Technion, Israel Institute of Technology, in 1963 and 1967 and the Ph.D. degree from Princeton University in 1970, all in electrical engineering. From 1970 to 1976 he was with Systems Control, Inc., Palo Alto, California. Currently he is Board of Trustees Distinguished Professor in the Dept. of Electrical and Computer Engineering and Marianne E. Klewin Professor in Engineering at the University of Connecticut. He is also Director of the ESP (Estimation and Signal Processing) Lab. His current research interests are in estimation theory, target tracking and data fusion. He has published over 500 papers and book chapters in these areas and in stochastic adaptive control. He coauthored the monograph *Tracking and Data Association* (Academic Press, 1988), the graduate texts *Estimation and Tracking: Principles, Techniques and Software* (Artech House, 1993), *Estimation with Applications to Tracking and Navigation: Algorithms and Software for Information Extraction* (Wiley, 2001), the advanced graduate texts *Multitarget-Multisensor Tracking: Principles and Techniques* (YBS Publishing, 1995), *Tracking and Data Fusion* (YBS Publishing, 2011), and edited the books *Multitarget-Multisensor Tracking: Applications and Advances* (Artech House, Vol. I, 1990; Vol. II, 1992; Vol. III, 2000). He has been elected Fellow of IEEE for “contributions to the theory of stochastic systems and of multi-target tracking.” He has been consulting to numerous companies and government agencies, and originated the series of Multitarget-Multisensor Tracking short courses offered via UCLA Extension, at Government Laboratories, private companies and overseas. During 1976 and 1977 he served as Associate Editor of the IEEE Transactions on Automatic Control and from 1978 to 1981 as Associate Editor of *Automatica*. He was Program Chairman of the 1982 American Control Conference, General Chairman of the 1985 ACC, and Co-Chairman of the 1989 IEEE International Conference on Control and Applications. During 1983–87 he served as Chairman of the Conference Activities Board of the IEEE Control Systems Society and during 1987–89 was a member of the Board of Governors of the IEEE CSS. He was a member of the Board of Directors of the International Society of Information Fusion (1999–2004) and served as General Chairman of FUSION 2000, President of ISIF in 2000 and 2002 and Vice President for Publications in 2004–13. In 1987 he received the IEEE CSS Distinguished Member Award. Since 1995 he is a Distinguished Lecturer of the IEEE AESS and has given numerous keynote addresses at major national and international conferences. He is co-recipient of the M. Barry Carlton Award for the best paper in the IEEE Transactions on Aerospace and Electronic Systems in 1995 and 2000 and recipient of the 1998 University of Connecticut AAUP Excellence Award for Research. In 2002 he received the J. Mignona Data Fusion Award from the DoD JDL Data Fusion Group. He is a member of the Connecticut Academy of Science and Engineering. In 2008 he was awarded the IEEE Dennis J. Picard Medal for Radar Technologies and Applications, and in 2012 the Connecticut Medal of Technology. He has been listed by *academic.research.microsoft* (top authors in engineering) as #1 among the researchers in Aerospace Engineering based on the citations of his work. He is the recipient of the 2015 ISIF Award for a Lifetime of Excellence in Information Fusion.





**Peter Willett** (F'03) received his B.A.Sc. (engineering science) from the University of Toronto in 1982, and his Ph.D. degree from Princeton University in 1986. He has been a faculty member at the University of Connecticut ever since, and since 1998 has been a Professor. His primary areas of research have been statistical signal processing, detection, machine learning, data fusion and tracking. He also has interests in and has published in the areas of change/abnormality detection, optical pattern recognition, communications and industrial/security condition monitoring. He is editor-in-chief of *IEEE Signal Processing Letters*. He was editor-in-chief for *IEEE Transactions on Aerospace and Electronic Systems* (2006–2011), and was Vice President for Publications for AESS (2012–2014). He is a member of the IEEE AESS Board of Governors 2003–2009, 2011 to present. He was General Co-Chair (with Stefano Coraluppi) for the 2006 ISIF/IEEE Fusion Conference in Florence, Italy and for the 2008 ISIF/IEEE Fusion Conference in Cologne, Germany, Program Co-Chair (with Eugene Santos) for the 2003 IEEE Conference on Systems, Man & Cybernetics in Washington DC, and Program Co-Chair (with Pramod Varshney) for the 1999 Fusion Conference in Sunnyvale.

# INTERNATIONAL SOCIETY OF INFORMATION FUSION

ISIF Website: <http://www.isif.org>

## 2015 BOARD OF DIRECTORS\*

2013–2015	2014–2016	2015–2017
Jean Dezert	Sten F. Andler	Joachim Biermann
Gee-Wah Ng	Murat Efe	Frederik Gustafsson
Anne-Laure Jousset	Lyudmila Mihaylova	Jesús García

\*Board of Directors are elected by the members of ISIF for a three year term.

## PAST PRESIDENTS

Darin Dunham, 2014	Darko Musicki, 2008	Yaakov Bar-Shalom, 2002
Wolfgang Koch, 2013	Erik Blasch, 2007	Pramod Varshney, 2001
Roy Streit, 2012	Pierre Valin, 2006	Yaakov Bar-Shalom, 2000
Joachim Biermann, 2011	W. Dale Blair, 2005	Jim Llinas, 1999
Stefano Coraluppi, 2010	Chee Chong, 2004	Jim Llinas, 1998
Elisa Shahbazian, 2009	Xiao-Rong Li, 2003	

## SOCIETY VISION

The International Society of Information Fusion (ISIF) is the premier professional society and global information resource for multidisciplinary approaches for theoretical and applied information fusion technologies.

## SOCIETY MISSION

### **Advocate**

To advance the profession of fusion technologies, propose approaches for solving real-world problems, recognize emerging technologies, and foster the transfer of information.

### **Serve**

To serve its members and engineering, business, and scientific communities by providing high-quality information, educational products, and services.

### **Communicate**

To create international communication forums and hold international conferences in countries that provide for interaction of members of fusion communities with each other, with those in other disciplines, and with those in industry and academia.

### **Educate**

To promote undergraduate and graduate education related to information fusion technologies at universities around the world. Sponsor educational courses and tutorials at conferences.

### **Integrate**

Integrate ideas from various approaches for information fusion, and look for common threads and themes—look for overall principles, rather than a multitude of point solutions. Serve as the central focus for coordinating the activities of world-wide information fusion related societies or organizations. Serve as a professional liaison to industry, academia, and government.

### **Disseminate**

To propagate the ideas for integrated approaches to information fusion so that others can build on them in both industry and academia.

## Call for Papers

The Journal of Advances in Information Fusion (JAIF) seeks original contributions in the technical areas of research related to information fusion. Authors are encouraged to submit their manuscripts for peer review <http://isif.org/journal>.

## Call for Reviewers

The success of JAIF and its value to the research community is strongly dependent on the quality of its peer review process. Researchers in the technical areas related to information fusion are encouraged to register as a reviewer for JAIF at <http://jaif.msubmit.net>. Potential reviewers should notify via email the appropriate editors of their offer to serve as a reviewer.